FIN SPACING INTERACTION IN FLUIDIZED BED HEAT EXCHANGERS

by

BURHAN MAHMUD A. AL-ALI

A thesis submitted for the Degree of

DOCTOR OF PHILOSOPHY

Department of Mechanical Engineering

The University of Aston in Birmingham

May 1976

"Seeking knowledge is an obligation for every muslim"

Prophet Mohamad

SUMMARY

The work presented in this thesis is concerned with the heat transfer performance of a single horizontal bare tube and a variety of finned tubes immersed in a shallow air fluidized bed.

Results of experimental investigations with the bare tube indicate that the tube position in the bed influences its performance particularly where fine bed materials are used. In some cases the maximum heat transfer is obtained with the tube in the particle cloud just above the dense phase fluidized bed - a phenomenon that has not been previously observed. This was attributed to the unusual particle circulation in shallow beds. The data is also presented in dimensionless correlations which may be useful for design purposes.

A close approximation to the bare tube data can be obtained by using the transient heating of a spherical probe and this provides a valuable way of accumulating a lot of data very rapidly.

The experimental data on finned tubes shows that a fin spacing less than twenty times the average particle diameter can cause a significant reduction in heat transfer due to the interaction which takes place between the particles and the surface of the fins. Furthermore, evidence

is provided to show that particle shape plays an important part in the interaction with spherical particles being superior to angular particles at low fin spacing/particle diameter ratio.

The finned tube data is less sensitive to tube position in the bed than bare tubes and the best performance is when the tube is positioned at the distributor. A reduction in bed depth decreases the thermal performance of the finned tube but in many practical installations the reduction in pressure drop might more than compensate for the reduced heat flux.

Information is also provided on the theoretical performance of fins and the effect of the root contact area between the fins and the tube was investigated.

ACKNOWLEDGEMENTS

The author wishes to express his gratitude and sincere thanks to Professor D.E. Elliott and Dr. J. Broughton for their invaluable advice and encouragement throughout the course of this work.

Thanks are also due to Dr. J. Howard for his advice and assistance during the prepation of this thesis.

Further thanks must go to the technical staff of the Mechanical Engineering Department for their help in the experimental work.

Finally, the author wishes to thank the Ministry of Higher Education and Scientific Research of IRAQ for their financial support and backing.

CONTENTS

page

CHAPTER 4

EXPERIMENTAL EQUIPMENT

CHAPTER 5

PLAIN TUBE WORK

page

CHAPTER 9

DISCUSSION OF RESULTS

CHAPTER 10

CONCLUSIONS AND SUGGESTIONS FOR FURTHER WORK

page

APPENDICES

NOMENCLATURE

Symbol	Definition
A	Cross-sectional area of general type of extended surface
A_{eff}	Effective surface area of finned tube
A_f	Surface area of fins
A_i	Tube inside area
A_m	Projected area of particle
A_o	Fin root area
A_T	Total surface area of finned tube
A_1, A_2	Constants
a	Constant
a_1, a_2	Constants
B_1, B_2	Constants
B	Shape factor
b_1, b_2	Constants
C	Circumference at any radius along fin
C_m	Circumference of particle projected area
C', C_o	Constants

Symbol	Definition
C_1	$\sqrt{R_o^4 + C_o^2}$
C_2	$\sqrt{(R_o + R_i)^4 + C_o^2}$
Cp_f	Specific heat of fluid
Cp_s	Specific heat of solids
C_R	Factor
C_s	Specific heat of spherical probe
C_w	Specific heat of water
D_b	Bed diameter
D_h	Diameter of heavy particles
D_i	Diameter of light particles
D_t	Diameter of fin root
D_f	Diameter at fin tip
D_p	Average particle diameter
D_{ti}	Tube inside diameter
g	Acceleration due to gravity
H	Heat transfer coefficient (general)
H_{BM}	Bed-to-metal heat transfer coefficient
H_i	Tube inside heat transfer coefficient
Hov.	Overall heat transfer coefficient

Symbol	Definition
h_o	Constant
I_o	Modified Bessel function of the first kind, zero order
I_1	Modified Bessel function of the first kind, first order
K_o	Modified Bessel function of the second kind, zero order
K_1	Modified Bessel function of the second kind, first order
K	Thermal conductivity of fin material
K_{air}	Thermal conductivity of air
K_f	Thermal conductivity of fluid
K_s	Thermal conductivity of solids
K_w	Thermal conductivity of water
L_f	Bed depth
L_{mf}	Bed depth at minimum fluidization conditions
L_t	Tube length
M	Mass of spherical probe
m	$\sqrt{2H/Kt}$
n	Number of fins
n*	Number of fins per metre
P	Constant

Symbol	Definition
Q	Heat transferred
Q_b	Heat entering fin from surroundings
Q_R	Heat conducted in the fin at radius R
$Q_{R+\delta R}$	Heat conducted in the fin at radius R+δR
R	Radius
R_o	Radius at fin root
R_e	Radius at fin tip
R_1	Distance of varying profile up the fin
S	Fin spacing
T	Temperature at any point in the fin
T_{b_1}, T_{b_4}	Bed temperatures
T_b	Average bed temperature
T_f	Average fin temperature
T_m	Metal surface temperature
T_o	Fin root temperature
T_s	Spherical probe temperature
T_{si}	Initial spherical probe temperature
T_w	Average water temperature
T_{wi}	Water temperature at tube inlet
T_{wo}	Water temperature at tube outlet

Symbol	Definition
t	Thickness of straight fins
U_f	Fluidizing velocity
U_{mf}	Minimum fluidizing velocity
U_{opt}	Fluidizing velocity at which the heat transfer coefficient attains maximum
V_b	Total bed volume
V_s	Actual volume of solids
V_w	Water velocity
W	Water flow rate
w	Thickness at any point along the fin
x	Fraction of heavy particles
X	Distance of vertical tube from bed axis
X_1	Fraction (by weight) of solids
z	Fin efficiency x fin effectiveness
$\beta, \beta_1, \beta_2, \beta_3$	Constants
ΔP	Pressure drop in bed
ΔR	Increment increase in radius
ΔT_{BW}	Temperature difference between ved and water
ΔT_w	Water temperature rise

Symbol	Definition
ε	Voidage
ε_f	Voidage at any fluidizing velocity
ε_{mf}	Voidage at minimum fluidizing velocity
η	Fin effectiveness
ϕ	Fin efficiency
λ	Factor
ψ	Angle, with fins of small root contact area
μ_f	Viscosity of fluid
μ_w	Viscosity of water
ρ_B	Bulk density of solids
ρ_h	Density of heavy particles
ρ_l	Density of light particles
ρ_f	Density of fluid
ρ_s	Particle density
Θ	(T_b-T)
Θ_o	(T_b-T_o)

Symbol	Definition

Dimensionless Groups

Ar	Particle Archimedes number $= \frac{gD_p^3 \rho_f (\rho_s - \rho_f)}{\mu^2_f}$
N	Fluidization index $= \frac{U_f}{U_{mf}}$
Nu	Particle Nusselt number $= \frac{H D_p}{K_f}$
Pr	Prandtl number $= \frac{Cp_f \mu_f}{K_f}$
Re	Particle Reynolds number $= \frac{D_p U_f \rho_f}{\mu_f}$
Re_{mf}	Particle Reynolds number at minimum fluidization $= \frac{D_p U_{mf} \rho_f}{\mu_f}$

CHAPTER 1

INTRODUCTION

INTRODUCTION

1.1 Fluidization

Fluidization is a process by which a mass of solid particles is transformed such that it exhibits liquid-like characteristics by the upward flow of gas or liquid through it.

Usually, the bed of solid particles is contained in a vessel supported by a porous plate through which the fluidizing medium is supplied. Before turning on the supply of the fluid, the bed is said to be packed. At low flow rates the fluid merely permeates through the voids between the particles without causing any disturbance to the packing of the particles. As the flow is increased, a state is reached where the drag and buoyancy forces acting on the particles are equal to their weight so that separation of the particles takes place. At this point the bed is said to be at minimum fluidization condition and the fluid velocity is termed the minimum fluidizing velocity.

When in this state, the bed starts to exhibit the liquid-like characteristics, e.g. the bed surface remains horizontal, bodies float on the surface or sink in the bed according to their densities and if an opening is made in the container wall, a jet of fluidized particles emerges.

Further increase in fluid flow results in different bed behaviour depending on whether the fluidizing agent is

a liquid or a gas. Liquid fluidized beds continue expanding smoothly and progressively with the rise in the fluid flow rate. With gas fluidized beds, however, the behaviour is quite different. As the gas flow is increased, large instabilities occur and bubbles are observed rising through the bed, movement of the solids takes place except with fine particles and the bed does not expand much beyond its volume at minimum fluidization.

The rise of bubbles through the bed causes lateral and vertical mixing of the particles by displacing the particles sideways and dragging them in their wakes respectively, thus making the motion of the particles a random process.

As the bubbles rise through the bed, they tend to coalesce and, if the bed is deep enough, they eventually form one large bubble. These types of beds are categorized as "deep" beds, having depths of greater than 50 cm. In beds of lesser depths, however, the absence of large bubbles gives the bed a more even bubbling pattern and due to the large number of bubbles present, better mixing is obtained.

The bubbles eventually burst at the surface throwing some particles above the surface of the bed. In shallow beds, where the number of bubbles is greater, a thick cloud of particles forms above the bed at high fluidizing velocities and forms a continuous part of the bed itself.

At high fluid velocities a point is reached where the drag forces are such that some of the particles become entrained in the gas escaping from the bed and are carried out with it.

1.2 Object of present work

The high mobility of particles in gas fluidized beds and hence the good mixing attained gives these beds two important features. Isothermal conditions are attained within the bed and high heat transfer rates are achieved to surfaces immersed in the bed due to the high rate of replacement of solids at the heat transfer surface. These features make a fluidized bed a good proposition in many applications where it can be used as a heat transfer medium. Elliott[1] reviewed some of the possible applications of fluidized beds particularly in total energy systems.

There has been a great deal of work done on studying the heat transfer between a fluidized bed and immersed surfaces. However, almost all the work had been done using deep beds except the work reported by Atkinson[2] and Yuditskii et al[3]. It was therefore the intention to study the heat transfer characteristics of single horizontal tubes, both finned and bare when immersed in a shallow gas-fluidized bed.

Average heat transfer coefficients around the bare tube were determined to explore the effect of particle size and density, fluidizing velocity and the location (vertically) of the tube in the bed. The latter effect had not been reported in previous work on deep beds.

A copper sphere was used as a heat transfer probe and it will be shown that it exhibits similar behaviour as a plain tube and may be used successfully to determine local

heat transfer coefficients in small beds or in checking the evenness of coefficients obtained in a particular bed.

The performance of finned tubes was investigated with particular attention being paid to the tube position, the fin spacing and its interaction with the particles. Use was made of non-conductive fins to examine the effect of the particle size/fin spacing ratio on the performance of the basic tube on which the fins are mounted.

An attempt was made at quantifying the critical spacing/particle size ratio, below which the heat transfer coefficient starts to drop, as this is an important parameter in heat exchanger design.

Particle shape and its effect on the interaction was also studied and an attempt was made at using some simple shape factor to characterise particles.

Some theoretical background is presented regarding the heat conduction in fins. A numerical solution of the governing differential equation was obtained and it was further extended to study the effect of the fin root profile on the performance of the fin. This method serves as a simulation of practical situations depending on how fins are mounted on tubes.

CHAPTER 2

REVIEW OF RELEVANT LITERATURE

REVIEW OF RELEVANT LITERATURE

2.1 Introduction

Some of the outstanding advantageous heat transfer properties of gas-fluidized beds were summarised by Botterill[4] as follows:

1. An extremely large area of contact between solid and fluid. This permits the achievement of high rates of heat transfer between the solid and the fluid and near isothermal equilibrium between bed particles and exit gases except with very shallow beds.

2. The reduction of temperature gradients to negligible proportions through the bulk of the bed as a consequence of the high degree of solids mixing.

3. High rates of heat transfer between the fluidized solids and immersed surfaces.

It is the third point listed above that is of direct relevance to the present work and consequently the review presented in this chapter will concentrate on this characteristic of gas fluidized beds.

Figure (2.1) illustrates the way in which the heat transfer coefficient between a fluidized bed and a surface immersed in it or the wall of the container varies with the fluid flow rate, i.e. with the fluid velocity through the bed (U_f). In the region where $U_f < Um_f$ (the minimum fluidizing velocity) the bed is "packed" where no movement of

the particles takes place and the heat transfer coefficient (H) is very low. After Um_f is reached, the heat transfer coefficient rises rapidly over a comparatively narrow range (the rising part of the curve). The rise is of one to two orders of magnitude for gas fluidized beds[7]. Up to a certain fluid velocity (U_{opt}), the heat transfer coefficient (H) increases due to the better particle circulation caused by increased bubbling. After the maximum, the heat transfer coefficient diminishes (the falling part of the curve) due to increasing proportion of the surface being blanketted by bubbles void of particles.

Research work on heat transfer between a gas fluidized bed and a surface "wetted" by the bed can be divided into two sections. The first concerns the theoretical aspects of the heat transfer process and the different models that have been proposed to describe it. The second includes the experimental work and empirical correlations that have been put forward to try and generalise the experimental results obtained.

In the following sections a review of the most relevant publications concering the fields of work mentioned above is presented. The reviewed work deals only with "low temperature" heat transfer, i.e. in fluidized beds of temperatures below about 500°C where radiation is negligible.

2.2 Models for heat transfer

A number of mathematical models have been suggested to describe the heat transfer process to surfaces wetted by

gas fluidized beds.

In earlier models, particularly those by Leva et al[15] and Levenspiel and Walton[13], the similarity between a bubbling fluidized bed and a boiling liquid led the workers to believe that the heat transfer was limited by a phenomenon which corresponded to the limiting laminar film as in conventional convective systems. The heat transfer was then considered dependent on the thickness of the boundary layer at the surface with the particles acting as turbulence promoters to erode away the film and reduce its thickness.

Later more successful models were postulated which consider the transient heat transfer between the bed and the surface. These models may broadly be divided into two categories. First those which consider the bed as a continuous gas and discrete particle two-phase system, and secondly, those which consider the two phases to be a continuous emulsion phase of particles and gas at minimum fluidizing condition and a discrete bubble phase devoid of particles. These models consider the unsteady conduction between the surface and either a single particle or an emulsion "packet" when either of them comes into contact with the surface.

Botterill and Williams[41] analysed the transient conduction between a single particle coming into contact or near contact with an immersed surface. A relaxation technique was used to solve the conduction equations which enabled isotherms to be drawn through the system for different particle residence times and different particle/gas

thermal properties. On comparing these results with experimental data, good agreement was particularly achieved when a gas film having a thickness equal to 10% of the particle diameter was assumed to surround the particle. The choice of the film thickness was apparently arbitrary and furthermore, the model was not suitable for long particle residence times since it considered temperature penetration depths up to one particle diameter.[44]

Botterill and Butt[42] extended the single particle model to consider two layers of particles, which improved the predicted heat transfer coefficient for long residence times.

Gabor[43], along the lines of the Botterill model proposed an "alternate slab model" in which he considered alternate layers of gas and solid. His solutions showed good agreement with experimental data but they were critically dependent upon the thickness of the gas layers in the model which was not based on strong physical evidence.

Ziegler et al[31], considered the unsteady conduction between a single particle and a gas film,which was assumed to be at the temperature of the heat transfer surface,where the particle never comes into direct contact with the surface. They also assumed that the particle residence time is defined by a gamma distribution function. Their results agreed well with experimental data and they concluded that

the solid thermal conductivity has negligible effect on the heat transfer coefficient.

The first model to consider the unsteady heat transfer between the emulsion phase and a surface was presented by Mickley and Fairbanks[26]. They considered the conduction to take place when a semi-permanent group of particles (called "packets")come into contact with the surface for a short time and then are returned to the bulk of the bed by bubble action. They assumed that these packets have constant thermo-physical properties, which are equal to those of the incipiently fluidized bed and are rigid and stationary during the process. To obtain the average heat transfer coefficient, they used a "stirring factor" which was not fully defined. Furthermore the assumption of constant properties of the packet is questionable.

Kubie and Broughton[45], in their model, used the packet theory but took into account the variation in the packing properties of the packets. They assumed that the packet properties near the wall can be represented as a function of the voidage which in turn was expressed as a function of the normal distance from the heat transfer surface. Good agreement with existing data was obtained and it appears that this model is the most successful proposed so far.

Syromyatnikov [46] presented a critical analysis of the packet theory. Through experiments conducted on bodies of various shapes and sizes he concluded that a gas film

does form periodically whose thickness was non-uniform. He also suggests that further development of the theory of heat transfer to surfaces in fluidized beds should be based on reliable experimental data on the local structural and hydrodynamic characteristics of fluidized beds close to a surface.

In addition to the problem of how heat is transferred to bodies in fluidized beds, evaluation of the particle or packet residence times is important to obtain the average heat transfer coefficient. Although there have been some attempts at measuring residence times, the problem is by no means resolved.

Residence times become particularly interesting when finned tubes are considered where some restriction of motion of particles takes place between the fins. No studies have yet been presented on this point.

2.3 Previous experimental work

A very comprehensive review of previous experimental work was presented by Zabrodsky[5]. More recent data was included by Kunii and Levenspiel[6] and by Davidson and Harrison[7] in their texts. The most recent of reviews has been presented by Botterill[8].

Previous experimental work has been conducted using different heat transfer surfaces which may be classified into the following categories:

a. The walls of the containing vessel
b. Vertical tubes
c. Horizontal tubes
d. Calorimeters and other surfaces
e. Extended surfaces.

the latter four being immersed in the fluidized bed.

Many of the workers have attempted to generalize their results by proposing empirical correlations. These correlations may be classified into three types according to which part of the H-U curve (figure 2.1) they are concerned with:

1. Correlations for the rising branch
2. Correlations for the maximum heat transfer coefficient which is important for design purposes.
3. Correlations for the falling branch after the maximum.

Correlations have also been proposed for the prediction of the gas velocity at which the maximum heat transfer coefficient is attained ($U_{opt.}$). These correlations, together with those for the falling branch of the H-U curve, will not be dealt with in this review as they are not of prime relevance to the work presented in this thesis and are of doubtful value outside the narrow range of bed/heat transfer surface configurations to which they refer.

The parameters that have generally been used to present heat transfer results and were found to be convenient for comparison of results of different workers[9] are the

following dimensionless groups

$$\text{Particle Nusselt number (Nu)} = \frac{HD_p}{K_f}$$

$$\text{Particle Archimedes number (Ar)} = \frac{gD_p^3\rho_f(\rho_s-\rho_f)}{\mu_f^2}$$

$$\text{Particle Reynolds number (Re)} = \frac{D_pU_f\rho_f}{\mu_f}$$

$$\text{Fluidization index (N)} = \frac{U_f}{U_{mf}}$$

More recently interest has arisen in a further fluidization index ($\frac{U_f-U_{mf}}{U_{mf}}$) being the ratio of the gas in bubble form to that in the continuous phase.

2.3.1 The walls of the containing vessel

A number of experimental investigations have been reported on heat transfer between a fluidized bed and the walls of the container. Some workers have proposed correlations based on their own work, while others proposed correlations based on many of other workers' data in the field.

Dow and Jakob[10] investigated heat transfer from steam heated walls to the fluidized beds using air with different types of fine solids at a temperature of 93-109°C. The heating sections of the walls were of 51-56 mm. diameter and 584-673 mm. height which indicates that "deep" beds were used. They proposed the correlation

$$Nu = 0.55\ Re^{0.8} \left(\frac{\rho_s Cp_s}{\rho_f Cp_f}\right)^{0.25} \left(\frac{D_b}{D_p}\right)^{-0.03} \left(\frac{D_b}{L_f}\right)^{0.65} \left(\frac{1-\varepsilon_f}{\varepsilon_f}\right)^{0.25} \qquad (2.1)$$

for the rising branch of the H-U curve

Van Heerden et al [11] employed a system where the bed was heated by an electric heater placed in the lower region while the walls of the container were water cooled. Different fluidizing gases were used with different types of solids whose size varied between 50 and 800 μm. The bed diameter used was 85 mm. and its height was 407 mm. while the bed temperature was approximately room temperature. They put forward the correlation

$$Nu = 0.58\ Pr^{0.5} B^{0.45} Re^{0.45} \left(\frac{Cp_s}{Cp_f}\right)^{0.36} \left|\frac{\rho_s(1-\varepsilon_{mf})}{\rho_f}\right|^{0.18} \qquad (2.2)$$

for the rising branch of the H-U curve, where B is a kind of a shape factor which is a measure of the deviation of the particles from the spherical shape [12].

Levenspiel and Walton [13] fluidized coal particles of sizes 132-1177 μm by air with air-cooled outside walls. Their correlation for the rising part of the H-U curve takes the conventional form

$$Nu = 0.6Pr\ Re^{0.3} \qquad (2.3)$$

Toomey and Johnstone [14] used an air-glass spheres system of size 55-848 μm with water cooled walls. The bed

diameter was 120mm and its depth varied between 335 and 625mm temperature was approximately 93°C. Their correlation takes the form

$$Nu = 3.75\ (Re_{mf} \log N)^{0.47} \qquad (2.4)$$

which covers the rising branch of the H-U curve also.

The work of Leva et al [15] was conducted on beds of diameters 51-102 mm. and heights 305-635 µm with temperatures of 126-212°C. Different solids were used as well as different gases for fluidization with the walls being steam heated. Their data was later incorporated in a correlation presented by Wen and Leva[16] together with the data of three other groups of investigators (10,11 and 14). The correlation is

$$Nu = 0.16 Pr^{0.4}\ Re^{0.76} \left(\frac{U_f^2}{gD_p}\right)^{-0.2} \left(\lambda \frac{L_{mf}}{L_f}\right)^{0.36} \qquad (2.5)$$

which also covers the rising branch of the H-U curve, where λ was defined by

$$\lambda = \frac{U_f - \text{superficial velocity for uniform expansion of bed}}{U_f}$$

Bartholemew and Katz[17] worked on beds of diameter 102 mm. and heights 469-4565 mm. fluidized by air and the walls being electrically heated. They proposed a correlation for the rising branch of the H-U curve of the form

$$Nu = Re\ Pr^{1/3} \left| \frac{1.56 + \ln(ReAr^{-2/3} - 0.012)}{-0.227\ Ar^{0.42}} \right| \qquad (2.6)$$

Another generalized correlation was presented by Wender and Cooper [19] which included the data of five

studies (10,14,15,17, and 18). The correlation is

$$\frac{Nu}{1-\varepsilon_f}\left(\frac{Cp_s\rho_s}{Cp_f\rho_f}\right) \times \frac{1}{1+7.5\ \exp\left|-0.44\frac{L_f}{D_b}\cdot\frac{Cp_s}{Cp_f}\right|} = f(Re) \quad (2.7)$$

where the function was only presented in graphical form which is shown in figure (2.2). This correlation is also for the rising branch of the H-U curve.

It is clear from the correlations presented above and other investigators data and correlations which were compared by Gelperin and Einstein (in 7), that the discrepancy between the data is very large which has always been attributed to the dependence of the heat transfer coefficient on particle circulation which is greatly affected by the scale of the equipment and in particular the aspect ratio of the bed (height/diameter).

From the different correlations, it can also be seen that the major factors affecting heat transfer are particle size and the thermo-physical properties of both solid and gas.

2.3.2 Vertical tubes

A number of investigations have been reported in the literature concerning vertical tubes, most of which originated in the 1950s. Correlations were also proposed for the rising branch of the H-U curve as well as for the maximum heat transfer coefficient. The correlations include a variety of dimensionless and dimensional quantities in

attempts to generalize heat transfer data to and from vertical tubes.

Baerg et al[20] worked on beds of 254 mm. height with a coaxial heater where they investigated the effect of particle size, bulk density, particle shape and the fluidizing velocity. They expressed their data in two equations. The first was

$$Nu_{max} = 278 \frac{D_p}{K_f} \log \left| \frac{0.0194\rho_B}{D_p} \right| \qquad (2.8)$$

for the maximum heat transfer coefficient and the second was

$$Nu = Nu_{max} - 312 \frac{D_p}{K_f} e^{\left|-0.0586 \ (\rho_f U_f - 0.0001975\rho_B)\right|} \qquad (2.9)$$

for the rising branch of the H-U curve, where ρ_B(inkg/m^3) was defined as the bulk density at the non-fluidized state, and D_p and K_f are in (m) and (W/m^{o}k) respectively.

In their work, Miller and Logwinuk [21] investigated heat transfer between a fluidized bed and a central vertical cooled tube. The bed height was not stated. The temperature of the bed varied between 40^{o}C and 212^{o}C. They proposed the dimensional equation

$$H = 0.499 \frac{K_s^{0.072} K_f^{2.4} (\rho_f U_f)^{.32}}{D_p^{0.961} Cp_f^{1.6} \mu_f^{0.8}} \qquad (2.10)$$

where H will be in (W/m^2 K). This equation deals with the rising portion of the H-U curve as it is in terms of U_F and could be modified and rewritten to include Nu and Re.

Vreedenberg[22,23] studied the performance of a single verticle water-cooled tube positioned along the axis as well as non-axially in very deep beds (1700 mm. high). He presented different correlations for fine-light particles and coarse-heavy ones. For fine-light particles he proposed the equations

$$\frac{H(D_b-D_t)}{K_f}\left(\frac{D_t}{D_b}\right)^{1/3} Pr^{-\frac{1}{2}} = 0.27 \times 10^{-15}\left|\frac{U_f(D_b-D_t)\rho_s}{\mu_f}\right|^{3.4} \quad (2.11)$$

for values of $\frac{U_f(D_b-D_t)\rho_s}{\mu_f} \leqslant 0.237 \times 10^6$, and

$$\frac{H(D_b-D_t)}{K_f}\left(\frac{D_t}{D_b}\right)^{1/3} Pr^{-\frac{1}{2}} = 2.2\left|\frac{U_f(D_b-D_t)\rho_s}{\mu_f}\right|^{0.44} \quad (2.12)$$

for $\frac{U_f(D_b-D_t)\rho_s}{\mu_f} > 0.237 \times 10^6$

For coarse-heavy particles he proposed

$$\frac{H(D_b-D_t)}{K_f}\left(\frac{D_t}{D_b} \times \frac{D_p}{D_b-D_t} \times \frac{1}{Pr}\right)^{1/3} = 0.105 \times 10^{-3}\left|\frac{U_f(D_b-D_t)}{\sqrt{gD_p^3}}\right|^2 \quad (2.13)$$

when $\frac{U_f(D_b-D_t)}{\sqrt{gD_p^3}} < 1070$, and

$$\frac{H(D_b-D_t)}{K_f}\left(\frac{D_t}{D_b} \times \frac{D_p}{D_b-D_t} \times \frac{1}{Pr}\right)^{1/3} = 240\left|\frac{U_f(D_b-D_t)}{\sqrt{gD_p^3}}\right|^{-0.1} \quad (2.14)$$

when $\frac{U_f(D_b-D_t)}{\sqrt{gD_p^3}} \geqslant 1070.$

The distinction between fine and coarse particles was made according to the quantity $\frac{\rho_s}{\rho_f}$ Re being smaller than 2050 or greater than 2550 respectively. As can be seen clearly all Vreidenberg's correlations deal with the rising zone of the H-U curve.

Wender and Cooper [19] presented another of their generalized correlations for heat transfer between a vertical tube and a fluidized bed. They correlated the data reported by Mickley and Trilling [14] and Mickley and Fairbanks [26] together with some additional commercial information into the equation

$$Nu=0.0119\ C_R(1-\varepsilon_f)\ \left(\frac{\rho_f}{\mu_f}\ Pr\right)^{0.43}\ Re^{0.23}\left(\frac{Cp_s}{Cp_f}\right)^{0.8}\left(\frac{\rho_s}{\rho_f}\right)^{0.66} \qquad (2.15)$$

where ρ_f is in Kg/m^3, μ_f is in Kg/m.sec. and C_p is a correction factor, originally given by Vreedenberg, [22] for non-axial tube location in the bed.

Gelperin et al (as in 9) presented a correlation in which they also allow for the tube position in the bed. The equation is

$$Nu = \frac{7.08\ \varepsilon_f}{1-\varepsilon_f} Re^{0.285}\ N^{-0.2}\ \left(1-\frac{2x}{D_b}\right) \qquad (2.16)$$

where x is the distance of the tube from the axis of the bed.

Other investigations with vertical tubes were done with tube bundles. In this case, the interaction between the tubes as well as the tubes arrangement becomes important as

the mechanism of heat transfer is affected at certain tubes positioning.

Similar to the case of heat transfer at the walls, the major concern of the workers has been to correlate data for the rising zone of the H-U curve. The correlations also show a wide range of dependence of the heat transfer coefficient on the different parameters.

2.3.3 Horizontal tubes

The earliest work on heat transfer between a fluidized bed and horizontal tubes immersed in it was done by Vreedenberg[24]. He used a single water-cooled horizontal tube situated at 850 mm. above the distributor in beds 1200mm deep. The parameters varied were fluidizing velocity, particle size, shape and density, tube diameter and the bed temperature. Vreedenberg observed that the heat transfer coefficient increased with increase in bed temperature as well as a decrease in the tube diameter. He then proposed two correlations for this data. One for fine-light particles for which he specified $Re\frac{\rho_s}{\rho_f}$ <2050, which is

$$Nu = 0.66\ Pr^{0.3}\ Re^{0.44} \left(\frac{D_p}{D_t}\right)^{0.56} \left(\frac{\rho_s}{\rho_f}\right)^{0.44} \left(\frac{1-\varepsilon_f}{\varepsilon_f}\right)^{0.44} \qquad (2.17)$$

and the other for coarse-heavy particles for which

$Re\frac{\rho_s}{\rho_f}$ >2550, which is

$$Nu = 420\ Pr^{0.3} Re^{0.3}\ Ar^{-0.3} \left(\frac{D_p}{D_t}\right)^{0.7} \qquad (2.18)$$

Both these correlations cover the rising branch of the H-U curve.

Gelperin (as in 9) proposed the correlation

$$Nu = 4.38 \left(\frac{1-\varepsilon_f}{\varepsilon_f}\right) \left(\frac{Re}{6(1-\varepsilon_f)}\right)^{0.32} \qquad (2.19)$$

Little can be said about the operating conditions as the original reference was not available in English.

Atkinson[2] studied heat transfer to a single water cooled horizontal tube immersed in shallow beds (25-62 mm deep). He studied the effects of bed height, bed size, bed material, tube position and bed temperature on the heat transfer coefficient. He also studied the performance of an oval tube as compared to the ordinary round one. He observed that the heat transfer coefficient decreased with increasing bed temperature which is contrary to the normal trend expressed by Vreedenberg, above, and other workers[8]. This discrepancy was not explained by the author. The other main feature of Atkinson's data was that the tube position was found to have a marked effect on the heat transfer coefficient, the higher value being obtained with the tube higher up the bed.

Another work with shallow beds was reported by Yuditskii and Zabrodskii[3]. They used a horizontal tube to investigate the "peculiarities" observed in shallow bed to tube heat transfer. Bed heights of 35-70 mm were used with fluidizing velocities up to 4m/sec. They reported an enhancement of the heat transfer coefficient

near the distributor plate which could have been due to an entry effect because of the type of distributor plate used. It was a grid with holes of diameter 1.65 mm. and a low free area which would give rise to jets being present. This means that the "quenching" zone (for the incoming hot air to attain bed temperature) could have been large, giving rise to higher bed temperatures at the bottom of the bed. In addition, the presence of the jets causes very vigorous particle motion, particularly at the level of air velocities used, which would enhance the heat transfer coefficient due to the decrease in residence time of the particles at the heat transfer tube.

Perhaps the most important feature of the performance of horizontal tubes in fluidized beds is that although there is much heat transfer surface exposed to the cross flow of solids moving under natural bubble induced circulation, two factors counter this advantage. One is the tendency for defluidized solids to form a stagnant pile on top of the tube which, although it is periodically disturbed, gives rise to very long residence times. The other is the tendency for bubbles to shroud the downward facing surface of the tube. This behaviour has been substantiated by measurements of local heat transfer coefficients made by various workers and is explained by Gelperin and Einstein (in 7) and Botterill[8].

Other work on horizontal tubes has been done (as in the case of vertical tubes) with tube bundles[32,52] where

the arrangement of the tubes in the bundle and the spacing between the tubes would be important. The effect of the tube spacing was clearly demonstrated by Elliott et al[52] where a single row of horizontal tubes was used. They reported that the heat transfer coefficient decreased markedly when the gap between the tubes was less than 70 mm.

2.3.4 Calorimeters and other surfaces

Among the other types of heat transfer surfaces used in fluidized beds are spheres, coils and wires.

Kunii and Levenspiel[6] briefly reviewed the works of Wicke and Fetling[27], Jacob and Osberg[28], Shirai[29], Shirai et al[30] and Zeigler et al [31] which included the use of a small cylindrical heater, a horizontal wire, a small heater, and a sphere respectively. Only Jacob and Osberg[28] proposed a correlation for the maximum heat transfer coefficient which is

$$H_{max} = ho\ (1-\varepsilon_f)(1-e^{-pK_f}) \qquad (2.20)$$

where ho and p are empirical constants defined in reference [28].

Other workers, namely Sarkirts, Traber et al, Obryadchikov and Kruglikov, and Kagan et al were mentioned by Aineshtein and Gelperin[9]. They all used coils in their investigations and proposed correlations for the rising branch of the H-U curve as well as for the maximum heat

transfer coefficient. As nothing was known about their experimental conditions because of the original references being in Russian as well as the further complication that arises with the coils arrangements, it was thought that stating the correlations would not serve any purpose.

2.3.5 Extended surfaces

Increasing the surface area of a heat transfer surface to obtain higher heat fluxes by the use of extended surfaces is not new. In fluidized beds it could be very advantageous to use extended surfaces as much higher heat transfer coefficients are obtained than gas-surface systems. In the case of a horizontal tube, in particular, it would be very advantageous to use extended surfaces if the arrangement helps to eliminate, or even minimise, the defluidized cap on the top of the tube.

Sinclair et al[37] and Baskakov and Filipovsky[38] have found that a flat plate is best arranged vertically in a fluidized bed in order to optimize heat transfer from the bed to the plate.

It appears, therefore, that the arrangement of a horizontal tube with vertically mounted fins immersed in the bed could be a profitable one.

The first published information on finned tubes in fluidized beds was given by Petrie et al[32]. They were concerned with the application of fluidized bed techniques to the calcination of radioactive wastes in which heat is

supplied to the bed from a liquid metal at 400°C flowing through tubes immersed in the bed. Helically wound fins on a basic tube as well as plain tubes arranged in horizontal bundles located in the lower regions of deep beds (approximately 900 mm. deep) were used. The basic tubes were 19 mm. in diameter and the fins (0.4 mm. thick and 10.3 mm. high) were either 197 fins/m or 433 fins/m in number. They showed that their data on plain tubes was in good agreement with Vreedenberg's correlation (equation 2.18). With finned tubes, they found that increasing the number of fins decreases the "fin effectiveness factor" (suggesting that the penetration of the particles between the fins was decreased as the fin spacing reduced[8]).

Similar results were reported by Bartel et al[33]. They used electrically heated single bare and finned tubes positioned horizontally at 200 mm. above the distributor plate in beds of spherical glass particles. The beds were 300 mm. in diameter and 560 mm. in height (unfluidized). The variables studied were particle size, fin thickness, fin height, and fluidizing velocity. They reported that their bare tube results were within 20% of Vreedenberg's. They defined a "fin effectivity factor" to relate the heat transfer coefficients of finned and bare tubes. Finally a mathematical model was used to correlate their data into a single equation containing all the variables.

Genetti et al [35] extended the work of Bartel et al[33] to study the effect of tube orientation on the heat transfer

coefficient using the same equipment. They observed that tube positions of 45^{o} and 60^{o} from the horizontal produced minimum values of the heat transfer coefficients of bare and finned tubes respectively.

Bartel and Genetti[34] extended their own work (in 33) to study the performance of the same finned tubes in bundle formations. The interesting observation made was that tubes with long fins were less sensitive to tube spacing than those with short fins. They also included a correlation for their data on the same lines as that presented for single tubes (in 33).

Investigations on the performance of single horizontal finned tubes which had longitudinal and transverse fins was studied by Natusch and Blenke[36]. Glass beads of sizes 110, 450 and 690 μm were used in beds 500 mm. deep in a steel container of 305 mm. diameter. The tubes, which were electrically heated, were maintained at $125^{o}C$ and positioned at 250 mm. from the distributor plate. For transverse fins, the thicknesses used were 0.5 mm, 1mm and 2 mm. The fin height varied from 7.5 mm. to 37.5 mm. and the fin pitch varied between 2 mm. and 10 mm. They concluded that longitudinal fins can only be used effectively at comparatively high fluidizing velocity. This restriction did not apply for a tube carrying two fins positioned in the vertical plane whose behaviour was found to be similar to a vertical plate. As for the transverse fins of thickness 1 mm., they observed that the effect of fin spacing on the heat transfer coefficient was small. In general they recommended that finned tubes

can be usefully employed in gas fluidized beds at gas velocities greater than 3 U_{mf} since the drop in the coefficient is compensated by the increase in heat transfer area and consequently high fluxes are achieved.

Atkinson[2] studied the performance of different types of finned tubes in shallow fluidized beds. The tubes tested included manufactured ones (with square and round fins) and commercial ones (with crimpled or extruded helical fins). Zircon sand (138 μm), silica sand (157 μm) and steel shot (432 μm) were used in beds of different configurations (round and rectangular) and heights that varied between 50 mm. and 150 mm. He concluded that the main geometric variable which influenced the heat transfer coefficient are basic tube diameter, fin height and fin spacing. He also observed that the heat transfer coefficient decreased with increasing bed temperature (similar to his observation with plain tubes). With square fins he observed an enhancement of the heat transfer coefficient when the finned tube was resting on the distributor plate which he attributed to the restriction of bubble coalescence before entry between adjacent fins.

2.3.6 Correlations for the maximum heat transfer coefficient

The maximum heat transfer coefficient is of prime importance in the design of heat exchangers employing fluidized beds since it is desirable for the equipment to run at the highest possible heat transfer coefficient for the given system.

In this respect many empirical correlations have been proposed in addition to the correlations by Baerg et al [20] (presented in section 2.3.2) and by Jacob and Osburg [28] (in section 2.3.4).

Maskaev and Baskakov [39] used very large particles in their investigations and they presented the correlation

$$Nu_{max} = 0.21\ Ar^{0.32} \qquad (2.21)$$

in the range $1.4 \times 10^5 < Ar < 10^8$.

Varygin and Martynushin (in 7) used a spherical silver calorimeter and proposed the equation

$$Nu_{max} = 0.86\ Ar^{0.2} \left(\frac{K_f}{K_{air}}\right)^{0.6} \qquad (2.22)$$

for $30 < Ar < 1.35 \times 10^5$

Gelperin et al [49] show that for heat transfer to immersed tubes

$$Nu_{max} = 0.7\ Ar^{0.22} \qquad (2.23)$$

over roughly the same range as for equation (2.22)

Zabrodsky [5], through an analysis of experimental data on low temperature beds proposed the dimensional equation

$$Nu_{max} = 0.431\ Ar^{0.2} \left(\frac{\mu^2_f}{g\rho_f k_f^2}\right)^{0.2} \qquad (2.24)$$

Gelperin and Einstein (in 7) have presented a comparison between the data and correlations of different workers

and comment *that the empirical correlations are only valid within the limits of the experimental conditions on which they are based* which is the view expressed by Zabrosky[5] as well.

2.3.7 Discussion

The major observations that can be made from the available literature is that almost all the work on heat transfer in fluidized beds has been done on deep beds whose behaviour is expected to be different from shallow beds since in the latter the number of bubbles reaching the surface is greater and hence the particle circulation could be quite different from that in deep beds.

Concerning finned tubes, no comprehensive study of the effect of fin spacing could be found. This aspect of the performance of finned tubes is one of the most crucial in using such tubes in conjunction with fluidized beds. Fin height and thickness can be optimized and evaluated from standard works on fins if the heat transfer coefficient is assumed to be constant over the length of the fin.

To obtain a fair evaluation of the performance of finned tubes it becomes necessary to study the performance of plain tubes because of the unanimous opinion that each experimental arrangement has its own performance.

One of the points concerning horizontally immersed tubes which has not been fully studied is the tube position.

In deep beds, the general opinion was summed up by Ainshtein and Gelperin[9] where they said: "the magnitude of H_{max} (or Nu_{max}) is, for a given system (particles-agent), relatively independent of the location of the heat transfer surface, its construction or even the type of distributor plate". In shallow beds, however, in both of the reported works (2 and 3), the position of the heat transfer surface had a marked effect on the performance although their observations were contradictory to each other.

As for the correlations offered, the ones for the maximum heat transfer coefficient appear to be in better agreement than those for the rising branch of the H-U curve. It is also evident that the relationship $Nu_{max} = a_1 Ar^{b_1}$ is substantially true and could be used as a guide line for future correlations. However, for the rising zone correlations, Nu is found expressed as a power function of Re which itself can be written as NRe_{mf}. Re_{mf} can be expressed as a function of Ar, and hence the correlation can take the form $Nu = a_2 N^{C_2} Ar^{b_2}$. The other variables that have been included in the different correlations are constant for any particular system. Expressing the correlation in this form seems to be reasonable, particularly as Gelperin and Einstein[7] point out that the exponent of Re in the relationship $Nu = aRe^b$ is not constant.

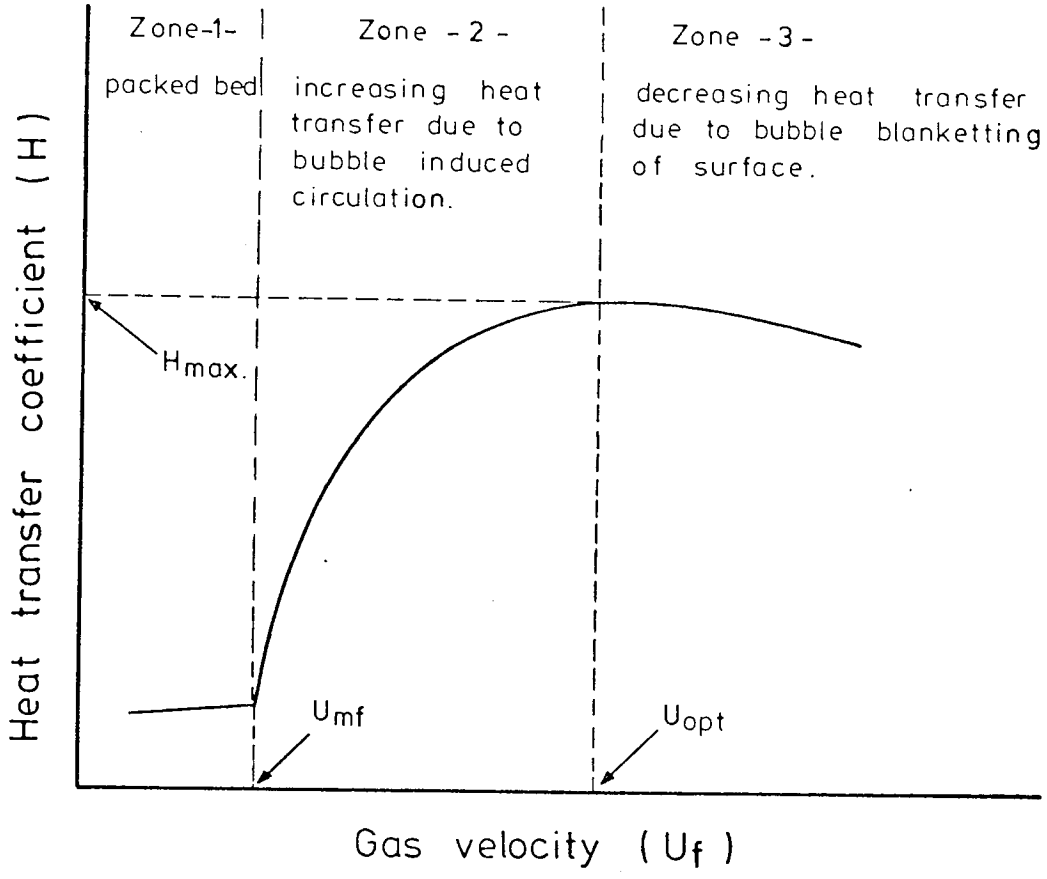

FIG. (2·1) TYPICAL DEPENDENCE OF THE HEAT TRANSFER COEFFICIENT ON GAS VELOCITY

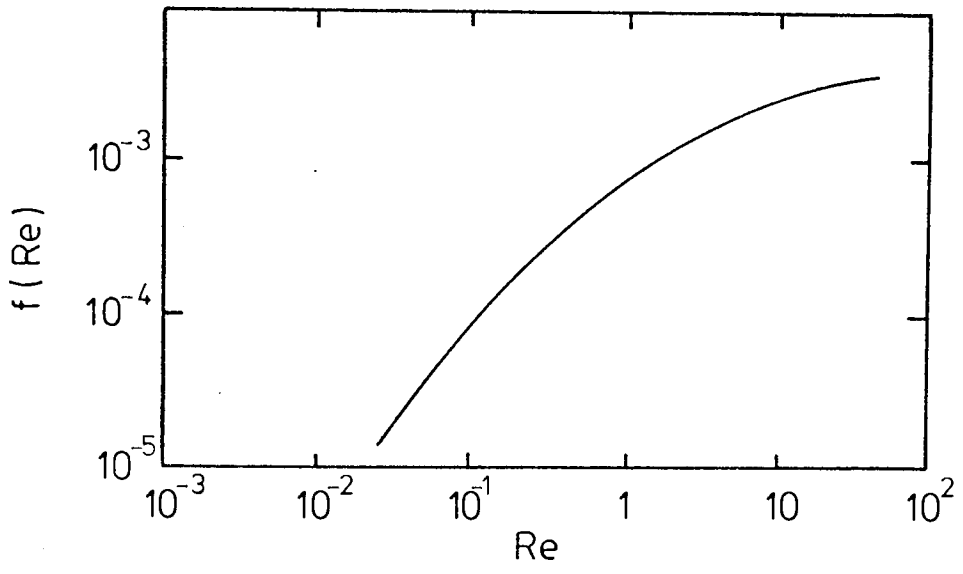

FIG. (2·2) CORRELATION FOR HEAT TRANSFER AT THE CONTAINER WALLS [FROM WENDER & COOPER (19)]

CHAPTER 3

SOME THEORETICAL CONSIDERATIONS

SOME THEORETICAL CONSIDERATIONS

3.1 Introduction

The work described in this chapter is concerned with the theoretical aspect of heat conduction in circumferential fins of rectangular cross section. The general equation is derived and two solutions of the equation are presented. The effect of the root area of the fin is also discussed.

3.2 Assumption for the heat flow equation

It is necessary that a number of assumptions are made to make the derivation of the governing equation possible. These are:

1. The heat flows through the fin at steady state. i.e. independent of time. This is particularly true in shallow beds with the presence of frequent bubbles. In deep beds, however, with intermittent bubbles, validity of this assumption becomes questionable.
2. The fin material is homogeneous and isotropic.
3. There are no heat sources in the fin itself.
4. The heat flow to the fin surface at any point is directly proportional to the temperature difference between the surrounding medium and the surface at that point.
5. The thermal conductivity of the fin is constant.
6. The bulk temperature of the surrounding medium is constant.
7. The temperature at the base of the fin is uniform.
8. The heat flow is in the radial direction only i.e. there are no temperature gradients across the thickness of the fin because the thickness is small compared to the length.

3.3 Theoretical treatment of fins

3.3.1 The general equation for extended surfaces

For the derivation of the general equation governing one dimensional steady state heat flow in an extended surface, consider a small element in an extended surface having a cross sectional area (A) and circumference (C), as shown in Figure (3.1). In the steady state, the element conducts Q_R and $Q_{R+\delta R}$ of heat, and receives heat Q_b from the surrounding material. An energy balance of the element gives

$$Q_R = Q_{R+\delta R} + Q_b \tag{3.1}$$

Q_b can be expressed, according to assumption (4) in section (3.2), as

$$Q_b = H\ C\ \delta_R\ (T_b - T) \tag{3.2}$$

where H is the heat transfer coefficient, T_b is the temperature of the surroundings and T is the temperature of the element under consideration. $Q_{R+\delta R}$ can be expressed as

$$Q_{R+\delta R} = Q_R + \frac{dQ_R}{dR}\ \delta_R \tag{3.3}$$

Q_R can be expressed in terms of Fourier's basic equation of conduction as

$$Q_R = K\ A\ \frac{dT}{dR} \tag{3.4}$$

Equations (3.1), (3.2), (3.3) and (3.4) yield

$$-\delta R \left| \frac{d}{dR}\ (KA\ \frac{dT}{dR}) \right| = H\ C\ \delta R\ (T_b - T) \tag{3.5}$$

therefore

$$-KA\frac{d^2T}{dR^2} - K\frac{dA}{dR}\frac{dT}{dR} = H\,C\,(T_b-T) \qquad (3.6)$$

Let $\theta = T_b-T$, hence $\frac{d\theta}{dR} = -\frac{dT}{dR}$ and $\frac{d^2\theta}{dR^2} = -\frac{d^2T}{dR^2}$

Equation (3.6) can now be written as

$$KA\frac{d^2\theta}{dR^2} + K\frac{dA}{dR}\frac{d\theta}{dR} = HC\theta \qquad (3.7)$$

Equation (3.7) is the general heat flow equation for extended surfaces of any profile. It can be found quoted by many of the workers in this field the most notable of whom was Gardner [47].

3.3.2 Equation for circumferential fins of rectangular profile

The type of fin under consideration is illustrated in figure (3.2) for which

$$A = 2\pi Rt \quad \text{and} \quad C = 4\pi R$$

where t is the fin thickness

equation (3.7) becomes

$$\frac{d^2\theta}{dR^2} + \frac{1}{R}\frac{d\theta}{dR} - m^2\theta = 0 \qquad (3.8)$$

where $m^2 = \frac{2H}{Kt}$

3.3.3 Fin temperature profile

The analytical solution of equation (3.8) is readily available in the literature [47,48]. Gardner [47] obtained a solution for the following boundary conditions.

1. at $R=R_o$, $\Theta=\Theta_o$ at the fin root
2. at $R=R_e$, $\frac{d\Theta}{dR} = 0$ at the fin tip

Gardner's solution is

$$\frac{\Theta}{\Theta_o} = \frac{K_1(mR_e)\ I_o\ (mR) + I_1(mR_e)\ K_o(mR)}{I_o(mR_o)\ k_1(mR_e) + I_1(mR_e)\ K_o(mR_o)} \qquad (3.9)$$

where

I_o is modified Bessel function of the first kind and zero order

K_o " " " " of the second kind and zero order

I_1 " " " " of the first kind and first order

K_1 " " " " of the second kind and first order

A detailed explanation of the solution with the boundary conditions used is presented in Appendix (1). Equation (3.9) is limited to the boundary conditions considered and is only applicable to fins of uniform thickness. Although analytical solutions exist for fins of non-uniform thickness[47], applying these solutions to composite fins (i.e. fins of two or more distinctly different profiles from tip to root) becomes tedius. Composite fins can be used as a mould to simulate the cases of fins of uniform thickness whose profiles near the root change because of the process of fitting them on the centre tube.

A numerical solution of equation (3.7) was therefore made for fins of non-uniform thickness. The validity of

the method was verified by comparing the results of this numerical method, when applied to a uniform fin, with Gardner's analytical solution. The method of solution and a flow chart of the computer programme are presented in Appendix (2).

Figure (3.3) shows the temperature difference (θ) distribution along a fin with the following specifications

1. fin height = 12.5 mm.
2. fin thickness = 1.6 mm.
3. temperature difference at the root = $80^{o}C$
4. heat transfer coefficient = 0.5 kW/m^2K

It is evident from the figure that the two solutions are very close with a maximum discrepancy of 0.6% of the analytical value at the tip of the fin.

3.3.4 Fin efficiency and effectiveness

Efficiency and effectiveness are two quantities originally used by Gardner[47] to characterise the performance of extended surfaces.

Fin efficiency is defined as the ratio of the actual heat transferred through the fin to the heat transferred if the whole fin is at the root temperature. (i.e. it is of infinite thermal conductivity).

Analytically an expression can be derived for the fin efficiency which is

$$\phi = \frac{2R_o}{m(R_e^2-R_o^2)} \left| \frac{I_1(mR_e)K_1(mR_o)-I_1(mR_o)K_1(mR_e)}{I_o(mR_o)K_1(mR_e)+I_1(mR_e)K_o(mR_o)} \right| \qquad (3.10)$$

Numerically the efficiency is evaluated from the knowledge of the temperature gradient at the root of the fin and hence the heat flux together with the heat transfer coefficient, the areas and the temperature at the root.

The derivation of the analytical expression for the fin efficiency and its evaluation numerically are given in Appendix (3).

Fin effectiveness (η) is defined as the ratio of the actual heat transferred through the fin to the heat transferred through the same root area if the fin was not present.

Actual heat transferred = $H A_f(T_f-T_b)$

Therefore
$$\eta = \frac{A_f(T_f-T_b)}{A_o(T_o-T_b)} \tag{3.11}$$

From the definition of the efficiency

$$\phi = \frac{T_f-T_b}{T_o-T_b} \tag{3.12}$$

and hence
$$\eta = \frac{A_f}{A_o}\,\phi \tag{3.13}$$

The fin efficiency is a measure of the effect of having an additional resistance in the path of the heat flux. Accordingly, the efficiency decreases with increasing fin height with the same fin thickness. This is clearly shown in Figure (3.4), which also shows the efficiency evaluated from the analytical and numerical solutions of the governing heat equation (3.8).

The fin effectiveness is a measure of the advantage of having an extended surface with the increased area available for heat transfer to the surrounding medium. However, it is inherent in the definition of the effectiveness that the temperature at the root of the fin remains the same whether the fin is or is not present while it is very likely that the temperature changes with the existence of the fin. For this reason the fin effectiveness could give a misleading interpretation of the advantage of having an extended surface.

Figure (3.5) shows the effect of increasing the fin height and hence the surface area on the effectiveness. When the fin height exceeds 20 mm. the rate of rise in the effectiveness declines indicating that it is not very advantageous to increase the fin height beyond this value.

When designing an extended surface, a compromise has to be made between increasing the effectiveness and decreasing efficiency. A quantity which reflects the combined effect of effectiveness and efficiency is the product of the efficiency and effectiveness. The variation of this new quantity (z) with fin height is shown in Figure (3.6) and shows that the optimum fin height is 20-25 mm.

3.4 Effect of root profile

In the previous sections throughout the derivation of the equation (3.8) and the evaluation of performance characteristics, one inherent assumption was that the area of contact between the fin and the tube has the same width as the fin itself. However, when fins are soldered, brazed

(as in the present work) or mechanically fitted on tubes, the situation may arise where the width of the area of fin contact with the tube is larger or smaller than the thickness of the fin itself. In such cases, the performance of the fin will change.

To investigate these two cases it is essential that a numerical solution of the governing differential equation be used together with a new differential equation for the first part of the fin near the root. The derivations of the new equations is part of the original work described in this thesis.

3.4.1 Fins with large root contact area

This case represents the situation where fins are soldered or brazed on tubes and the corners at the root are not as square as earlier assumed but as shown in figure (3.7).

To obtain the differential equation for the first part of the fin, we shall use the original equation (3.7)

$$KA\frac{d^2\Theta}{dR^2} + K\frac{dA}{dR}\frac{d\Theta}{dR} = HC\Theta$$

It is assumed that the first part of the fin near the root is of hyperbolic shape up to distance R_1 along the fin. By considering an element at radius R, and of thickness w, we get

$$A = 2\Pi R w \tag{3.14}$$

But the equation of the profile gives

$$\frac{w}{2} R = \text{constant } (C') \tag{3.15}$$

from (3.14), $\frac{dA}{dR} = 2\Pi (R\frac{dw}{dR} + w)$

and from (3.15), $\frac{w}{2} + \frac{R}{2} \frac{dw}{dR} = 0$

Hence, $\frac{dA}{dR} = 0$

Therefore equation (3.7) becomes

$$\frac{d^2\Theta}{dR^2} - \frac{2H}{KC_o} R \Theta = 0 \tag{3.16}$$

where $C_o = 2C'$

The solution for a fin of such root profile is numerical since no analytical solution could be found for composite fins. The solution is the same as the one described in Appendix (2) except that equation (3.16) is used for the distance up to R_1 along the fin instead of equation (3.8).

For evaluating the efficiency of such fins, the surface area becomes

$$A_f = 2\Pi \left| (C_2 - C_1 + \frac{C_o}{2} \ln(\frac{C_2 - C_o}{C_2 + C_o}) - \frac{C_o}{2} \ln(\frac{C_1 - C_o}{C_1 + C_o}) \right| + \Pi (R_e^2 - (R_o + R_1)^2) \tag{3.17}$$

where $C_2 = \sqrt{(R_o+R_1)^4+C_o^2}$

$C_1 = \sqrt{R_o^4+ C_o^2}$

A flow chart of the computer programme used for the solution of equations (3.16) and (3.8) and obtaining the effectiveness and efficiency together with evaluating the surface area for the above described fin is presented in Appendix (4). For each fin height considered, the value of R_1 was varied from 1 mm. to 5 mm. in steps of 1 mm. so that the range of increase in the root area is 5.5 to 28.6%.

Figures (3.9) and (3.10) show the variation of the efficiency and effectiveness with fin height for the five cases mentioned above respectively.

It may be concluded that the effect of increasing the fin root area on the efficiency is negligible, as can be seen from Figure (3.8). However, the effectiveness is affected by this change in area quite markedly. But it is only the efficiency that will be used for evaluating the heat transfer coefficient in the present practical work. So the assumption to treat the fins as having a rectangular uniform thickness profile will be valid.

3.4.2 Fins with small root contact area

This case represents the situation where fins are mechanically fitted on tubes. The analysis is carried out by simulating the reduction in area as curving the edges inwards into the fin as arcs of a circle of radius R_1, as shown in Figure (3.8).

The thickness of an element at radius R is given by

$$W = t-2R_1(1-\cos\psi) \tag{3.18}$$

where ψ is the angle made with the base of the straight section of the fin.

Therefore, the area of the element is

$$A = 2\pi R\left[t-2R_1(1-\cos\psi)\right] \tag{3.19}$$

$$\frac{dA}{dR} = 2\pi\left[t-2R_1(1-\cos\psi\right] - 4\pi RR_1\sin\psi\frac{d\psi}{dR} \tag{3.20}$$

but $R = R_o + R_1(1-\sin\psi)$

$$\frac{dR}{d\psi} = -R_1\cos\psi$$

and $$\frac{d\psi}{dR} = -\frac{1}{R_1\cos\psi}$$

Equation (3.20) becomes

$$\frac{dA}{dR} = 2\pi\left[t-2R_1(1-\cos\psi)\right] + 4\pi\tan\psi \tag{3.21}$$

using the general equation (3.7), we get

$$K.2\pi R\left[t-2R_1(1-\cos\psi)\right]\frac{d^2\Theta}{dR^2} + K\{2\pi\left[t-2R_1(1-\cos\psi)\right]+4\pi R\tan\psi\}\frac{d\Theta}{dR}$$

$$= H4\pi RO$$

$$\text{Hence } \frac{d^2\Theta}{dR^2} + \frac{\left[2R\tan\psi+t-2R_1(1-\cos\psi)\right]}{R\left[t-2R_1(1-\cos\psi)\right]}\frac{d\Theta}{dR} = \frac{2\Theta H}{K\left[t-2R_1(1-\cos\psi)\right]}$$

(3.22)

and the surface area of the fin is

$$A_f = 2\left[\pi^2 R_1 (R_o+R_1) - 2\pi R_1^2 + \pi(R_e^2 - (R_o+R_1)^2)\right]$$

When solving equation (3.22) using the same numerical technique as in Appendix (4), it was found that for this case, the numerical process was unstable. The reason for instability is not known but probably the numerical process itself may have been unsuitable for fins of such profile where the first portion of the fin is diverging where the instability appeared to occur. It was decided that locating the reason and curing it was to be left for future investgation where another numerical technique might be used. It was therefore decided that only the change in area at the root and the surface area was taken into account while treating the fin as a uniform thickness one from root to tip for evaluating the temperature gradient at the root.

This case of bad thermal contact was only considered theoretically since the main experimental work was later conducted with fins which were brazed on the tube and hence they had a large root contact area. However, experimental verification for the bad contact case was left for future work, although some data was presented by Singh[51], where crimped fins were used, which were wound round the tube, and their performance was found to be inferior to good contact fins.

For the present analysis, five cases were considered for each fin height. The radius R_1 was varied from 0.05mm. to 0.45mm. which means that the contact area changed by 70% to 10% of the straight fin area for each fin height considered.

Figures (3.11) and (3.12) show the variation of the efficiency and the effectiveness with the reduction in root area respectively. The efficiency in this case is the only affected parameter since it involves the root and surface areas of the fin, while the effectiveness only uses one area, that of the root.

Not much importance could be attached to the variation of the efficiency as the solution does not take into account the effect of the fin profile on the temperature gradient at the root.

In the design of finned tube heat exchangers in fluidized beds, the heat transfer process considered in isolation would not be sufficient for the overall optimisation of the system. Other important factors would have to be taken into consideration, e.g. the relative cost of the heat transfer surface, the bed containment cost, and the pumping power cost. However, the theory can be used as a guide in such design problems.

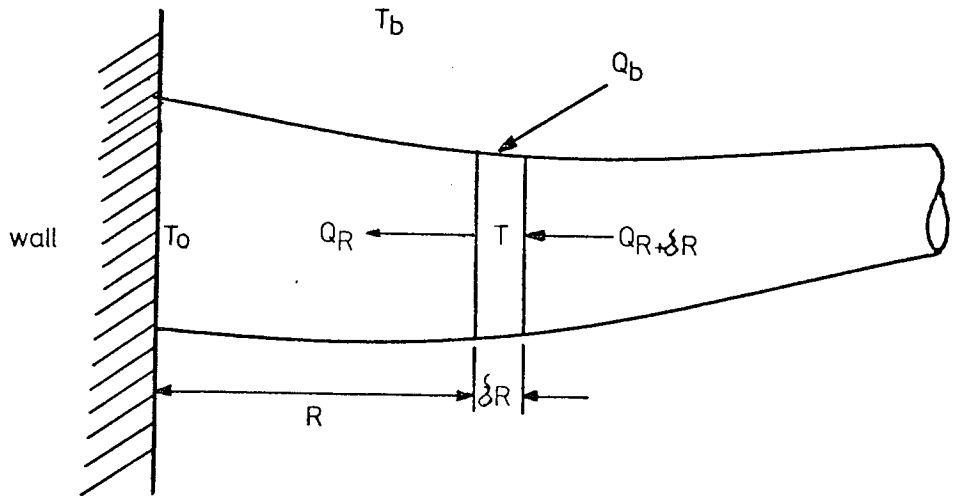

FIG.(3.1) GENERAL TYPE OF EXTENDED SURFACE

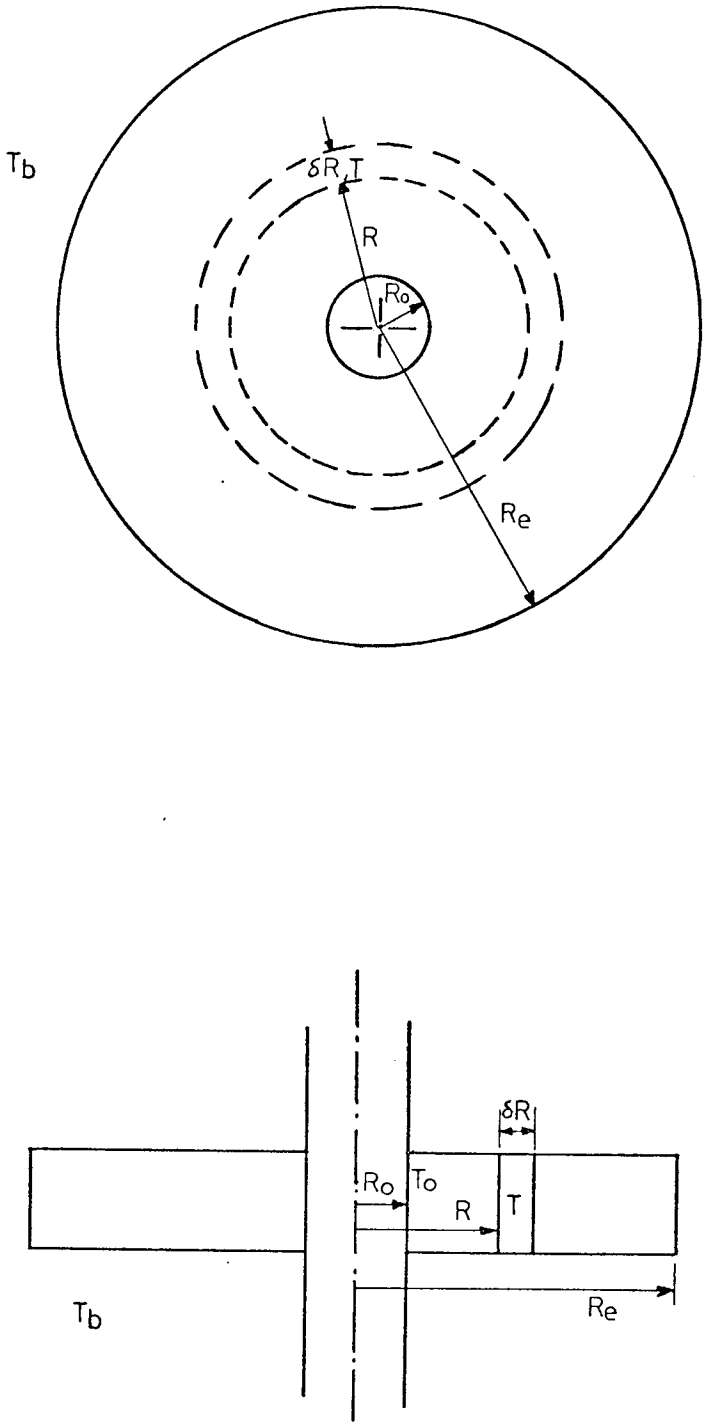

FIG.(3.2) SCHEMATIC DIAGRAM OF CIRCUMFERENTIAL FIN OF RECTANGULAR PROFILE

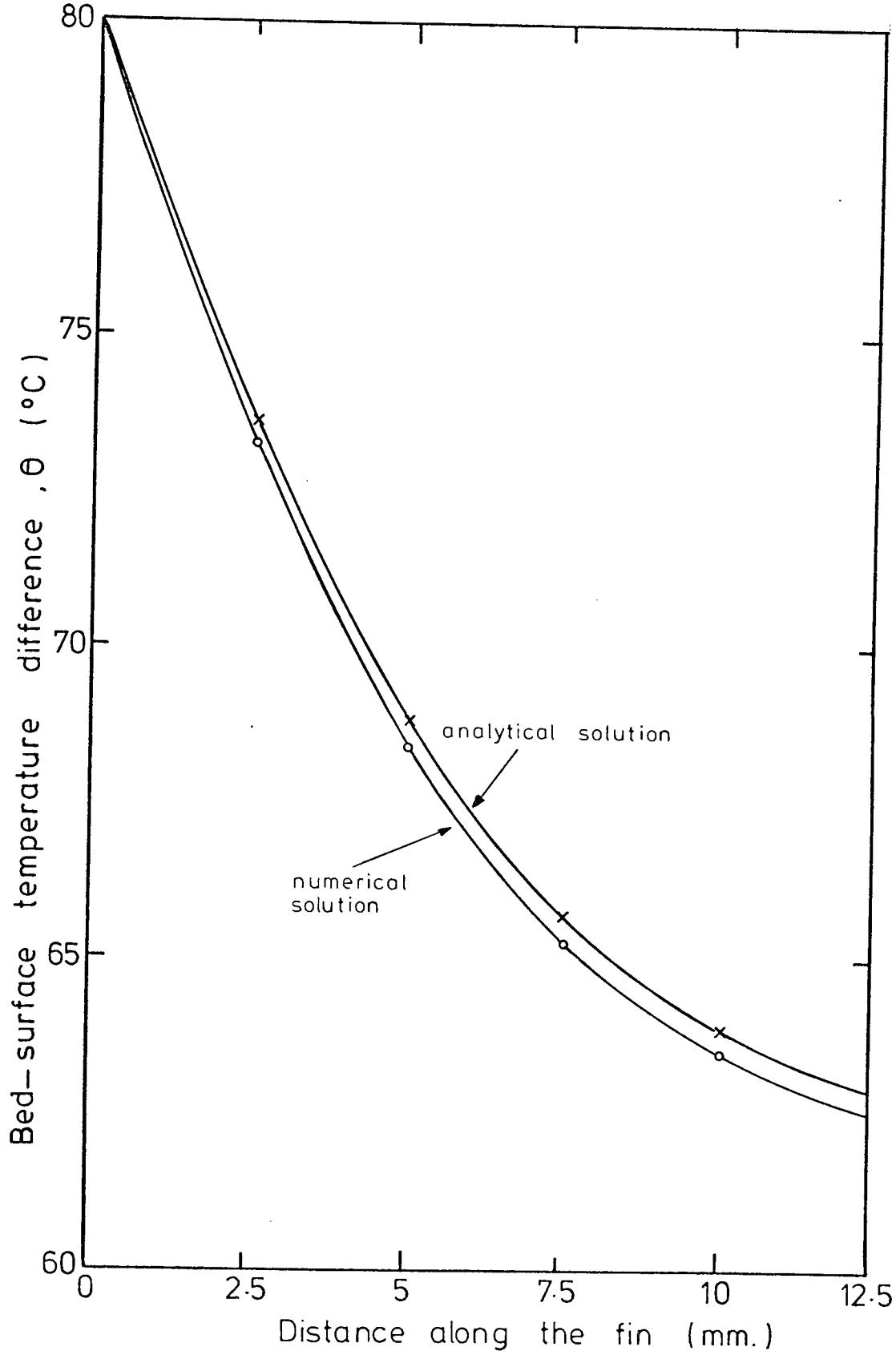

FIG. (3·3) TEMPERATURE DISTRIBUTION ALONG A CIRCUMFERENTIAL FIN OF RECTANGULAR PROFILE

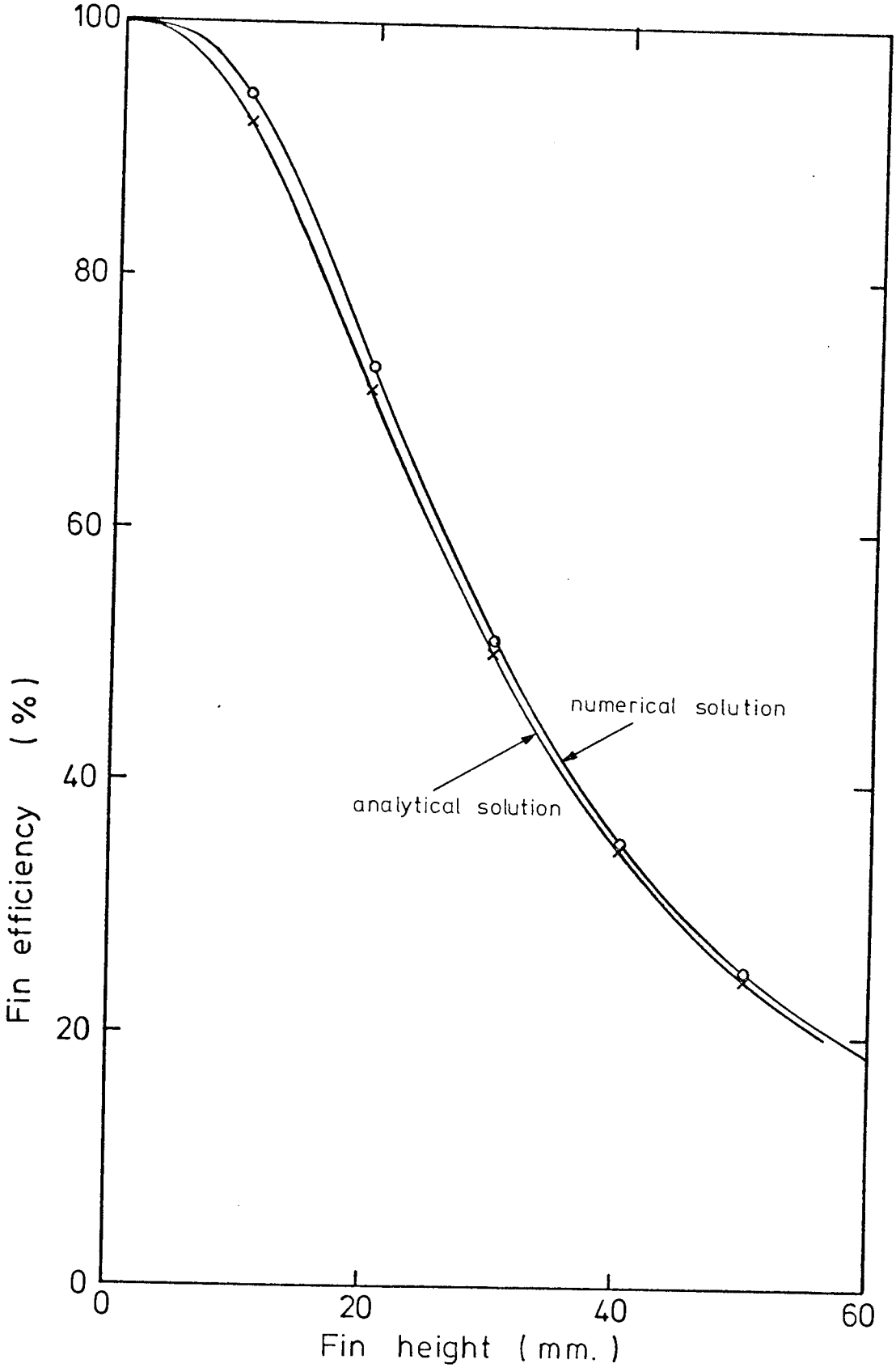

FIG.(3.4) VARIATION OF FIN EFFICIENCY WITH FIN HEIGHT.

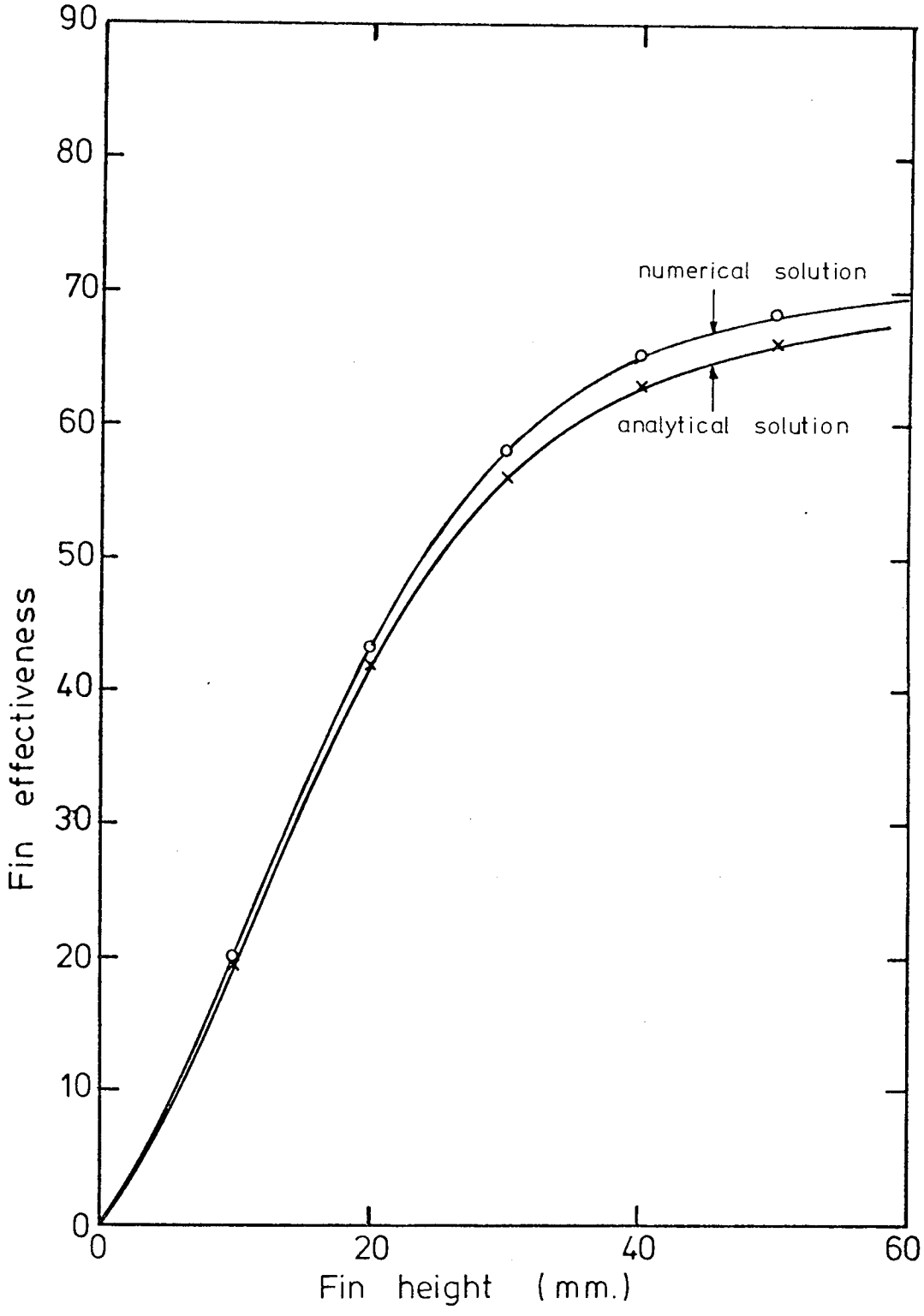

FIG.(3.5) VARIATION OF FIN EFFECTIVENESS WITH FIN HEIGHT

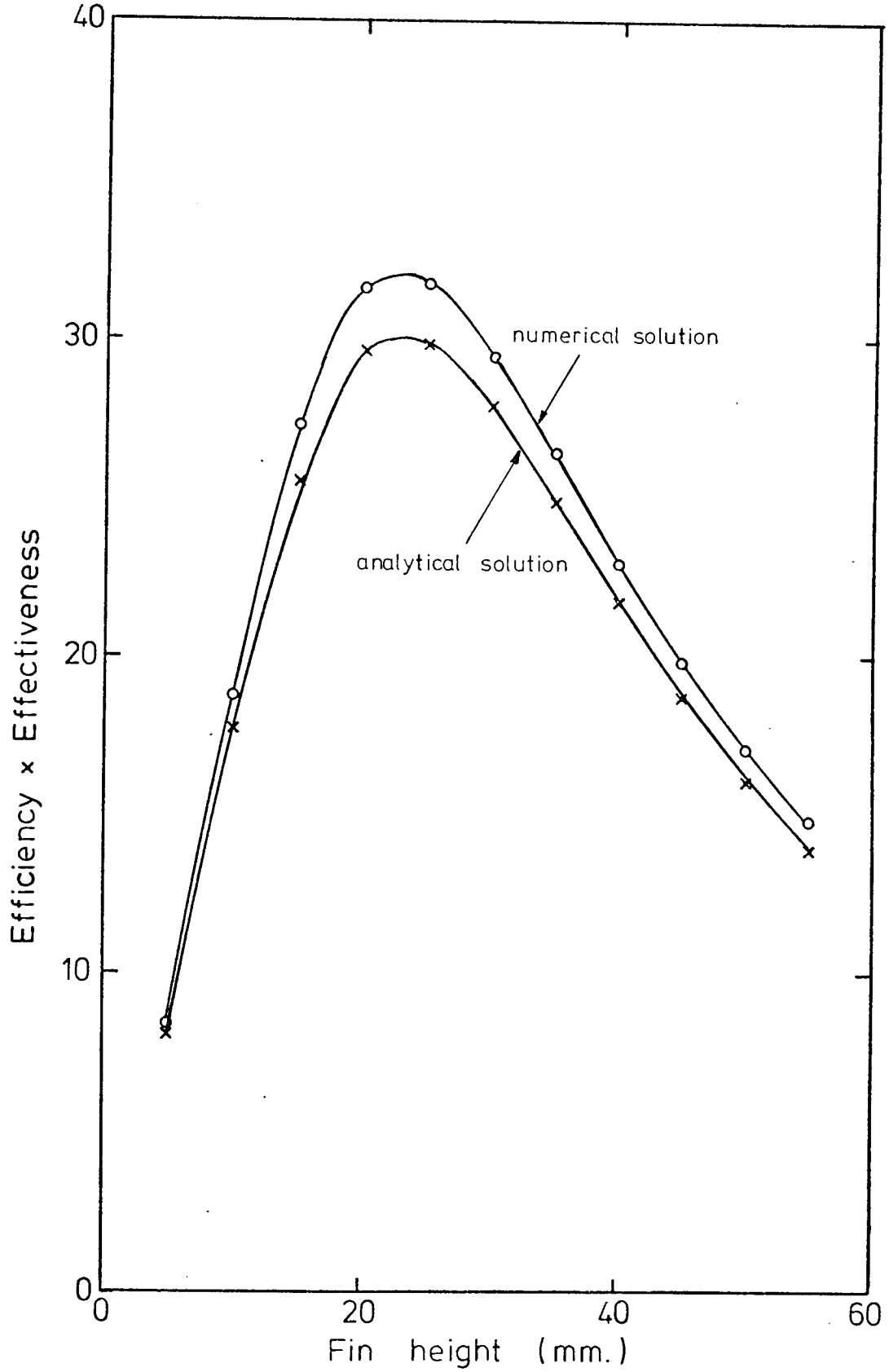

FIG.(3.6) VARIATION OF (EFFICIENCY x EFFECTIVENESS) WITH FIN HEIGHT

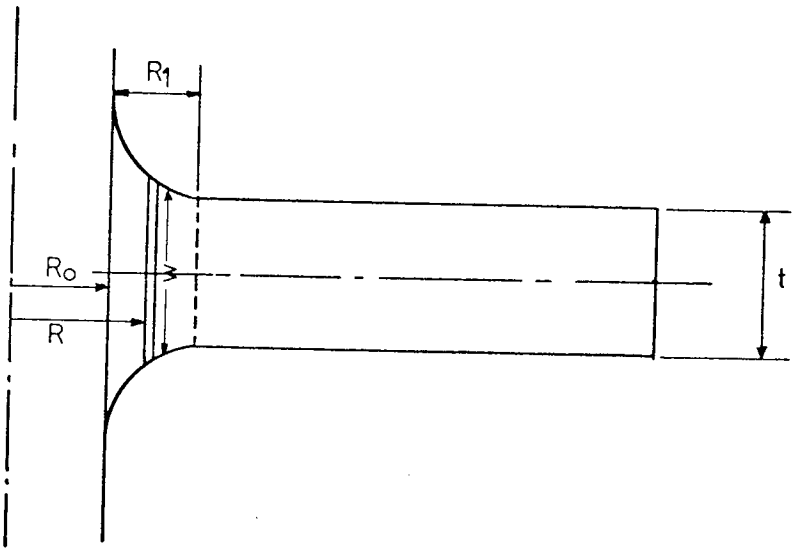

FIG.(3.7) FIN WITH LARGE CONTACT AREA

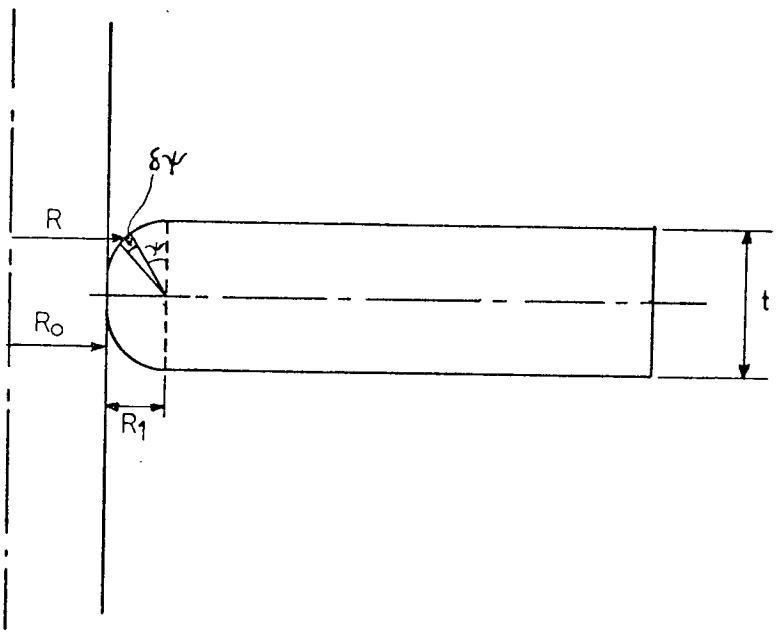

FIG.(3.8) FIN WITH SMALL CONTACT AREA

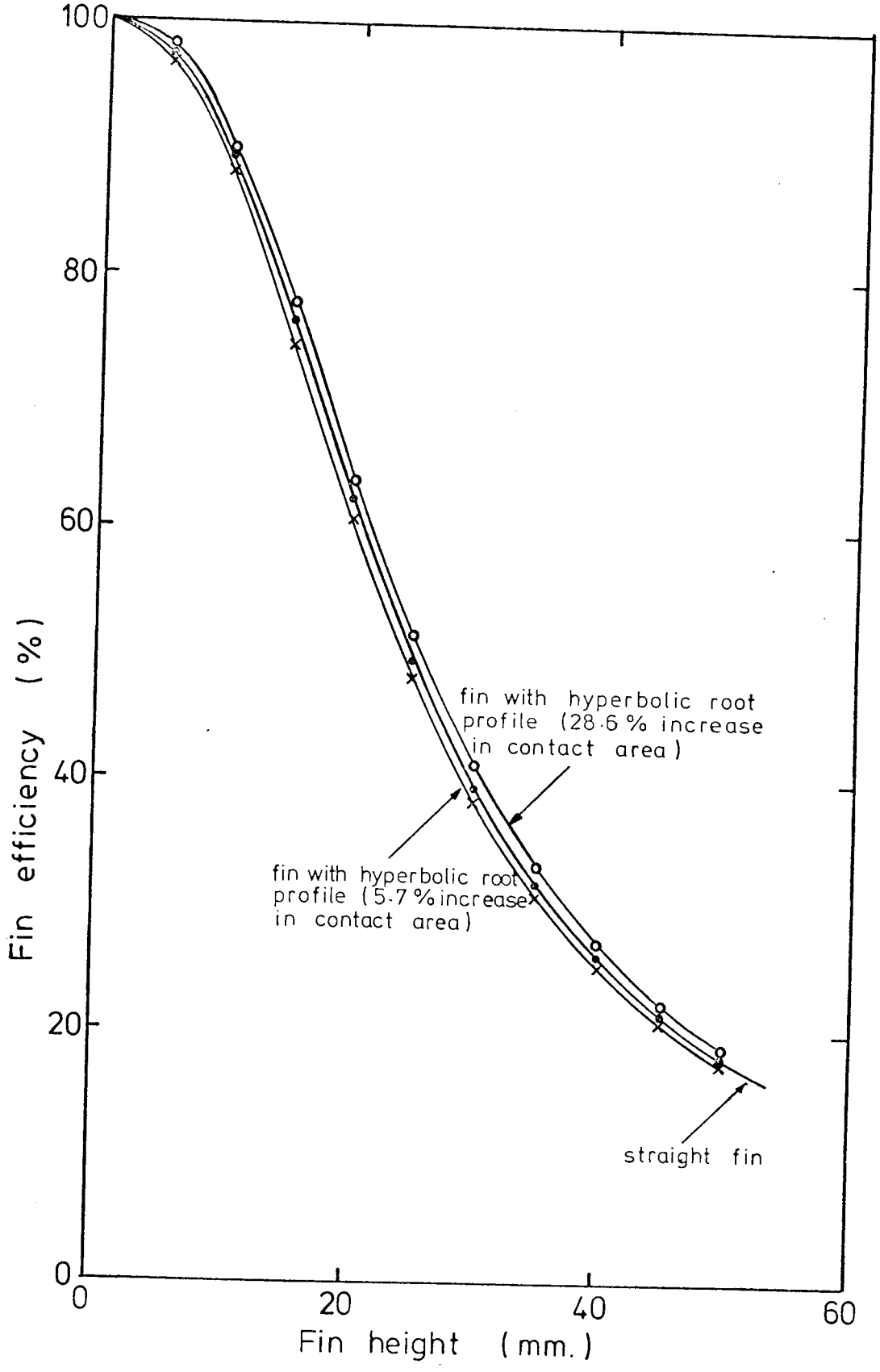

FIG.(3.9) EFFICIENCY OF FINS WITH LARGE CONTACT AREA

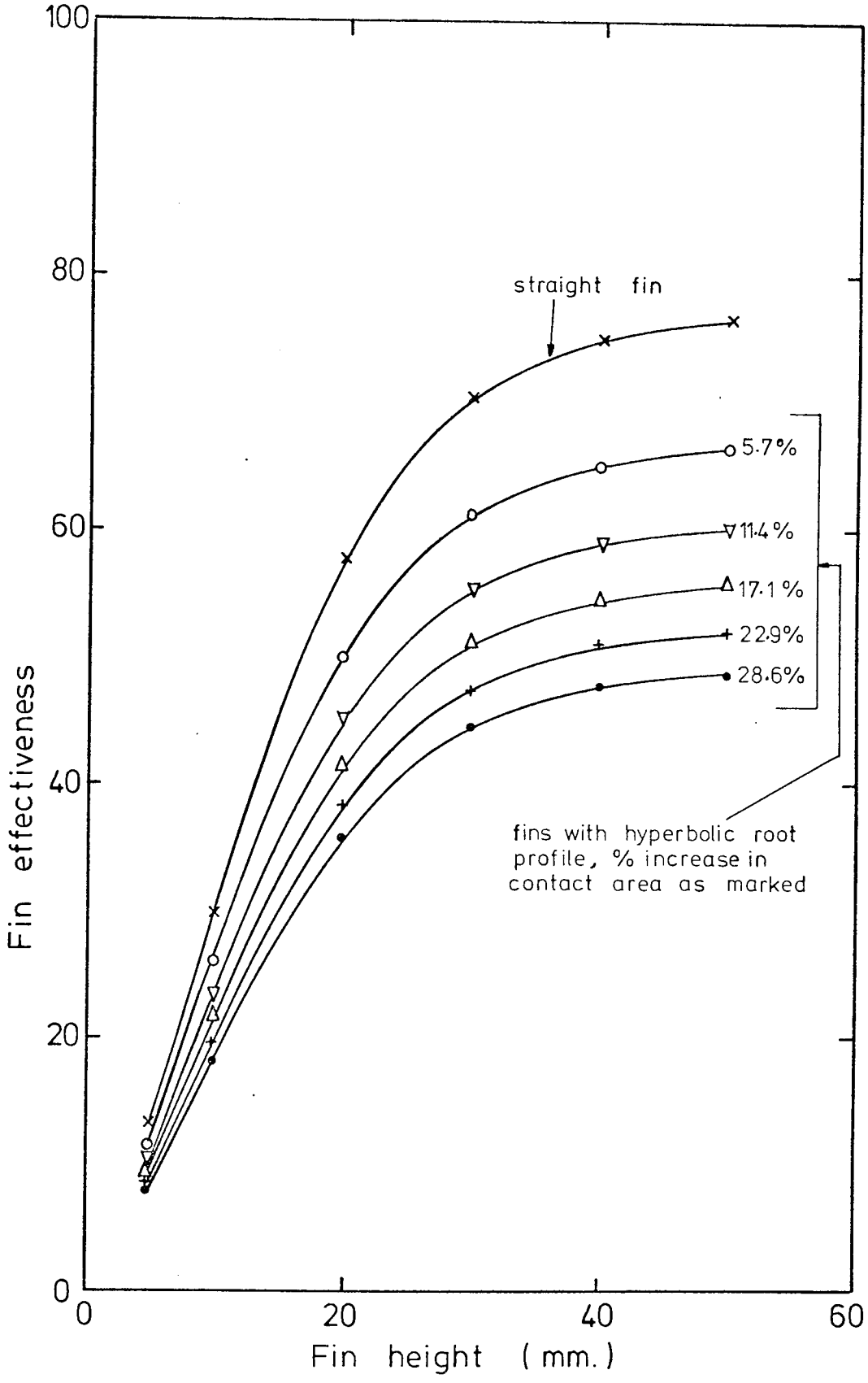

FIG. (3·10) EFFECTIVENESS OF FINS WITH LARGE CONTACT AREA

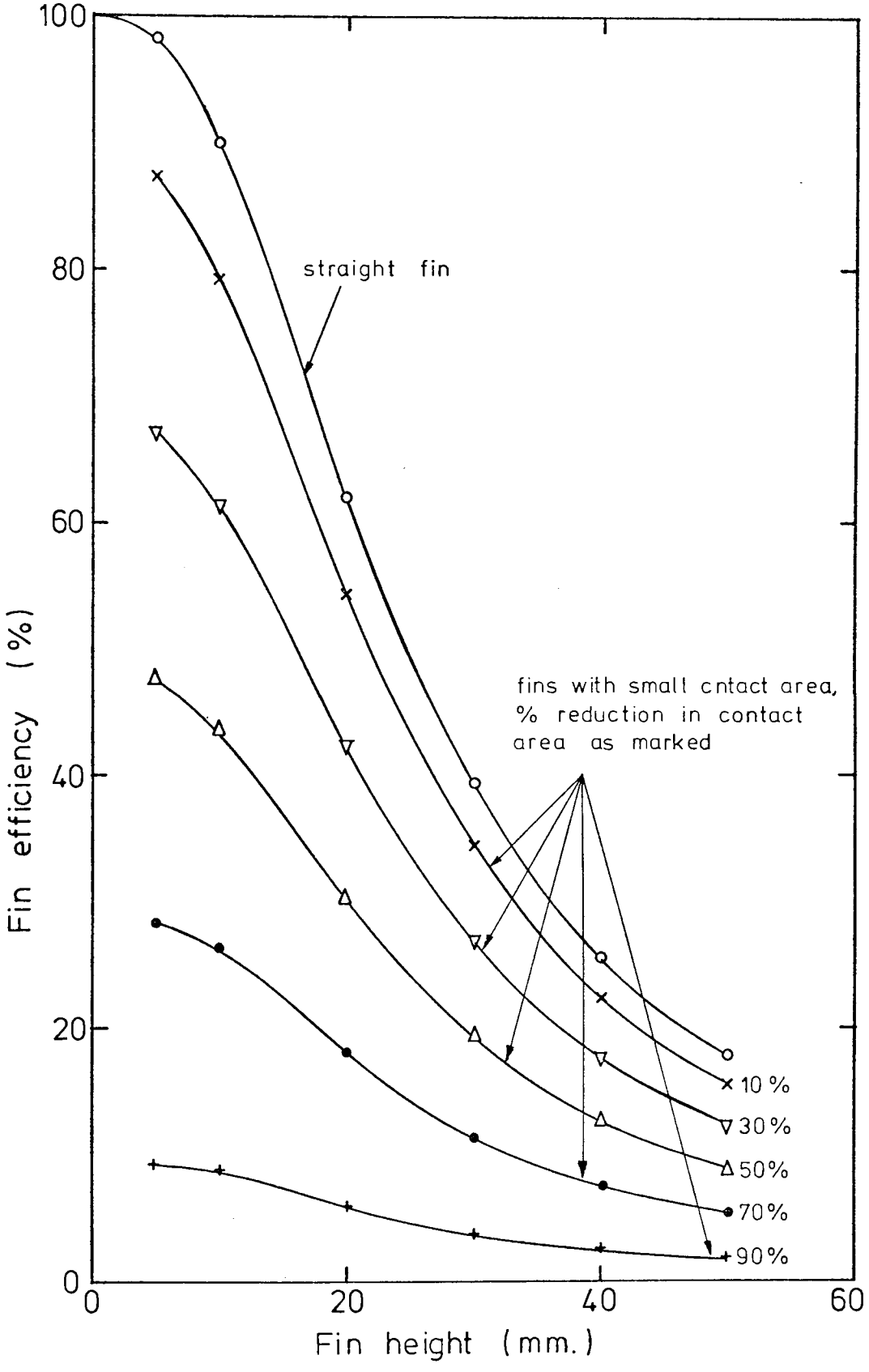

FIG.(3·11) EFFICIENCY OF FINS WITH SMALL CONTACT AREA

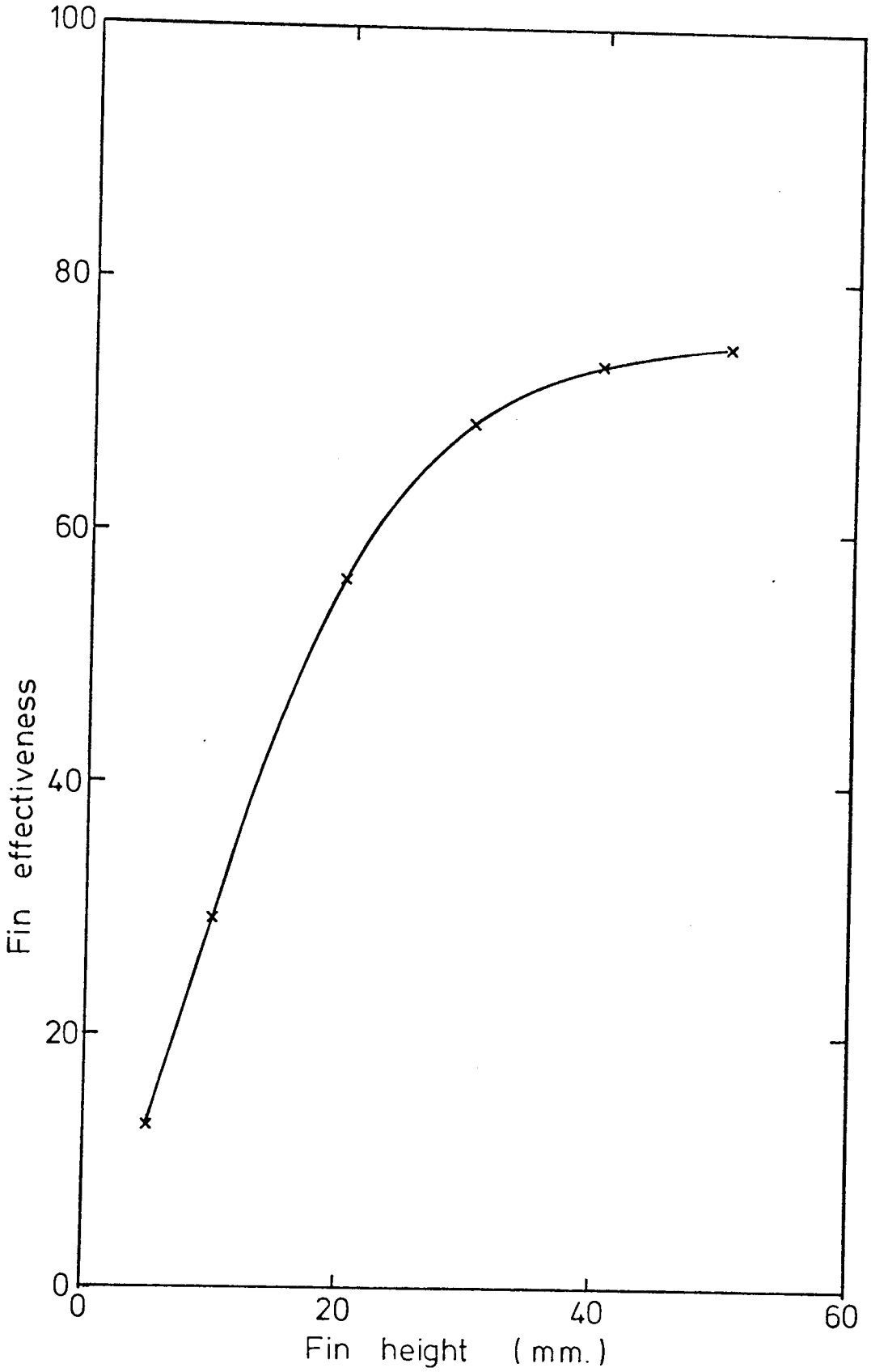

FIG.(3·12) EFFECTIVENESS OF FINS WITH SMALL CONTACT AREA

CHAPTER 4

EXPERIMENTAL EQUIPMENT

EXPERIMENTAL EQUIPMENT

4.1 The Main test rig

4.1.1 Introduction

The test rig described here was needed to carry out all the heat transfer experiments. It was initially designed to cater for relatively high heat rates which were expected with heat transfer elements of large surface area, i.e. finned tube exchangers with large number of fins. However, when the finned tube test elements were designed later, it was decided to make shorter elements having fewer fins, thus saving time, effort and material, while keeping within reasonable error limits the results to be obtained. Consequently, the rig was not used to its full capacity regarding heat transfer rates.

A general photograph of the essential parts of the test rig is presented in figure (4.1). Hot air was supplied from a fan through an electric heater to the bed which was maintained at a steady temperature by water cooled test elements (plain or finned tubes) which were immersed in it.

4.1.2 The bed and air distribution

The fluidized bed container was made with the dimensions 60 cm long x 15 cm wide x 30 cm high. Figure (4.2) shows an exploded view of the bed and the air distribution system, and a close-up view of the arrangement is shown in the photograph

in figure (4.3). The height of 30 cm later proved to be insufficient and perspex guard walls were erected on top of the bed to prevent losing a lot of material by elutriation when using fine solids or high fluidizing velocities.

The distributor plate used to diffuse the air uniformly through the bed was a pierced sheet of metal with all the holes inclined to the plane of the plate in one direction, namely along the length of the bed. The material is known as "conidur sheet". Trials were made with the plate assembled into the rig with the holes in two alternative configurations - where the holes directed the air longitudinally in two opposite directions. The uniformity of fluidization in the bed was unaffected by the configuration of the assembly.

The pressure drop characteristics of the distributor plate were investigated using the arrangement described in Appendix (5). In addition to using the probe described, which was to monitor the pressure above the plate, a pressure tapping was made in the wind box beneath the bed and connected to the other end of the inclined manometer so that a measure of the differential pressure across the distributor plate was obtained. Figure (4.4) shows the pressure drop across the distributor plate at different flow rates and at room temperature.

The arrangement of the air distribution system can be seen clearly in figure (4.2). The air was passed through a box to which a five-hole manifold section was

attached, which in turn was fixed to the wind box underneath the distributor plate. To obtain uniform fluidization, particularly at low air flow rates, a plate with 25mm. diameter holes punched in it was placed horizontally in the wind box directly above the openings of the manifold. Furthermore, the space between the punched plate and the distributor plate was packed with copper wool to increase the overall pressure drop of the air and obtain even more uniform fluidization.

4.1.3 Bed material

Two types of bed material were used - namely, silica sand and blown alumina. Each material was sieved using sieves calibrated to B.S.410. Three size ranges of the silica sand (100-200 μm, 200-300 μm and 300-400 μm) and one size range of the alumina (1000-1200 μm) were obtained. Two samples were then taken from the first sand size range (from two different sources) for the bare tube and finned tube experiments. Only one sample was used from each of the other three size ranges (two sand and one alumina) for the two sets of experiments.

Two important properties of the materials were required, namely size and density. The size was determined by carrying out a sieve analysis on a quantity from each sample prepared. The results are presented in Appendix (6) where the concept of a mean particle diameter is also discussed. The density of the materials was measured using a standard specific gravity bottle. An account of the method and the results are given in Appendix (6).

4.1.4 The air circuit

A schematic diagram of the air circuit is shown in figure (4.5). The air was supplied from a $1\frac{1}{4}$ horse power, 440 volts, three-phase fan unit supplied by "Sekomak Air Products". The fan was capable of supplying 5000 litres/minute of air measured at 15°C and atmospheric pressure with a maximum pressure head of about 70 cm. water gauge. The air flow rate was metred using an orifice plate of 50.34 mm. diameter with corner pressure tappings. A 3 m length of pipe of 76.2 mm. inside diameter was used between the fan and the orifice plate due to the need for fully developed flow of the air at the orifice. The length of the pipe was equivalent to 40 times its diameter as specified by the British standards. The pressure tappings were connected to an inclined manometer to measure the pressure drop across the orifice from which the flow rate was then calculated. The orifice was checked against the largest capacity rotameter available in the laboratory which was of maximum capacity 3500 litres/minute. The calibration curve which was then extrapolated to cover the whole operating range of the fan, is shown in figure (4.6).

4.1.5 The water circuits

A schematic diagram showing the arrangement of the water circuits used is given in figure (4.7). The loop ABCD is a closed mains water circuit supplying the test

element. The water was pumped round by a three-phase, $\frac{3}{4}$horse power pump. The flow rate was controlled by the valve Vm after the pump and was measured by rotameter Rm. Two thermometers were inserted at points B and C to measure the water temperatures before and after the test element.

To stabilize the temperatures of the water in the main circuit an open circuit was incorporated in the system. The supply came from the mains through a constant head tank. It was fed into the main circuit at point A before the pump so that good mixing takes place within the pump before it goes through to the test element and it is taken out of the main circuit at point D. The amount of the stabilizing water was controlled by the valve Vs on the outlet side and is measured by rotameter Rs. Two themometers, of range 0-100^{o}C and accurate to 1^{o}C, were inserted on the open circuit just before the water entry into the main circuit and just after its exit to record the water temperatures. These temperatures, together with the flow rate given by rotameter Rs served as a check on the heat flux that was being transferred from the fluidized bed to the water through the test element.

4.2 Instrumentation

4.2.1 Water flow measurement

The water flow rates in both the main and stabilizing circuits were measured by rotameters supplied by "GEC ELLIOTT Process Instruments Limited". The one used in the

main water circuit (Rm) was capable of metering 20 litres/minute while the second one on the stabilizing circuit had a maximum capacity of 10 litres/minute. They were both made of a tapered glass tube with the scale marked in centimetres and using a stainless steel float. The calibration curves of both rotameters Rm and Rs were supplied by the manufacturers and are presented in figures 4.8 and 4.9 respectively.

4.2.2 Temperature measurement

The measurement of water temperatures before and after the test element which gave the temperature rise of the water passing through the heat transfer section immersed in the bed was made by using two very sensitive and accurate thermometers. They were graduated to read down to $0.05^{o}C$ and each had a maximum error of $0.03^{o}C$ with an operating range of $0-25^{o}C$. These thermometers were calibrated and certified by the N.P.L. and hence no further calibration was carried out. Thermocouples, of the chromel-alumel type were used to record the bed temperature. Four thermocouples were made in the laboratory and were positioned in the bed such that they were free to move within the bed as outlined in figure 4.10. This arrangement was made because a temperature gradient was observed along the bed, and although it was small ($8^{o}C$ per metre), it was decided to use the log-mean temperature difference between the bed and the water in computing the overall heat transfer coefficient.

The thermocouples were connected through a multiswitch box to a "solartron 2000" digital voltmeter of accuracy 0.01% and range 0-10mV. The common cold junction from the switch box was passed through a reference junction cell supplied by "Delristor", which had an oil bath kept at $0^{o}C$, using a special probe provided.

Figure (4.11) shows a photograph of the instruments used and mentioned above together with a twin channel temperature pen recorder which was used to record temperature traces of a spherical heat transfer probe, which when plunged in the bed, served as another method of measuring heat transfer coefficient in a fluidized bed for comparison with the tube data.

4.3 Test rig for voidage measurement

The test rig used for voidage measurement was made of transparent perspex sheet. An exploded view of the rig is shown in figure (4.12). It is basically a fluidized bed column having a 2" square cross-section and 12" height. The air supply used was the main line of the laboratory which was fed through a control valve to an air box beneath the bed. The distributor plate used which was fixed between the air box and the bed was a porous plastic sheet having a fairly high pressure drop characteristic. The height of the fluidized bed was observed visually and was measured by a flexible scale attached to one side of the column.

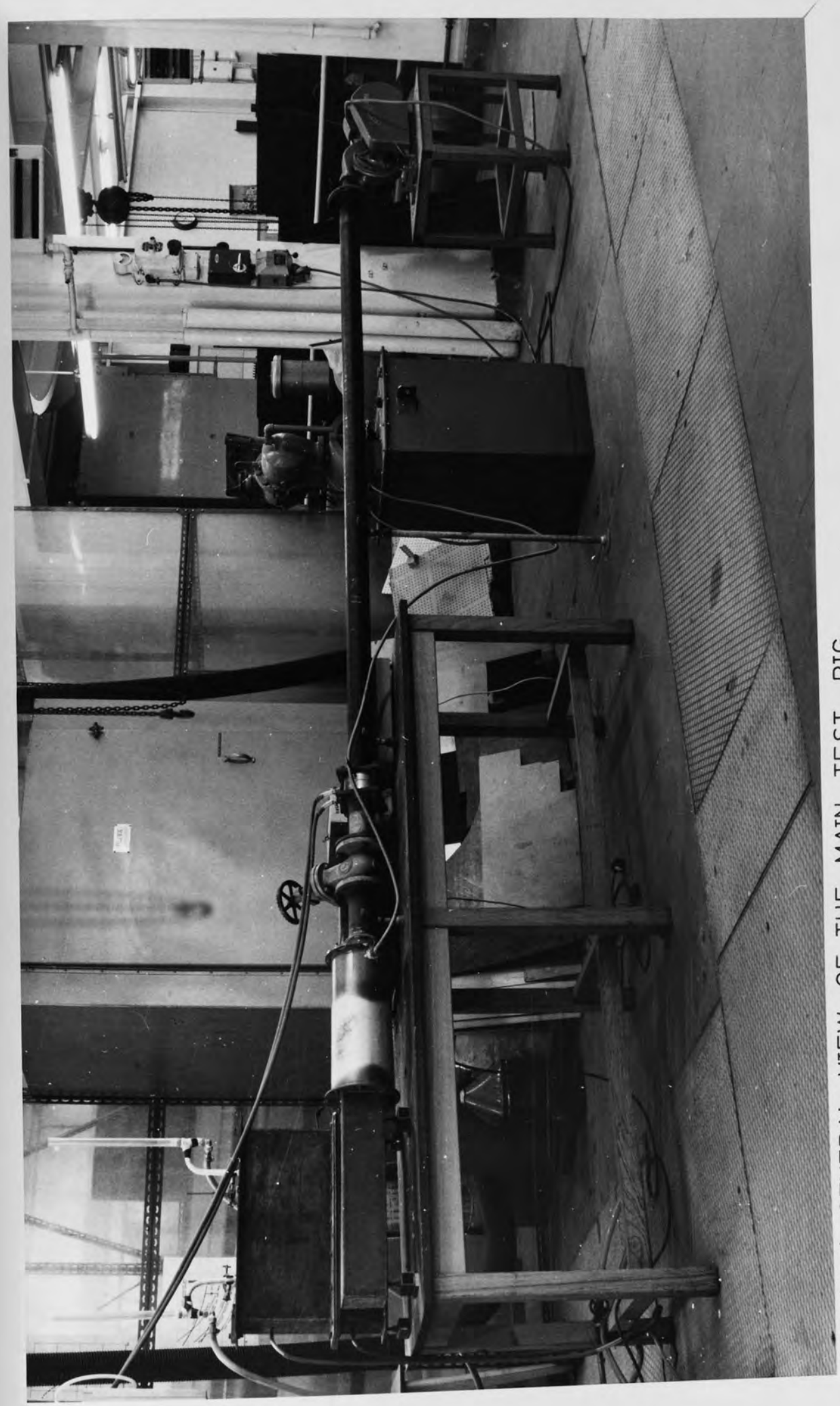

FIG. (4.1) GENERAL VIEW OF THE MAIN TEST RIG

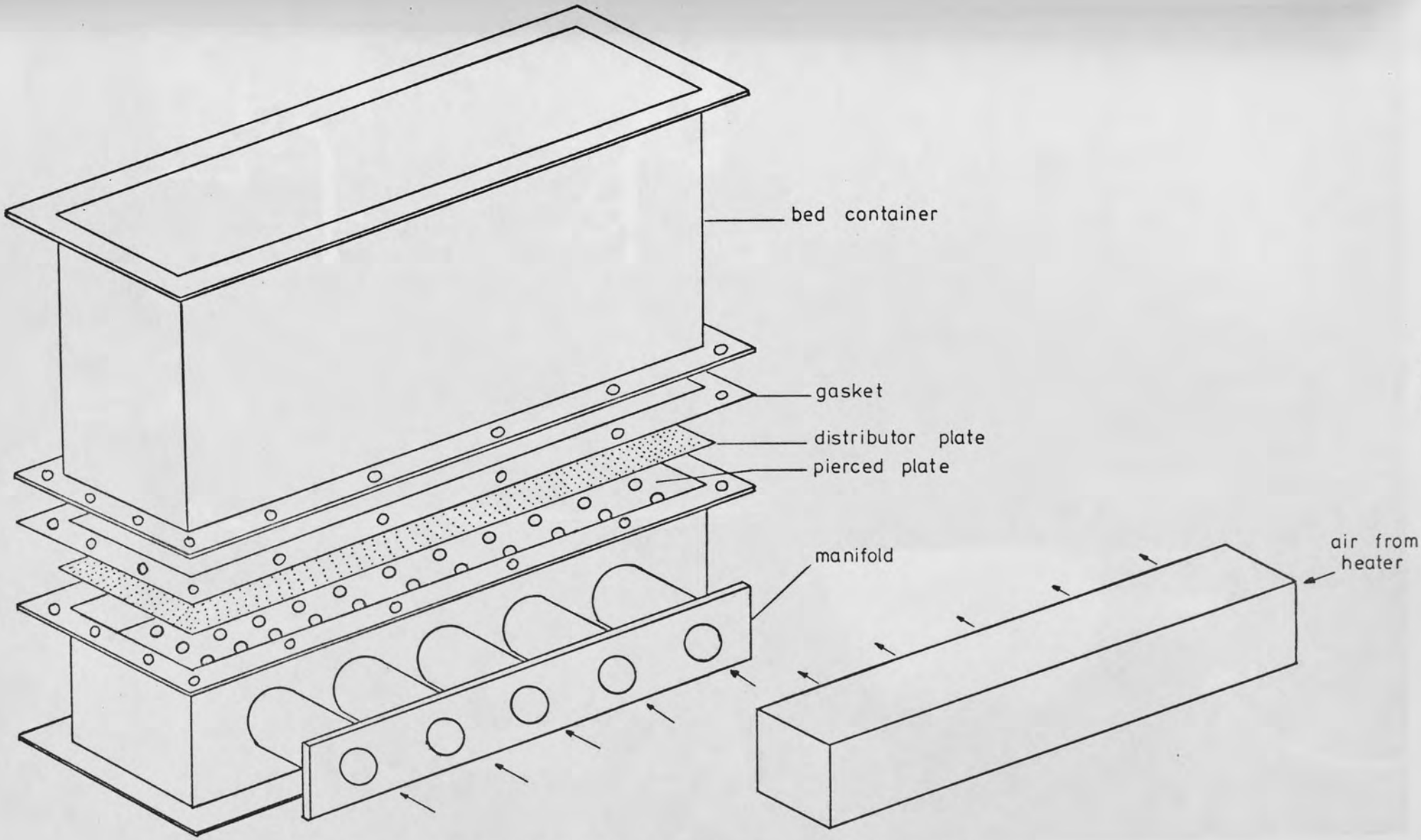

FIG. (4.2) EXPLODED VIEW OF MAIN BED

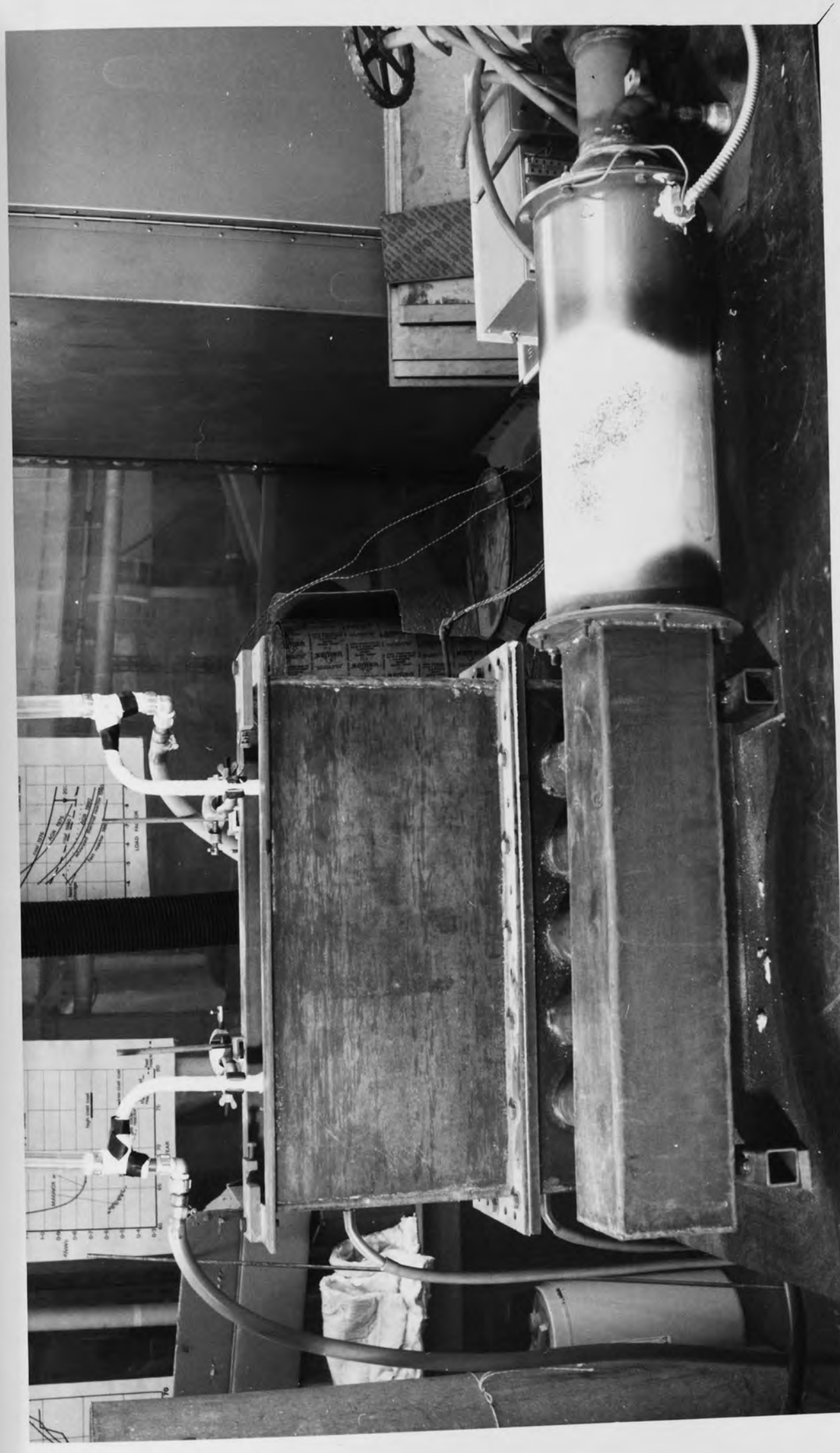

FIG. (4.3) CLOSE-UP VIEW OF THE BED

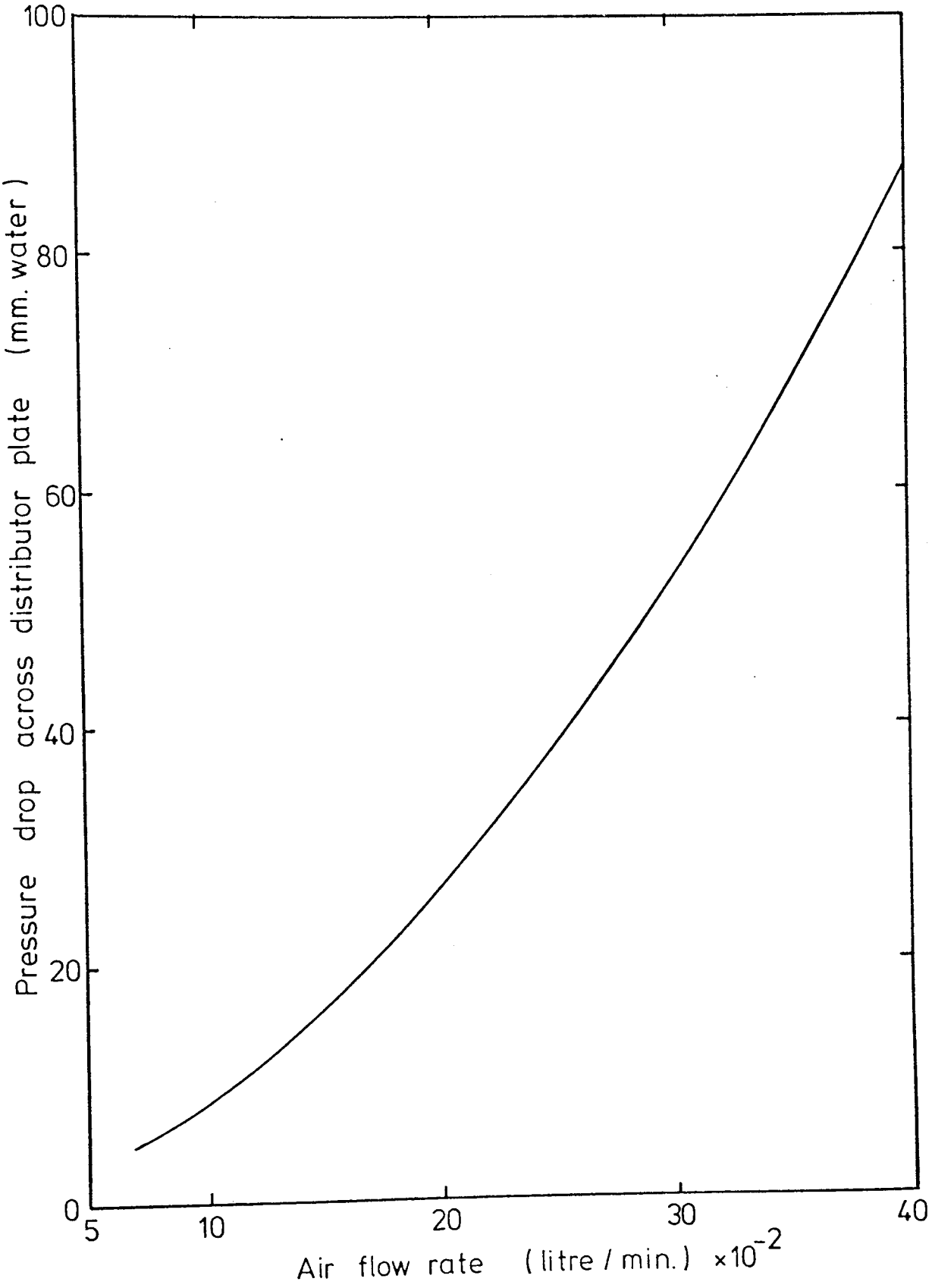

FIG.(4.4) PRESSURE DROP CHARACTERISTICS OF DISTRIBUTOR PLATE

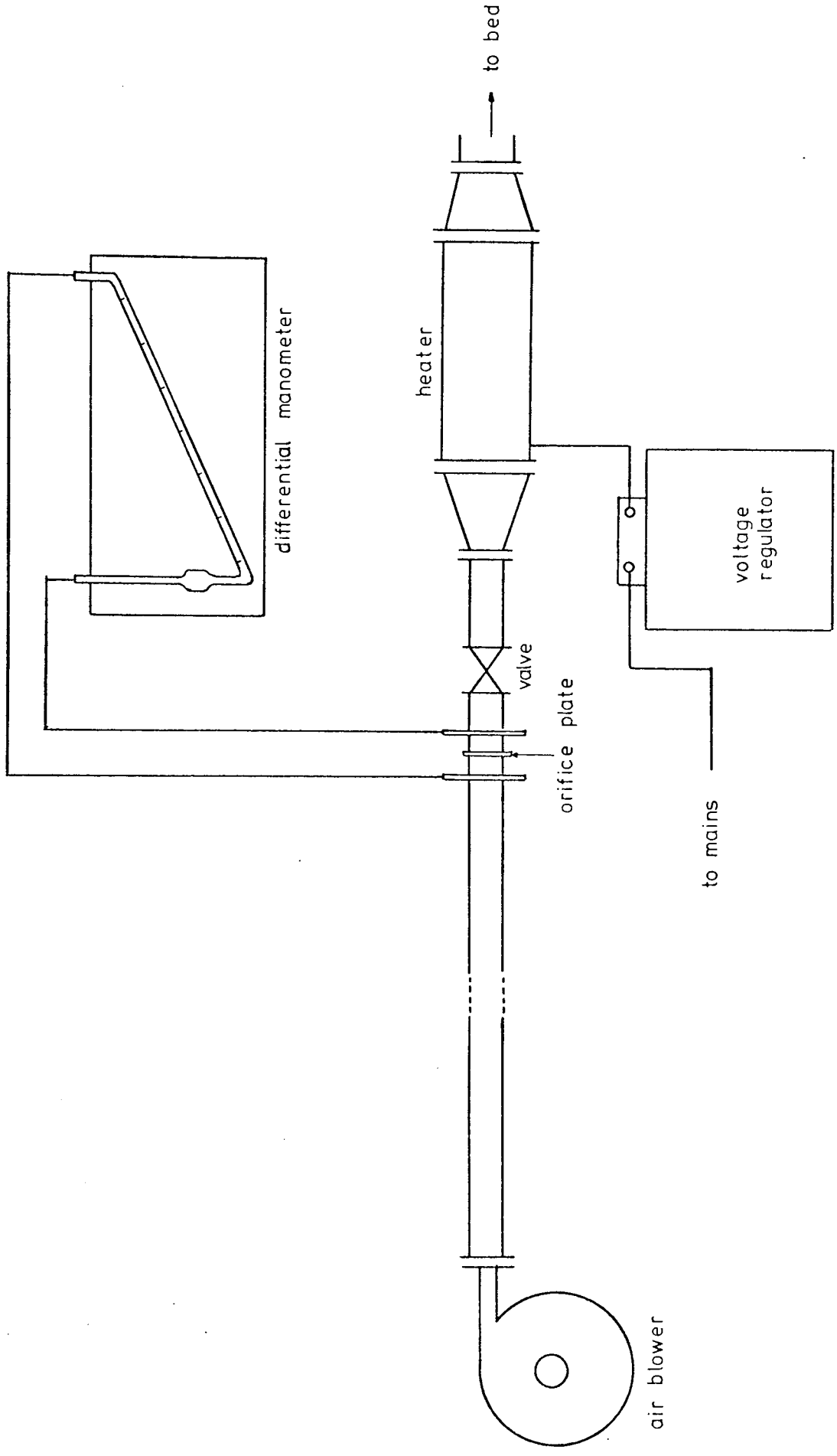

FIG. (4.5) SCHEMATIC DIAGRAM OF THE AIR CIRCUIT

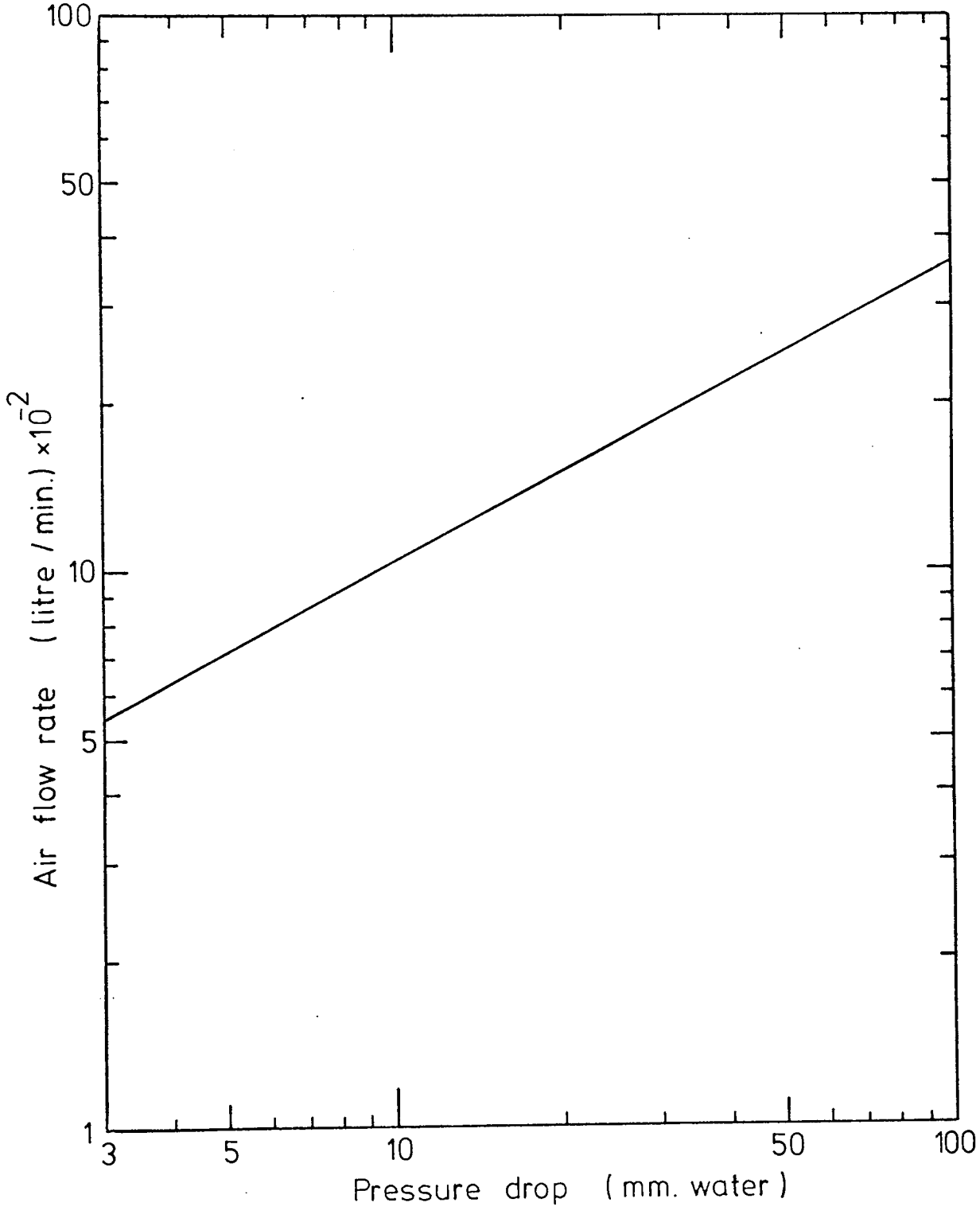

FIG. (4.6) CALIBRATION OF THE ORIFICE PLATE

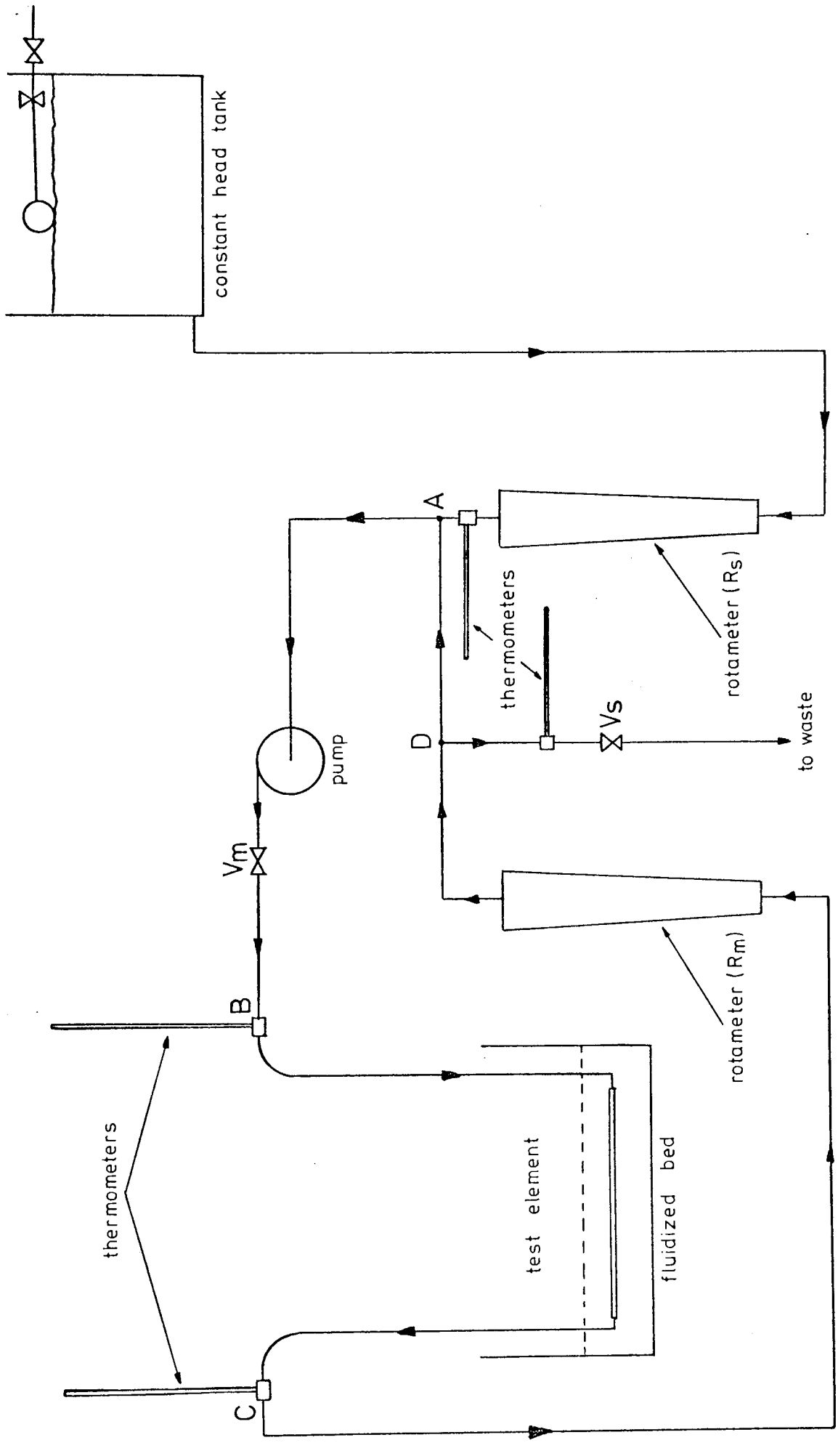

FIG. (4.7) SCHEMATIC DIAGRAM OF THE WATER CIRCUITS

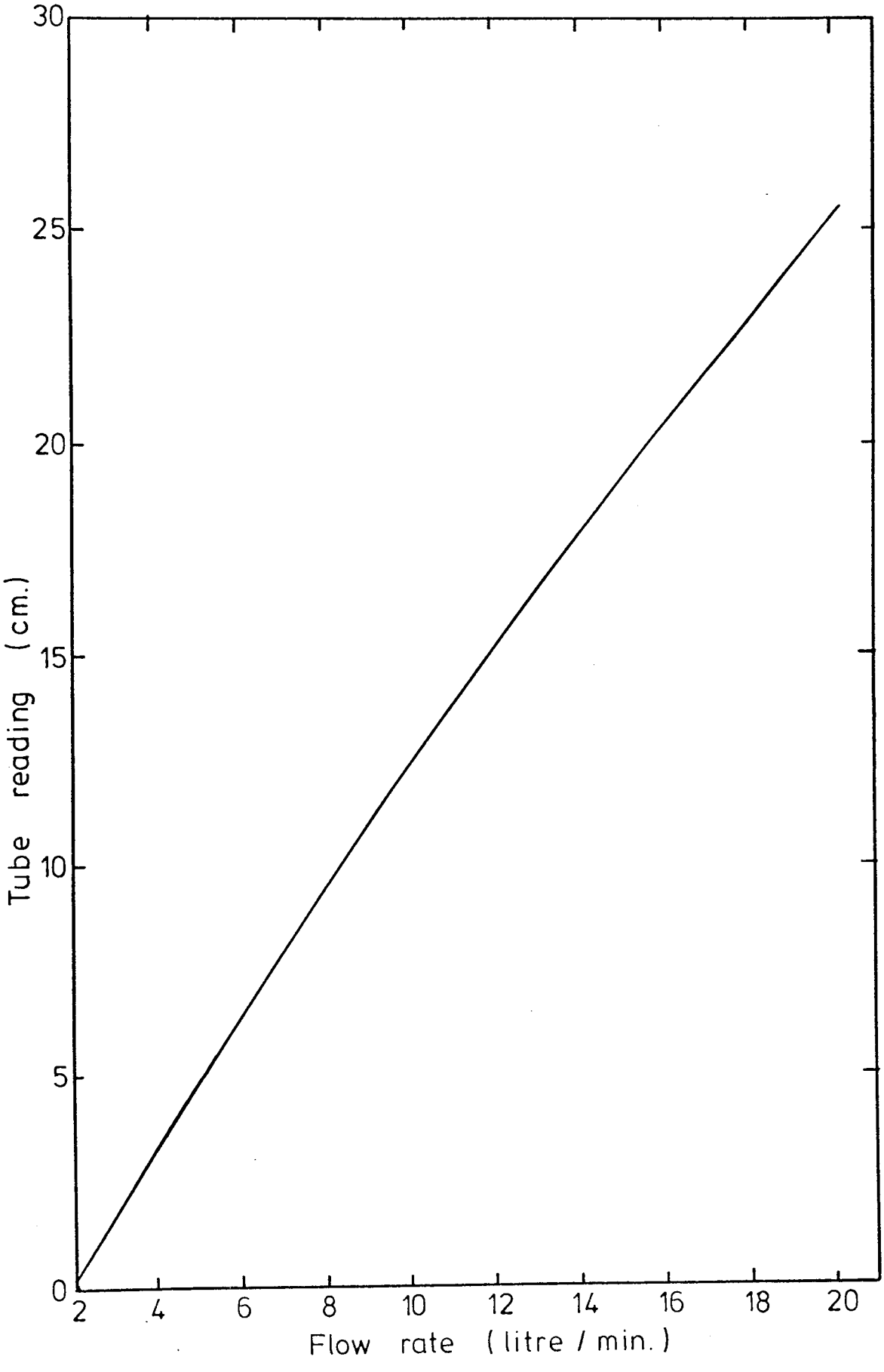

FIG.(4.8) CALIBRATION CURVE FOR ROTAMETER (R_m)

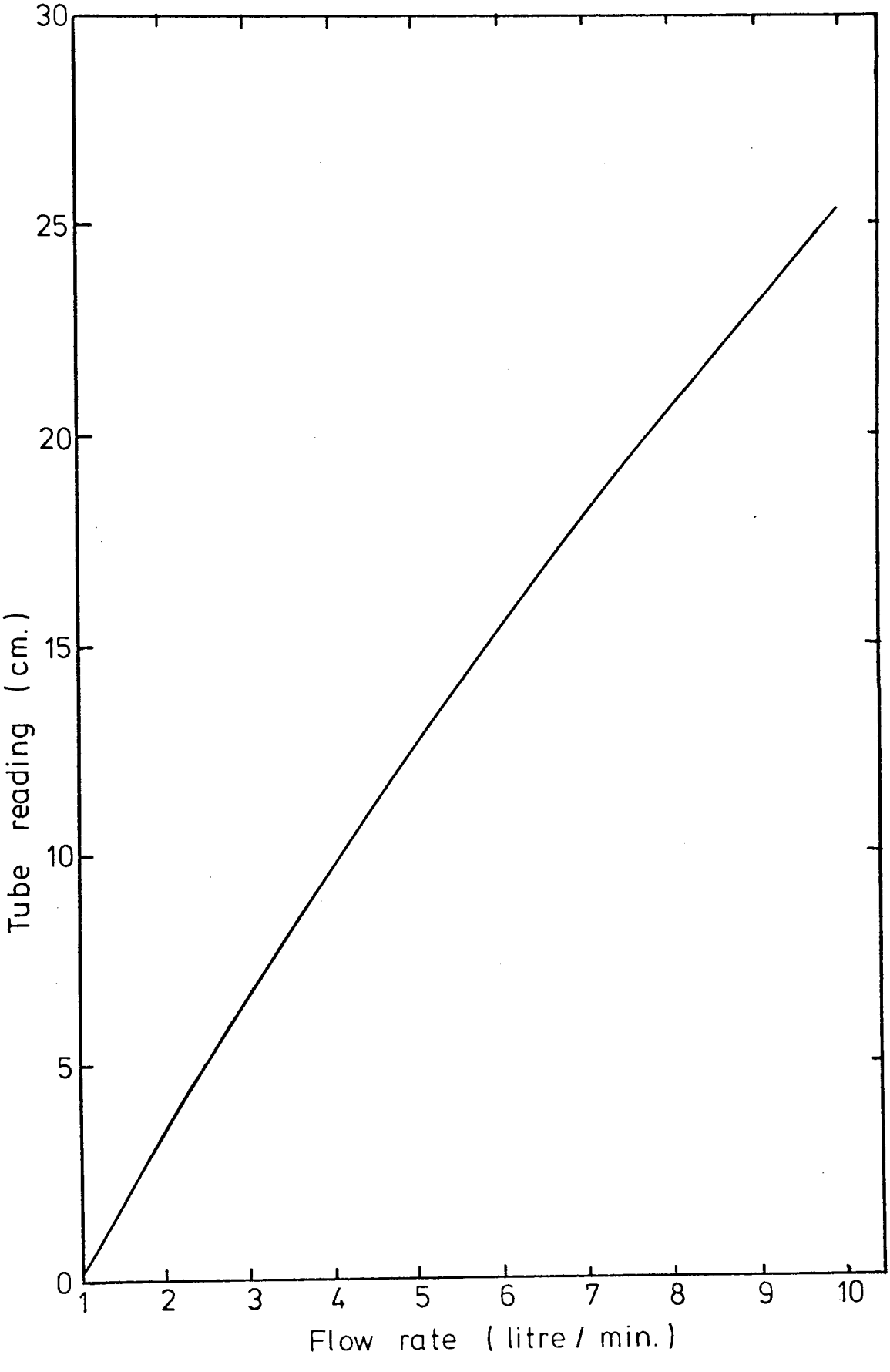

FIG. (4.9) CALIBRATION CURVE FOR ROTAMETER (R_S)

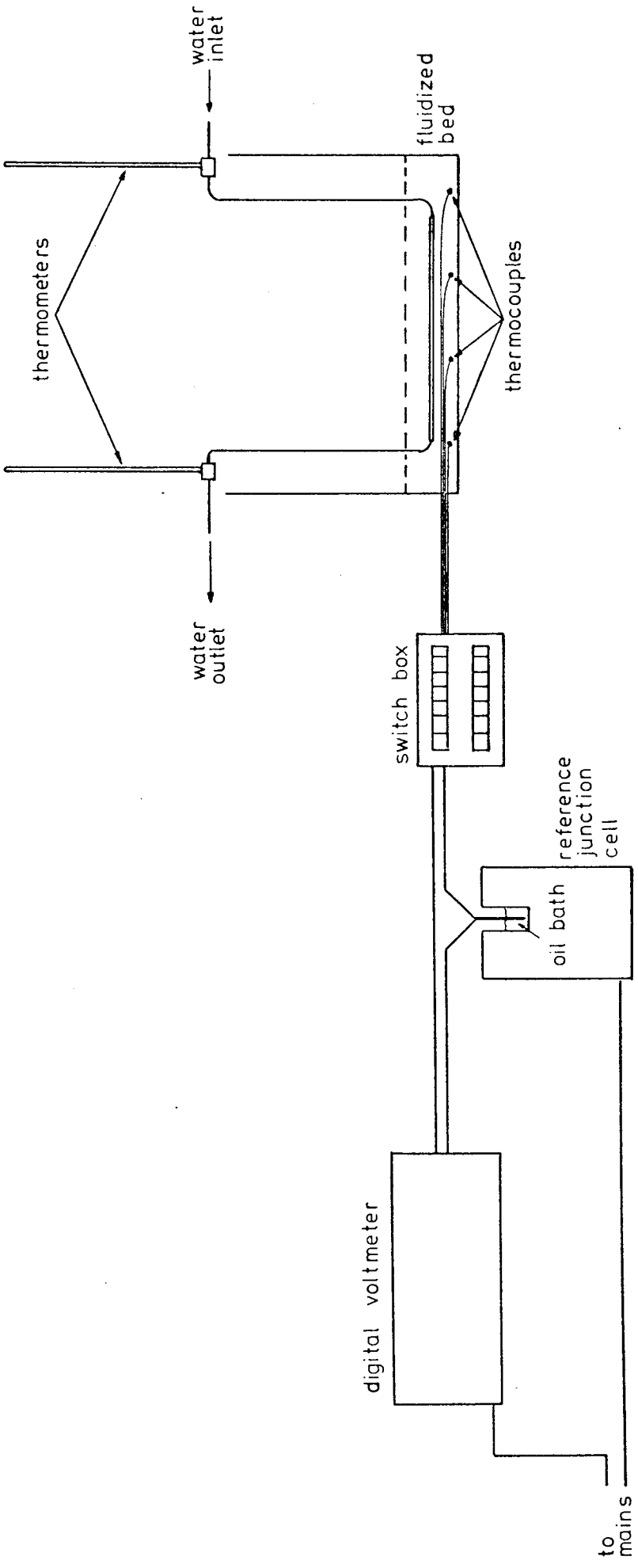

FIG. (4.10) INSTRUMENTATION FOR TEMPERATURE MEASUREMENT

FIG. (4·11) INSTRUMENTATION FOR TEMPERATURE MEASUREMENT

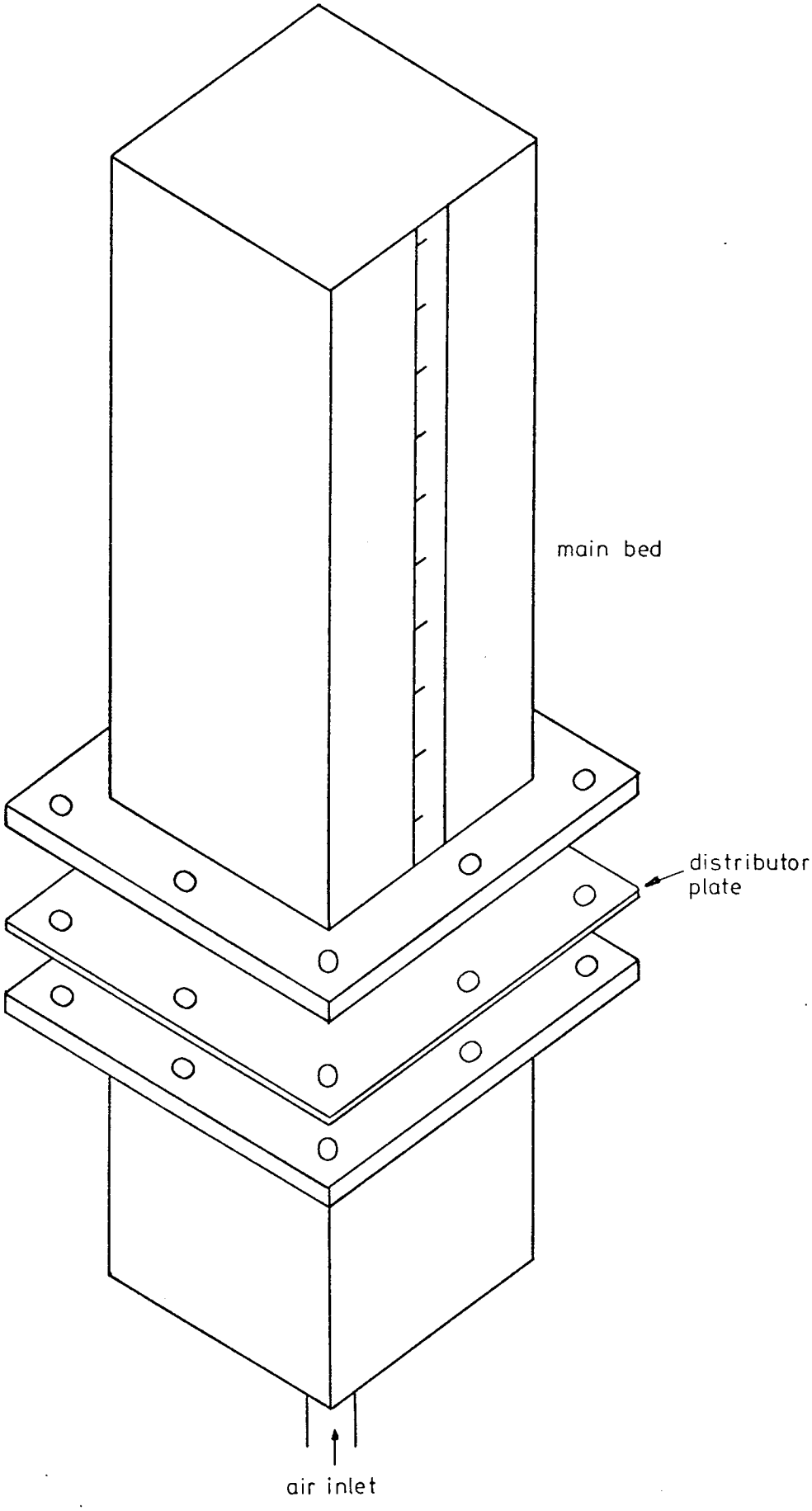

FIG. (4.12) EXPLODED VIEW OF THE RIG USED FOR VOIDAGE MEASUREMENT

CHAPTER 5

PLAIN TUBE WORK

PLAIN TUBE WORK

5.1 Introduction

It was mentioned in Chapter 2 that very little data existed at the time of starting this work on heat transfer in shallow fluidized beds. It was also noted that the data available in the literature gives the impression that the bed geometry has some effect on the heat transfer performance of the bed.

To study the performance of extended surfaces, it is desirable that data on bare tubes be known so that a clear idea could be obtained about the advantage of using extended surfaces as heat exchangers. Knowledge of heat transfer characteristics of bare tubes also helps to indicate, to some extent, effects that take place when fins are added on to a tube. In particular the part played by particle motion, mixing and the interaction between the fin arrangement and the fluidized bed.

It was therefore decided to study the performance of a single horizontal bare tube to establish the basic data against which performance a finned tubing could be compared.

5.2 Experimental technique used

The technique used was to calculate the bed-surface heat transfer coefficient from the experimentally determined overall heat transfer coefficient (bed-water) and an estimate of the heat transfer coefficient at the inner surface of the tube. The latter estimate was made using the relationship

$$Nu = f(Re, Pr)$$

The overall coefficient (Hov.) was evaluated from the measurement of :-

1. water flow rate (W)
2. Water inlet and outlet temperatures (Twi and Two respectively)
3. Bed temperatures (Tb_1, Tb_2, Tb_3 and Tb_4) *

and hence (Hov) was computed using the expression

$$Hov. = \frac{W.Cw.\ (Tw_o - Tw_i)}{\pi\ D_t\ L_t x \text{ Temperature difference}} \qquad (5.1)$$

where Cw is the specific heat of water.

It was found while measuring bed temperature that a temperature gradient exists along the bed in a direction opposite to the flow of water inside the tube. It was, therefore, decided that a log-mean temperature difference should be used for evaluating the overall heat transfer coefficient. This L.M.T.D. was obtained by using the expression

$$LMTD = \frac{(Tb_1 - Tw_o) - (Tb_4 - Tw_i)}{\ln\left|\frac{(Tb_1 - Tw_o)}{(Tb_4 - Tw_i)}\right|} \qquad (5.2)$$

It was thought originally that the heat transfer coefficient between the water and the inside of the tube could be computed from the famous Dittus-Boelter equation[53]

---

* Suffixes 1,2,3 and 4 for the bed temperatures start from the end where the water is flowing out.

$$Nu = 0.023\ Re^{0.8}\ Pr^{0.4} \qquad (5.3)$$

But if the conditions for applying this expression are to be met, the flow has to be very high (Re> 10000), which means that the rise in the water temperature would be very small, unless the heat flow is very large, leading to serious errors in $(Tw_o - Tw_i)$ in equation (5.1). It was therefore decided to work with a low flow rate (R≈8700) and to obtain a separate correlation for the present working system to allow the inside heat transfer coefficient to be obtained. This is explained in detail in the next section.

When the inside and overall coefficients are known, the bed-surface heat transfer coefficient (H_{BM}) is computed by using the relationship

$$\frac{1}{Hov} = \frac{1}{Hi} + \frac{1}{H_{BM}} \qquad (5.4)$$

It may be noted here that in expression (5.4) the resistance to the heat flow of the tube wall is neglected for the reason that the wall thickness is very small and the thermal conductivity of the tube material is very high so that the resistance itself (thickness/conductivity) is small compared to the film resistances on the inside and the outside of the tube ($1/H_i$ and $1/H_{BM}$ respectively).

5.3 Evaluation of the tube inside heat transfer coefficient

As can be seen from standard works on turbulent heat transfer to and from fluids flowing inside tubes [53,54].

the empirical expressions are of the form

$$Nu = B_1 Re^{0.8} Pr^{B_2} \tag{5.5}$$

i.e. $$\frac{Hi\ Dt_i}{K_w} = B_1 \left(\frac{V_w Dt_i \rho_w}{\mu_w}\right)^{0.8} \left(\frac{C_w\ \mu_w}{K_w}\right)^{B_2}$$

The properties of the water C_w, μ_w, K_w and ρ_w along the tube were not greatly affected by temperature as the temperature rise is small, which means that they can be considered as constants.

Hence expression (5.5) can be written as

$$Hi = \text{constant (a)}\ V_w^{.8} \tag{5.6}$$

Then equation (5.4) becomes

$$\frac{1}{Hov} = \frac{1}{a\ V_w^{.8}} + \frac{1}{H_{BM}} \tag{5.7}$$

Tests were carried out at a fixed fluidizing velocity and at the same tube position while the water flow rate was varied for each particle size used.

It was, however, noticed that the overall heat transfer coefficient was greatly affected by the position of the tube in the bed, namely the distance above the distributor plate. It was then decided that a preliminary series of tests had to be carried out to find the position giving the optimum coefficient so that the main calibration tests could be done.

Three types of particles were used for these calibration tests. They were all sand but of different size. The properties of these solids are shown in table (5.1).

From the calibration tests, the values obtained for Hov and V_w were plotted as $1/_{Hov}$ against $1/_{V_w^{\cdot 8}}$ using equation (5.7) as the guide line anticipating a linear relationship. Typical results for each particle size are shown in figure (5.1). The straight lines through each set of points were obtained using the least squares technique. For each set of points the slope of the line is 1/a and the intercept is $1/H_{BM}$.

To obtain a unified value of the constant (a) for all particles, the value of the intercept $(1/H_{BM})$ for each set of tests was subtracted from (1/Hov) and the result was plotted against $(1/V_w^{\cdot 8})$. The resulting plot is shown in figure (5.2). The correlation between the two variables $(1/Hov - 1/H_{BM})$ and $(1/V_w^{\cdot 8})$ was done on an ICL 1905 digital computer using a standard statistical package programme. The slope of the regression line was found to be 0.081 which is the value of (1/a) in equation (5.7). Hence equation (5.7) becomes

$$\frac{1}{Hov} = \frac{0.081}{V_w^{\cdot 8}} + \frac{1}{H_{BM}} \qquad (5.8)$$

It can be seen from figure (5.2) that the scatter about the regression line is large which obviously induces

an error in the final resulting values of H_{BM} computed later, but this error in the value of the constant and hence Hi will not affect the value of H_{BM} greatly. This will become clear in section (5.6) where the errors involved in this work will be discussed.

5.4 Evaluation of the minimum fluidizing velocity

Many attempts have been made to provide expressions from which the minimum fluidizing velocity may be calculated from fluid and particle properties. Most of these are based on equating the pressure drop across the bed to the weight of the particles. The following expression is then obtained

$$\frac{\Delta P}{L_{mf}} = (1-\varepsilon_{mf})(\rho_s-\rho_f)g \qquad (5.9)$$

Expressions for the pressure drop across a fixed bed (applied at minimum fluidization conditions) such as that of Ergun[6] are then used

$$\frac{\Delta P}{L_{mf}} = \frac{150(1-\varepsilon_{mf})^2}{\varepsilon^3_{mf}} \frac{\mu_f U_{mf}}{D^2_p} + 1.75\left(\frac{1-\varepsilon_{mf}}{\varepsilon^3_{mf}}\right) \frac{\rho_f U^2_{mf}}{D_p} \qquad (5.10)$$

By equating the pressure drop given by (5.9) and (5.10) and rearranging, the general expression

$$Ar = 150\left(\frac{1-\varepsilon_{mf}}{\varepsilon^3_{mf}}\right) Re_{mf} + \frac{1.75}{\varepsilon^3_{mf}} Re^2_{mf} \qquad (5.11)$$

is obtained.

Approximations have been proposed by many workers to simplify this expression [6] but perhaps the most universal is the one proposed by Goroshko et al (in 7)

$$Re_{mf} = \frac{Ar}{f_1 + f_2\sqrt{Ar}} \qquad (5.12)$$

where $f_1 = \frac{150(1-\varepsilon_{mf})}{\varepsilon^3_{mf}}$ and $f_2 = \frac{1.75}{\varepsilon^3_{mf}}$

The variations of f_1 and f_2 with ε_{mf} is illustrated in figures (5.3) and (5.4) respectively. It can be noticed that f_1 in particular is quite sensitive to the change in ε_{mf}. Equation (5.12) was used for evaluating the minimum fluidizing velocity. The value of ε_{mf} was determined experimentally, which is fully explained with the results in the next section.

5.5 Experimental results

5.5.1 Variable tube position

Experiments were carried out to determine the dependence of the heat transfer coefficient (H_{BM}) on the position of the tube vertically in the bed at given fluidizing velocities, particle sizes and bed depths. The bed temperature was kept at about 100°C for all tests.

5.5.1.a Variable tube position at different particle sizes

For these tests, the static (unfluidized) bed height was kept at 50 mm. The fluidizing velocity for each particle size used was set at the value which was expected

to give maximum heat transfer coefficient. In addition to the three sand samples mentioned earlier, blown alimina of average size 1100 μm was used. The properties of this sample is seen in table (5.1). This blown alumina is very spherical and smooth, but hollow at the same time, which made it less dense than the sand.

The results of these experiments are shown in figure (5.5).

5.5.1.b Variable tube position at different fluidizing velocities

These experiments were done using one type of particles (sand) and one particle size (253 μm). The static bed height was again fixed at 50 mm. Three fluidizing velocities were used, one on the rising zone of the H-U curve and the other two after the heat transfer coefficient had attained its maximum value. The results are shown in figure (5.6).

5.5.1.c Variable tube position for different bed depths

The sample used here was sand of average size 253 μm. The fluidizing velocity used was 0.37 m/sec. which is the same fluidizing velocity as that used with the sample indicated in figure (5.5), i.e. the heat transfer coefficient was at the maximum value for a bed height of 50 mm.

Three static bed heights were used, 50 mm., 35 mm. and 28 mm.

Figure (5.7) shows the results obtained. To facilitate comparison between the three curves and correct interpretation, another plot is given in figure (5.8). In this figure the heat transfer coefficient is plotted against the ratio of the tube centre line from the distributor plate to the static bed height.

5.5.2 Voidage determinations

The voidage fraction at minimum fluidization condition (ε_{mf}) for each particle size used for the heat transfer investigations was measured experimentally so that the minimum fluidizing velocity (U_{mf}) could be evaluated using equation (5.12).

The test rig used is the one described in Chapter 4.

Small amounts of the sample were weighed and added to the bed. Each time a new amount was added, the air supply was turned on to fluidize the sample. The air flow was then reduced until no bubbles were observed in the column while it was still fluidized. The height of the sand column was then measured. The results were plotted in cumulative fashion as can be seen in figures (5.9), (5.10), (5.11) and (5.12). The lines drawn were obtained by the least squares technique.

The slope of these lines was then used to obtain the ratio of the volume of solids to the total bed volume, and the voidage is then calculated using the equation

$$\varepsilon_{mf} = 1 - \frac{V_s}{V_b} \qquad (5.13)$$

where V_s is the volume of solids

V_b is the total volume of the bed.

The results of these experiments are presented in table (5.2), and compared with packed bed values which were determined experimentally.

5.5.3 Variable fluidizing velocity

These tests were carried out to establish the dependence of the heat transfer coefficient on the fluidizing velocity for different particle sizes while keeping the rest of the variables (static bed height and the tube position) for each experiment constant. The static bed height was kept at 50mm., while the tube was positioned (within the bed) to give the maximum heat transfer coefficient corresponding to the particle size under test which was known from the experiments reported in section (5.5.1.a)

The results obtained for the four particles of sizes 134 μm, 253 μm, 345 μm and 1100 μm are shown in figures (5.13), (5.14), (5.15) and (5.16) respectively, together with respective deep bed values obtained from the correlation presented by Zabrodsky [5] for the maximum heat transfer coefficient.

To show the dependence of the heat transfer coefficient on particle size the four curves of (5.13), (5.14), (5.15) and (5.16) were plotted together and are shown in figure (5.17).

5.6 Error analysis

From equation (5.4)

$$\frac{1}{H_{BM}} = \frac{1}{Hov} - \frac{1}{Hi} \qquad (5.14)$$

The errors in H_{BM} arise due to errors in either Hov or Hi. These errors can be calculated from the relationship

$$\delta H_{BM} = \frac{\partial H_{BM}}{\partial Hov} \delta Hov + \frac{\partial H_{BM}}{\partial H_i} \delta H_i \qquad (5.15)$$

where δH_{BM}, δHov and δH_i are the errors in H_{BM}, Hov and H_i respectively. Therefore

$$\delta H_{BM} = \frac{H_i^2}{(Hi - Hov)^2} \delta Hov - \frac{Hov^2}{(Hi-Hov)^2} \delta H_i \qquad (5.16)$$

Dividing both sides of equation (5.16) by H_{BM} and rearranging, we get

$$\frac{\delta H_{BM}}{H_{BM}} = \frac{H_i}{(H_i-Hov)} \frac{\delta Hov}{Hov} - \frac{Hov}{(H_i-Hov)} \frac{\delta H_i}{H_i} \qquad (5.17)$$

The terms $\frac{\delta H_{BM}}{H_{BM}}$, $\frac{\delta Hov}{Hov}$ and $\frac{\delta H_i}{H_i}$ represent the percentage errors in H_{BM}, Hov and H_i respectively.

The effect of the errors in Hov and H_i on H_{BM} will now be considered.

A typical value of H_i used for this analysis, calculated from expression (5.6) using the value of the constant (a) from figure (5.2) together with the value of V_w used for all the heat transfer experiments, was 10.57 $kW/m^2\ ^oK$.

Fig. (5.18) shows the result of the investigation of the errors induced in H_{BM} due to arrors in Hov using equation (5.17).

The investigation of the errors induced in H_{BM} arising from errors in H_i is shown in figure (5.19).

To determine the overall errors involved in the heat transfer investigations, the following assumptions were made

1. The main error in Hov lies in the heat flux measurement and in particular the temperature rise of the water since $Hov = \frac{W\ C_w(T_{wo}-T_{wi})}{A_t}$

2. The main error in H_i lies in the constant (a) as $H_i = aV_w^{.8}$ but there will be a ±1% error to be expected in the water flow.

The error in the temperature rise is the maximum error in the reading of the thermometers which was ±3%. This gave an error induced in H_{BM} of ±3.15%.

The error in the constant (a) was obtained from figure (5.2) where the two dotted lines of the standard deviation (otherwise called the "standard error of estimate") in the regression analysis carried out are shown. The standard deviation was calculated to be ±0.082. This gave a maximum percentage error in (a) of ±10% which was evaluated at a value of 0.8 (i.e. at the lowest value of a that was practically obtained). This error in (a) induces an error of ±0.5% in H_{BM} which was calculated from figure (5.19).

Hence the total error induced in H_{BM} due to the errors in Hov and H_i would be ±3.65%.

Table (5.1)

Material	Dp (μm)	Density (Kg/m^3)
sand	134	2709
sand	253	2684
sand	345	2662
Blown Alumina	1100	1777

Table (5.2)

Material	Voidage (ε_{mf})	Voidage of packed bed
sand (134 μm)	.481	.457
sand (253 μm)	.463	.445
sand (345 μm)	.44	.426
Alumina (1100μm)	.484	.469

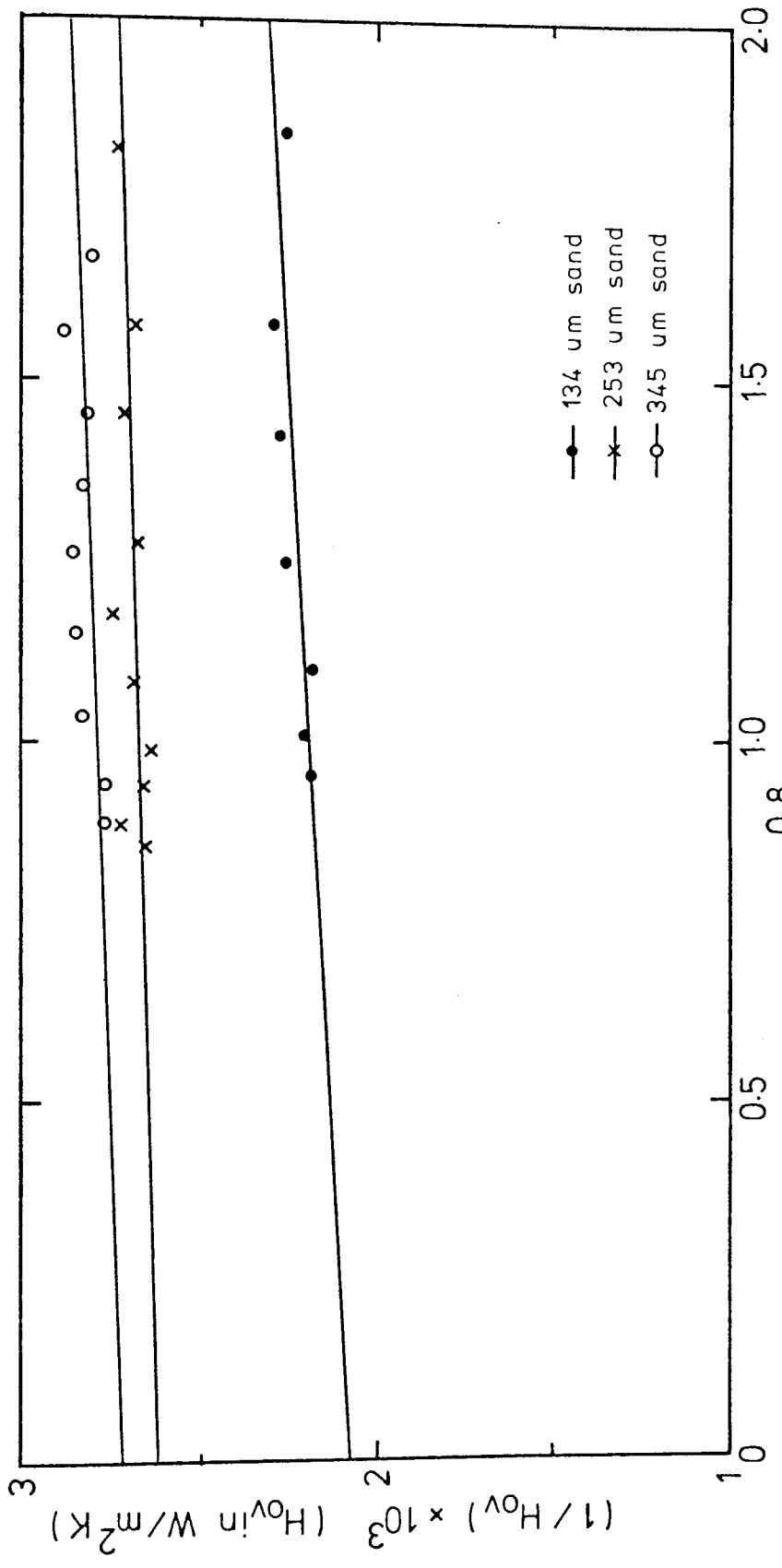

FIG. (5.1) CALIBRATION CURVES FOR THE TUBE INSIDE HEAT TRANSFER COEFFICIENT

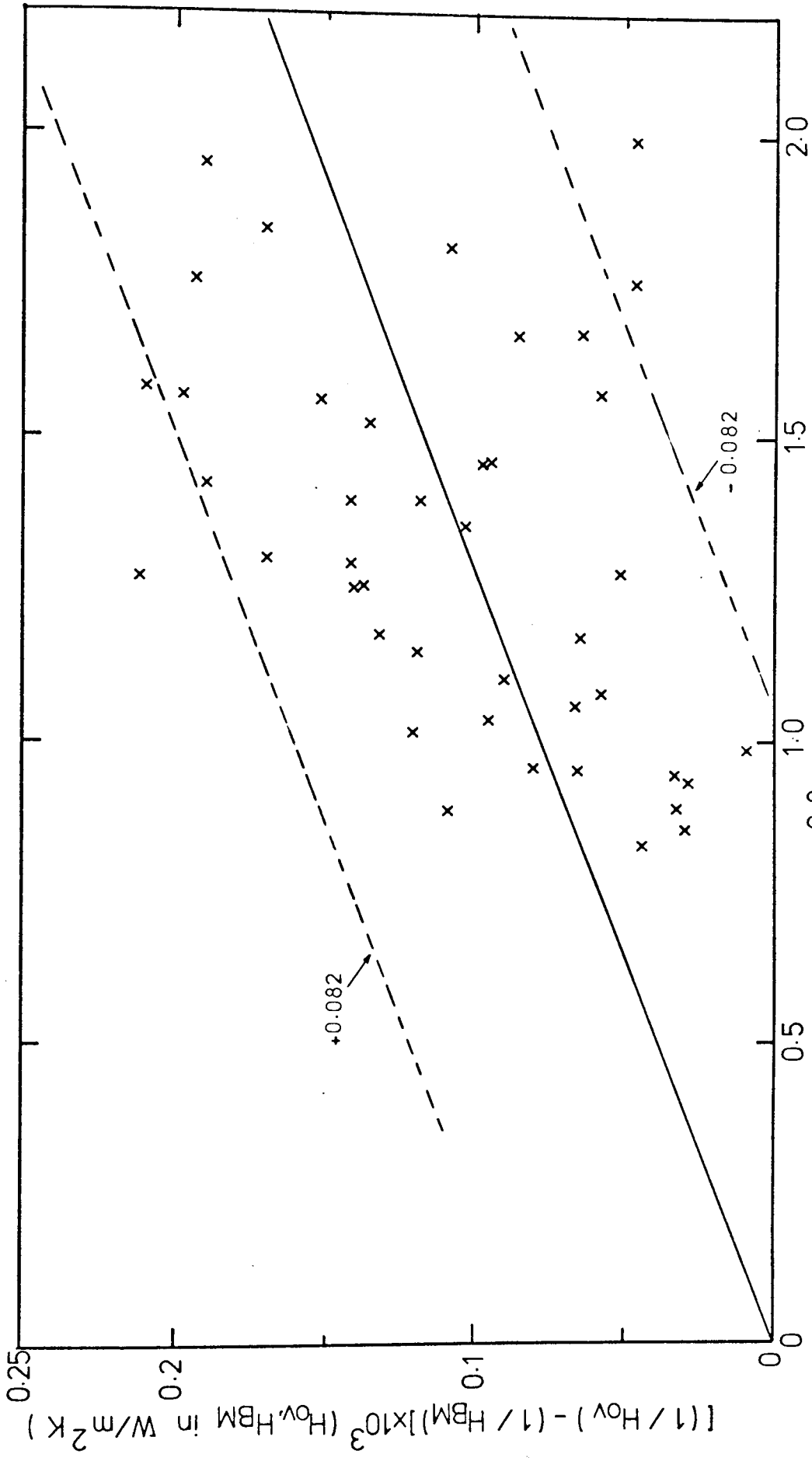

FIG. (5.2) CALIBRATION CURVE FOR THE TUBE INSIDE HEAT TRANSFER COEFFICIENT

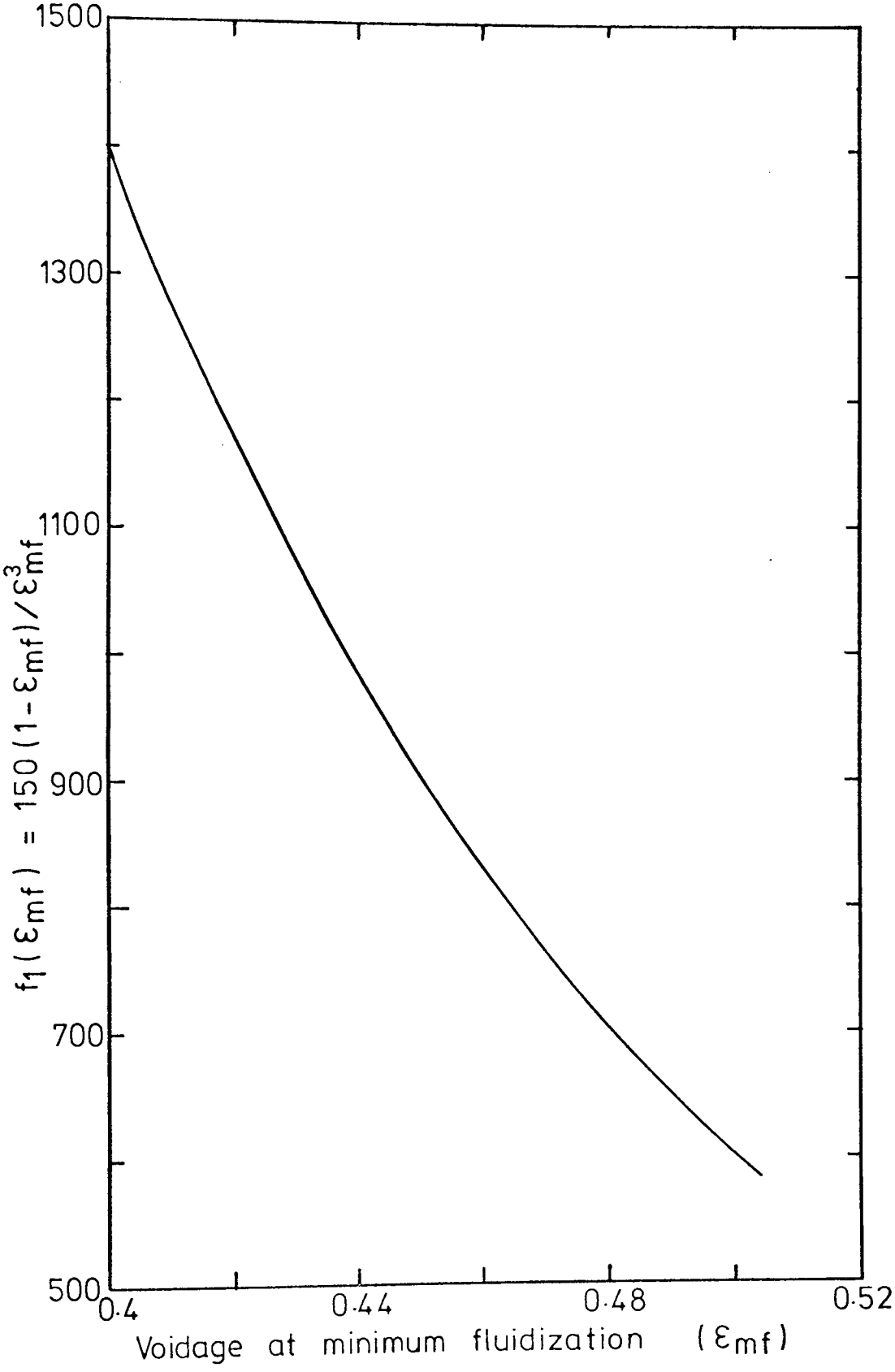

FIG. (5·3) VARIATION OF $f_1(\varepsilon_{mf})$ WITH VOIDAGE

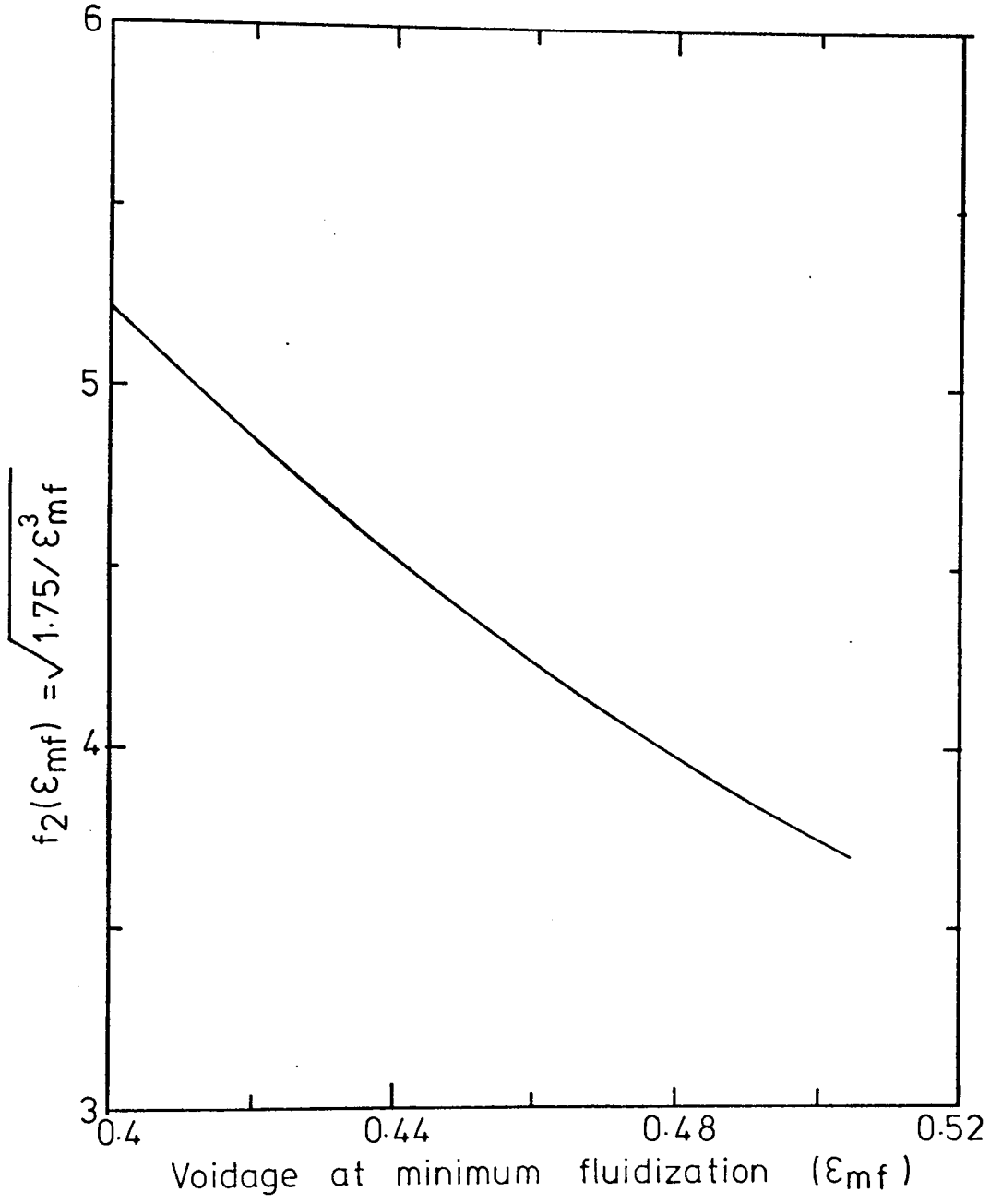

FIG. (5·4) VARIATION OF $f_1(\varepsilon_{mf})$ WITH VOIDAGE

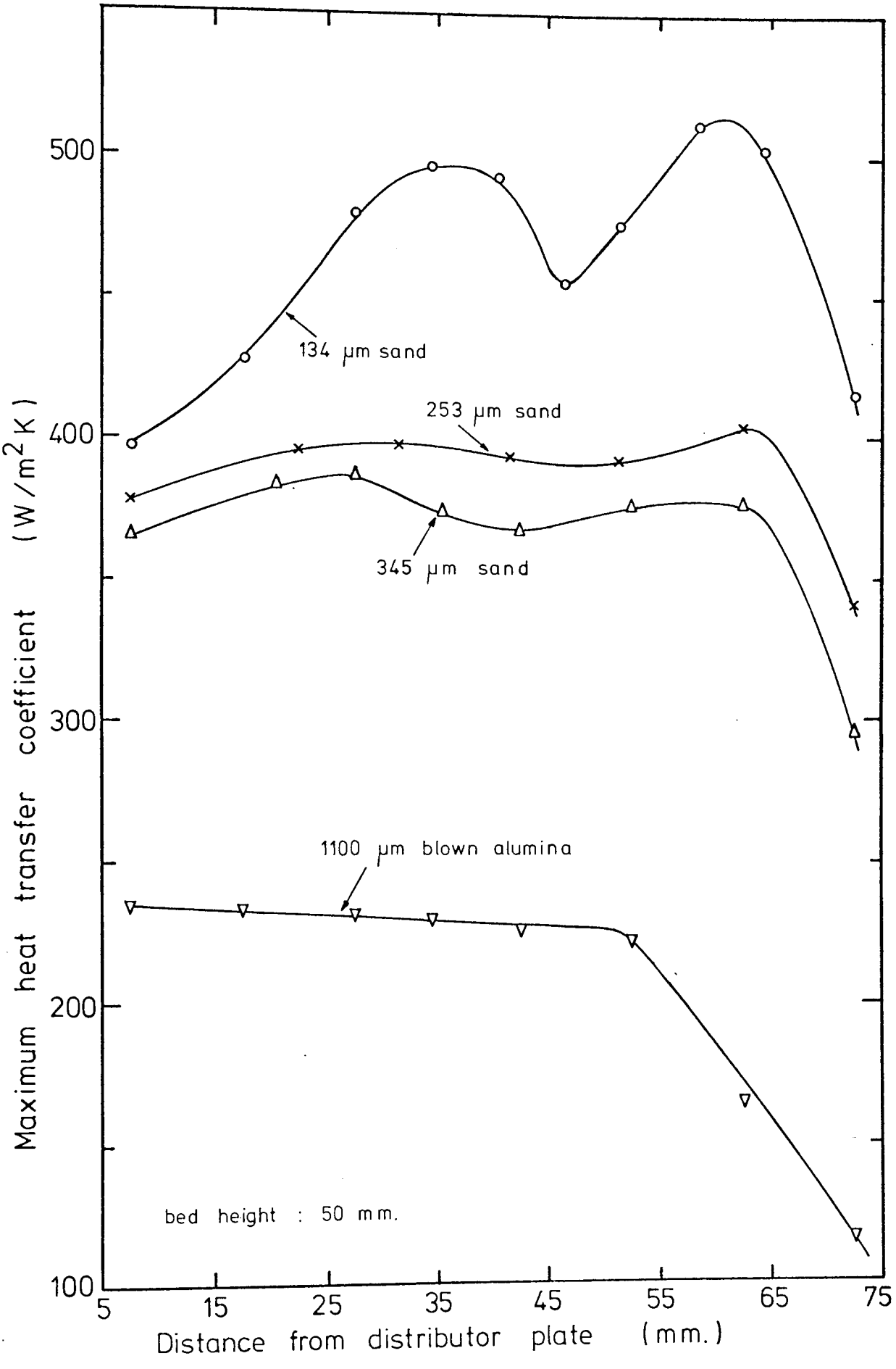

FIG. (5·5) EFFECT OF TUBE POSITION ON THE HEAT TRANSFER COEFFICIENT FOR DIFFERENT PARTICLE SIZES

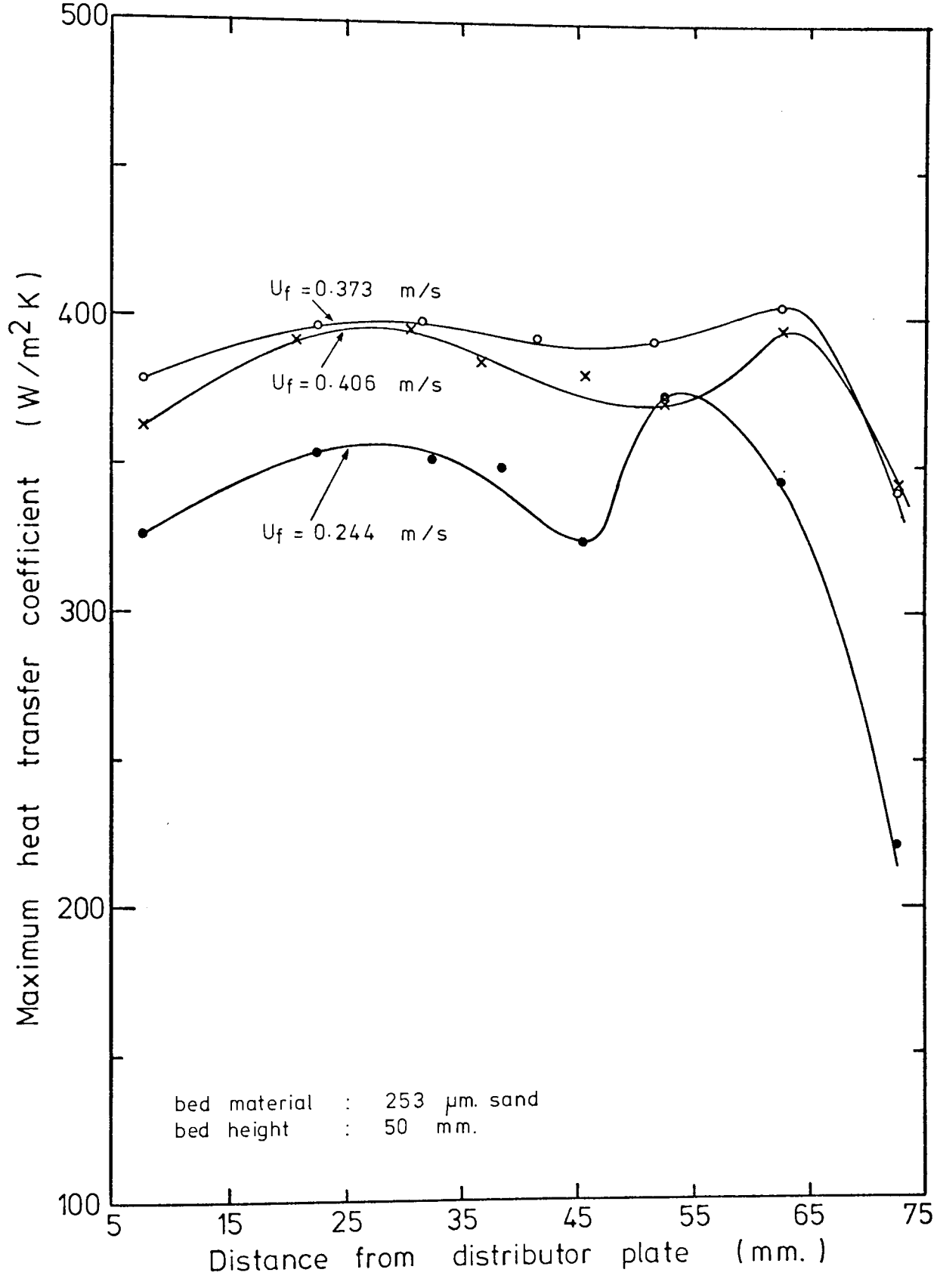

FIG. (5·6) EFFECT OF TUBE POSITION ON THE HEAT TRANSFER COEFFICIENT AT DIFFERENT FLUIDIZING VELOCITIES

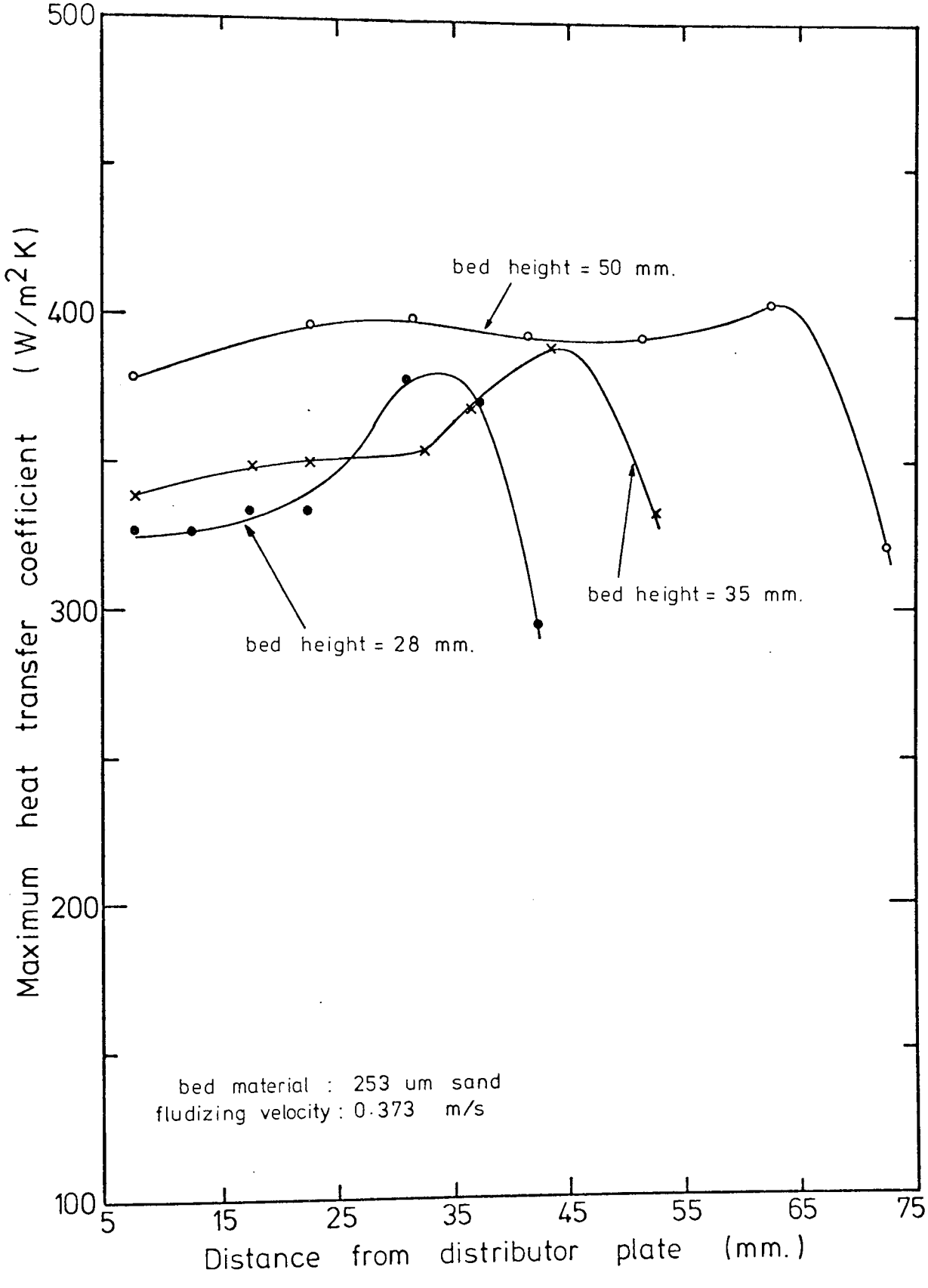

FIG. (5.7) EFFECT OF TUBE POSITION ON THE HEAT TRANSFER COEFFICIENT FOR DIFFERENT BED HEIGHTS

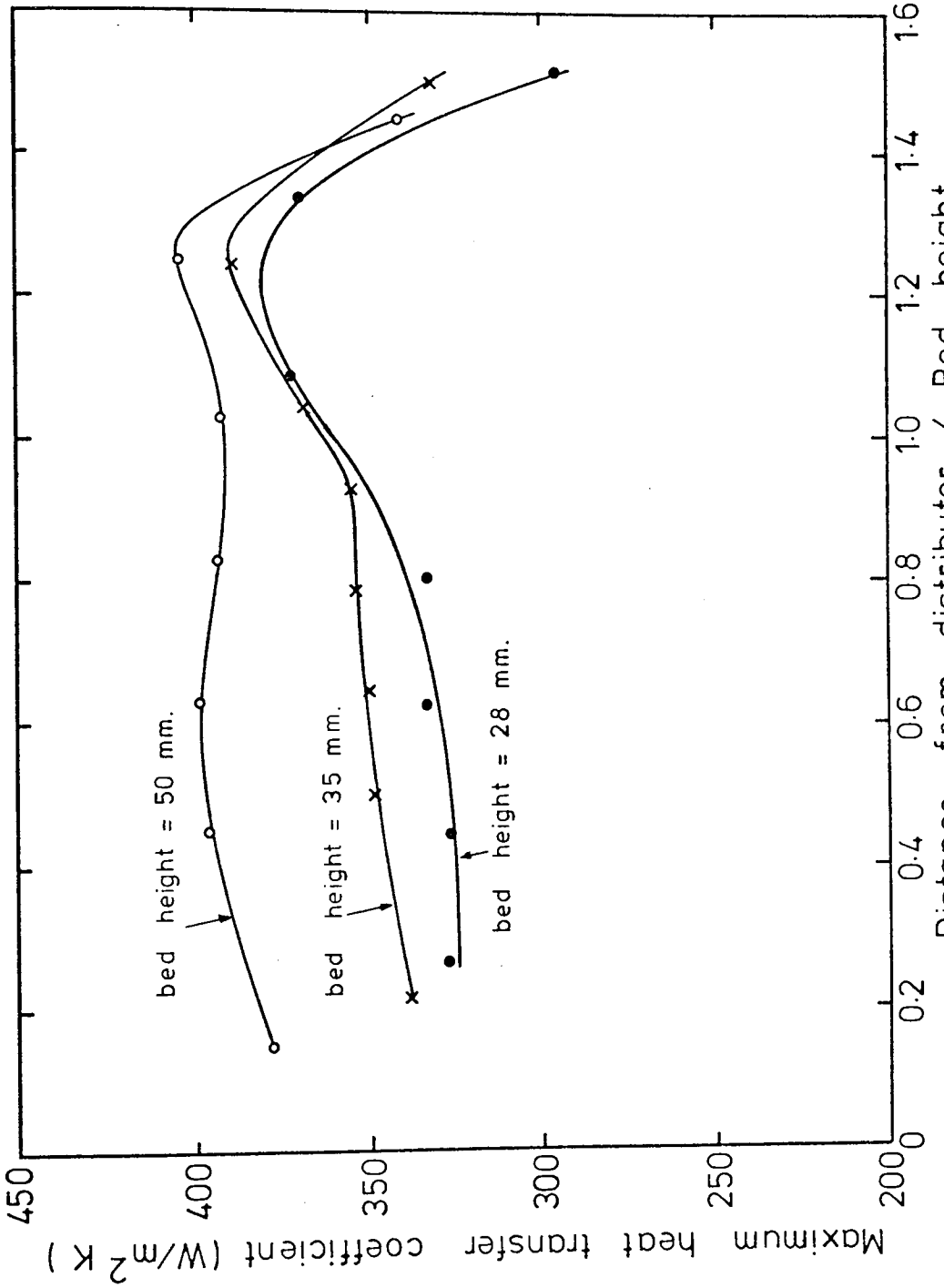

FIG. (5.8) EFFECT OF RELATIVE TUBE POSITION ON THE HEAT TRANSFER COEFFICIENT FOR DIFFERENT BED HEIGHTS

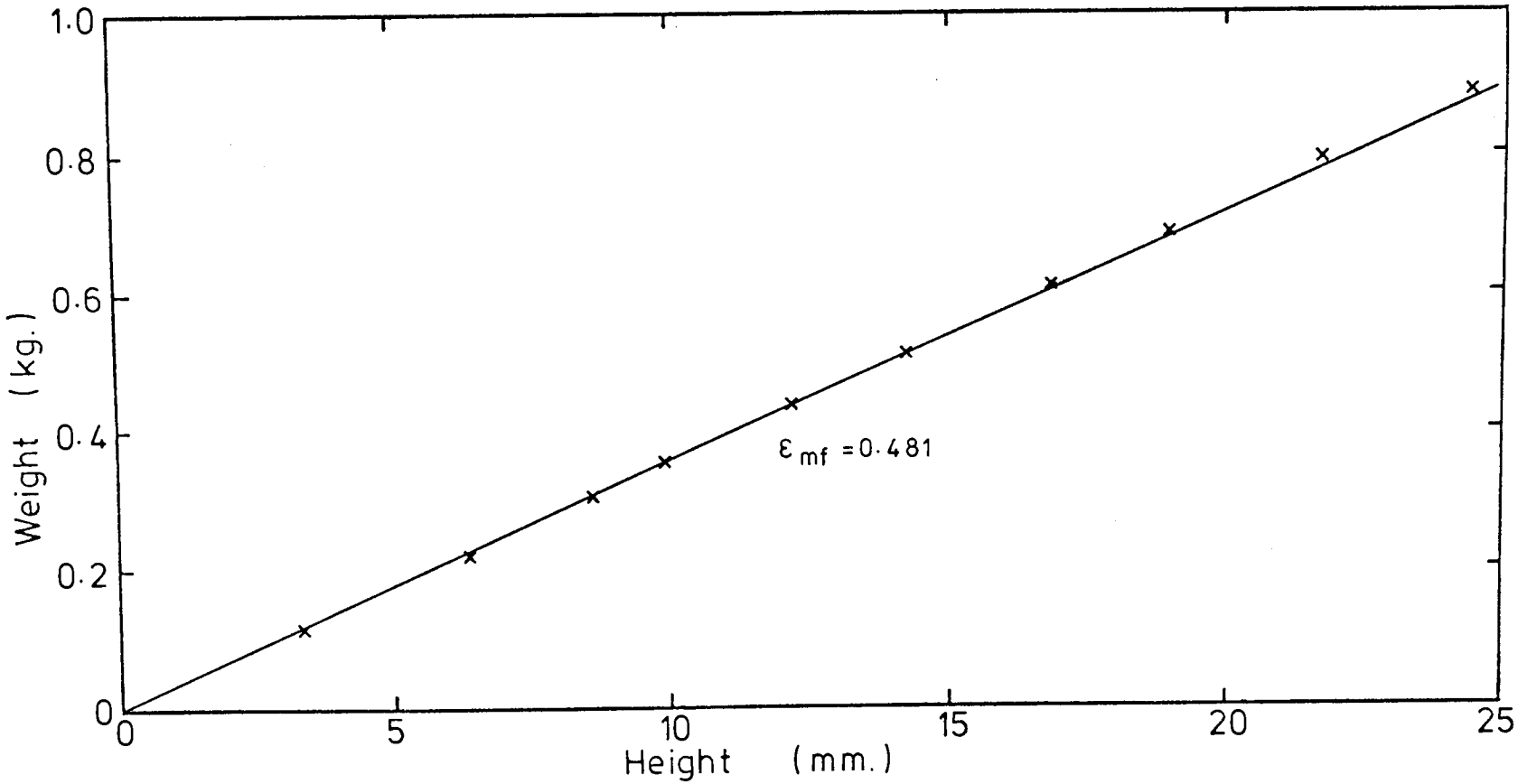

FIG. (5.9) VOIDAGE MEASUREMENT (134 μm. sand)

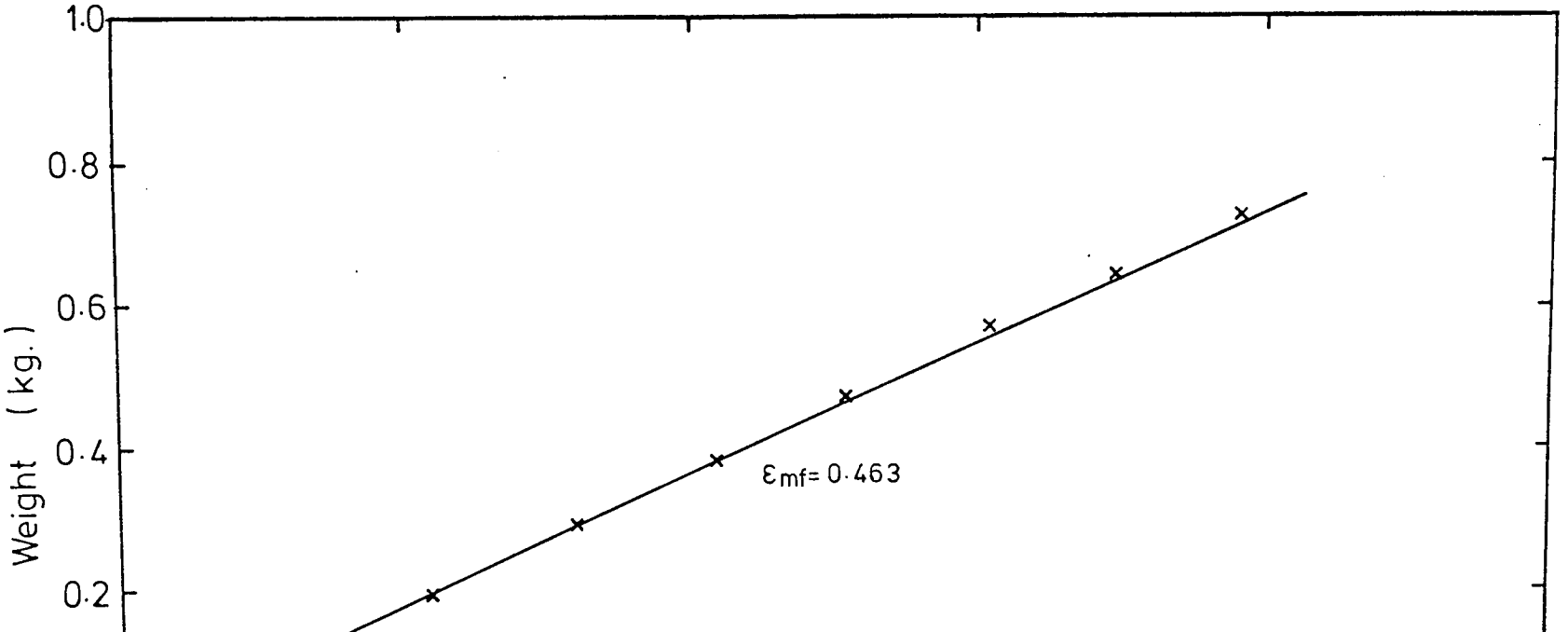

FIG. (5·10) VOIDAGE MEASUREMENT (253 μm. sand)

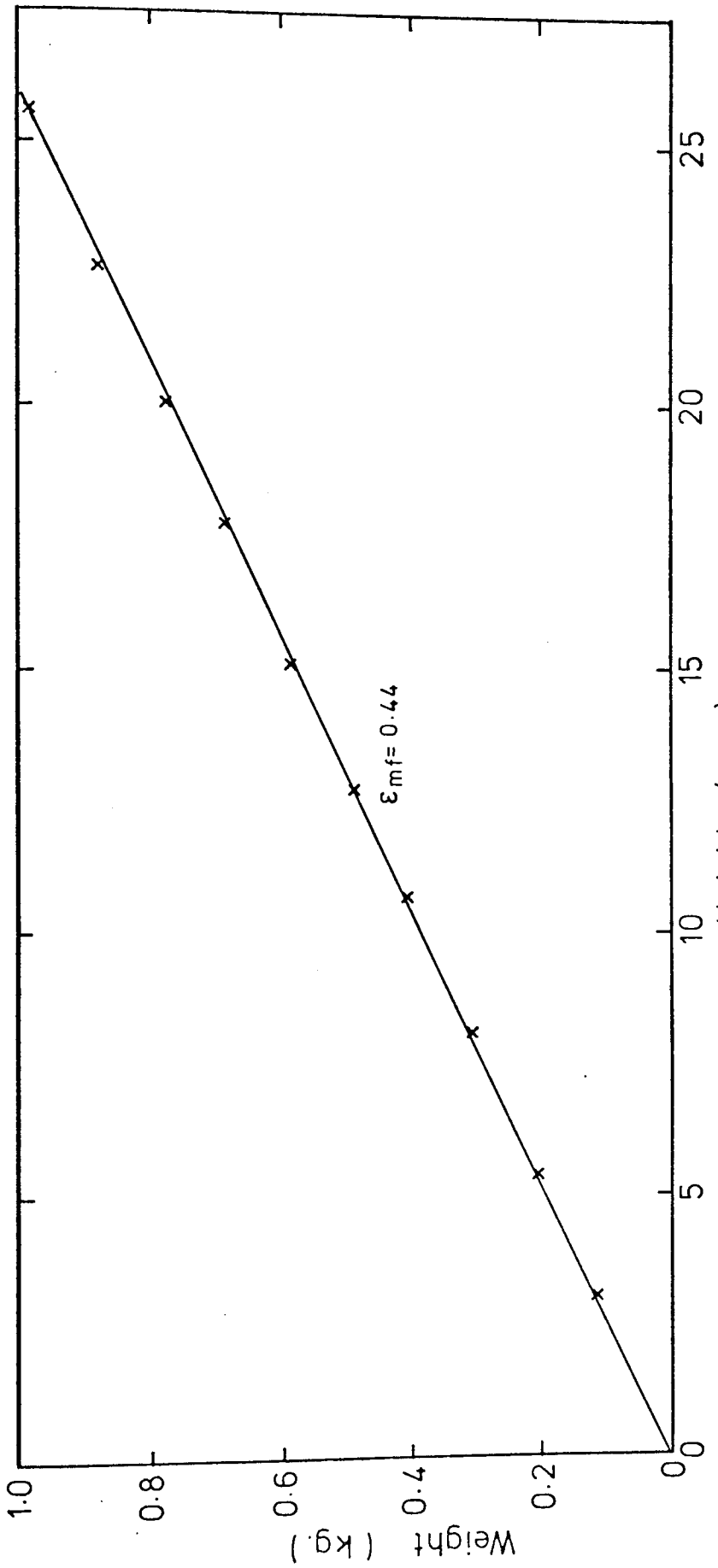

FIG.(5.11) VOIDAGE MEASUREMENT (345 μm. sand)

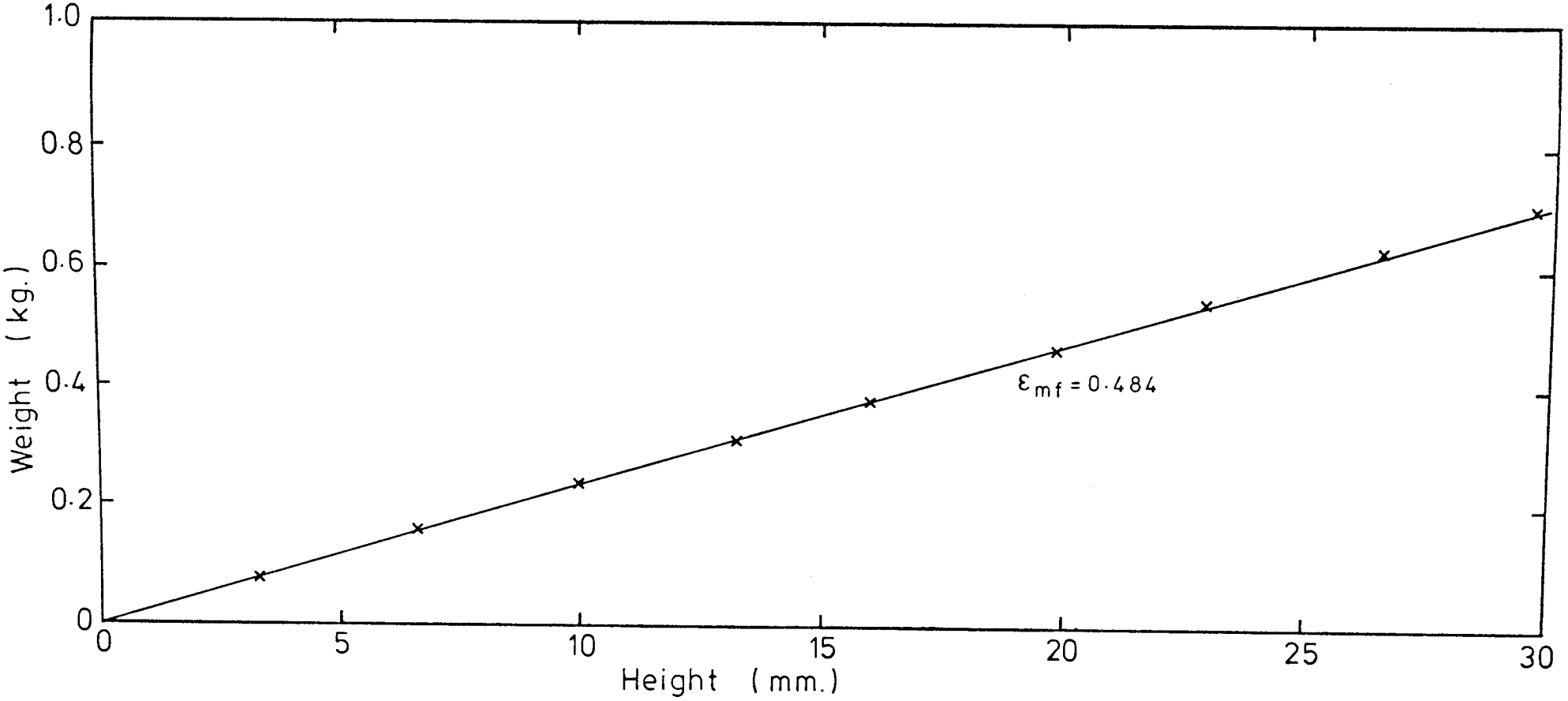

FIG.(5.12) VOIDAGE MEASUREMENT (1100 μm. alumina)

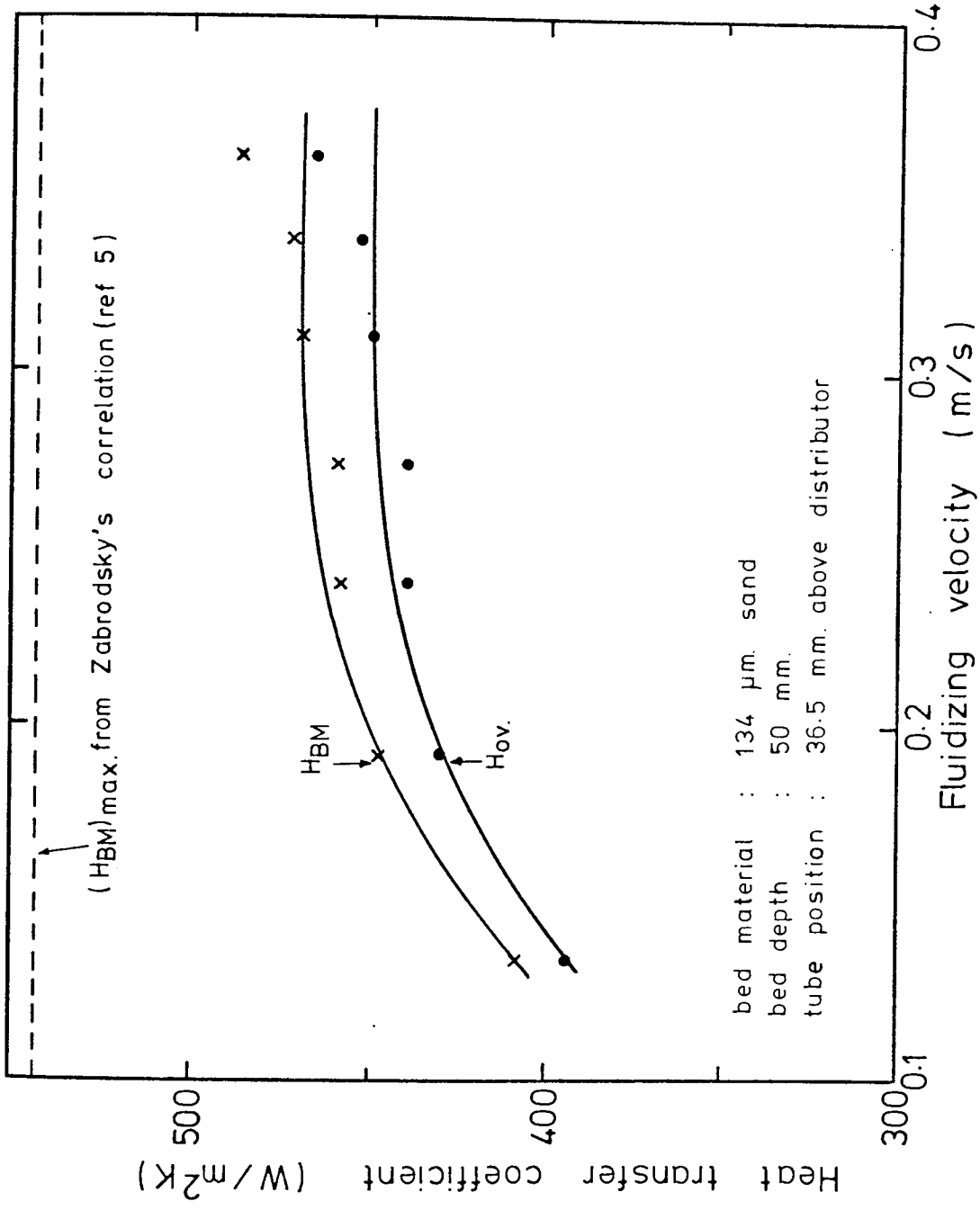

FIG. (5.13) DEPENDENCE OF THE HEAT TRANSFER COEFFICIENT ON FLUIDIZING VELOCITY

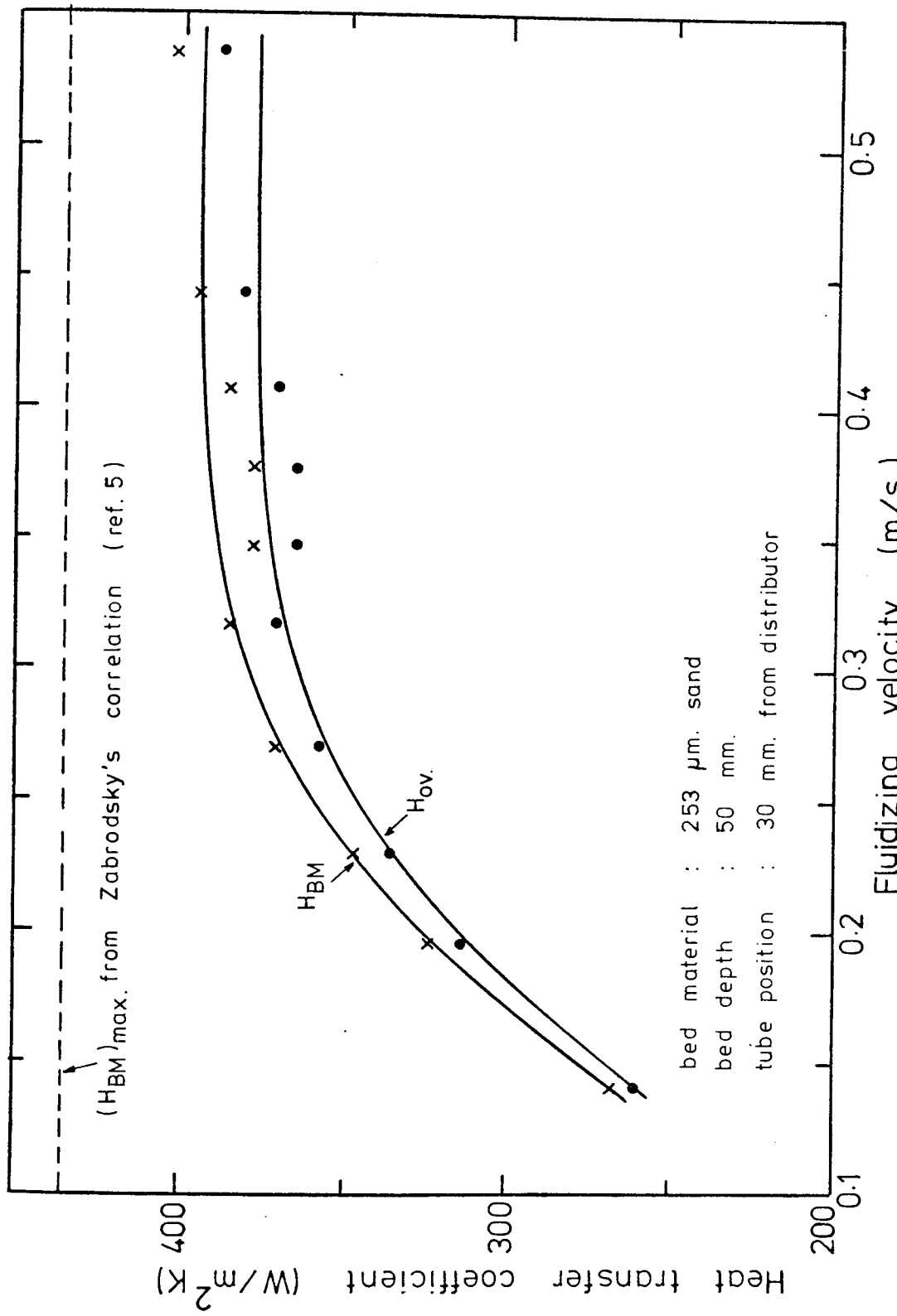

FIG. (5.14) DEPENDENCE OF THE HEAT TRANSFER COEFFICIENT ON FLUIDIZING VELOCITY

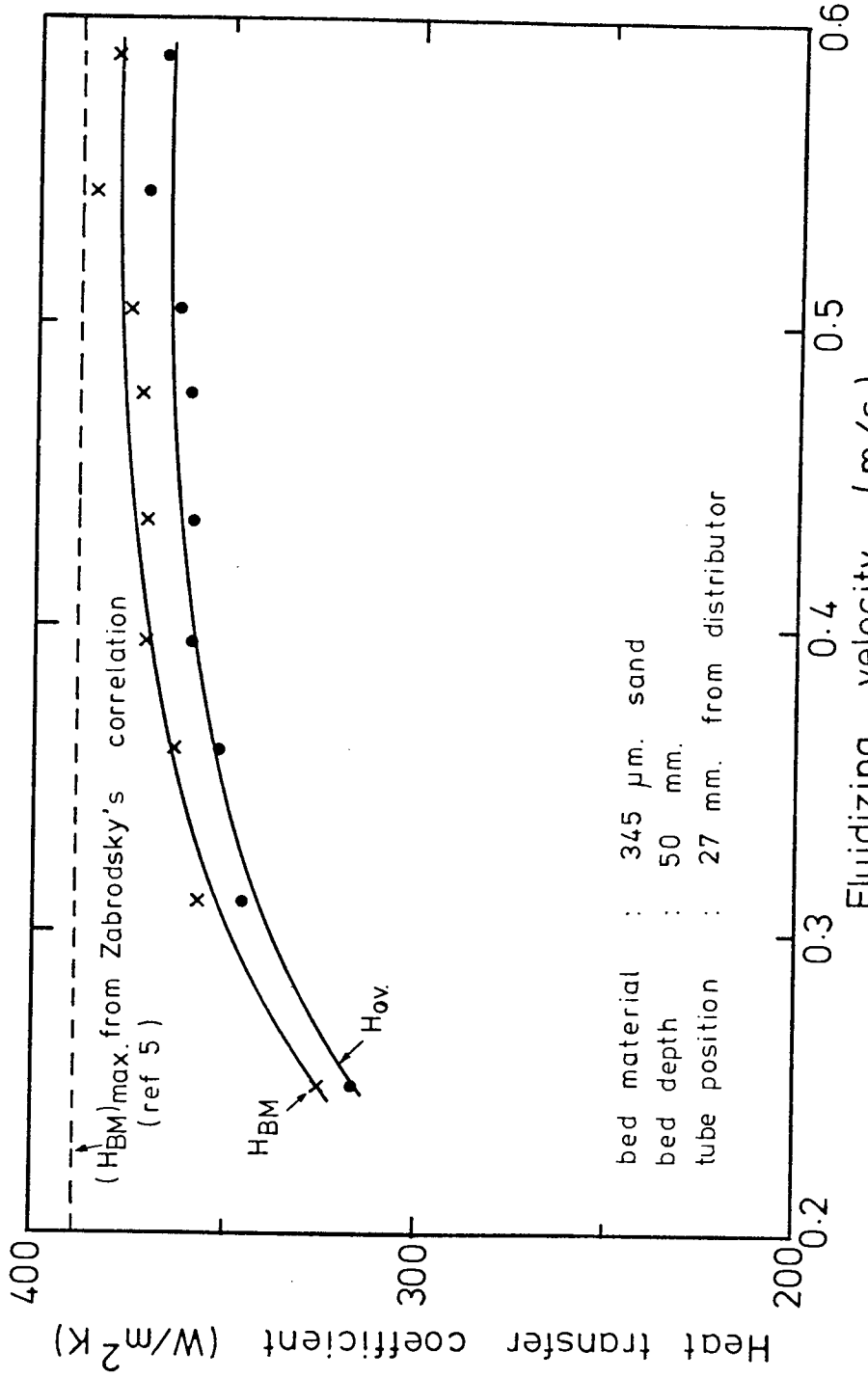

FIG. (5.15) DEPENDENCE OF THE HEAT TRANSFER COEFFICIENT ON FLUIDIZING VELOCITY

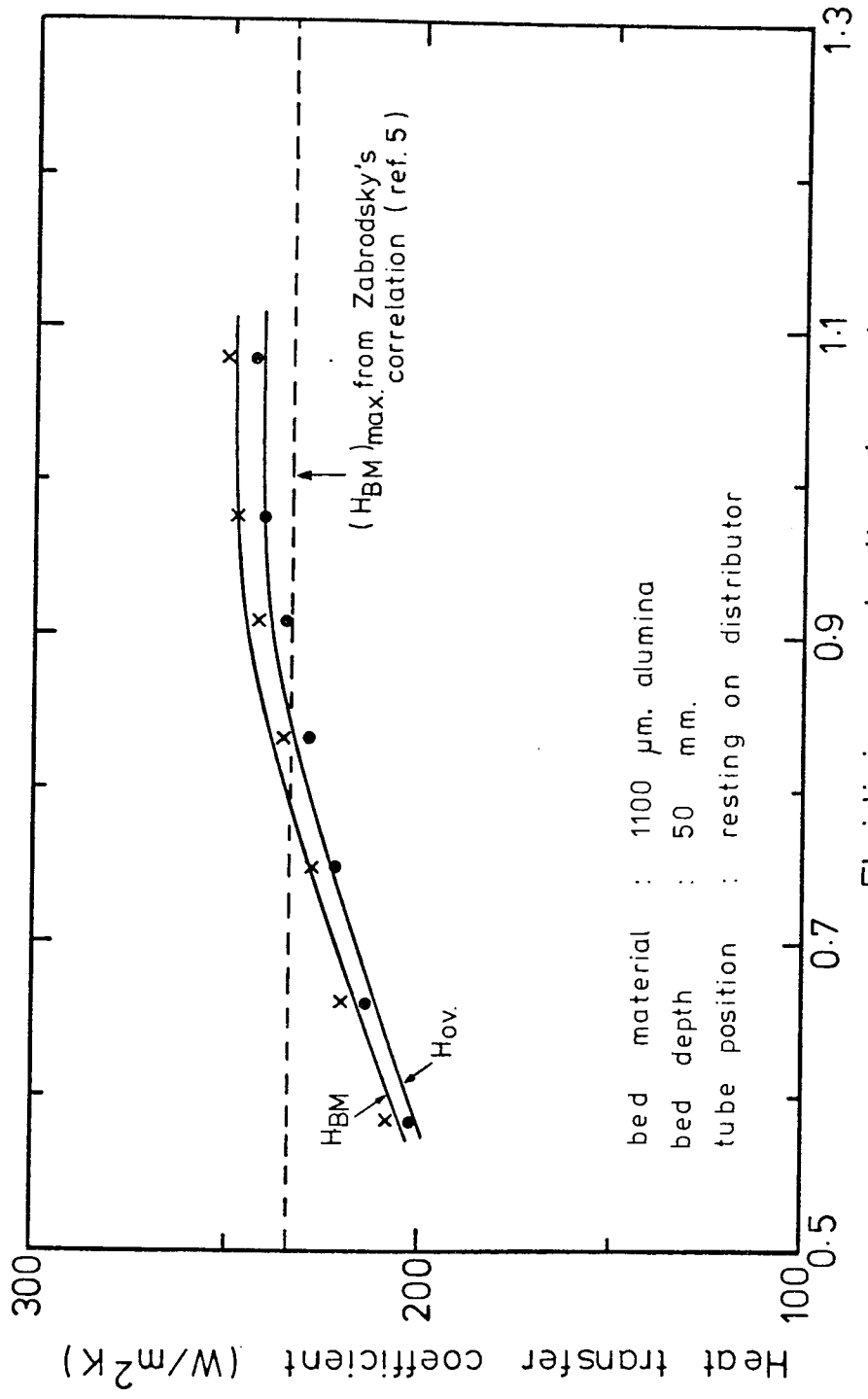

FIG. (5·16) DEPENDENCE OF THE HEAT TRANSFER COEFFICIENT ON FLUIDIZING VELOCITY

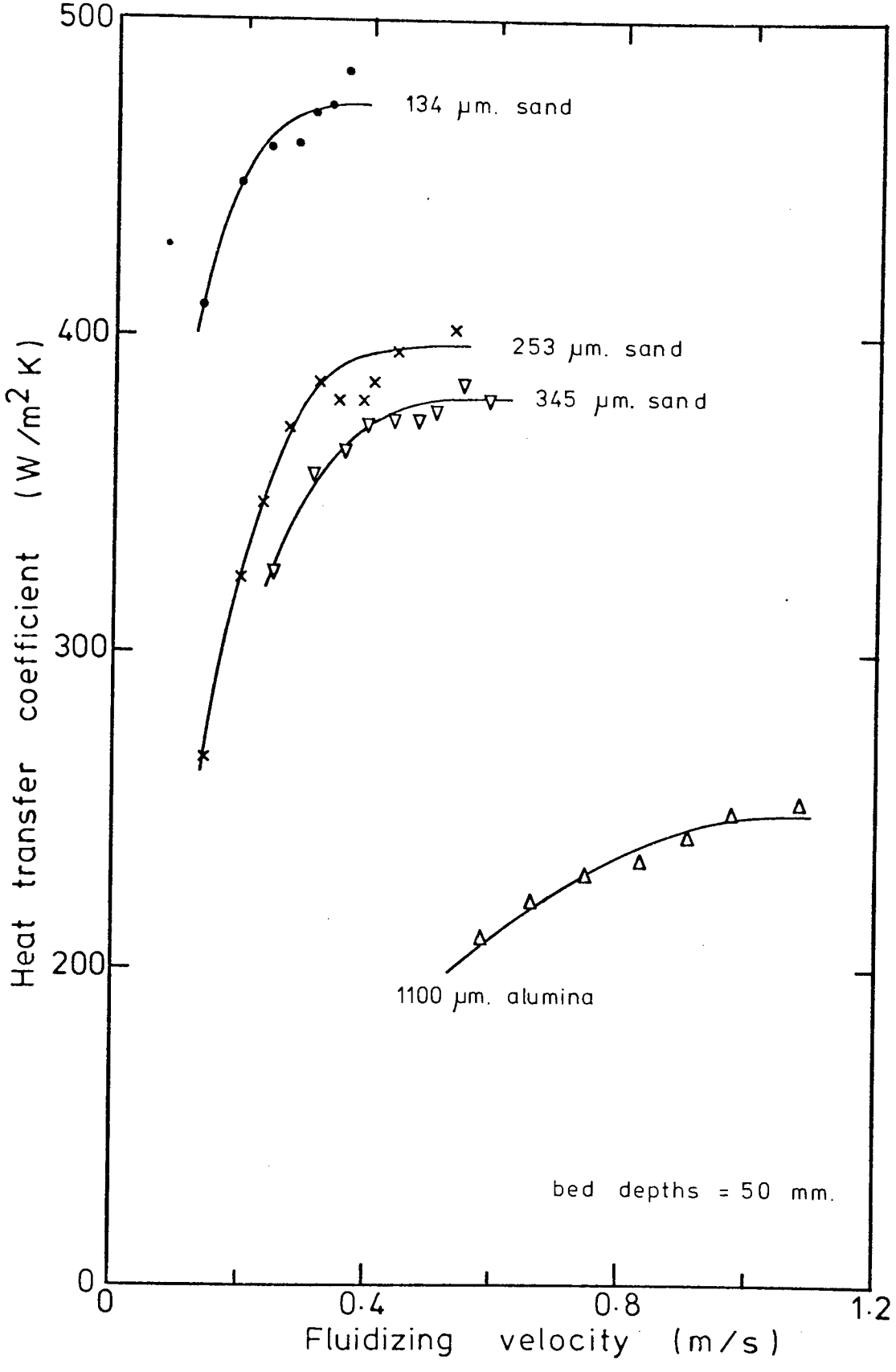

FIG. (5·17) DEPENDENCE OF THE HEAT TRANSFER COEFFICIENT ON PARTICLE SIZE

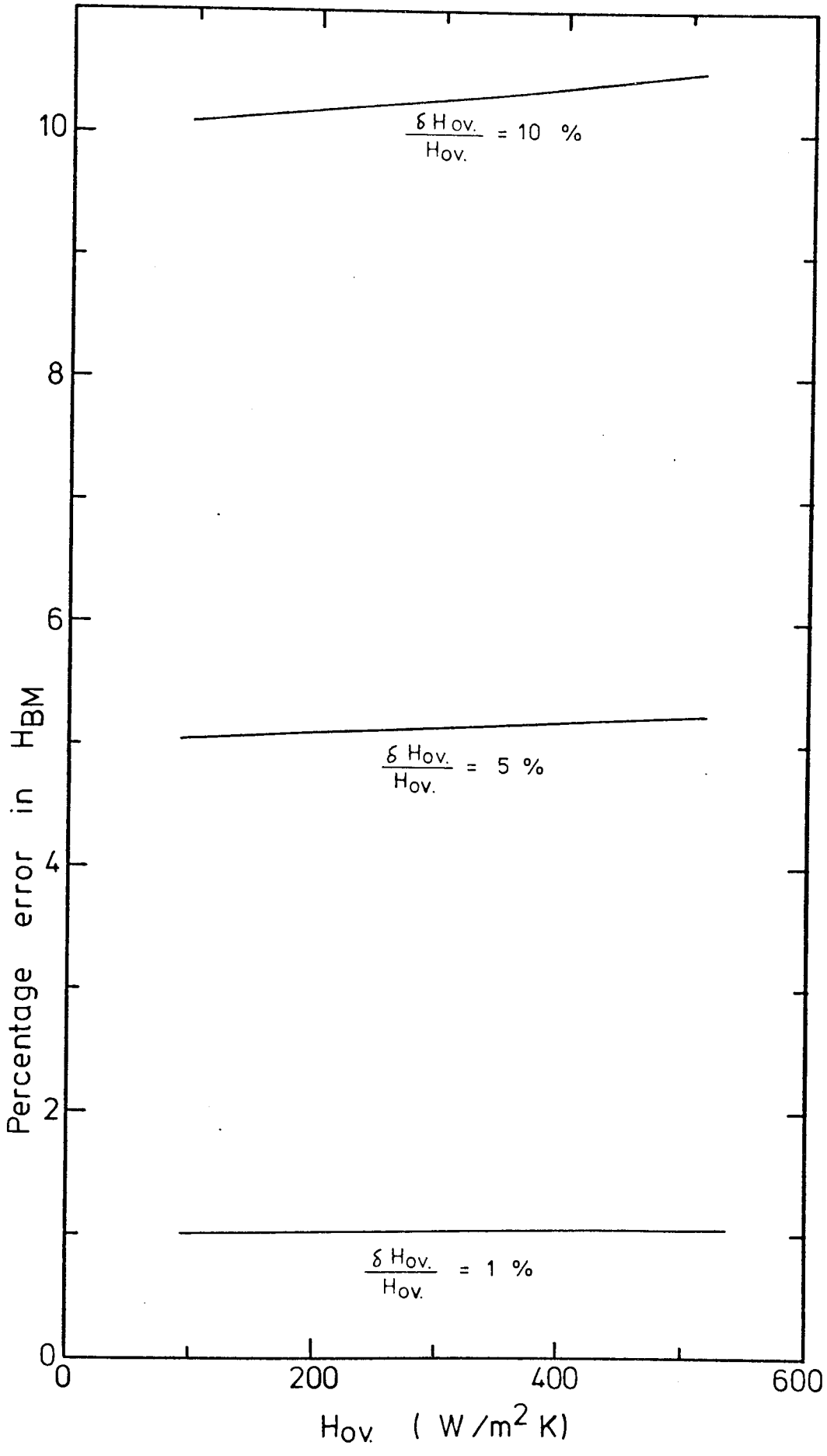

FIG. (5.18) EFFECT OF ERRORS IN $H_{ov.}$ ON ERRORS IN H_{BM}

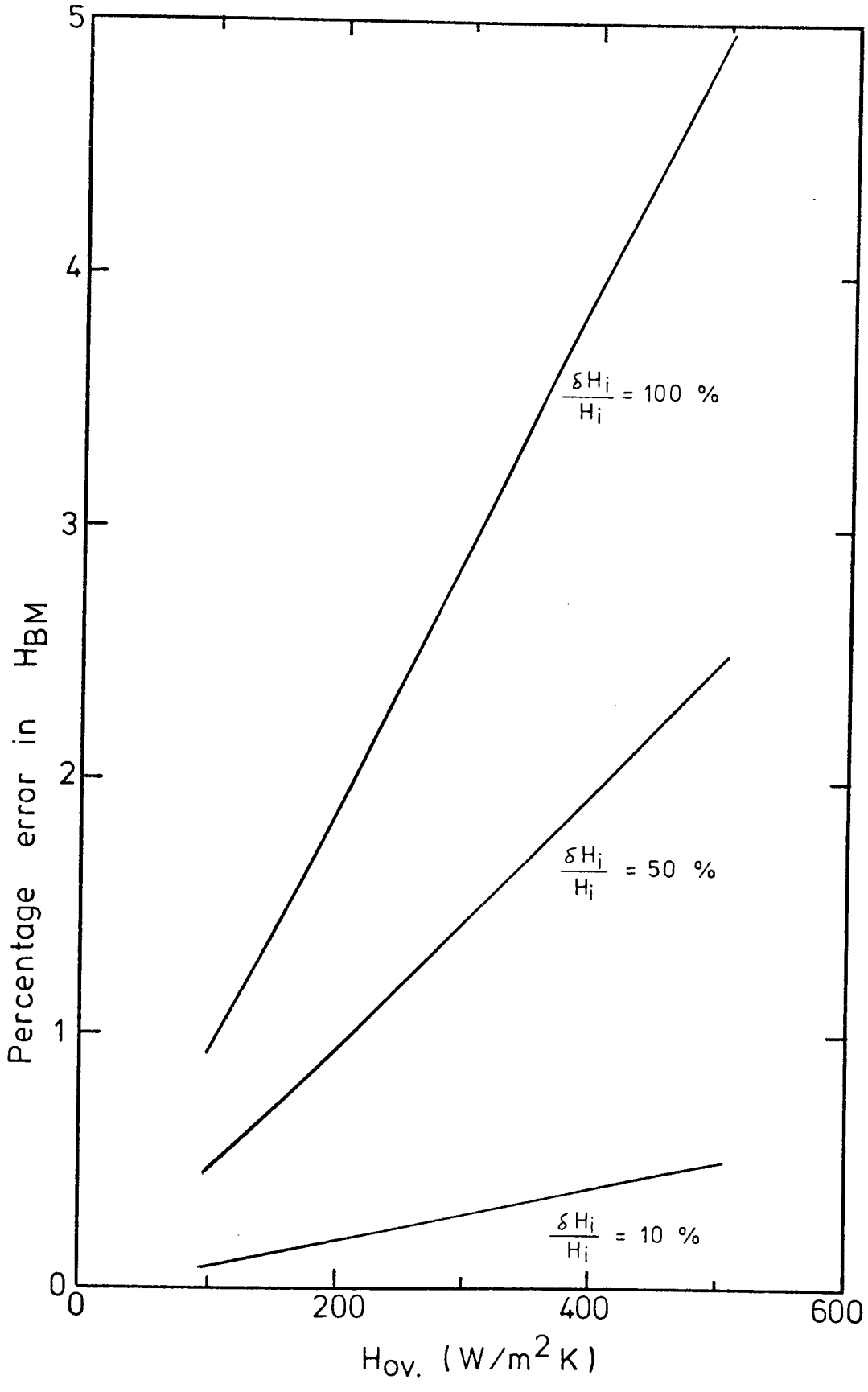

FIG. (5.19) EFFECT OF ERRORS IN H_i ON ERRORS IN H_{BM}

CHAPTER 6

THE SPHERE PROBE

THE SPHERE PROBE

6.1 Introduction

A heat transfer probe of sperical shape was used to obtain values of the heat transfer coefficient between a fluidized bed and the probe for comparison with data obtained from the plain tube experiments. The object being to be able to correlate between probe and tube thus allowing many more experiments to be done very quickly covering a wide range of conditions.

Due to the fact that most of the heat transfer takes place when the solid particles come into contact with the immersed object, the local motion of the particles and hence the heat transfer will be affected by the shape of the solid immersed in the bed.

A spherically shaped probe serves as an approximate representation of a plain horizontal tube since some similarity in the profile of both objects exists.

The effect of probe shape on indicated heat transfer coefficient has not been investigated but a spherical probe is commonly used and the effect was not thought to be large.

Gelperin et al 1968[7] investigated local heat transfer coefficients round a horizontal tube measuring the local heat fluxes and temperature differences in individual zones round the perimeters of tubes from 20 to 80 mm. diameter immersed in a bed of quartz sand (dp=160 μm) of height 385 mm. and fluidized by air. His results show that the distribution of

the heat transfer coefficient is such that it is optimum at the sides, as shown in figure (6.1). The results also show that the distribution is strongly dependent on the fluidizing velocity and the diameter of the tube.

Baskakov et al [55] investigated the local heat transfer coefficient round a sphere by obtaining the temperature profile round a 40 mm. glass sphere placed at the centre of a bed of corundum particles (Dp=320 μm.) at 200 mm. from the distributor plate and then developing a mathematical expression to calculate local heat transfer coefficients. His results are shown in figure (6.2).

A comparison between Baskakov's results and Gelperin's with 40 mm. tube diameter and approximately equal fluidizing velocity reveals that the distribution of the heat transfer coefficient is very similar in both cases, with very little local variation at $U_f >> U_{mf}$.

6.2 Description of the probe and its principle

The probe itself was a copper sphere of 14.27 mm. diameter. A small hole was drilled into the sphere up to the centre into which a stainless steel sheathed chromel-alumel type thermocouple was silver soldered so that the temperature at the centre of the sphere could be measured. When in use, the thermocouple was connected directly to a

pen type temperature recorder and a trace of the rise of the sphere temperature with time was obtained. The general arrangement of the probe is shown in Figure (6.3) and a typical temperature trace is presented in Figure (6.4).

In principle the copper sphere was considered an isothermal one since the thermal conductivity of copper is very large and hence the temperature measured at the centre can be regarded as the temperature of the whole sphere. Using this assumption a simple expression was obtained to calculate the heat transfer coefficient from the transient trace (shown in figure 6.4) which was

$$\ln \left| \frac{T - T_s}{T - T_{si}} \right| = - \frac{H A_s}{MC_s} \quad t \qquad (6.1)$$

The derivation of the equation is presented in Appendix (7).

Values of T_s at 5-second time intervals were obtained from the trace (shown in Figure (6.4)) and a log-linear plot of $\left(\frac{T - T_s}{T - T_{si}}\right)$ against time t was produced. The slope of the resulting straight line gave the quantity $\frac{HA_s}{MC_s}$ in equation (6.1) from which the sphere surface average heat transfer coefficient was then calculated knowing A_s, M and C_s. A typical log-linear plot is shown in Figure (6.5).

6.3 Experiments carried out and results

Two sets of experiments were carried out. One was to check the effect of the position of the sphere on the heat transfer coefficient at a constant fluidizing velocity and

the other was to confirm the variation of the heat transfer coefficient with the fluidizing velocity at one sphere position. For the latter, the sphere was placed such that it was in the same position as the bare tube in the corresponding experiments done previously (reported in section (5.5)).

The experimental procedure carried out using the spherical probe was of the same nature as that using the bare tube previously reported in Chapter (5), for the reason that the results were intended to serve as a confirmation of those obtained with the bare tube.

All the tests were done using silica sand of average size 134 μm., the reason being that it showed the greatest sensitivity to the position of the bare tube in the previous tests (Chapter 5).

The lateral position of the sphere throughout the tests was on the longitudinal axis of the bed.

Results of these tests are presented in Figures (6.6) and (6.7).

6.4 Discussion

It is evident from the results presented in Figures (6.6) and (6.7) that the two results obtained from the bare tube

and sphere tests are in fairly good agreement with each other.

Both sets of results show the same trend. Concerning the effect of the position of the immersed object, the heat transfer coefficient is highest at two positions; one where the object is within the limit of the static bed and the other is where the object is in the lean phase of the bed above the static bed height of 50 mm. They are also both consistent in exhibiting that the maximum value of the heat transfer coefficient occurs in the cloud at a distance of about 60 mm. from the distributor plate, i.e. outside the dense phase of the bed. As far as the effect of the fluidizing velocity is concerned, the well-known phenomenon that the heat transfer coefficient rises with fluidizing velocity, attaining a maximum after a certain velocity ($U_{opt.}$) is reached, is clearly shown. The difference between the two cases (bare tube and spherical probe) is that there is less scatter of the data points with the sperical probe than with the bare tube. This may be attributed to the fact that less sources of error, which could have only been in the temperature recorder, than those associated with the bare tube. This leads to $U_{opt.}$ being identified more easily by using the spherical probe.

Quantitatively, the two sets of results are in close agreement as well. In figure (6.6) it is noticed that the heat transfer coefficients for the sphere are less than 5% lower than the bare tube data, except at the position 70 mm.

above the distributor plate where the object is virtually in the airstream and very few particles are thrown up to make contact with it. At this position, it is probable that more particles per unit surface area are likely to hit the bare tube than the sphere because of the larger surface area of the tube being exposed across the flow of the air. In Figure (6.7), however, the rising part of the curve for the sphere is about 7% lower than the corresponding part for the tube, while at the flat portion, the two curves are within 1% of each other.

On the whole, the sphere results were found to be more reproducible than those of the tube, which can be attributed to the fact (as mentioned earlier) that less sources of error are encountered with the spherical probe.

It may be concluded that the sperical probe offers a simple and reliable method for studying heat transfer characteristics of bare tubes in fluidized beds.

To demonstrate the versatility of the probe, it was used to carry out a check on heat transfer coefficients obtained at different points along the bed. This test was carried out with the probe located 30 mm. above the distributor plate at a fluidizing velocity of 0.252 m/sec. The results are presented in Figure (6.8). The main observation is that the coefficient values on the left hand side of the bed are higher than on the right hand side (with a maximum dispersion of about 4%) which was, probably, because of the existence of a temperature

gradient in the horizontal direction along the bed giving about $5^{o}C$ temperature difference along the bed, with the lowest temperature on the right hand side. The temperature gradient was thought to be due to heat losses in the air duct.

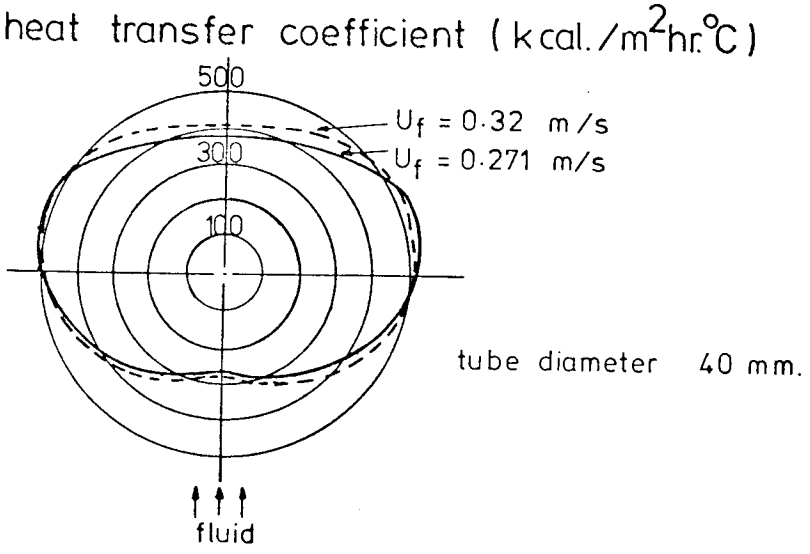

FIG. (6·1) LOCAL HEAT TRANSFER COEFFICIENTS FROM HORIZONTAL TUBES
[Gelperin et al (in 7)]

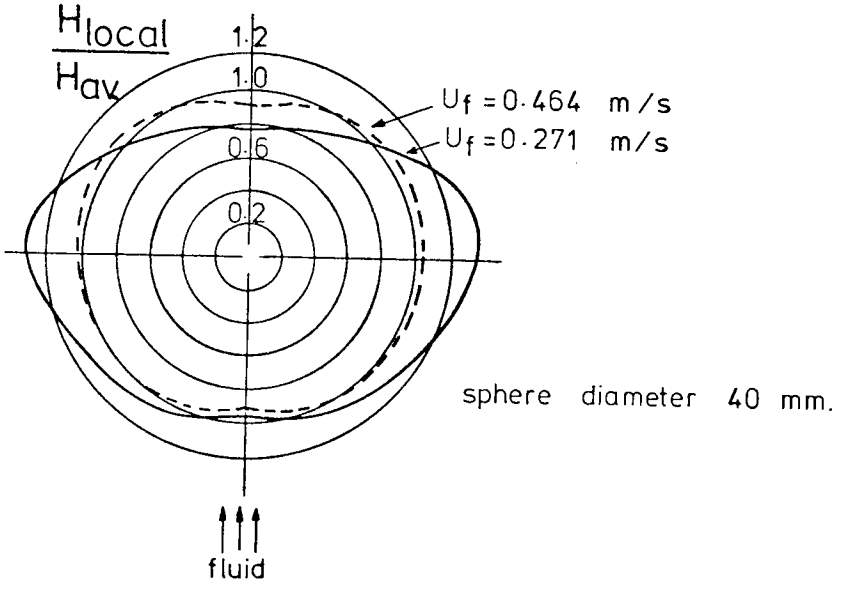

FIG. (6·2) LOCAL HEAT TRANSFER COEFFICIENTS FOR A SPHERE
[Baskakov et al. (55)]

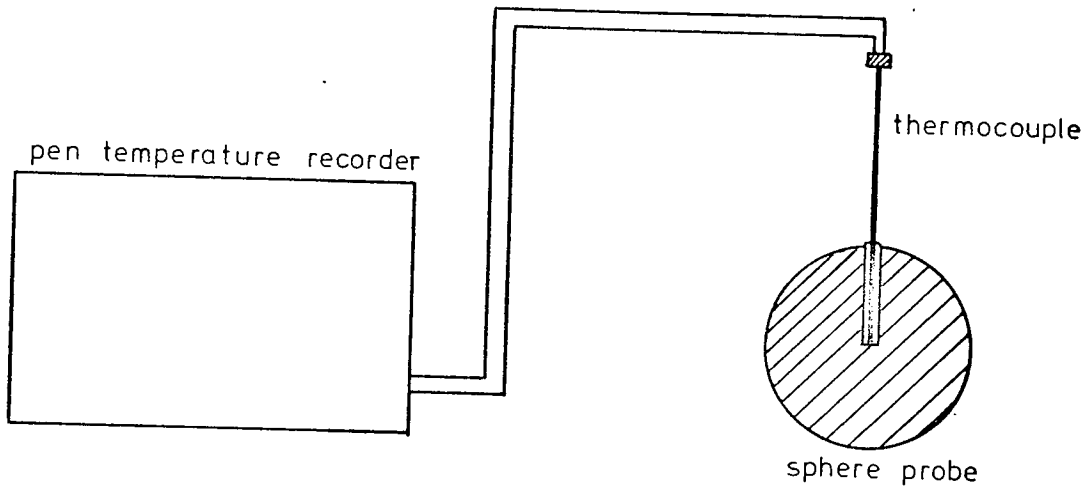

FIG. (6.3) ARRANGEMENT OF THE SPHERE PROBE

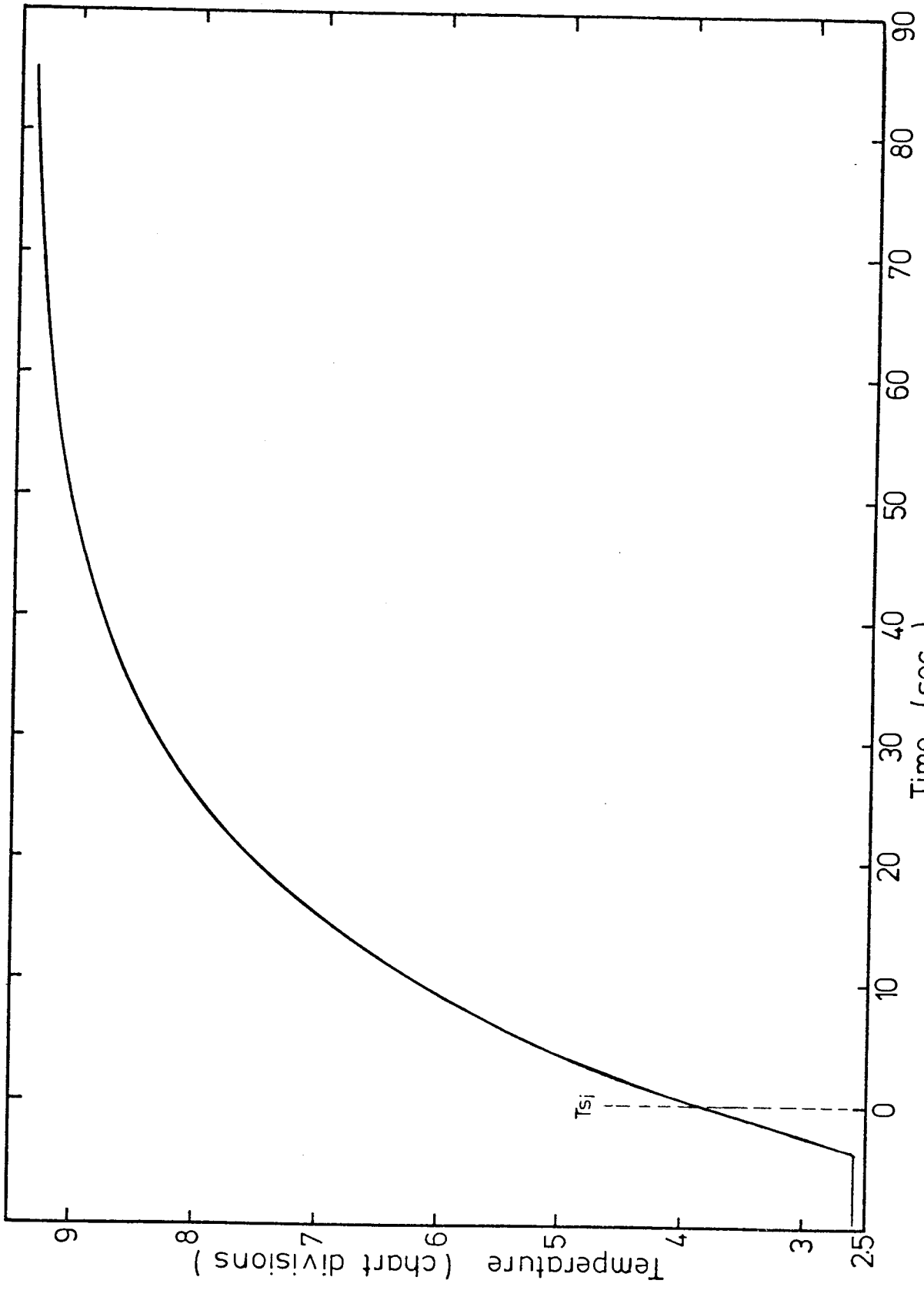

FIG.(6.4) TYPICAL TEMPERATURE TRACE OF THE SPHERE PROBE

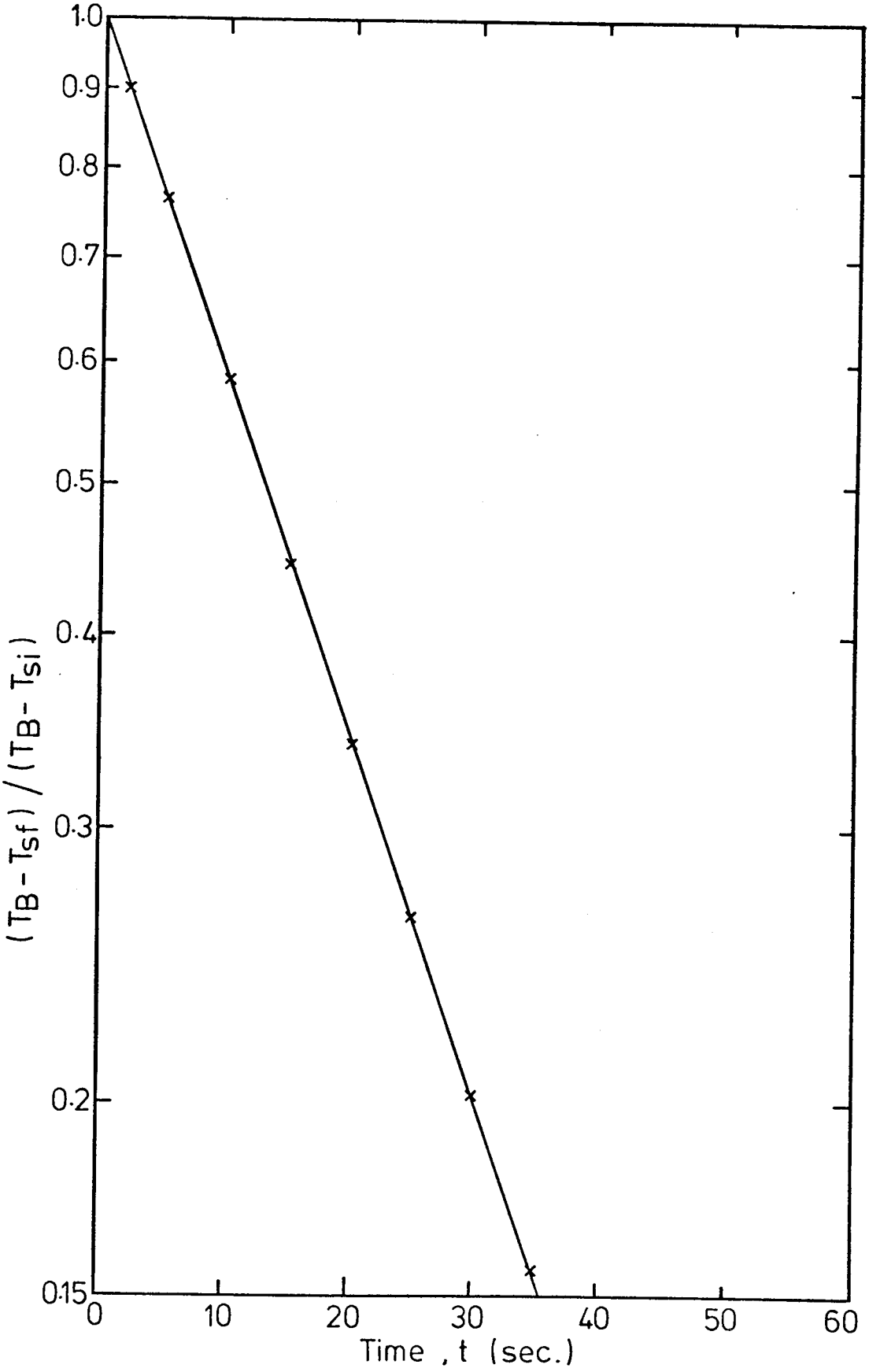

FIG.(6.5) TYPICAL LOG-LIN. PLOT FOR THE SPHERE PROBE

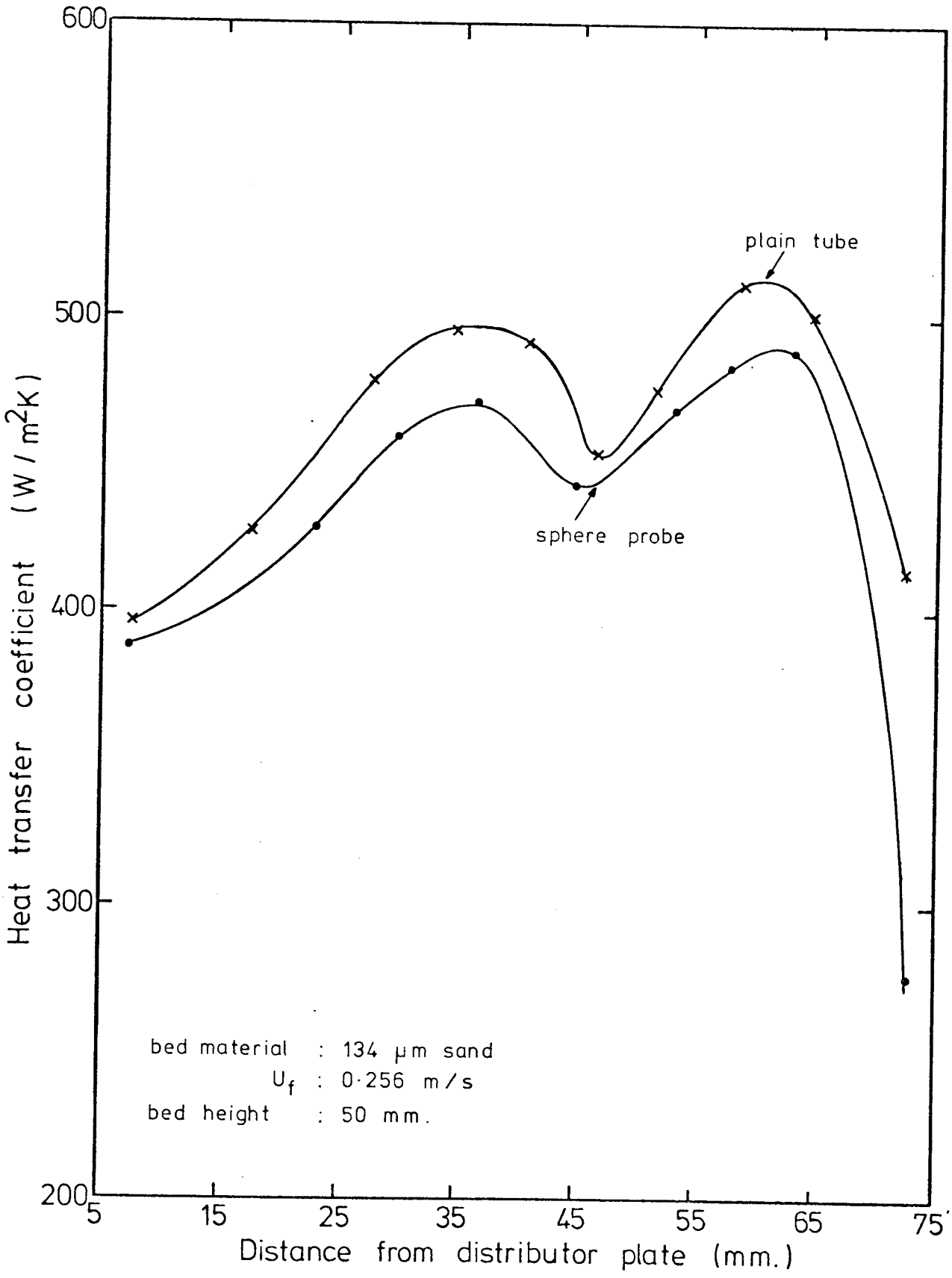

FIG. (6·6) COMPARISON BETWEEN SPHERE AND PLAIN TUBE RESULTS

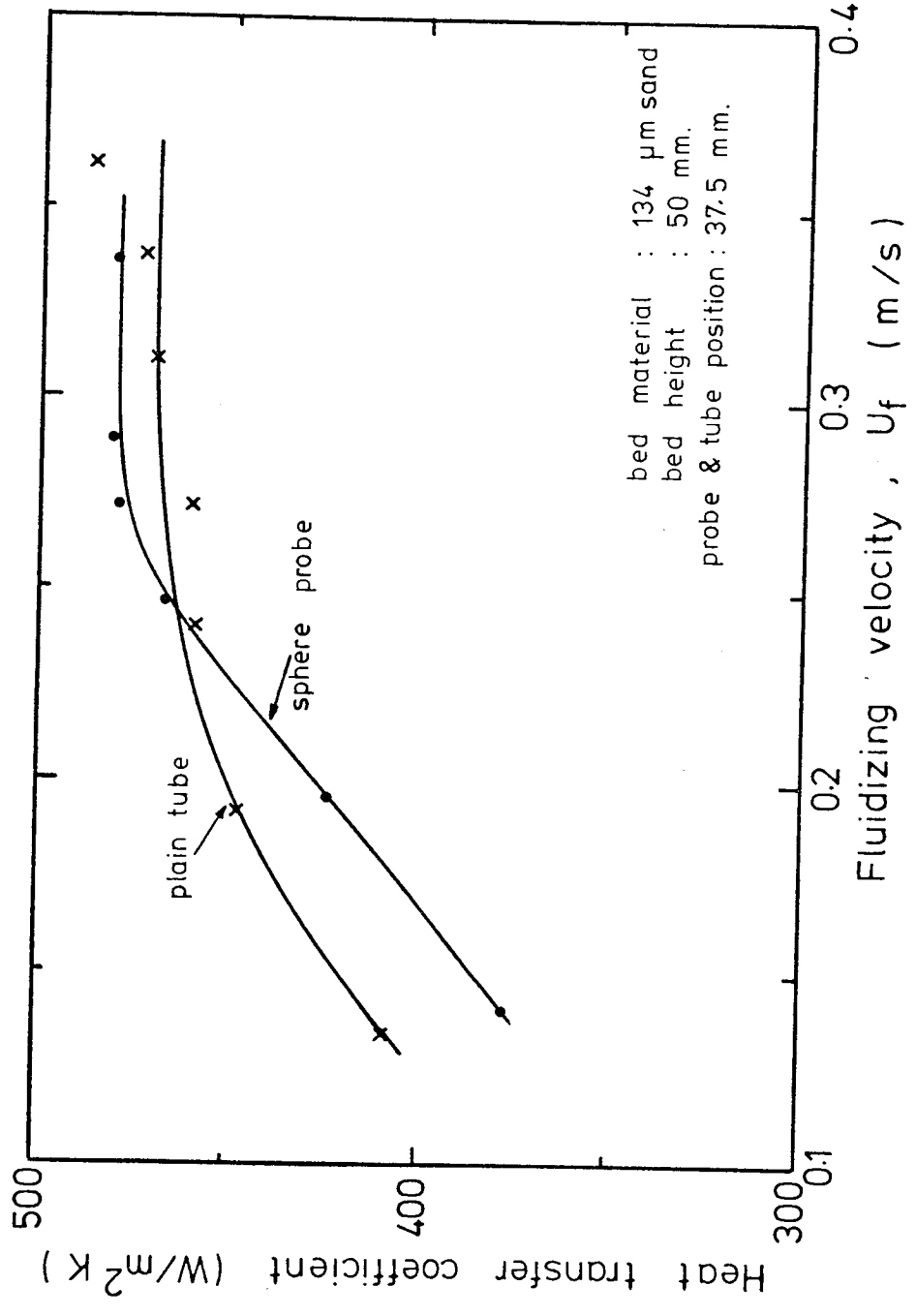

FIG. (6.7) COMPARISON BETWEEN SPHERE AND PLAIN TUBE RESULTS

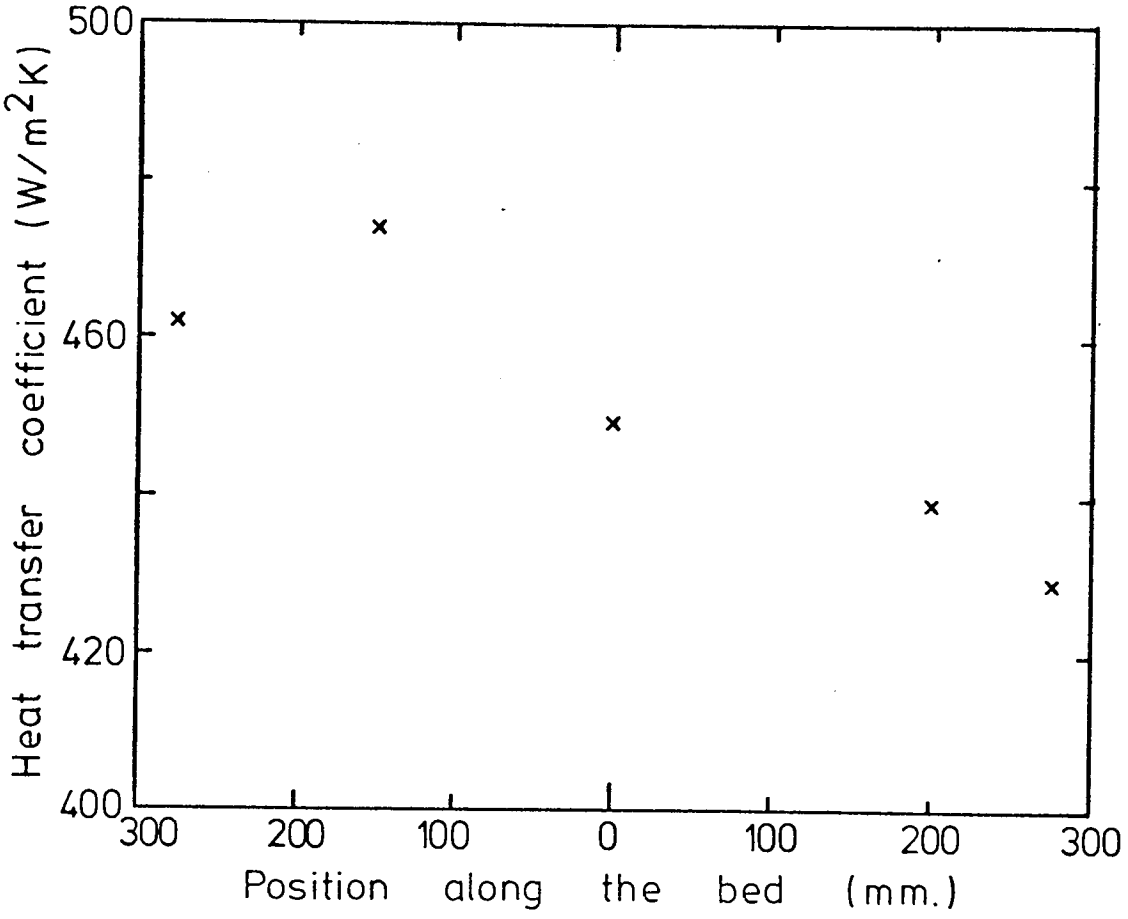

FIG. (6.8) HEAT TRANSFER COEFFICIENT AT POINTS ALONG THE BED

CHAPTER 7

USE OF NON-CONDUCTIVE FINS

USE OF NON-CONDUCTIVE FINS

7.1 Introduction

When the fins are fitted on to a tube to increase the heat transfer area, it is expected that the heat transfer coefficient for the whole system, when calculated on the basis of the total area, will be less than that of the bare tube alone because of the presence of the resistance to heat flow in the fins themselves.

In a fluidized bed, the heat transferred to an immersed object is governed by the particle motion and circulation which dictates the residence time of the particles at the heat transfer surface.

Hence, when finned tubes are used in fluidized beds, the movement of particles between the fins and their interaction with the centre tube is a major factor influencing heat transfer. This poses the following question:- Would the movement of particles between the fins be affected in such a way that the heat transferred at the centre tube is influenced directly?

The work described in this chapter was carried out to investigate this question. The general idea was that non-conductive fins were used on a tube whose dimensions were the same as the tube used for the bare tube investigation. The heat transfer coefficients obtained were compared with those obtained with the bare tube.

7.2 Description of the system

In Figure (7.1) the general arrangement of the non-conductive fins is given. The circular fins were made of perspex 3mm. thick and 24mm. high. They were firstly force-fitted on the tube (which was of 15mm. diameter) and then the end two fins were fixed on to the tube with an adhesive (Araldite) after the fins were spaced at 3mm. intervals. To hold the fins together firmly, a groove was machined at the edge of all of them (as shown in Figure (7.1)) and a strip of perspex was fixed in the groove with an adhesive.

The main test rig (described in Chapter 4) was used for this investigation.

7.3 Experiments carried out and results

A short series of tests was carried out using three different bed materials which were:

1. Silica sand of average size 134 μm
2. Silica sand of average size 253 μm
3. Blown alumina of average size 1100 μm

Since this investigation was solely intended to establish the effect of the presence of the fins on the heat transfer coefficient at the centre tube, all three tests were done using the one test element made with the fin spacing at 3mm.

With each bed material used, the test element was placed at the position where the heat transfer coefficient

of the bare tube attained a maximum value within the limit of the unfluidized bed depth. This position was the same place where the bare tube had been positioned for the tests mentioned in Section (5.5.3).

The results of this investigation are presented in Figures (7.2), (7.3) and (7.4) for the three bed materials mentioned above respectively.

7.4 Discussion

Computation of the results of this investigation was done in exactly the same manner as that adopted for the bare tube work (Chapter 5). The only exception was that the calibration of the heat transfer coefficient at the inside of the tube carried out for the bare tube investigation was used in the present work to evaluate the bed-to-tube heat transfer coefficient.

The area of tube, used for calculating the heat transfer coefficient, was that exposed to the bed only, which was approximately half that of the equivalent bare tube.

The water flow rates used were less than those for the bare tube because of the smaller heat rates involved. This led to smaller temperature rises for the same flow. The procedure adopted was to reduce the flow rate until the water temperature rise was of the same order of magnitude as that associated with the bare tube. The reason for this procedure was that inaccuracies in water temperature measurement was the major source of error in the experiments

leading to significant error in the computed heat transfer coefficient. It was, therefore, intended that the percentage error in the temperature rise should be kept to the same order of magnitude as that associated with the bare tube investigations.

In looking through the results in Figures (7.2), (7.3) and (7.4), the following observations can be made.

1. The presence of fins increases the heat transfer coefficient on the centre tube.
2. The heat transfer coefficient exhibits the same trend with the fluidizing velocity, i.e. it rises at diminishing rate becoming asymptotic to a maximum value.
3. The maximum heat transfer coefficient is attained at a slightly higher fluidizing velocity than that attained with the bare tube.

The major feature of these results is a significant rise in the heat transfer coefficient especially in the case of the 1100 μm spherical blown alumina where H_{BM} nearly doubled in spite of the fact that the fin spacing/particle size ratio was less than 3:1. This feature will be discussed in greater detail in chapter (9) together with the other finned tube results since it became apparent later that particle shape and its interaction with the surface was a very important factor.

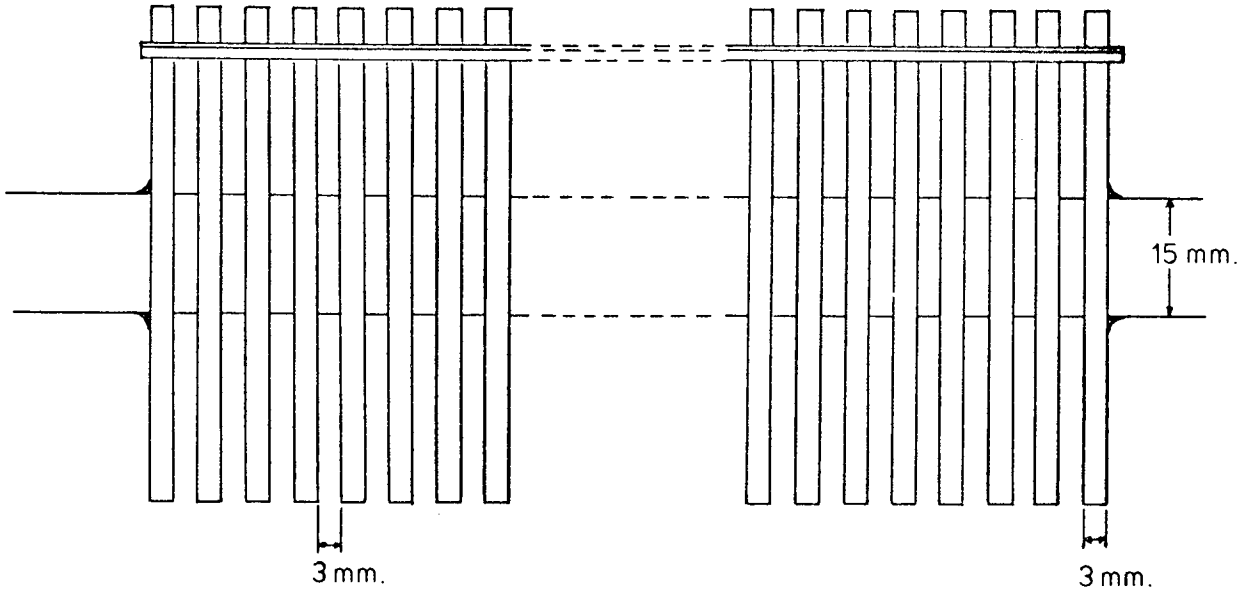

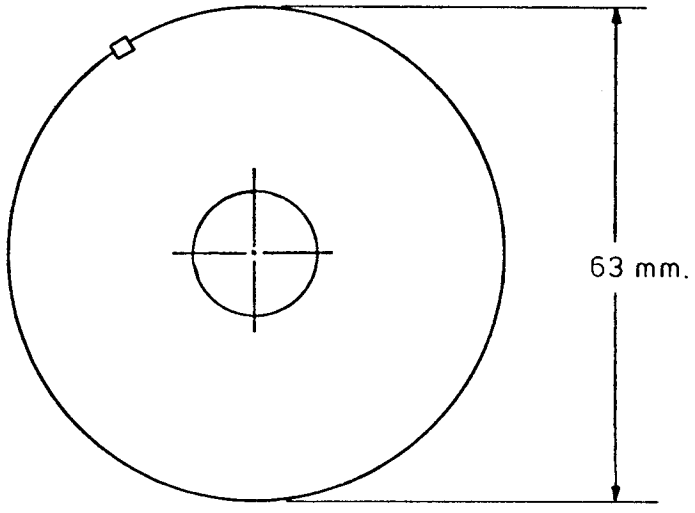

FIG. (7·1) ARRANGEMENT OF NON-CONDUCTIVE FINS

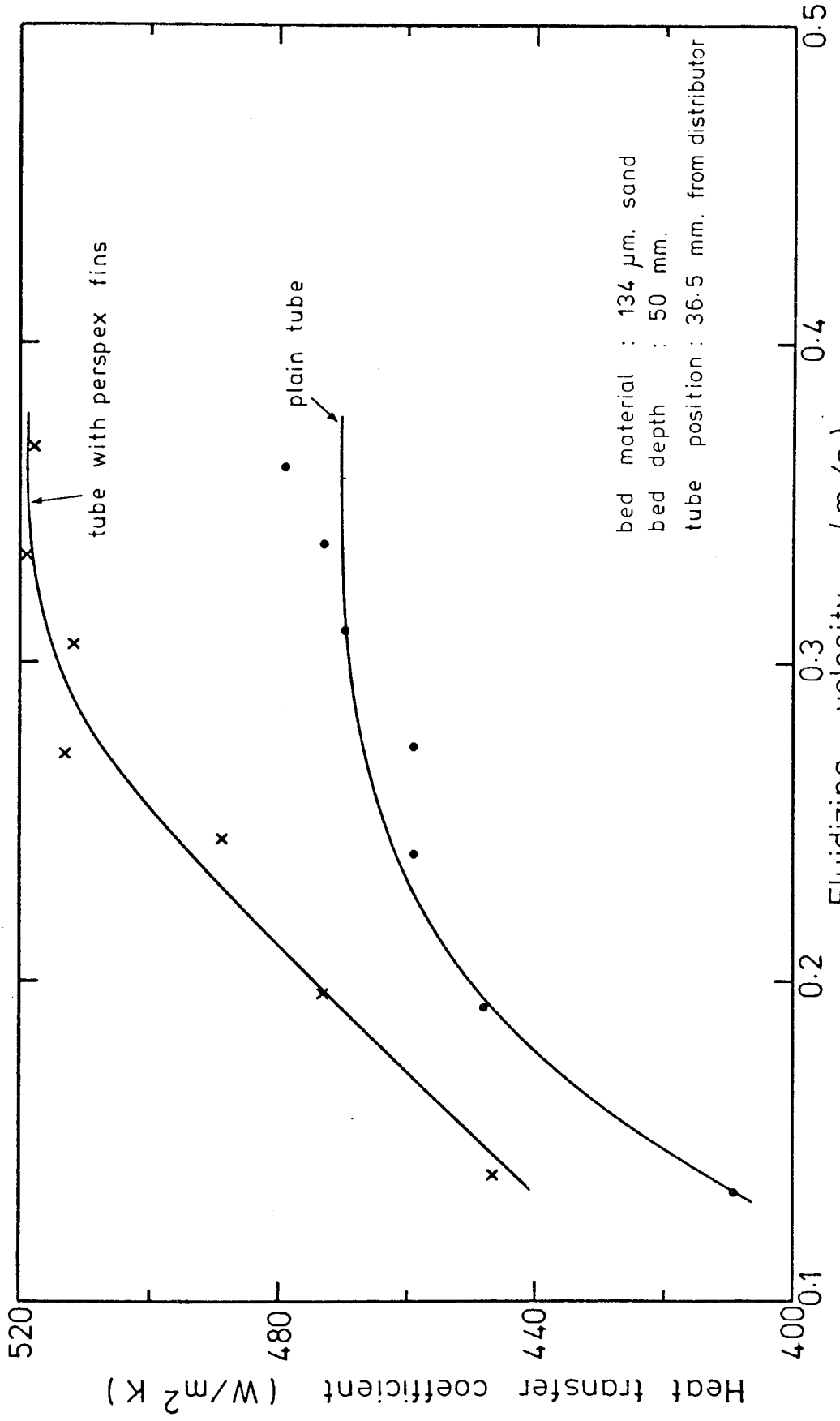

FIG. (7.2) COMPARISON OF PERFORMANCE OF TUBE WITH PERSPEX FINS WITH PLAIN TUBE

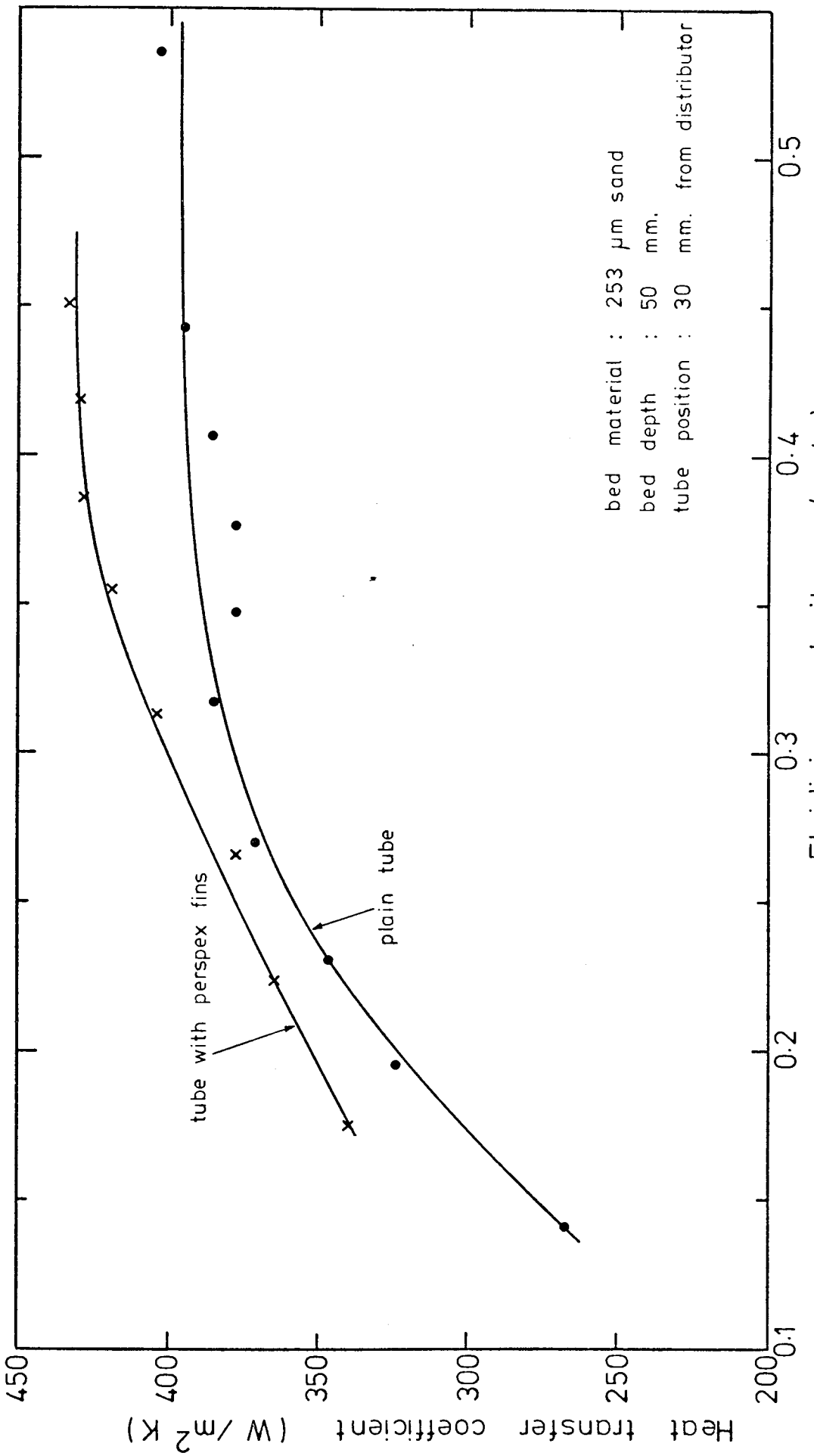

FIG. (7.3) COMPARISON OF PERFORMANCE OF TUBE WITH PERSPEX FINS WITH PLAIN TUBE

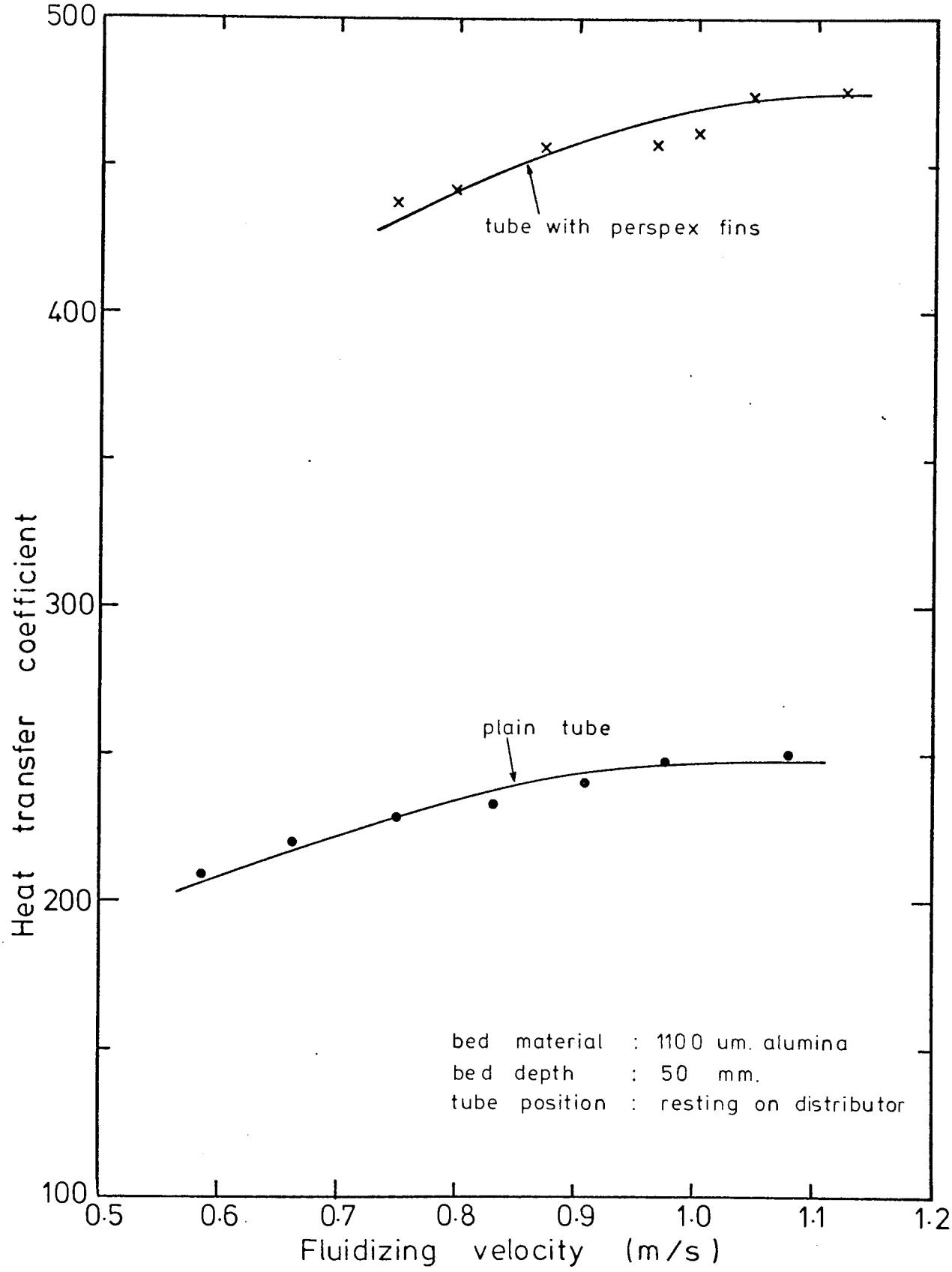

FIG. (7.4) COMPARISON OF PERFORMANCE OF TUBE WITH PERSPEX FINS WITH PLAIN TUBE

CHAPTER 8

FINNED TUBE WORK

FINNED TUBE WORK

8.1 Introduction

The work described in this chapter was carried out to study the performance of finned tubes in a shallow bed (maximum unfluidized height 50 mm.) with particular attention being paid to the position of the tube and the effect of fin spacing.

The issue of tube position was investigated because of the marked effect the position had on the plain tube results (presented in chapter 5) and it was thought that a comparison would be fruitful. Furthermore, Atkinson [2] reported that tube position did show some effect when square fins were used and in particular higher heat transfer coefficients were obtained with the finned tube resting on the distributor.

Fin spacing is naturally expected to be a major factor in optimizing the heat transfer performance of finned tubes in fluidized beds. For good heat transfer the particles must be able to penetrate between the fins quite freely so that no gas "pockets" or packed solids result and maximum contact between solids and surface is achieved.

Other fin variables (namely height and thickness) were thought to be mainly geometrical factors and their influence could be evaluated from previous work on fins (such as Gardner [47]). Although fin height might take part in the

interaction with solids movement and influence the performance it was thought that the effect would not be large compared to that of the spacing.

8.2 Evaluation of the heat transfer coefficient

The test rig used for these finned tubes experiments was that used previously for the plain tube tests which is presented in chapter 4. The measurements that were taken for evaluating the heat transfer coefficient were

1. water flow inside the tube
2. water temperature at inlet and outlet of the tube
3. bed temperature

The principle adopted to present the bed-to-surface heat transfer coefficient (H_{BM}), was to use the water-to-bed overall heat transfer coefficient (Hov.), based on the total external area of the finned tube, and the inside heat transfer coefficient (water-to-tube (Hi)) based on the inside area of the tube. The procedure employed was as follows:

1. The overall heat transfer coefficient (Hov.) was computed using the equation

$$\text{Hov.} = \frac{Q}{A_T \text{ X LMTD}} \qquad (8.1)$$

Q is the heat flux and was calculated from the equation

$$Q = W \text{ X } C_w \text{ X } (Tw_o - Tw_i) \qquad (8.2)$$

A_T is the total surface area of the finned tube and is given by

$$A_T = \pi\left(\frac{D_f^2 - D_t^2}{4} \times 2 \times n + (n-1)D_t S\right) \qquad (8.3)$$

where n is the number of fins and S is the fin spacing.

The Log-mean temperature was used (as for the case of plain tubes) because of the temperature variation in the bed, and is given by

$$LMTD = \frac{(T_{b_1} - T_{wo}) - (T_{b_4} - T_{wi})}{\ln\left(\frac{T_b - T_{wo}}{T_{b_4} - T_{wi}}\right)} \qquad (8.4)$$

2. The inside heat transfer coefficient (Hi) was evaluated using the Dittus-Boelter equation

$$Nu = 0.023\ Pr^{0.4} Re^{0.8} \qquad (8.5)$$

which was quite valid since the water flow rates used gave Re values in excess of 10000 (approximately 20000) which is the condition specified for using the equation [53].

3. The bed-to-surface heat transfer coefficient (H_{BM}) was then calculated using the relationship

$$\frac{1}{Hov.\ A_T} = \frac{1}{H_i A_i} + \frac{1}{H_{BM}\ A_{eff}} \qquad (8.6)$$

where A_{eff} is the effective area and is given by

A_{eff} = bare tube area between the fins + effective fins area which is written as

$$A_{eff} = \pi \left((n-1)S\, D_t + \left(\frac{D_f^2 - D_t^2}{2}\right) n\, \emptyset\right) \qquad (8.7)$$

where $\emptyset$ is the fin efficienty which is included to account for the resistance of the fins. The derivation of equation (8.6) is given in appendix (8). As the effective area depends on the value of the fin efficiency ($\emptyset$) which in turn depends on the heat transfer coefficient (H_{BM}) (see equation (3.10)), an iterative process was necessary for calculating H_{BM}. This was carried out with the aid of a programable calculator (HP9830) using "BASIC" as the programme language. The initial value of H_{BM} taken for the iteration was assumed to be the value of Hov. A detailed explanation of the iteration process together with the flow diagram of the programme are provided in appendix (8).

8.3 The finned tubes

The elements used for all the experiments were manufactured in the laboratory. They were made of copper (approximately 1.6mm) thick, with an outside diameter of 44 mm. The basic tube was also a copper one with 15 mm. outside diameter, which meant that the fin height was 14.5mm. According to the theoretical analysis

(chapter 3), the fin height chosen was reasonable since its efficiency would be quite high (figure 3.4) while maintaining a high effectiveness (figure 3.5). Three values of the fin spacing were chosen 2mm., 3mm., and 5mm. which gave a wide range of values of spacing-to-particle size ratios to be investigated.

The choice of the length of the test elements was made keeping in view the following

1. Saving time and material in fabricating the elements
2. Obtaining a reasonable water temperature rise
3. The error in the heat transfer coefficient would be of reasonable proportion.

For the latter an error analysis was made to evaluate approximately the expected error in H_{BM} due to the errors expected in the water temperatures in relation to the number of fins.

Equations (8.1) and (8.2) yield an expression for Hov. as

$$Hov. = \frac{W \ C_{pw}}{A_T} \left[\frac{\Delta T_w}{\Delta T_{BW}}\right] \qquad (8.8)$$

where ΔT_w and ΔT_{BW} are the water temperature rise and the "LMTD" respectively.

From equation (8.6) an expression was obtained for H_{BM} as

$$H_{BM} = \frac{Hov.\ A_T H_i A_i}{A_{eff}(H_i A_i - Hov.A_T)} \qquad (8.9)$$

The error in H_{BM} due to an error in Hov was calculated from the expression

$$\frac{\delta H_{BM}}{H_{BM}} = \frac{H_i A_i A_T}{A_{eff.}(H_i A_i - Hov.A_T)} \times \frac{\delta Hov.}{Hov.} \qquad (8.10)$$

which was obtained on the principle outlined in the error analysis for the plain tube work (chapter 5). From equation (8.8), it can be noticed that the error in Hov. is equivalent to that in ΔT_w if the assumption is made that the other quantities constitute no sources of error. Consequently expression (8.10) becomes

$$\frac{\delta H_{BM}}{H_{BM}} = \frac{H_i A_i A_T}{A_{eff.}(H_i A_i - Hov.A_T)} \times \frac{\delta(\Delta T_w)}{\Delta T_w} \qquad (8.11)$$

Combining equations (8.11) and (8.9), we get

$$\frac{\delta H_{BM}}{H_{BM}} = \frac{H_{BM} A_{eff.}}{Hov.\ A_T} \times \frac{\delta(\Delta T_w)}{(\Delta T_w)} \qquad (8.12)$$

in which $(Hov.A_T)$ was then substituted from (8.8)

to give

$$\frac{\delta H_{BM}}{H_{BM}} = \frac{H_{BM} A_{eff.} \Delta T_{Bw}}{W C_w \Delta T_w} \times \frac{\delta(\Delta T_w)}{\Delta T_w} \qquad (8.13)$$

To evaluate ΔT_w equations (8.8) and (8.6) were combined to give

$$\Delta T_w = \frac{H_i A_i H_{BM} A_{eff.} \Delta T_{BM}}{W C_w (H_{BM} A_{eff.} + H_i A_i)} \qquad (8.14)$$

The error analysis was carried out, evaluating ΔT_w first for values of H_{BM} varying between 100 and 500 W/m^2k. The area $A_{eff.}$ was evaluated from the expression

$$A_{eff.} = \pi [D_t(1-n^*t) + \frac{\emptyset n^*}{2} (D_f^2 - D_t^2)] \qquad (8.15)$$

where t is the fin thickness and n* is the number of fins per metre length of tube. The values of $\emptyset$ were calculated from equation (3.10) (Chapter 3) for each value of the heat transfer coefficient used.

The flow of water was assumed to give Re=20000 from which H_i was evaluated using equation (8.5) and ΔT_{BW} was taken as 85^oC.

The result of the error analysis is presented in figure (8.1) using values of n* 50 to 300 fins/metre for a tube length of 100 mm. For the spacings chosen 2,3 and 5mm. the corresponding numbers of fins per metre were approximately 279, 219 and 153 which meant that the expected error, would not be greater than 9% even at a low value of 100 W/m^2K. It was therefore decided that the elements were to be approximately 100 mm. long since all the conditions stated previously have been satisfied. A photograph of the elements can be seen in figure (8.2).

8.4 Bed materials

Four bed materials were used for the finned tube tests, three of the materials were the same ones used for the bare tube tests, namely sand of size ranges 200-300 μm and 300-400 μm, and alumina of size range 1000-1200 μm. The fourth one was a new quantity of sand of size range 100-200 μm which was supplied from a different source.

The properties of the bed materials were determined as explained in appendix (6) and are shown in table (8.1). The voidage for the new fine sand was also measured and was found to be the same as that for the sand of size 134 μm used for the bare tube. The values of the voidage for the bed materials are also presented in table (8.1).

8.5 Experimental results

The choice of the fin spacings of 2,3 and 5mm., together with the particle sizes used, enabled a reasonably wide range of particle size (D_p) / fin spacing(s) ratios to be employed for the investigations. These ratios, together with the number of fins for each element are shown in table (8.2).

Throughout the experiments, the bed temperature was maintained at about 100°C.

8.5.1 Variable tube position

Experiments were carried out to establish the variation of the heat transfer coefficient with the position of the tube in the bed. Three sets of experiments were conducted using different particles, different fluidizing velocities and different bed heights for the three elements of finned tubes, i.e. the fin spacing was varied throughout the tests.

8.5.1 a Variable tube position at different particle sizes

The settled bed height for these tests was kept at 50mm. The fluidizing velocity chosen for each particle size used was fixed at a value that was expected to correspond to the maximum heat transfer coefficient for the particles under test. This was done with the help of a quick scanning test varying the fluidizing velocity and locating roughly the velocity at which the heat transfer coefficient reached its maximum. All four bed materials were used in these tests.

The results of these experiments are presented in figures (8.3), (8.4), (8.5) and (8.6) corresponding to particle sizes of 151 μm, 253 μm, 345 μm and 1100 μm respectively.

8.5.1.b Variable tube position at different fluidizing Velocities

Similar to the experiments reported in section (5.5.1.b) one particle size was used for these tests and the static bed height was 50 mm. The fluidizing velocities used were 0.239 m/sec., 0.324 m/sec and 0.4 m/sec., the lowest one was to correspond to the rising region of the H-U curve.

The results obtained are shown in figures (8.7), (8.8) and (8.9) corresponding to the three fin spacings of 2,3 and 5 mm. respectively.

8.5.1.c Variable tube position for different bed heights

These experiments were carried out using the 253 μm sand as the bed material. The Fluidizing velocity was fixed at0.324 m/sec. Similar to the tests with the bare tube, the bed heights used were 50, 35 and 28 mm. The results are presented in figures (8.10), (8.11) and (8.12) for fin spacings of 2,3 and 5mm. respectively. In the "a" parts of the figures the heat transfer coefficient is seen plotted against the distance from the distributor plate while in the "b" parts the coefficient was plotted against the ratio of the distance from the distributor to the static bed height so that a relative plot was obtained to outline the effect of the bed height more clearly.

8.5.2 Variable fluidizing velocity

These experiments were carried out to determine the effect of the fluidizing velocity on the heat transfer coefficient using different particle sizes for the three finned tubes.

Based on the results reported in the previous section (8.5.1) the tubes were positioned at the bottom of the bed resting on the distributor plate, since no variation of the heat transfer coefficient was observed previously as the tube position was changed near the distributor except for the

fine sand (151 μm) which can be seen in figure (8.3). The static bed height for these tests was fixed at 50 mm.

The results are presented in figures (8.13), (8.14), (8.15) and (8.16) corresponding to particle sizes of 151μm, 253 μm, 345 μm and 1100 μm respectively.

Table - 8.1 -

Properties of bed materials for finned tubes tests

material	size (μm)	density (kg/m^3)	voidage (Emf)
silica sand	151	2660	0.481
silica sand	253	2685	0.463
silica sand	345	2709	0.44
Blown alumina	1100	1777	0.484

Table - 8.2 -

Finned tubes used for experiments

Particle size (D_p) (μm.)	fin spacing(s) / particle size (D_p) ratio		
	fin spacing 2mm. (Number of fins 28)	fin spacing 3mm. (Number of fins 22)	fin spacing 5mm (Number of fins 15)
151	13.2	19.8	33.02
253	7.9	11.9	19.8
345	5.8	8.7	14.5
1100	1.8	2.7	4.5

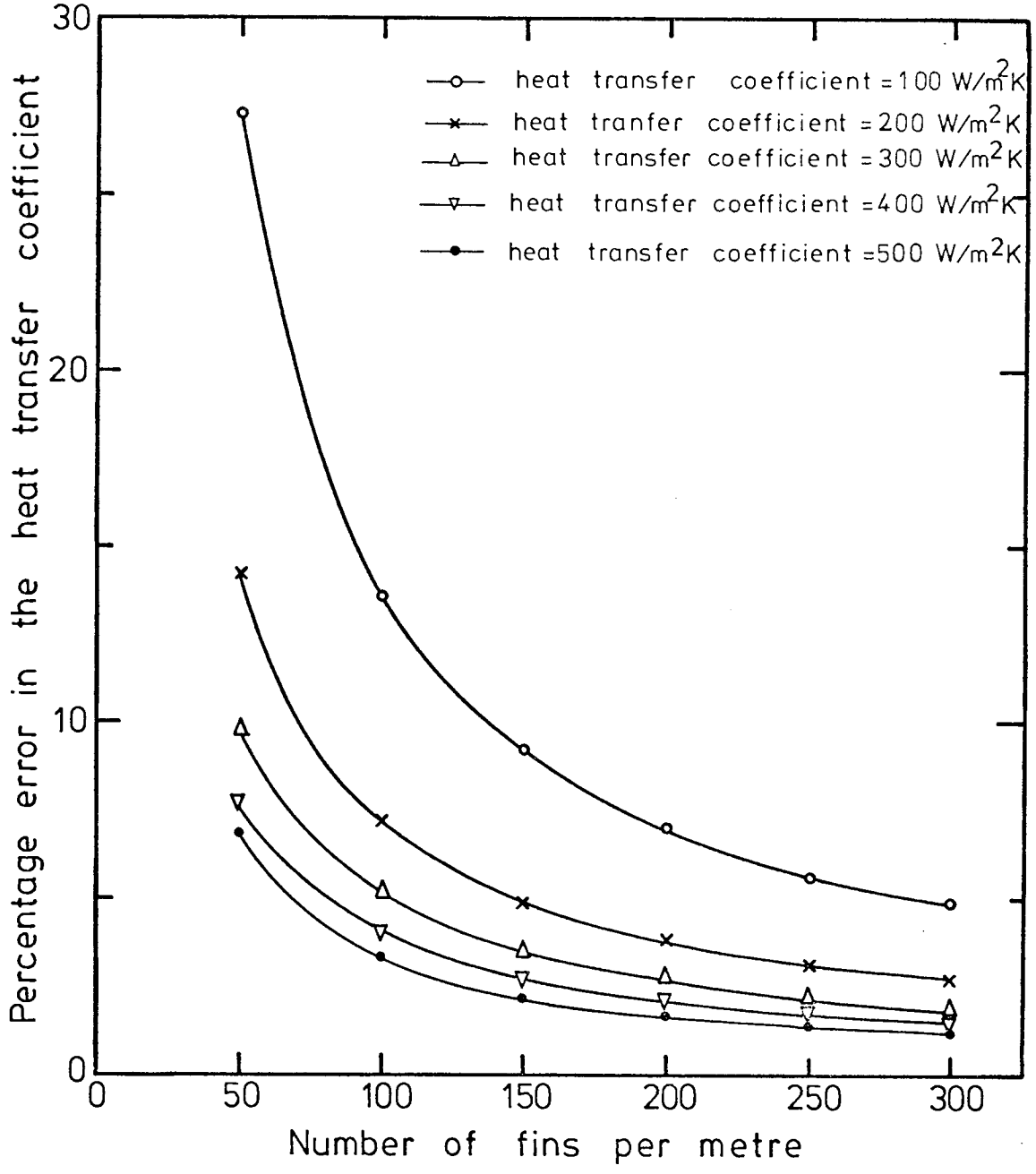

FIG. (8.1) ERROR ANALYSIS FOR A FINNED TUBE 100 mm. LONG

FIG.(8.2) THE FINNED TUBE ELEMENTS

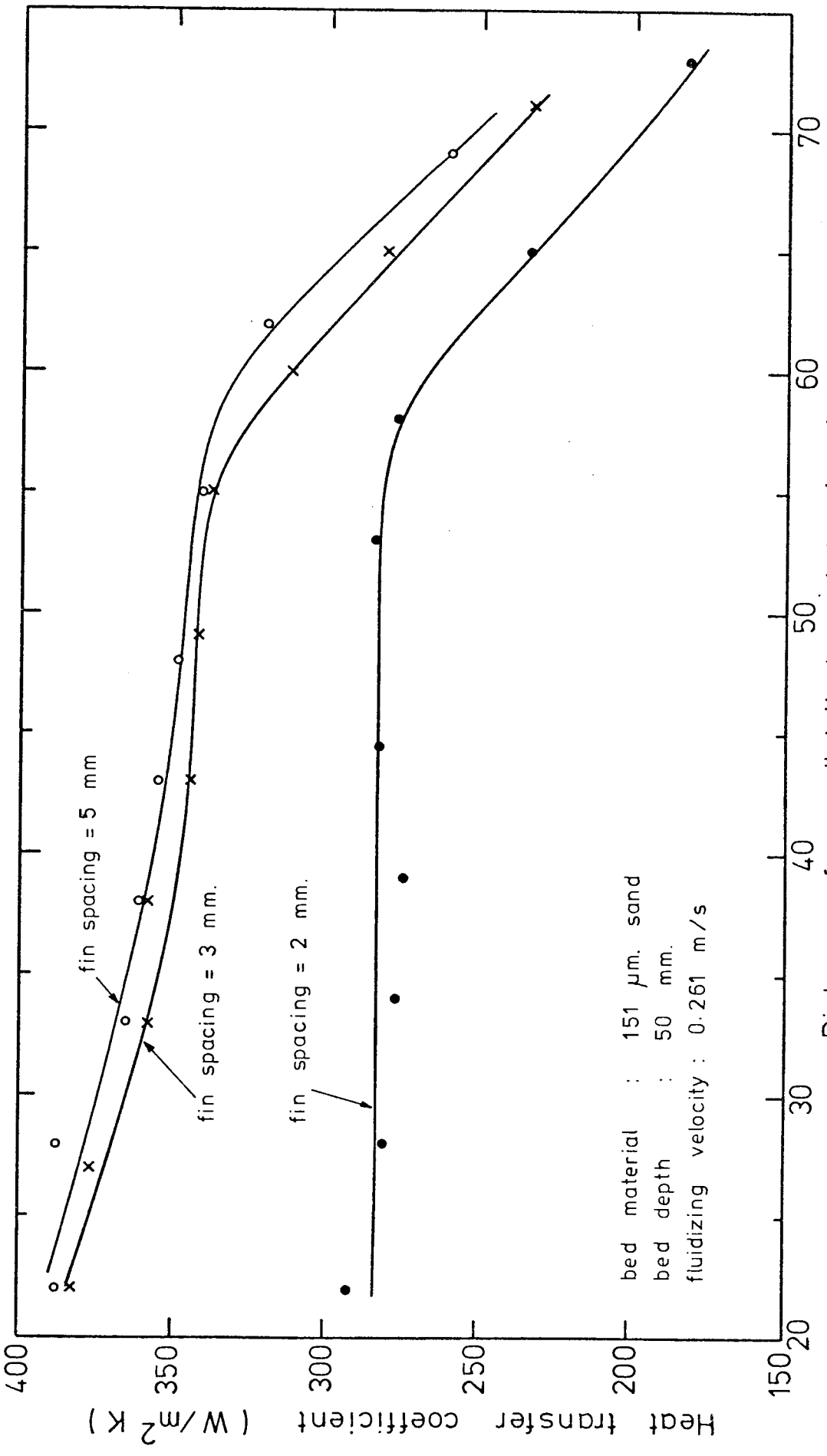

FIG. (8.3) VARIATION OF THE HEAT TRANSFER COEFFICIENT WITH TUBE POSITION FOR DIFFERENT FIN SPACINGS

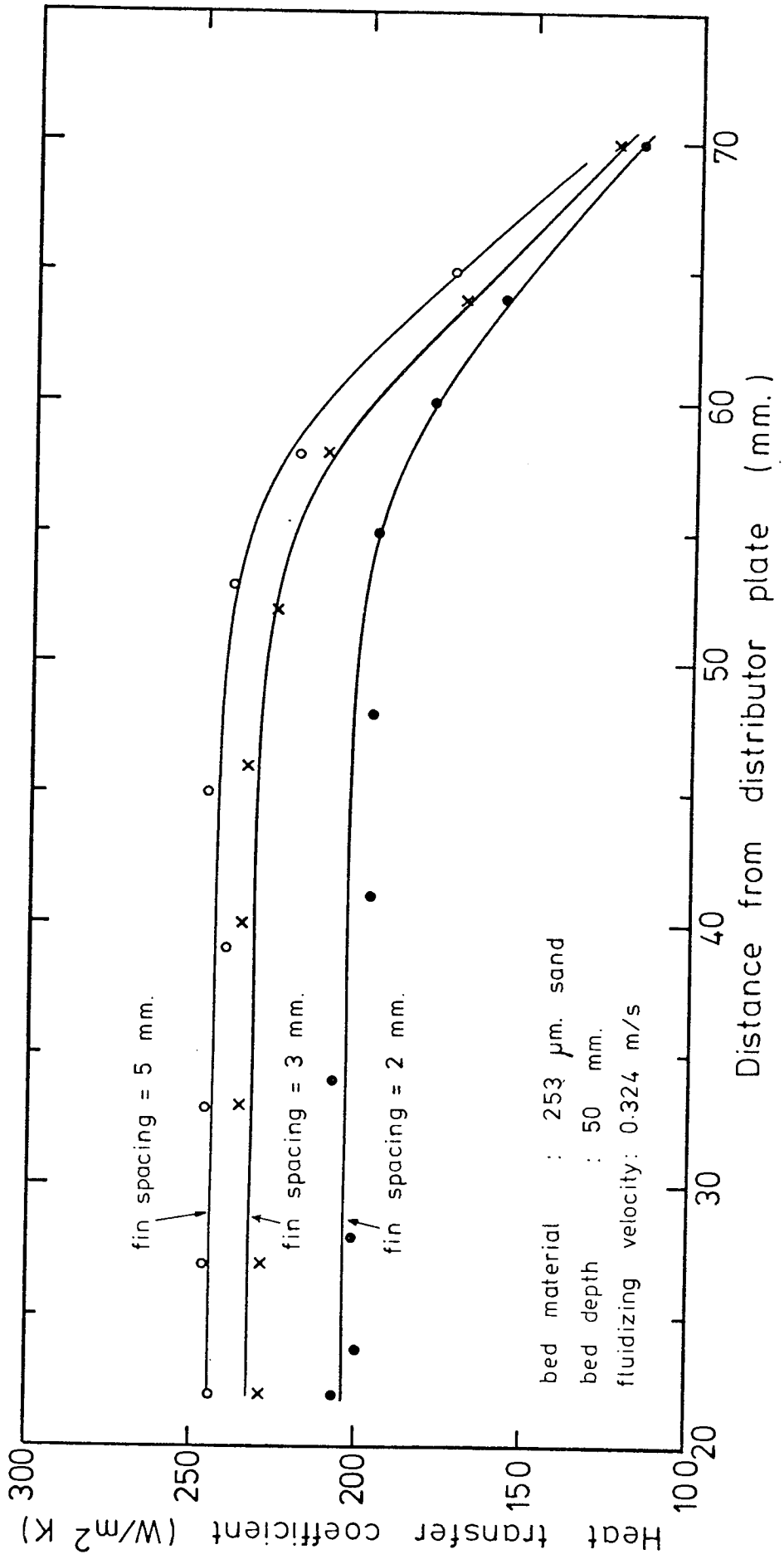

FIG. (8.4) VARIATION OF THE HEAT TRANSFER COEFFICIENT WITH TUBE POSITION FOR DIFFERENT FIN SPACINGS

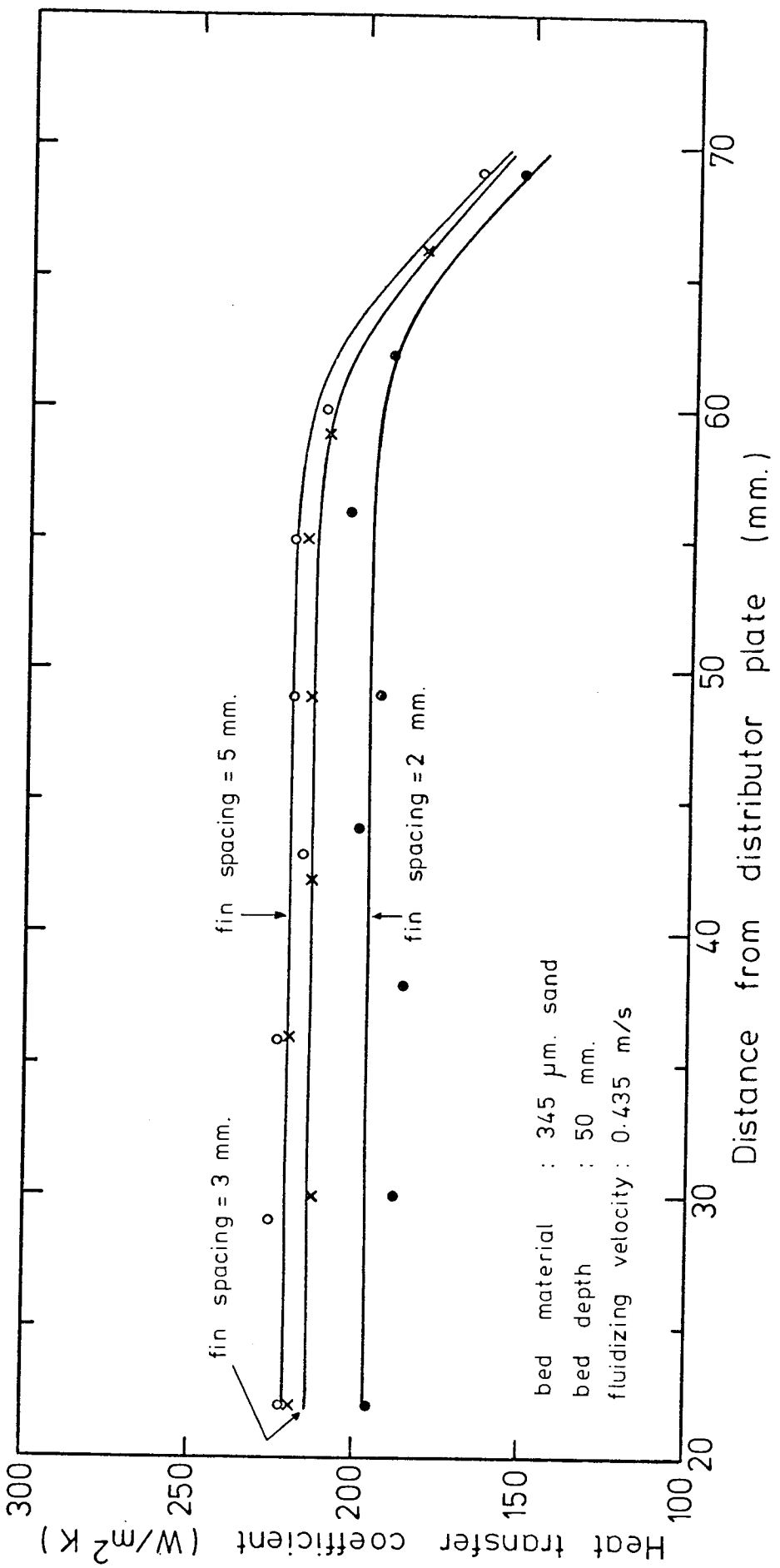

FIG. (8.5) VARIATION OF THE HEAT TRANSFER COEFFICIENT WITH TUBE POSITION FOR DIFFERENT FIN SPACINGS

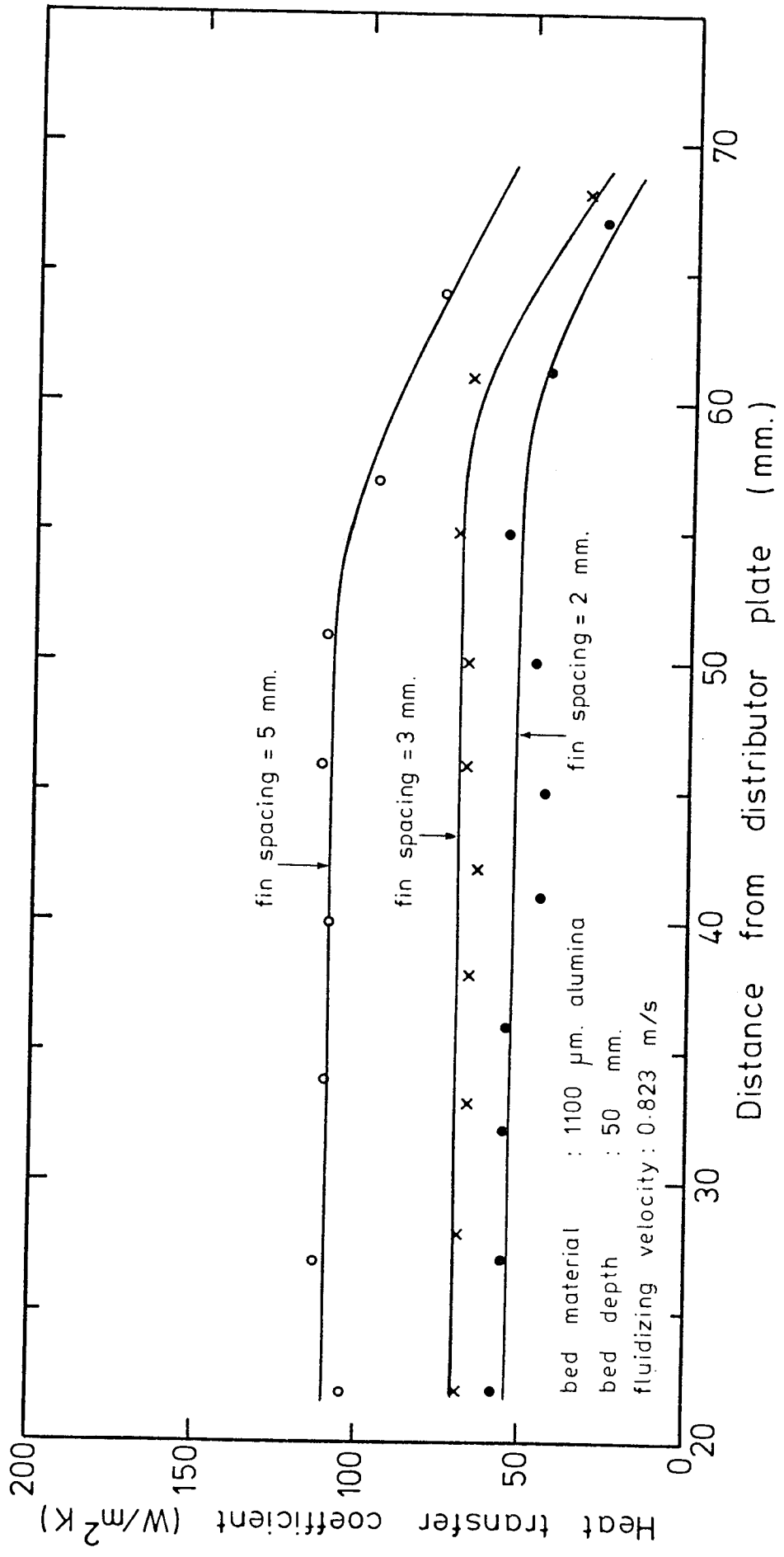

FIG. (8.6) VARIATION OF THE HEAT TRANSFER COEFFICIENT WITH TUBE POSITION FOR DIFFERENT FIN SPACINGS

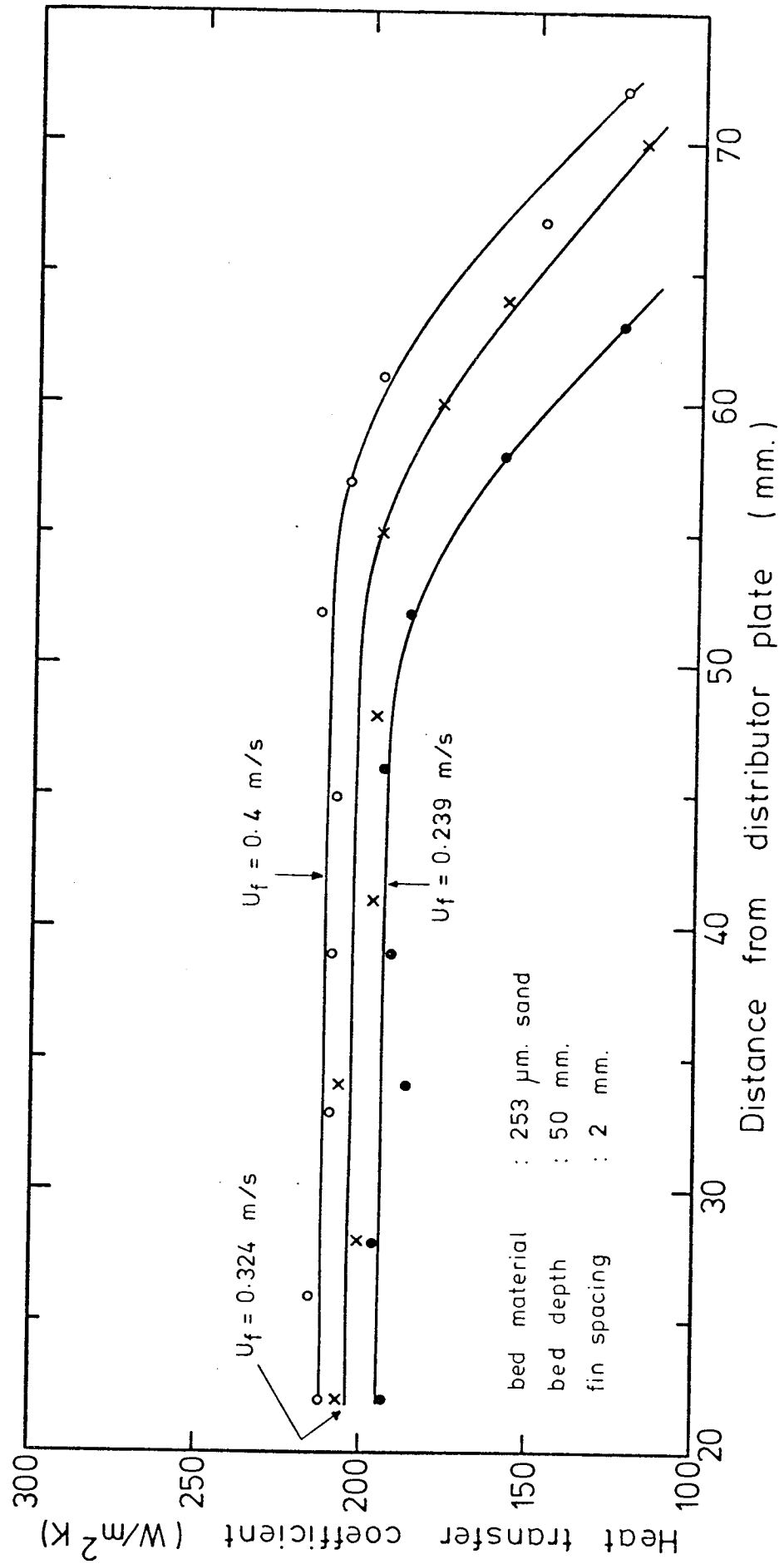

FIG. (8.7) VARIATION OF THE HEAT TRANSFER COEFFICIENT WITH TUBE POSITION AT DIFFERENT FLUIDIZING VELOCITIES

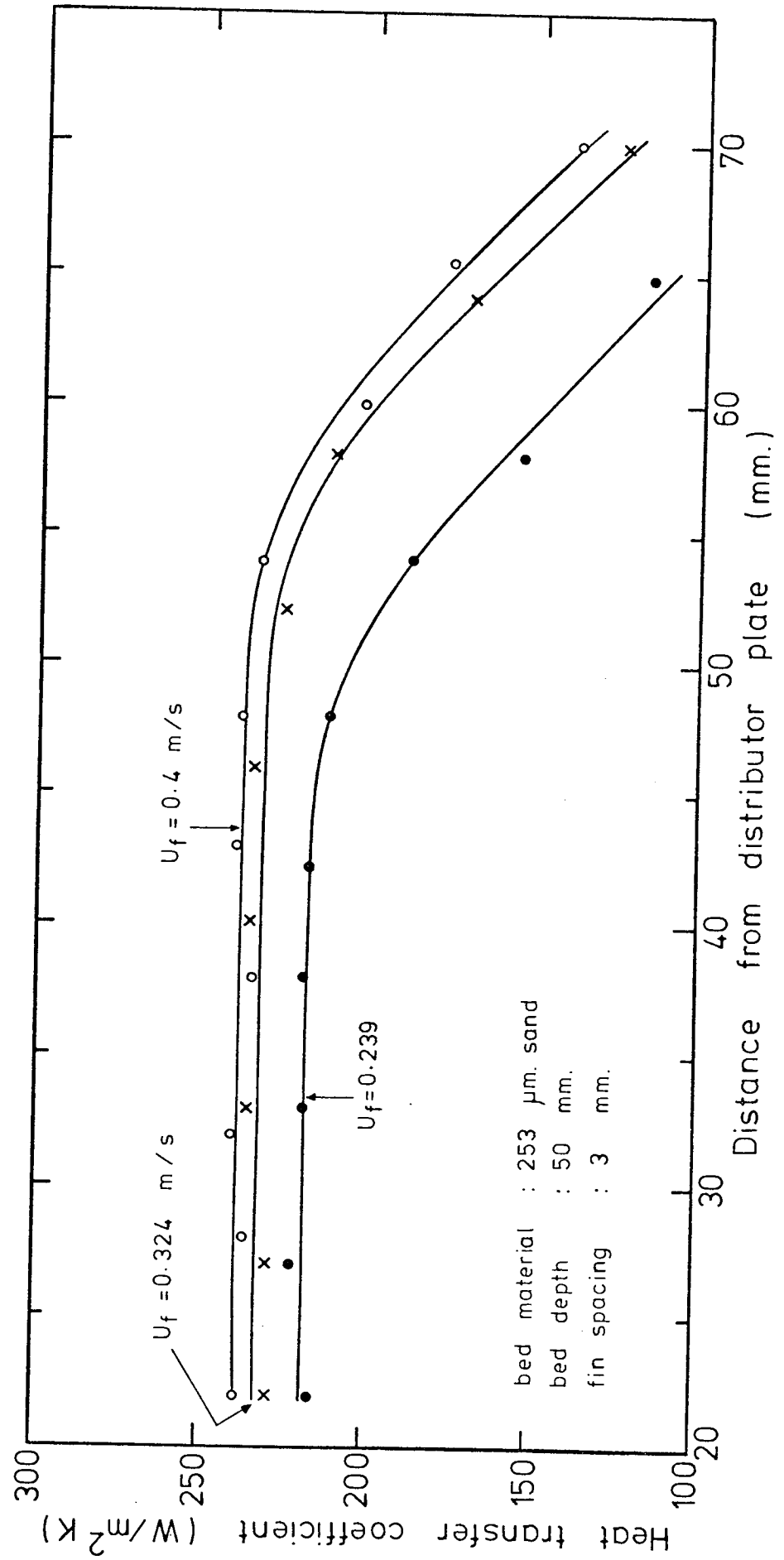

FIG. (8.8) VARIATION OF THE HEAT TRANSFER COEFFICIENT WITH TUBE POSITION AT DIFFERENT FLUIDIZING VELOCITIES

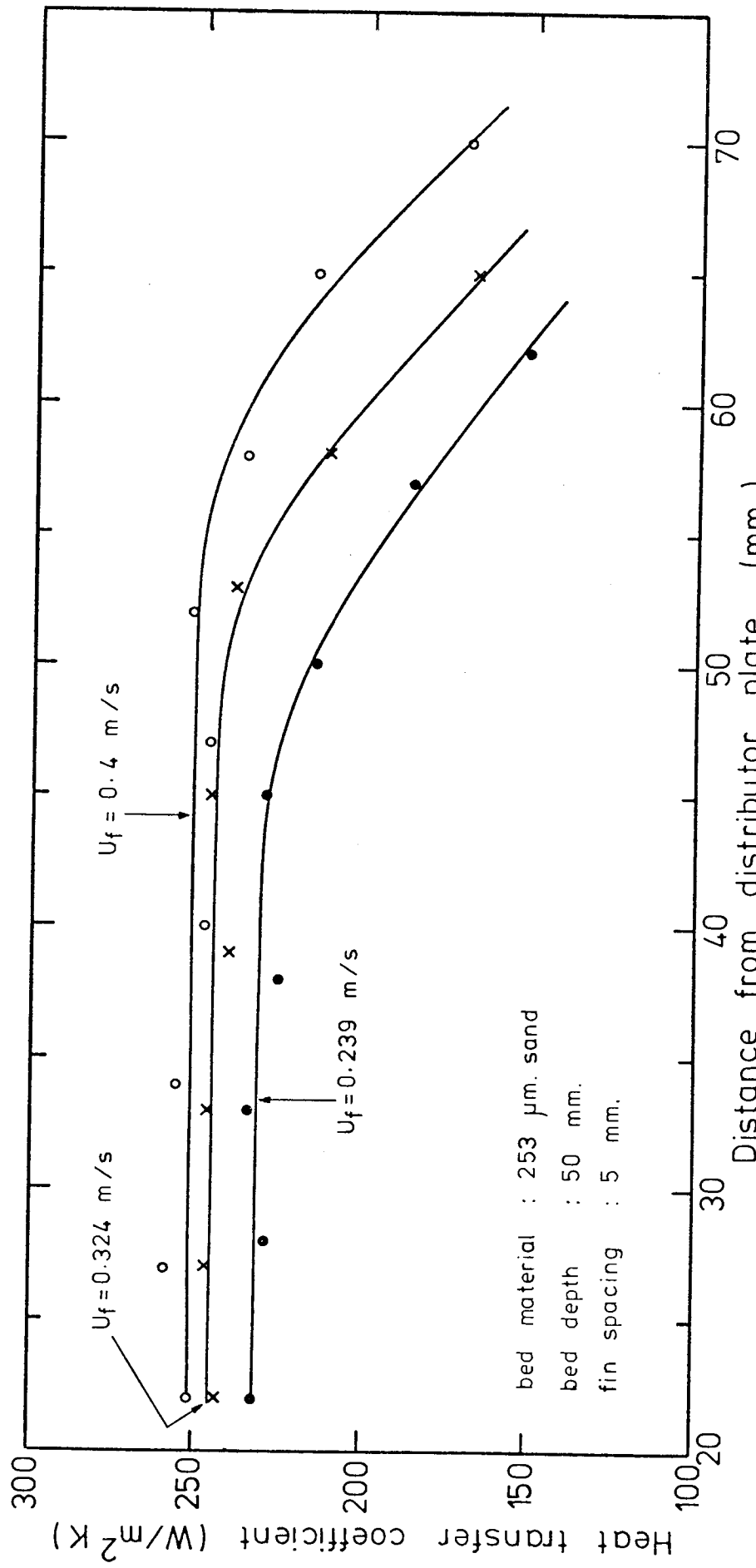

FIG. (8.9) VARIATION OF THE HEAT TRANSFER COEFFICIENT WITH TUBE POSITION AT DIFFERENT FLUIDIZING VELOCITIES

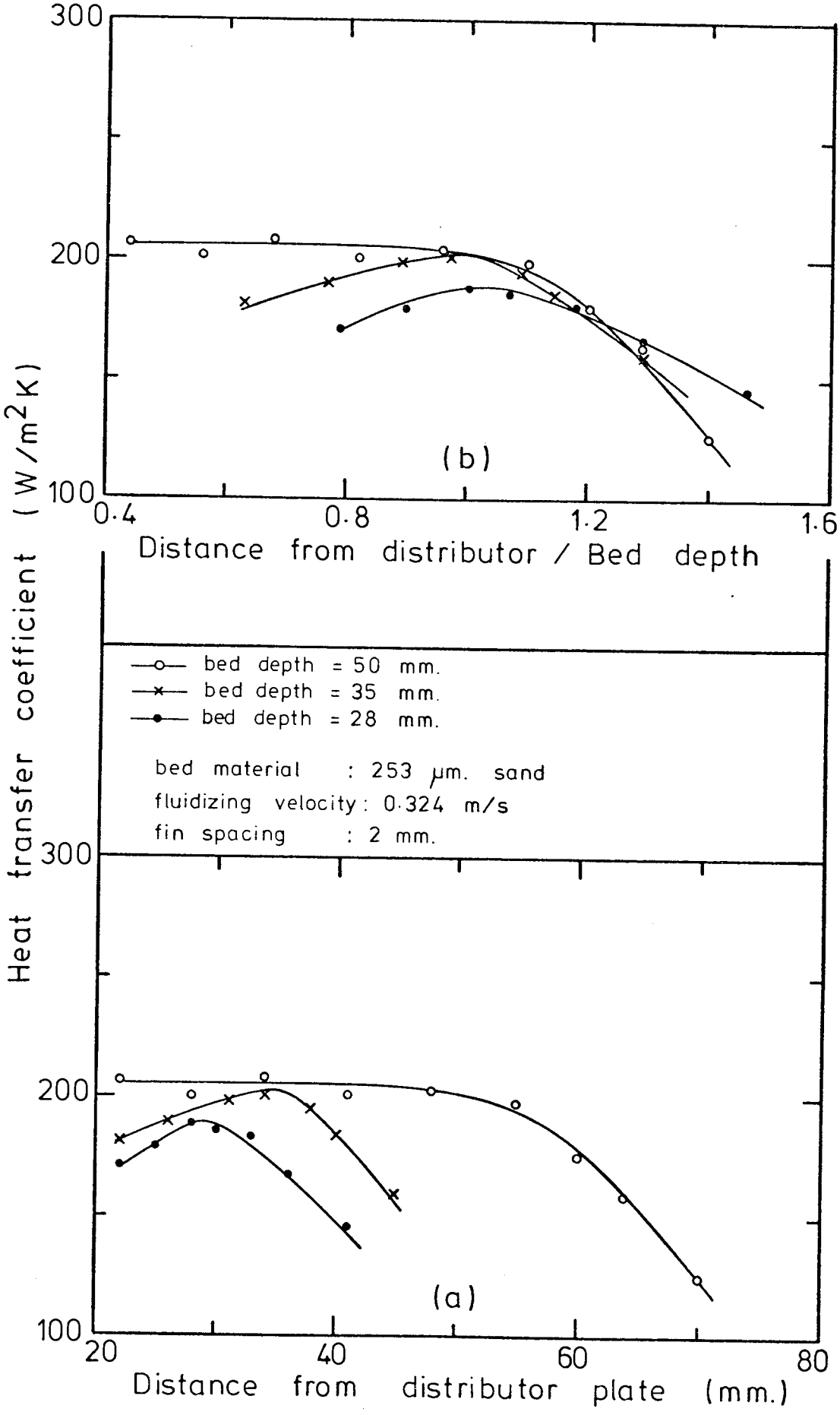

FIG.(8·10) VARIATION OF THE HEAT TRANSFER COEFFICIENT WITH TUBE POSITION FOR DIFFERENT BED DEPTHS

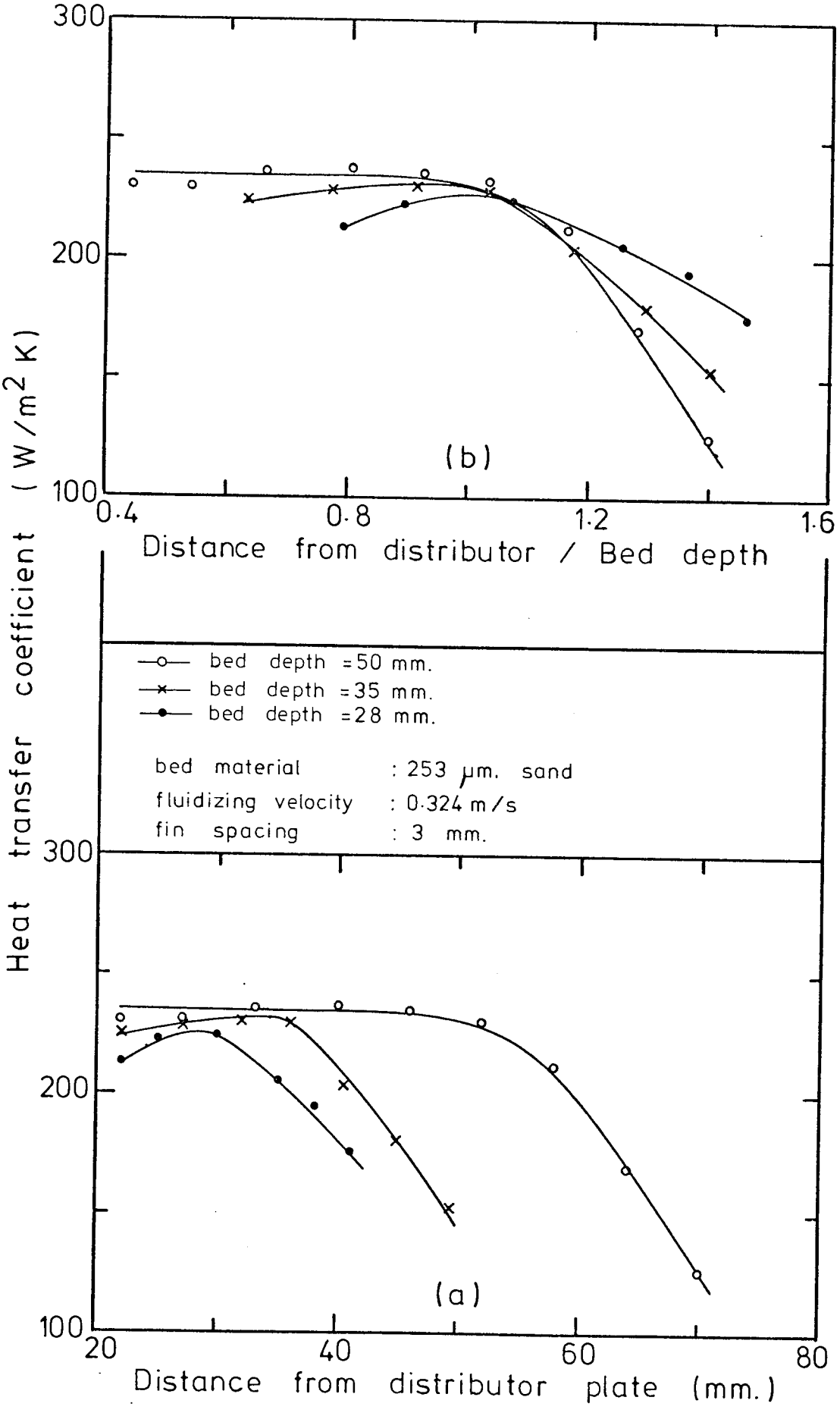

FIG. (8·11) VARIATION OF THE HEAT TRANSFER COEFFICIENT WITH TUBE POSITION FOR DIFFERENT BED DEPTHS

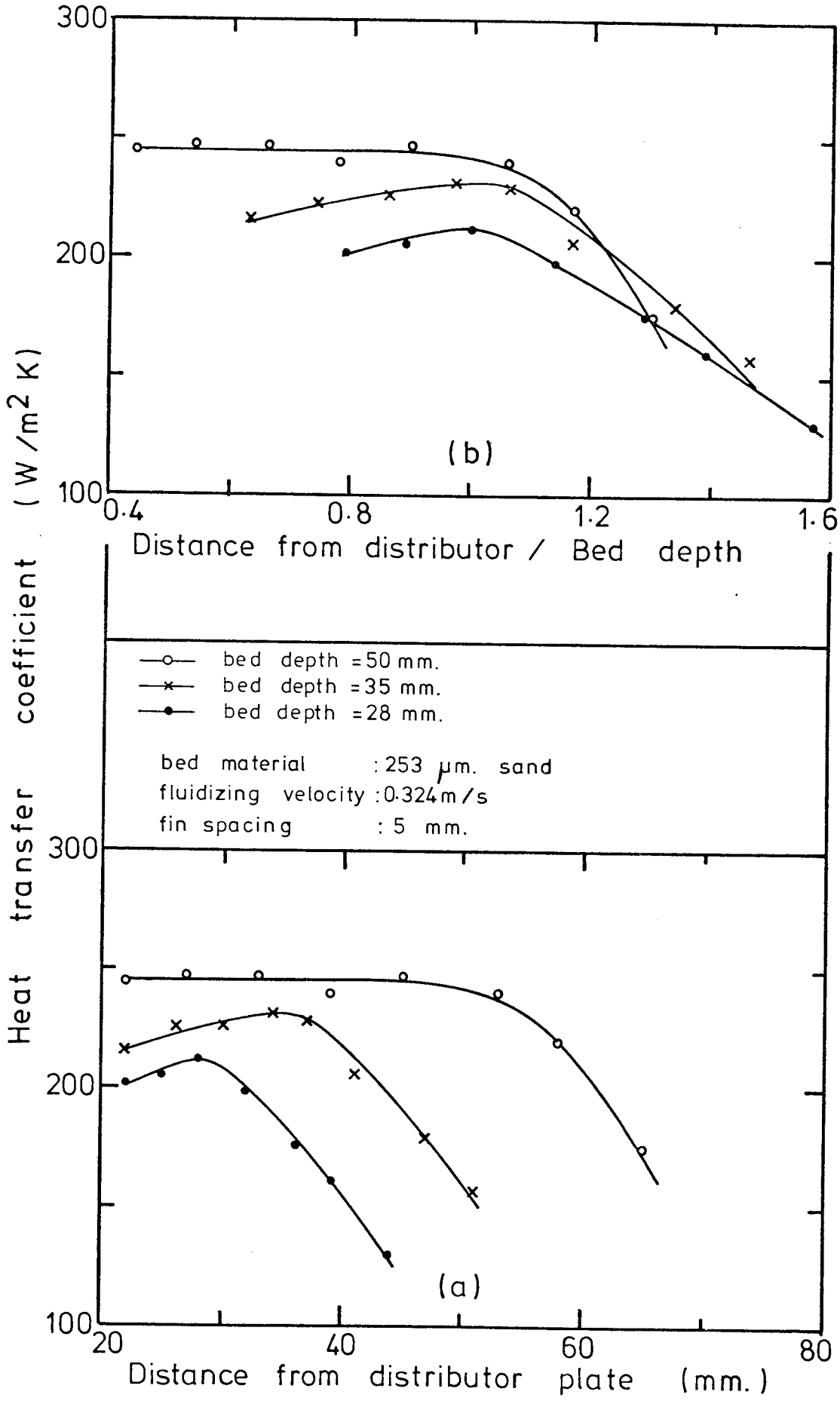

FIG. (8·12) VARIATION OF THE HEAT TRANSFER COEFFICIENT WITH TUBE POSITION FOR DIFFERENT BED DEPTHS

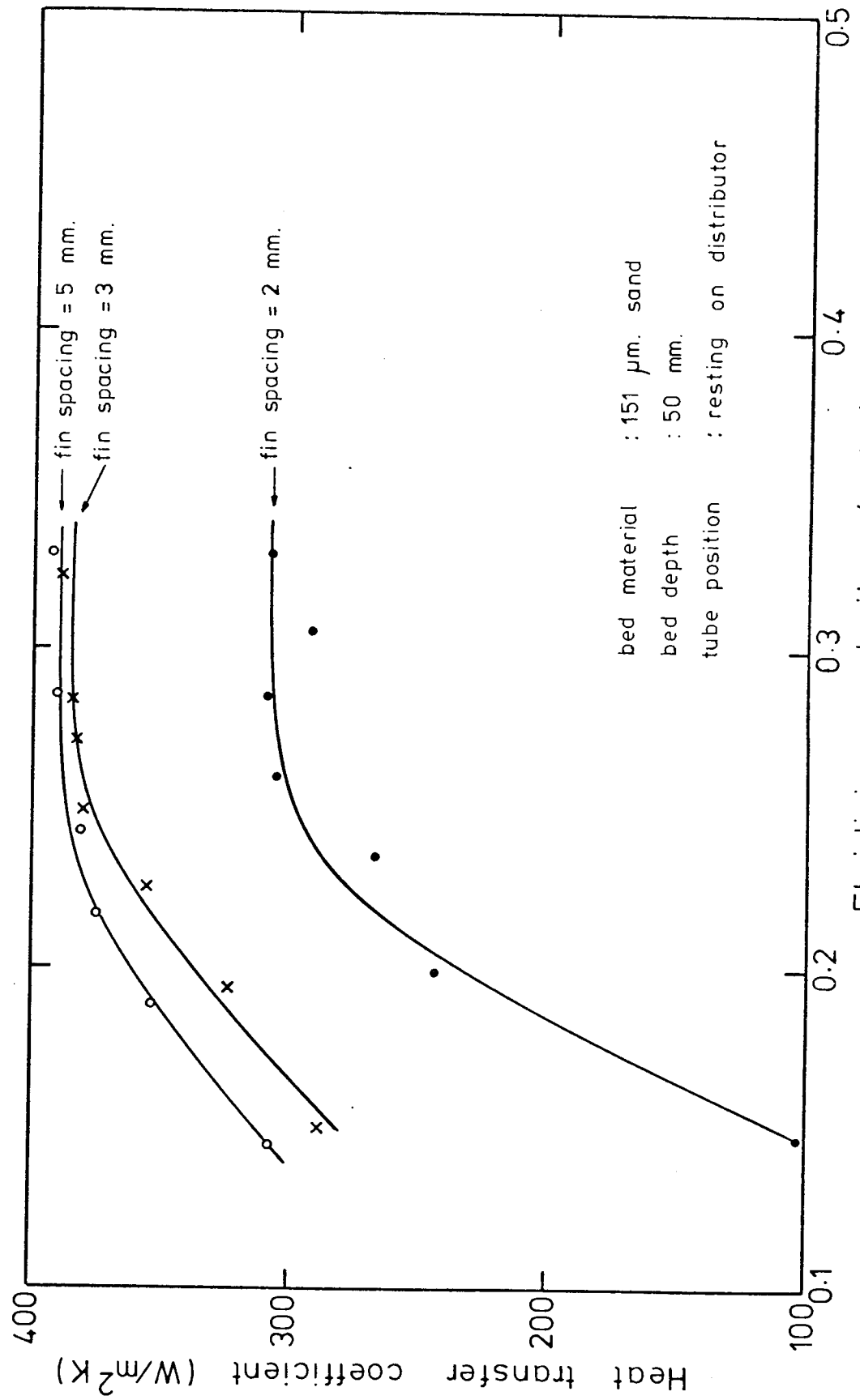

FIG. (8.13) VARIATION OF THE HEAT TRANSFER COEFFICIENT WITH FLUIDIZING VELOCITY FOR DIFFERENT FIN SPACINGS

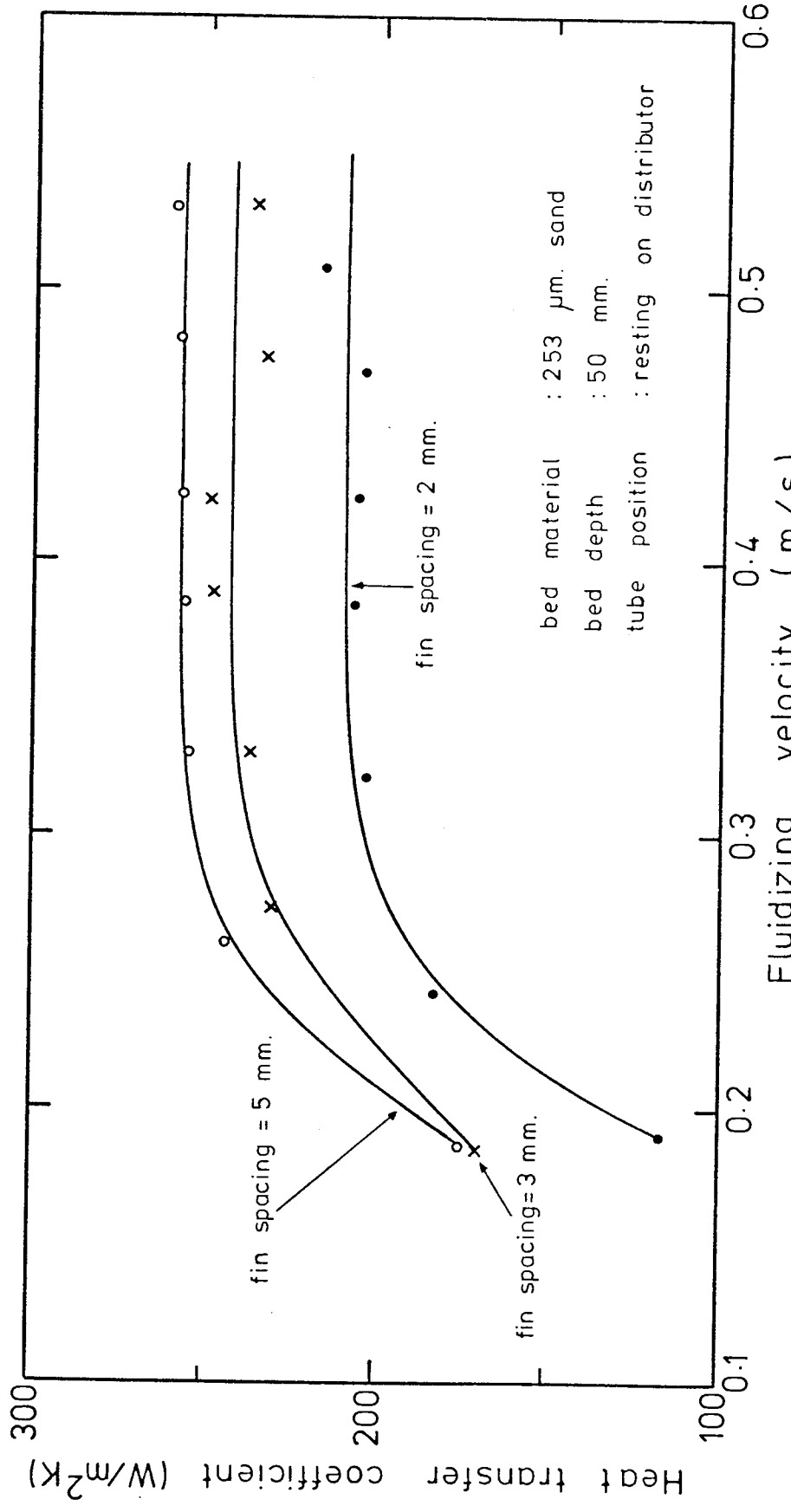

FIG. (8.14) VARIATION OF THE HEAT TRANSFER COEFFICINT WITH FLUIDIZING VELOCITY FOR DIFFERENT FIN SPACINGS

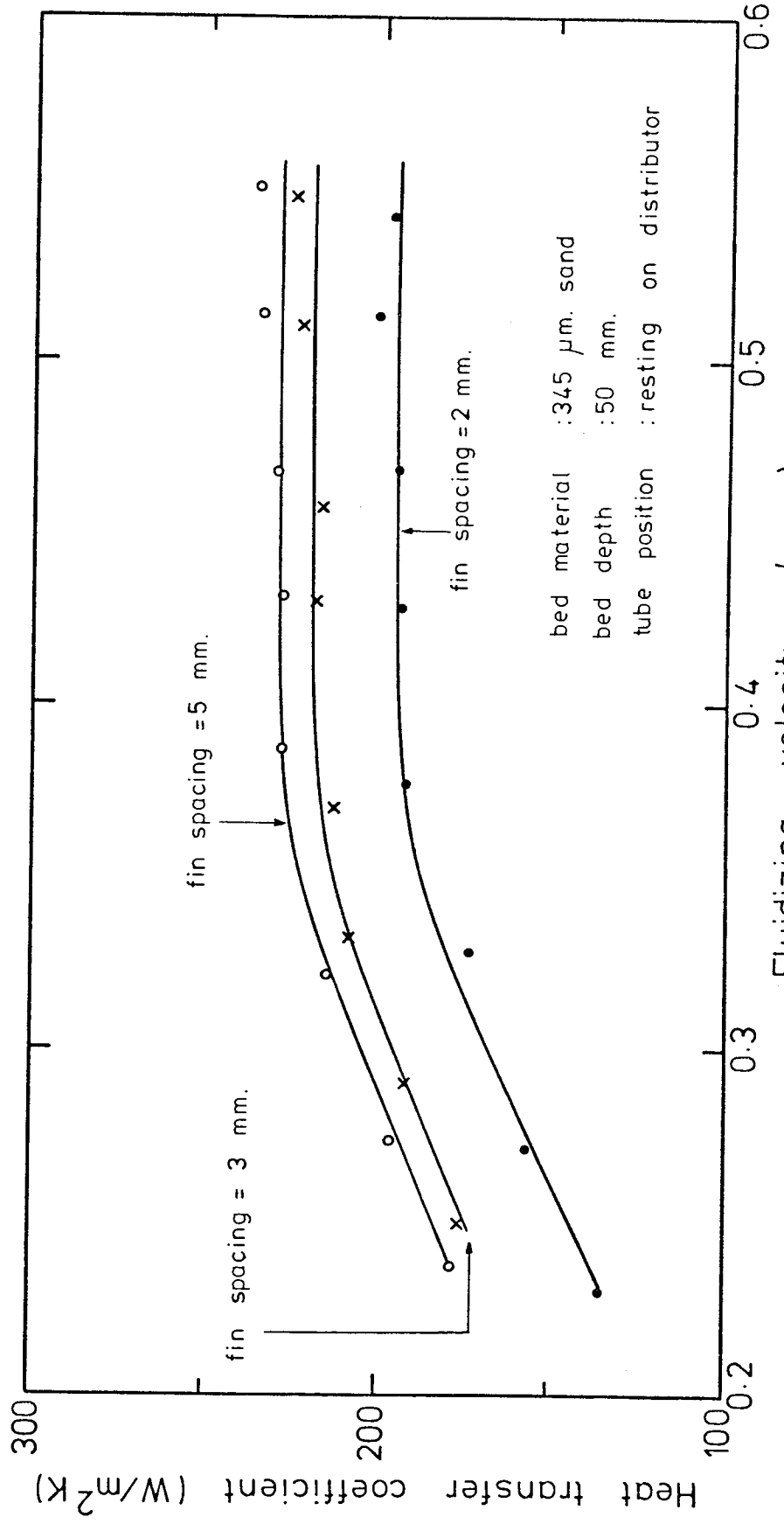

FIG. (8.15) VARIATION OF THE HEAT TRANSFER COEFFICIENT WITH FLUIDIZING VELOCITY FOR DIFFERENT FIN SPACINGS

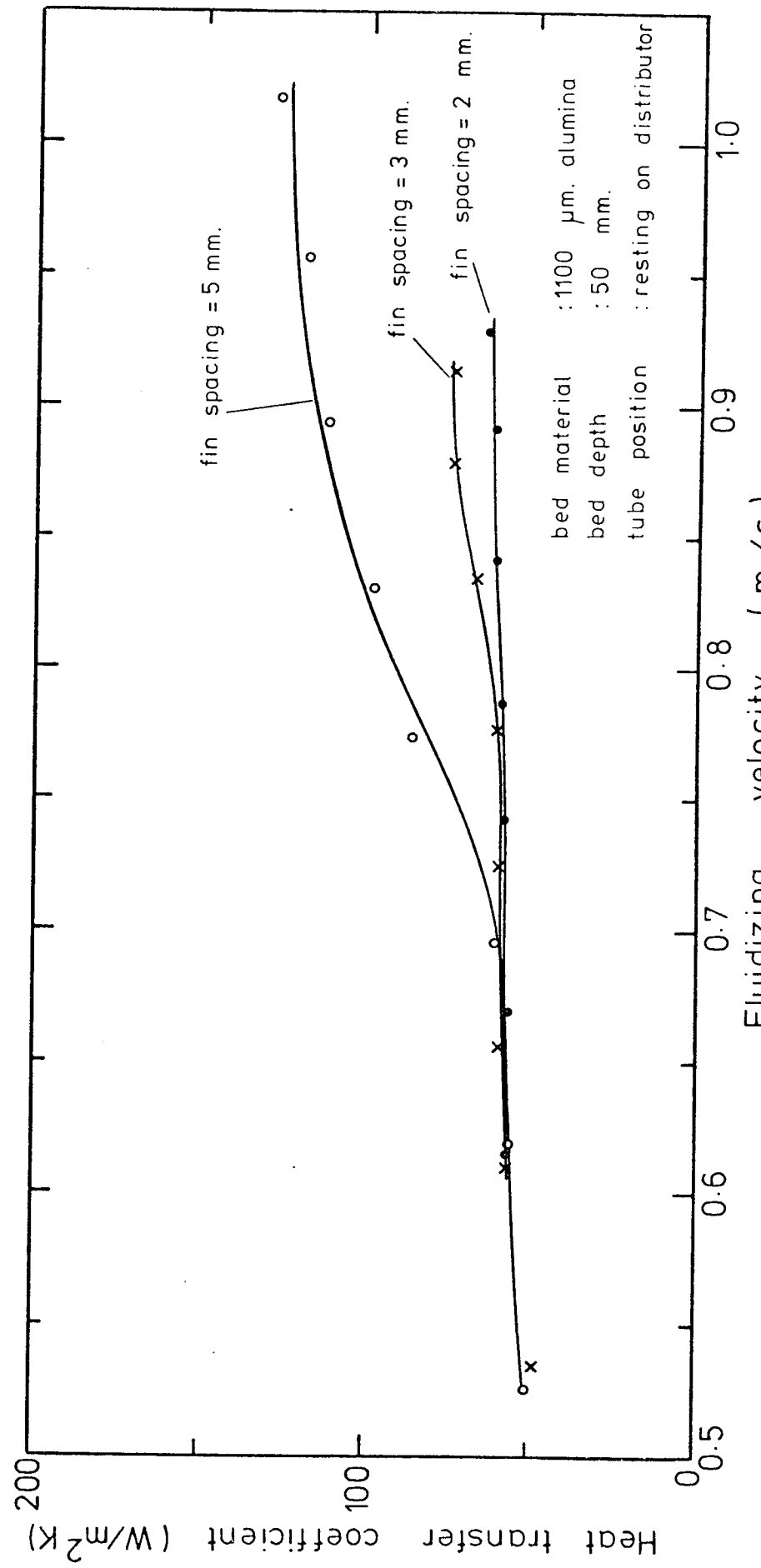

FIG. (8·16) VARIATION OF THE HEAT TRANSFER COEFFICIENT WITH FLUIDIZING VELOCITY FOR DIFFERENT FIN SPACINGS

CHAPTER 9

DISCUSSION OF RESULTS

DISCUSSION OF RESULTS

9.1 Plain tube work

As explained previously, the performance of a plain tube immersed in the bed was studied so as to serve as a reference with which results of finned tubes could be compared. However, as most of the studies of heat transfer in fluidized beds have been concerned with deep beds the investigations were extended to cover in particular, the effect of the tube position in the bed which is a contra-versial aspect as was pointed out in chapter (2).

9.1.1 Effect of tube position

The variation of the heat transfer coefficient with the position of the tube in the bed was investigated.as outlined in chapter 5, using different particle-sizes and with different fluidizing velocities and bed heights.

The results, that were presented in figures (5.6),(5.7) (5.8) and (5.9), clearly show that the tube position does have a significant effect on the heat transfer coefficient. This is contrary to the view expressed by Ainshtein and Gelperin[9] regarding deep beds and relatively in agreement with the observation made by Yuditskii and Zabrodskii[3] with shallow beds, although the trend they showed was quite different from the trends here. Atkinson[2], who is the only other worker to use shallow beds, concluded that the tube position did not have a significant effect on the heat transfer coefficient , although some of his data indicated that some effect

was present. This variation of the heat transfer coefficient with tube position indicates that the circulation of particles in shallow beds is markedly different from that in deep beds and that the configuration of the distributor/ shallow bed itself might be important.

9.1.1.a Effect of tube position at different particle sizes

The results in figure (5.5) show the influence of tube position on heat transfer for different particle sizes. It is noticeable that the influence of tube position becomes more pronounced as the particle size decreases. With alumina (1100 μm), the best heat transfer coefficient is obtained with the tube resting on the distributor plate with a steady slow decline until the tube leaves the bed. With sand, however, a different behaviour is observed. The coefficient shows two peak values, one with the tube inside the dense phase and the other with the tube situated in the dilute phase above the bed i.e. in the "cloud".

It is known from previous research by Rowe and Everett[57] and Hager and Thomson[58], where bubble behaviour around immersed tubes was viewed by X-rays, that bubbles adhere to the immersed tube and hence an envelope of bubbles forms around the sides and lower face of the tube, thus obstructing particles from coming near enough to the tube for heat transfer to take place. Because the bubbles grow in size as they move up the bed, this envelope would become thicker and at the surface of the bed the resistance to

particles coming into contact with the tube is, apparently, large enough to cause a drop in the heat transfer coefficient which is evidenced by the sand particles in figure (5.5). Counteracting this effect is the vigorousness of the particle motion which is caused by the bubbles. Near the distributor plate, where the bubbles start to form, the particle motion is expected to be relatively slow causing the heat transfer coefficient to be low because of the long residence time of particles at the surface. As the bubbles move up the bed, growing in size, the particle motion becomes more vigorous and hence the residence time of the particles decreases giving a rise in the heat transfer coefficient. It appears that at a particular level in the bed the two effects combine to give an optimum value of the heat transfer coefficient. The location of this point apparently moves up the bed as the particle size decreases.

In addition to the two factors mentioned above, the top surface of the tube becomes covered by a "cap" of defluidized particles which is practically stationary. This effect was described by Botterill[8] and the cap was clearly visible during the current experiments when the tube was located near the surface of the bed.

At tube positions in the lean phase (cloud) above the bed, another peak value of the heat transfer coefficient was obtained for the sand only. The cloud forms when particles are thrown up by the bubbles as they burst at the surface of the bed. The heat transfer in this region depends

on the number of particles which can come into contact with the tube. It was observed that as the particle size decreased the cloud became thicker implying that more particles came into contact with the tube. Consequently the heat transfer coefficient attained a higher value in the cloud than that in the bed with the finest sand used (134 μm). This variation was confirmed by the results obtained with the spherical probe presented in chapter (6).

During the experiments it was also observed that the "cap" was slightly reduced in size as the tube was moved out of the bed and into the cloud which would obviously contribute in enhancing the heat transfer coefficient.

9.1.1.b Effect of tube position at different fluidizing velocities

The results presented in figure (5.6) show the variation of the heat transfer coefficient with tube position at three fluidizing velocities 0.244 m/sec, 0.373 m/sec and 0.406 m/sec, using one particle size (253 μm sand). At the lowest fluidizing velocity the heat transfer coefficient in the dense phase was expected to be lower than that for the other two velocities because it corresponds to a point on the rising part of the H-U curve as can be seen in figure (5.14). It is noticeable that the drop in the coefficient in the lean phase is not as large as that in the bed and that the peak value is attained at a lower position because of the less intense motion of the particles due to the low fluidizing velocity.

The other two curves in figure (5.6) correspond to velocities where the heat transfer coefficient is near its maximum as can be seen from figure (5.14). At the highest fluidizing velocity, it is possible that the effect of bubbles enveloping the tube becomes a limiting factor and hence may be the cause of the depression in the coefficient at the surface of the bed.

9.1.1.c Effect of tube position at different bed depths

Figure (5.7) shows the variation of the heat transfer coefficient with tube position for different bed depths of 50 mm., 35 mm. and 28 mm. using 253 μm sand at a fluidizing velocity of 0.373 m/sec. To compare the results more accurately the heat transfer coefficient was plotted against the relative position of the tube, i.e. using the ratio of the distance from the distributor to the static depth of the bed. This is shown in figure (5.8).

The drop in the heat transfer coefficient with decreasing bed depth may be attributed to two possible reasons. Firstly the decrease in bed depth causes the bed expansion to be larger thus resulting in increasing bed voidage and less particle/surface contacts. Secondly, the lower the bed depth, the smaller would be the bubble size at the upper region of the bed which contributes to decreasing particle motion.

It is noticeable, however, that in the lean phase, the decrease in the heat transfer coefficient as the bed depth is reduced is not as high in proportion as the drop in the dense phase coefficient. The drop in the lean phase coefficient would be caused by the reduction in the number

of particles in the cloud due to the smaller bubbles that occur in the shallower beds. This phenomenon (of the decrease in the lean phase coefficient being less than that in the dense phase coefficient as the bed depth is decreased) could imply that the ratio of the weight of particles in the lean phase to the weight of particles in the dense phase increases with a decrease in bed depth.

It is also noticeable that the maximum heat transfer coefficient is attained at the same relative position as defined by tube height above the distributor/bed depth.

9.1.2 Effect of fluidizing velocity

The results of tests conducted to establish the variation of the heat transfer coefficient with fluidizing velocity, which were presented in figures (5.13), (5.14), (5.15) and (5.16), show that the H-U characteristics in the shallow beds (50 mm deep) are similar to the well-established trend mentioned previously in chapter (2), which was based on deep beds data.

The figures also show the corresponding values of the maximum heat transfer coefficient for each particle size as obtained from the Zabrodsky's correlation (equation 2.24) which was for deep beds. It is noticeable from figure (5.16) that the 1100 μm alumina gives a better performance in shallow beds than in deep beds since the maximum heat transfer coefficient attained is higher than that given by Zabrodsky's correlation.

To observe the influence of particle size, the four curves mentioned above were plotted together and are shown

in figure (5.17). Qualitatively, the influence of particle size is the same as for deep beds, i.e. the smaller the particle size, the higher the heat transfer coefficient which is mainly due to more particles contacting the surface when the particle size is reduced.

9.1.3 Proposed correlations

9.1.3a Correlation for the rising part of the H-U curve

The results in figure (5.17) were used to formulate a correlation for the rising branch of the H-U curve using the dimensionless groups Nu, Ar and N. The correlation was envisaged to be of the form

$$Nu = \beta_1 N^{\beta_2} Ar^{\beta_3} \qquad (9.1)$$

For this purpose the results in figure (5.17) were plotted on log-log scales in terms of the Nu against N as shown in figure (9.1). For each curve, the rising branch was located. The least squares technique was then used to determine the slope and the intercept term for each curve. This gave a relationship of the form

$$Nu = \beta N^{\beta_2} \qquad (9.2)$$

After taking the average of the slopes an overall value of β_2 was obtained and values of β were corrected correspondingly. The four equations (one for each particle size) were

$$Nu = 0.933\ N^{0.354} \quad \text{(for 134 μm sand)} \qquad (9.3)$$

$$Nu = 1.844\ N^{0.354} \quad \text{(for 253 μm sand)} \qquad (9.4)$$

$$Nu = 2.719\ N^{0.354} \quad \text{(for 345 μm sand)} \qquad (9.5)$$

$$Nu = 6.798\ N^{0.354} \quad \text{(for 1100 μm alumina)} \qquad (9.6)$$

The four values of β were then plotted against their corresponding values of the Archimedes number (Ar). This is shown in figure (9.2). A regression analysis was carried out and it gave

$$\beta = 0.2\ Ar^{0.331} \qquad (9.7)$$

The final correlation then became

$$Nu = 0.2\ N^{0.354} Ar^{0.331} \qquad (9.8)$$

9.1.3.b Correlation for the maximum heat transfer coefficient

For the maximum heat transfer coefficient, the correlation anticipated was of the form

$$Nu_{max} = \alpha_1 Ar^{\alpha_2} \qquad (9.9)$$

For this, values of the maximum heat transfer coefficient from the four curves in figure (5.17) were used together with six other values obtained from other experiments done at bed temperatures ranging between 75°C and 150°C using sand samples of sizes 134 μm and 253 μm to vary the values of Ar while using the same bed materials. The results were plotted as Nu_{max} against Ar and are shown in figure (9.3). A regression analysis yielded the correlation

$$Nu_{max} = 0.562\ Ar^{0.255} \qquad (9.10)$$

Correlation (9.8) was compared with data taken from Atkinson[2] and is shown in figure (9.4) where fairly good agreement is indicated bearing in mind that the distributor plates used in the two different sets of experiments were of

quite different designs.

Equation (9.10) was compared with the correlation offered by Zabrodsky[5] and with atkinson's data [2].This is shown in figure (9.5) and it indicates that good agreement is obtained.

The original data presented by Atkinson, which was used for comparison with correlations (9.8) and (9.10), is presented in Appendix (9).

9.2 Finned tube work

9.2.1 Effect of tube position

The results previously discussed concerning the plain tube prompted a similar investigation into the effect of the tube position on the heat transfer coefficient. With finned tubes, another important factor to be considered was fin spacing in relation to the particle size, fluidizing velocity and the bed depth.

9.2.1.a Effect of tube position for different particle size

The results of these investigations were presented in figures (8.3), (8.4), (8.5) and (8.6) for the bed materials sand (151 μm), sand (253 μm), sand (345 μm) and alumina (1100 μm) respectively. With each particle size three fin spacings were used 2mm, 3mm, and 5 mm. For the three sands the corresponding fluidizing velocities were set at a level where the heat transfer coefficient was expected

to have reached its maximum. For the alumina, the fluidizing velocity used was the same as that used with the bare tube test (chapter 5).

It appears that the heat transfer coefficient was unaffected by the position of the tube in the bed except where the fin spacing/particle size ratio (S/Dp) reached about 20 when it was observed that the best heat transfer coefficient was with the finned tube resting on the distributor plate. This may be attributed to the particle motion being hindered because the bubbles would not be able to penetrate freely between the fins thus reducing the intensity of the motion of particles. For S/Dp $\geq$ 20 the penetration of particles became apparently easier which was confirmed by the fact that the curves for 3mm and 5mm spacings in figure (8.3) were very close to each other. In these two curves it was noticed that the tube position begins to have an influence resulting in the best heat transfer coefficient being with the fins resting on the distributor. This could be attributed to the better penetration of the bubbles within the fins because of the small size at the distributor.

It can be seen from these results that the coefficient does not start to decline until the centre tube has cleared the height of the unfluidized bed (50 mm.). At this level the upper half of the fins are in the lean phase above the bed where good particle/surface contact still exists.

9.2.1.b Effect of tube position at different fluidizing velocities

Sand (253μm) was used for these investigations with fluidizing velocities 0.239 m/sec, 0.324 m/sec and 0.4 m/sec. The results shown in figures (8.7), (8.8) and (8.9) correspond to the three fin spacings 2mm, 3mm and 5mm respectively.

According to the explanation offered in the preceding section and with (S/dp) being less than 20 for all the results, the only distinguishing feature of these curves is the bed expansion which would obviously increase with the rise in fluidizing velocity, thus raising the point at which the heat transfer coefficient starts to drop. At the same time the heat transfer coefficient rises with rising fluidizing velocity because of improved penetration and movement of particles within the fins.

9.2.1.c Effect of tube position with different bed depths

As in the tests with the bare tube, three bed depths were used 50mm, 35mm, and 28mm. The bed material was 253 μm sand with 0.324 m/sec fluidizing velocity. The results were presented in figures (8.10), (8.11), and (8.12) for the fin spacings 2 mm, 3mm and 5mm. respectively. The "b" parts of the figures show the variation of the heat transfer coefficient with the relative position of the tube with respect to bed depth.

The figures show that with reduced bed depth the heat transfer coefficient in the lower region of the bed suffers the most reduction. This may be due to the bed expansion

being greater at lower bed depths which gives rise to a less dense bed and less number of contacts between the particles and the surface. Moreover, as the bed depth is decreased, the bubbles in the upper region of the bed become smaller thus reducing the intensity of particle motion in the lower region of the bed. However, as S/Dp increases (as in figure (8,12) when S/Dp= 19,7) and the motion of particles between the fins becomes easier, the reduction of the heat transfer coefficient at the peak points becomes more comparable with that obtained for the bare tube.

It is also evident, with bed depths of 35 and 28mm that the best heat transfer coefficient is obtained with the tube positioned at the surface of the bed. At this level, the upper half of the fins would be in the lean phase above the bed. It was, therefore, thought that some of the reduction in the heat transfer coefficient in the dense phase at the lower half of the finned tube was compensated for by the heat transfer in the lean phase at the upper half of the finned tube in spite of a reduction in the number of particles in the cloud because of the decrease in bed depth. This could mean that the ratio of the number of particles in the cloud to the number of particles in the dense phase increases as the bed depth decreases.

9.2.2 Effect of fluidizing velocity

It was intended that these investigations would show the behaviour of the heat transfer coefficient with the fluidizing velocity for the range of values of (S/Dp) available. The results were presented in figures (8.13),

(8.14), (8.15) and (8.16) corresponding to the particle sizes 151 μm, 253 μm and 345 μm and 1100 μm respectively.

The results clearly show the traditional trend of a rising zone of the coefficient after which a maximum value is attained. It will be seen from the figures that as S/ Dp is reduced, the circulation of particles within the fins becomes more restricted and when S/ Dp reaches a value below 5, the heat transfer coefficient does not increase much beyond the packed bed value. This is shown by the curve corresponding to 2mm fin spacing in figure (8.16).

9.2.3 Effect of fin spacing

It had been expected that the fin spacing would be an important factor in the performance of finned tubes in fluidized beds, and the experimental results show that the effect of fin spacing in relation to the particle size appears to be quite critical for particle movement and consequently for the heat transfer coefficient.

Figure (9.6) shows the dependence of the maximum heat transfer coefficient on (S/ Dp) for the four particle sizes used for the tests. The data was taken from figures (8.13), (8.19), (8.15) and (8.16). This figure together with the other four from which the data was taken, brings to attention the following :-

1. The value of S/ Dp of 20 appears to be a critical one, below which the maximum heat transfer coefficient starts to decline rapidly
2. The rate of reduction of the heat trasnfer coefficient appears to depend on the size and type of particles. It was observed that the decline was sharpest for 151μm sand.

3. For S/Dp<5, the particle movement is greatly obstructed and near total blockage of particles occurs between the fins.

Two possible causes of this interaction are :-

1. The mobility of the particles themselves between the fins.
2. The interaction between particles of different shape and surface profile with the surface of the fins which could give rise to lower particle mobility at the surface.

The first possibility was investigated by using mixtures of particles of two different kinds. Botterill et al [59] and McGuigan [60], who studied the viscosity of fluidized beds using a small scale viscometer, have reported that adding small proportions of coarse light particles to a bed of fine heavy ones resulted in reducing the viscosity of the beds. The reduction of the viscosity would imply an improvement in the particle mobility and consequently a better heat transfer performance would be expected. Experiments were carried out for three mixtures using 151 μm sand as the fine dense material and 1100 μm alumina as the coarse light material. The mixture ratios used were 95%-5%, 90% - 10%, and 80% - 20% by weight of sand and alumina respectively. The densities and average sizes of the mixtures were calculated from the equations quoted by Goossens et al [61] which are :

$$\frac{1}{\rho_m} = \frac{x}{\rho_h} + \frac{1-x}{\rho_l} \qquad (9.11)$$

and $$\frac{1}{D_m\rho_m} = \frac{x}{D_h\rho_h} + \frac{1-x}{D_l\rho_l} \qquad (9.12)$$

where suffixes l, h and m refer to the light material, the heavy material and the mixture respectively and x is the percentage by weight of the heavy material. As far as the segregation problem was concerned, no specific criterion was available to specify the exact conditions for segregation to take place. Goosens et al[61] have proposed a mathematical criterion, but it carries some serious weaknesses. Furthermore Rowe et al [62], in their studies on segregation, concluded that the density difference is the main cause of segregation while the effect of size is mainly to alter U_{mf} which is little affected when a lot of coarse material is added to the fine material. They further add that the degree of mixing depends very much on gas velocity and even strongly segregating mixtures can be mixed by using a sufficiently high gas velocity. With the experiments carried out no visible evidence was available of segregation taking place.

The results of the investigations with mixtures are shown in figures (9.7) and (9.8) showing the variation of the heat transfer coefficient with the tube position and the fluidizing velocity respectively as compared to the performance of the pure sand (151μm). The figures clearly show that the heat transfer coefficient declined with increase in the percentage of the coarse-light material which was quite the opposite to the expected enhancement. Although these

investigations were not conclusive, it was clear that the effect of the viscosity of the bed was minimal and far outweighed by the deleterious effect of the low fin spacing/particle size ratio of 5 :1 of the larger particles.

The second of the possibilities (i.e. the influence of particle shape) was thought to be the main reason responsible for the restriction of particle motion between the fins. This was investigated and is discussed in the next section.

9.2.4 Influence of particle shape and profile

Photographs of the three sand materials (151μm, 253μm and 345 μm) viewed on a projection microscope were taken to observe if there was any visible difference between the shapes and profiles of the materials that might cause the premature decline in the heat transfer coefficient when the finest sand was used. These microphotographs are presented in figure (9.9). The 1100 μm alumina was known to be round and smooth so that no photographs were thought necessary. The figure shows clearly that the 253 μm sand and the 345 μm sand are similar in sphericity and exhibit few sharp edges. The 151 μm particles have rougher profiles and numerous sharp edges although their sphericity is not very different from the other two. It was thought that this roughness was the most likely cause for the premature fall in the heat transfer coefficient of the 151 μm particles when a fin spacing/particle diameter ratio less than 20 was used.

Three attempts were made to characterise the particle shape and in particular the surface profile. The aim was to find a simple shape factor which can describe the roughness of the surface of the particles.

1. The angle of repose was considered as a first indication of particle shape. Measurements were taken of the open and closed angles of repose. For the closed angle of repose the samples were poured slowly into a heap and the angle the cone made with the horizontal was measured. For the open angle of repose the samples were poured into a box. The box was tipped to rest on one side and then brought back to rest on its base and the angle of the inclined surface of the sand made with the horizontal was then measured. The results of the average of five measurements for each material are presented in table (9.1). Although there is an indication that the 151 μm sand is less free flowing than the other two sands, the difference looks marginal. However, by comparing the results for the sands with those for the 1100 μm alumina (which was spherical and smooth), it appears that slight variations in the angle of repose are significant. Consequently it was felt that many more tests with a variety of particles would be necessary to form a firm conclusion.

2. The second method was based on the analogy of the flow of particles between the fins with liquids. The aim was to obtain a characteristic similar to the friction factor used for liquid flow. A specially constructed small rig was used for this purpose, a schematic diagram

of which is presented in figure (9.10). It mainly consisted of a wooden box with a sliding gate to hold the sand in the box before allowing it to flow downwards through the fins. The finned tube elements were fixed underneath the gate making sure that the sand could only flow out through the fins. The tests were carried out using all three finned tubes with each sample. Three measurements were recorded with each

combination of particle size and fin spacing and the average was then taken. The results are presented in figure (9.11) and show the flow of sand (kg/sec) as a function of (S/D_p). These results show that the flow of the 151 μm sand was more sensitive to fin spacing than the other two materials in addition to the observed dependence on particle size, which supported the initial proposition that particle shape and profile was a critical factor in the flow of solid particles between the fins. It is interesting to notice that, when the curves are extrapolated, they converge to a value of about 3 on the S/D_p axis corresponding to zero flow of solids. This value of 3 is used as a rough guide in hydraulic transport problems to indicate the limiting value of a pipe diameter in terms of particle size.

It was, however, unfortunate that the number of data points was not enough to obtain a quantitative interpretation of the results. Many finned tube elements with varying

spacing were needed for this purpose and, unfortunately, time was not available for the finned tubes to be made and it was left for future work.

3. The use of a shape factor derived from the profile of the particles was also considered. Many surface shape factors have been proposed[65,66] for which either the surface area of the particles or their three length dimensions (length, width and thickness) were required. Again due to the lack of time available, no experimental measurements could have been done for obtaining the actual surface area and all three dimensions of the particles. Consequently, it was decided to use a shape factor which could be obtained from the two dimensional projected images of the particles.

It has been suggested that the ratio of the Martin's diameter* to the Feret's diameter * of the particle could be used as a shape factor, but, as Church[63] outlined in his analysis, this involves many problems

---

* The Martin's and Feret's diameters are defined as the length of the line bisecting the area of the particle in a fixed direction and the projected length of the particle in the same direction respectively.[63]

and the number of particles to be used has to be of the order of magnitude of many hundreds. Another two dimensional shape factor was proposed by Hausner [64] which is given by

$$S.F. = \frac{C^2}{12.6\ A} \qquad (9.13)$$

where C is the circumference and A is the area of the image of the particle. The constant 12.6, which is equivalent to 4π, was inserted to give the shape factor a value of 1 for a sphere. It was decided to use this shape factor to characterise the sand materials.

Photographs similar to the ones shown in figure (9.9) were obtained such that 50 particles of each material could be considered. The circumference of each particle was measured with the aid of a "map reader" and the area was measured with a planimeter. The results are given in table (9.2). Although the results show that the shape factor for the 151 μm sand is slightly higher than the other two, which are closer, it was felt that the difference was not representative of the observed visible difference in profile. This was thought to be due to the error in measuring the circumference where it was very difficult to follow the profile of the particles (especially the 151 μm sand) very accurately in spite of the fact that five measurements were taken for each particle. It was therefore decided that the results were not conclusive enough to be reliable.

Finally, after three attempts were made to characterise particle shape, it was thought that, although none of the methods used was conclusive enough, the un-fluidized flow experiments were the most likely to yield

informative data. It was therefore concluded that further investigations were necessary to modify existing methods or use more definite ones to characterise particle performance with respect to fin spacing.

9.2.5 Proposed correlation

In spite of the effect of particle shape discussed in the preceding section, it was interesting to plot values representing the maximum heat transfer coefficient in dimensionless form (Nu_{max}) against the product of (Ar) and (S/D_p). This was actually similar to what was used for the bare tube data with the added factor (S/D_p). The plot is shown in figure (9.12). The values of Nu_{max} were obtained from figures (8.13), (8.14) and (8.15) for the sand bed materials. The values for the alumina were not used because the results in figure (8.16) do not indicate that the maximum heat transfer coefficient had been attained.

It was interesting to notice that a power relationship does exist between the two variables, Nu_{max} and $Ar(S/D_p)$ which is represented by the straight line which was obtained by the least squares technique. The equation of the line was found to be

$$Nu_{max} = 0.359 \left| Ar(S/D_p) \right|^{0.186} \qquad (9.14)$$

It is hoped that when a shape factor for the particles can be defined, it would be included in the generalised correlation which could certainly make the equation most useful for design purposes.

9.2.6 Comparison of results

Figure (9.13) shows a comparison between the correlation obtained with data taken from Natusch and Blenke[36] and from Atkinson [2] where fin heights were different from those used in the present work and are indicated on the figure. The original data from both sources is presented in Appendix (9).

Due to the varying experimental conditions any comparison would have to involve all the variables (expressed in dimensionless form). This would probably involve a complete dimensional analysis of all the data and it was decided that this task should be left for future work.

The results obtained for the mixtures of particles, which were given in figure (9.8), were also plotted to observe how they fitted with the trend of the main experimental data. The agreement can be seen to be quite good.

9.2.7 Influence of the fins on the centre tube

It was previously indicated in chapter (7), from results obtained with non-conductive fins, that the presence of fins does have an effect on the heat transfer coefficient at the centre tube because of the constrained motion of the particles. This effect was observed as an improvement in the heat transfer coefficient.

According to the investigations that followed on particle shape and its interaction with the surface of the fins, it may be concluded that the large increase in the heat transfer coefficient at the centre tube with particles of

1100μm) alumina (see figure 5.16) was due to this particle-surface interaction. With the alumina particles being round and smooth as well as the perspex being smooth, the particle could slide easily along the fin surface, thus enhancing particle motion between the perspex fins and reducing the residence time of the particles at the centre tube. This was evident during the experiments where the particles were observed moving very fast out of the space between the perspex fins while no such behaviour could be seen when the copper fins were used. Also the perspex fins were comparatively long and an effect similar to pneumatic transport through the fin gaps might have had a major effect.

Table 9.1

Angles of repose of sand bed materials

material	angle of repose (degrees)	
	closed	open
sand(151μm)	34.04	31.2
sand(253μm)	32.54	30.5
sand(345μm)	32.44	30.16
alumina(1100μm)	27.7	29.3

Table 9.2

Shape factors of sand bed materials

material	shape factor
sand(151μm)	1.192
sand(253μm	1.133
sand(345μm)	1.147

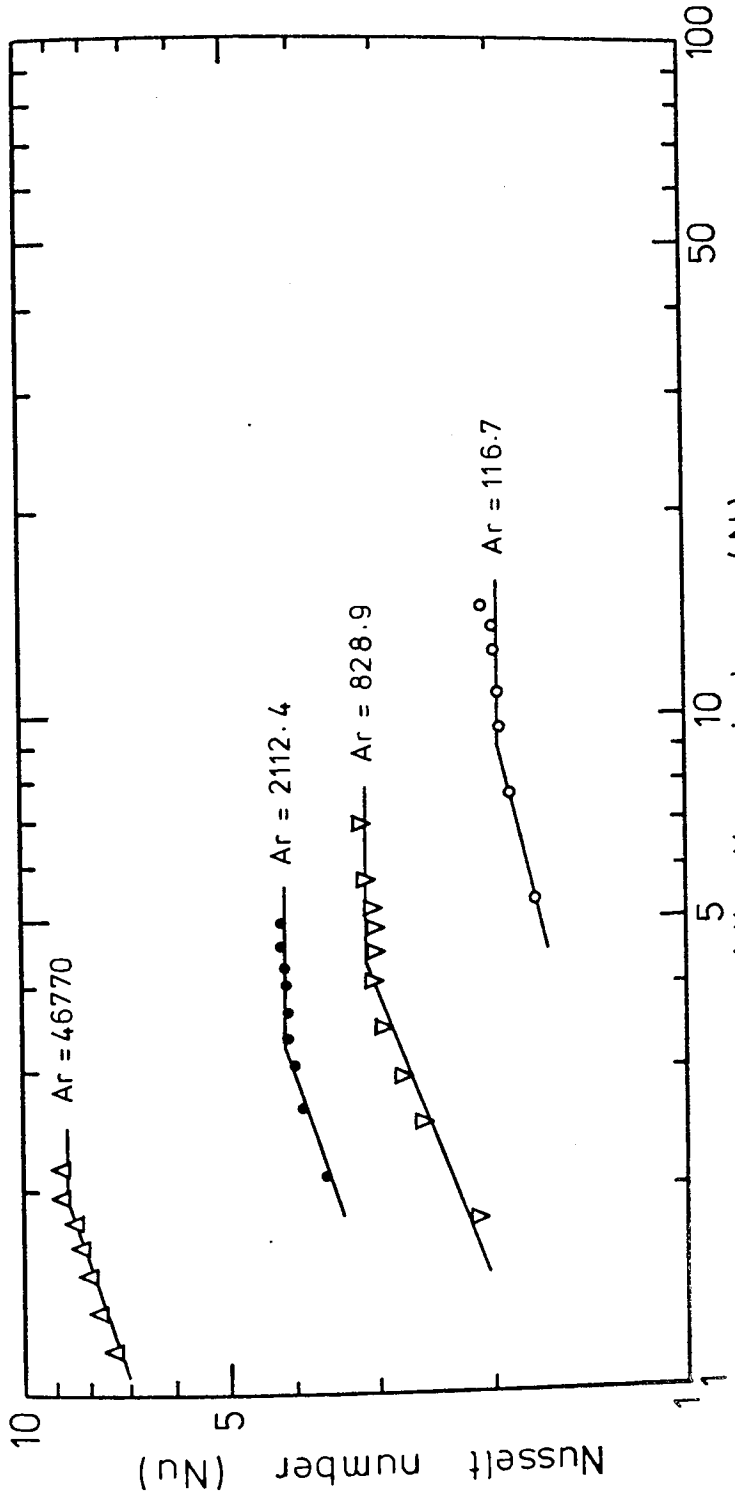

FIG. (9.1) VARIATION OF NUSSELT NUMBER WITH THE FLUIDIZATION INDEX

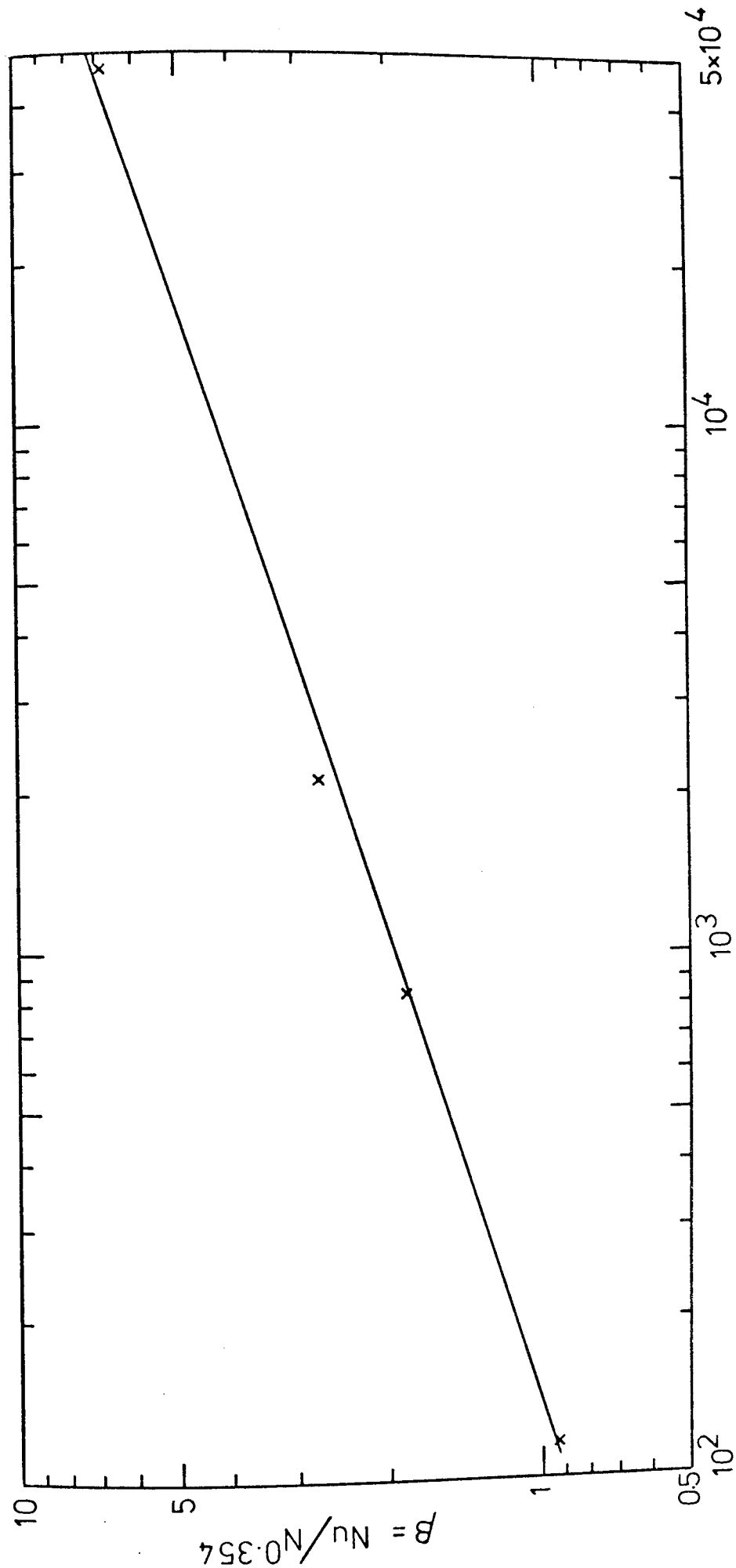

FIG.(9.2) CORRELATION FOR THE RISING BRANCH OF THE H-U CURVE

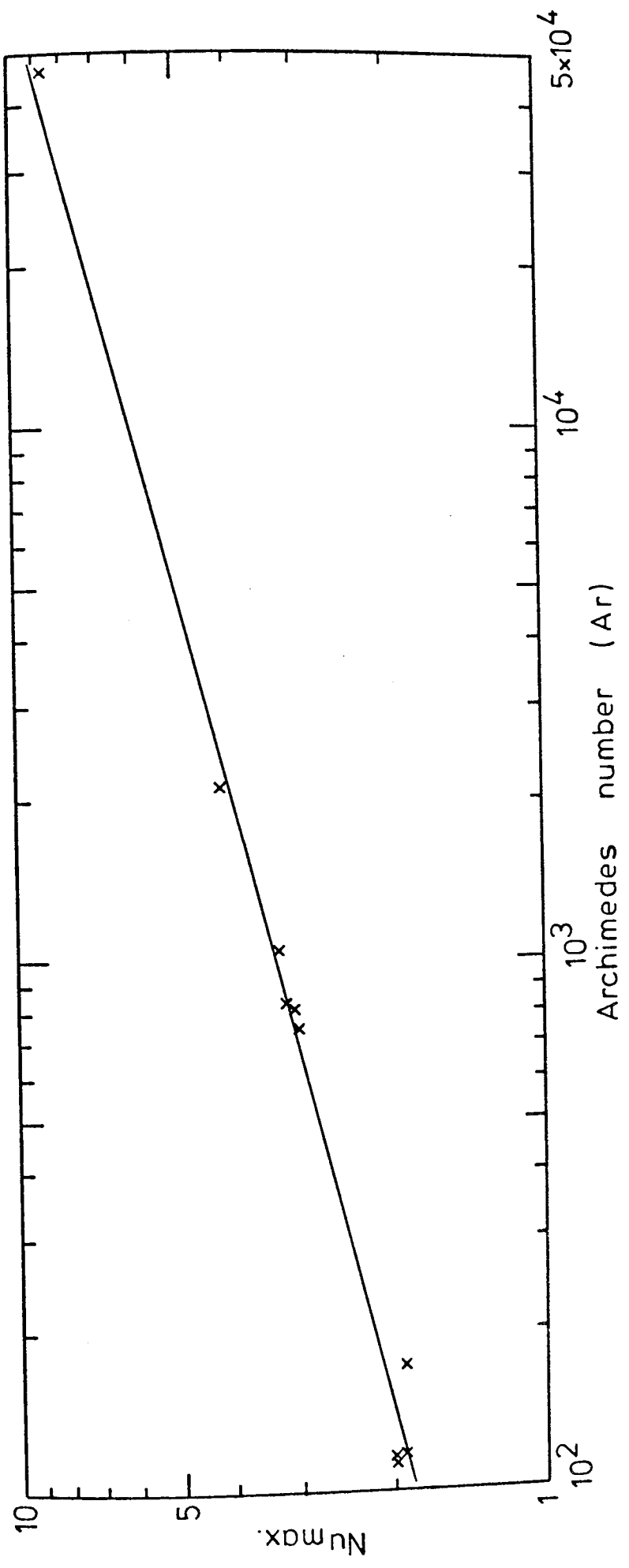

FIG.(9.3) CORRELATION FOR THE MAXIMUM HEAT TRANSFER COEFFICIENT

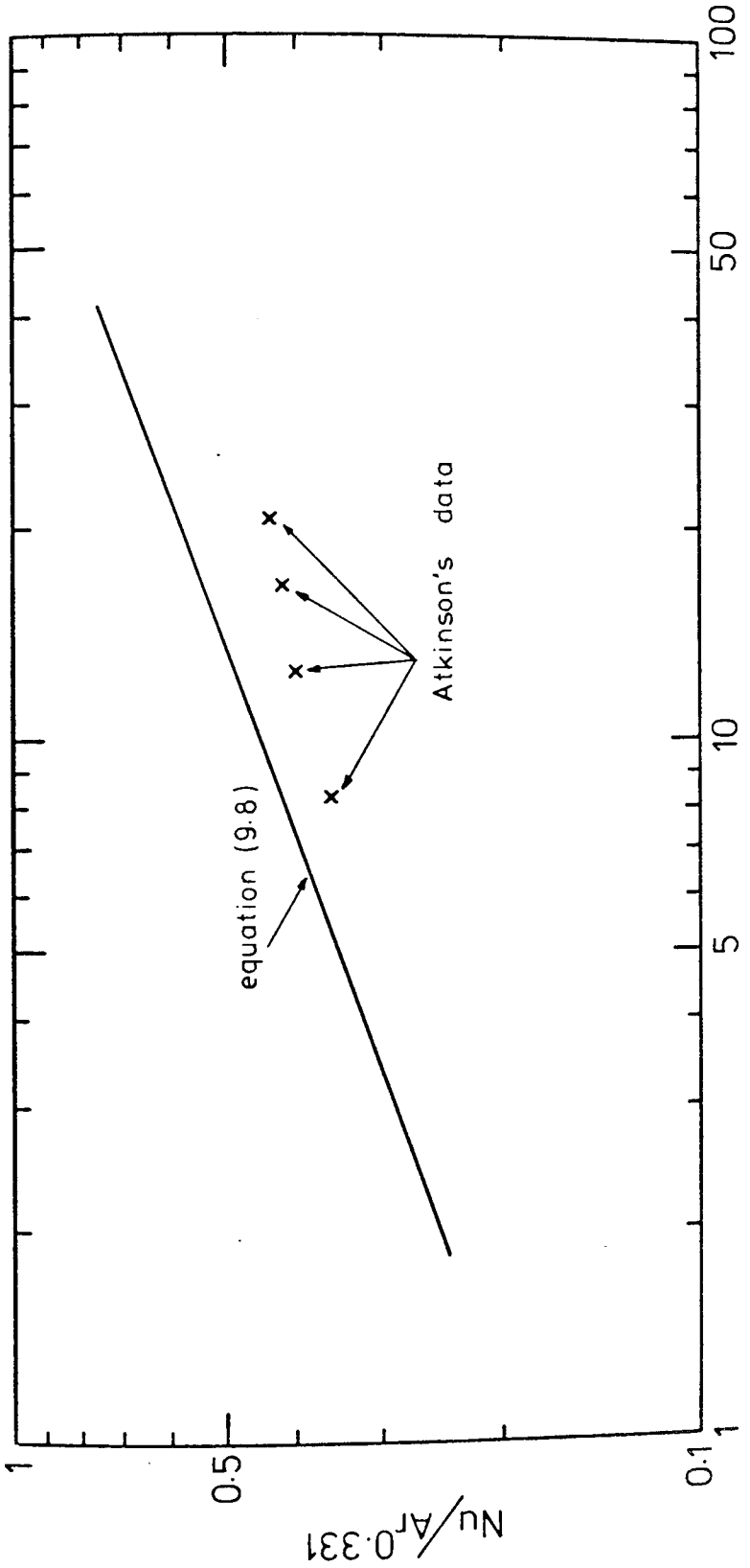

FIG. (9.4) COMPARISON OF CORRELATION (9.8) WITH DATA FROM ATKINSON (ref.2)

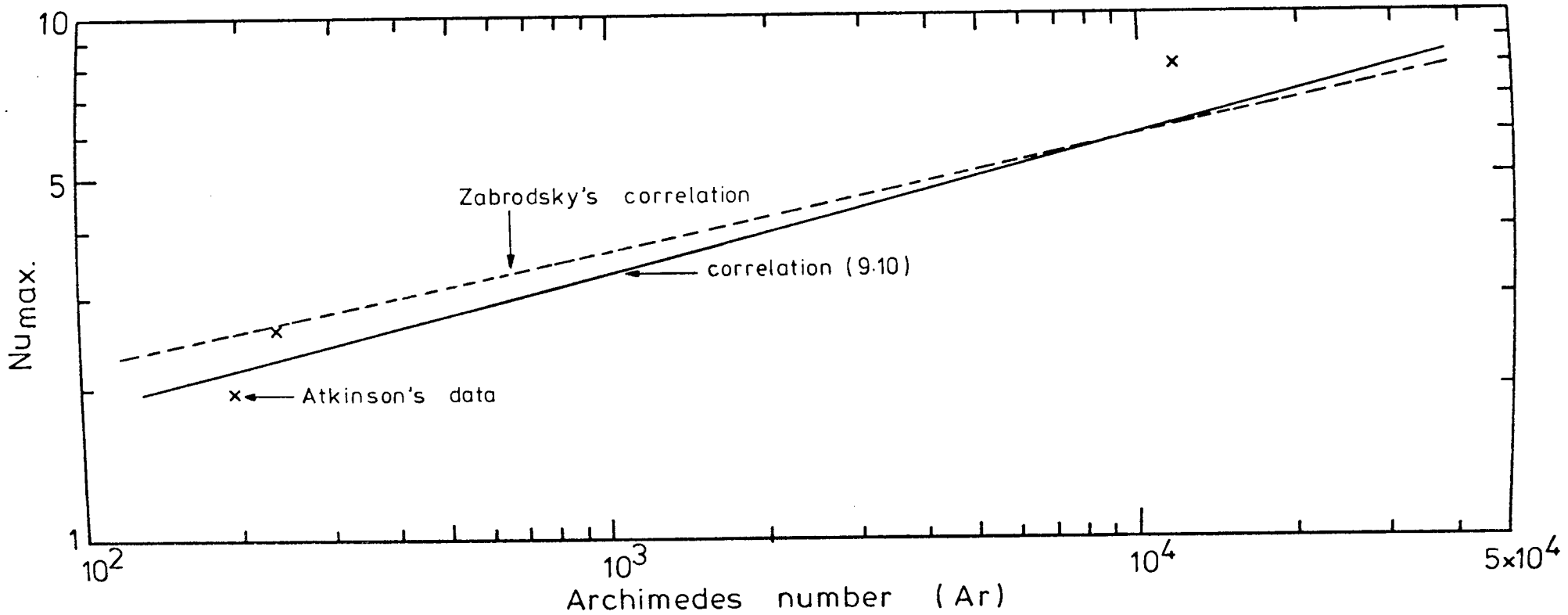

FIG. (9.5) COMPARISON OF CORRELATION (9.10) WITH DATA FROM ATKINSON (ref. 2) AND ZABRODSKY'S CORRELATION (ref. 5)

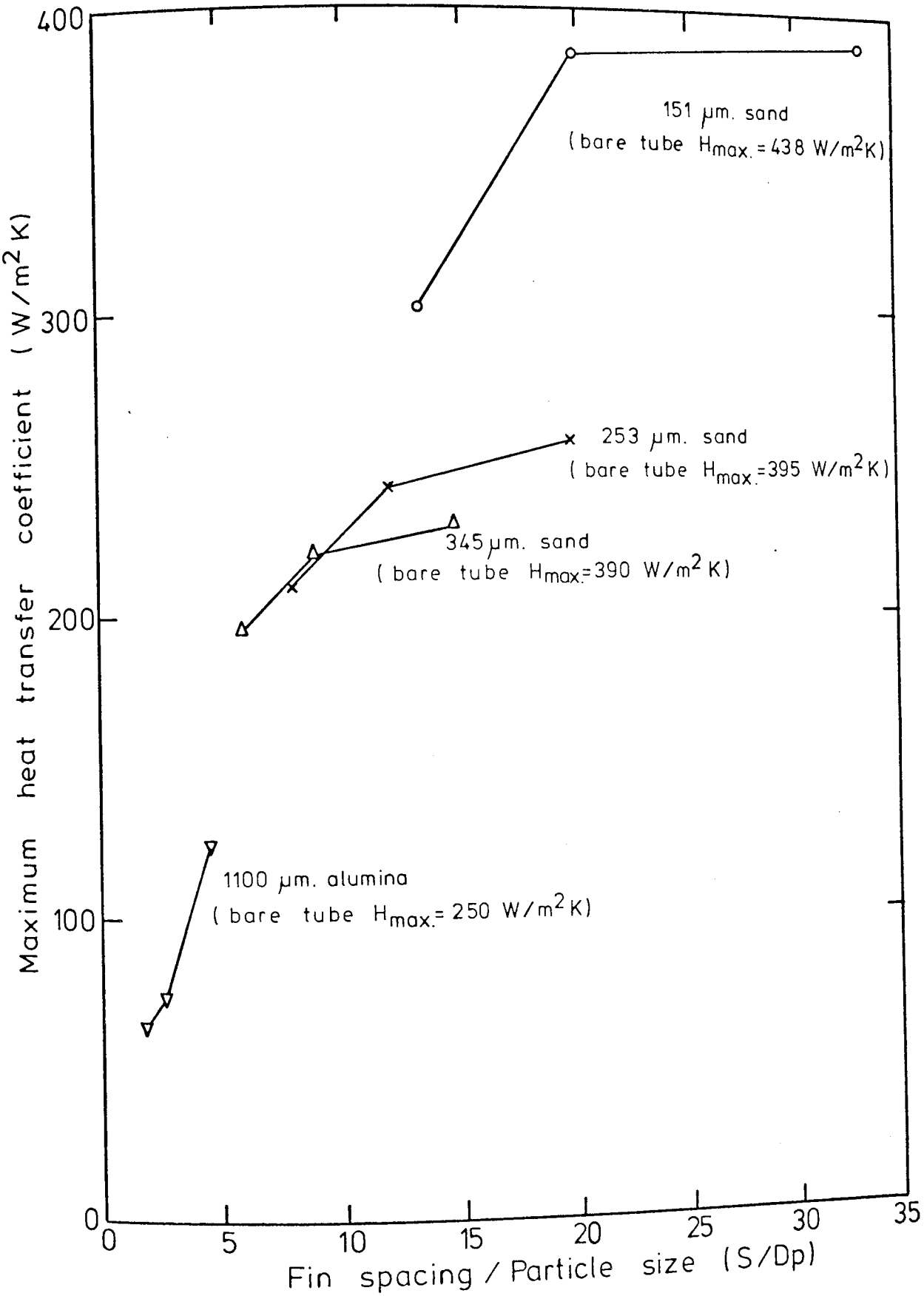

FIG. (9.6) INFLUENCE OF FIN SPACING ON THE HEAT TRANSFER COEFFICIENT

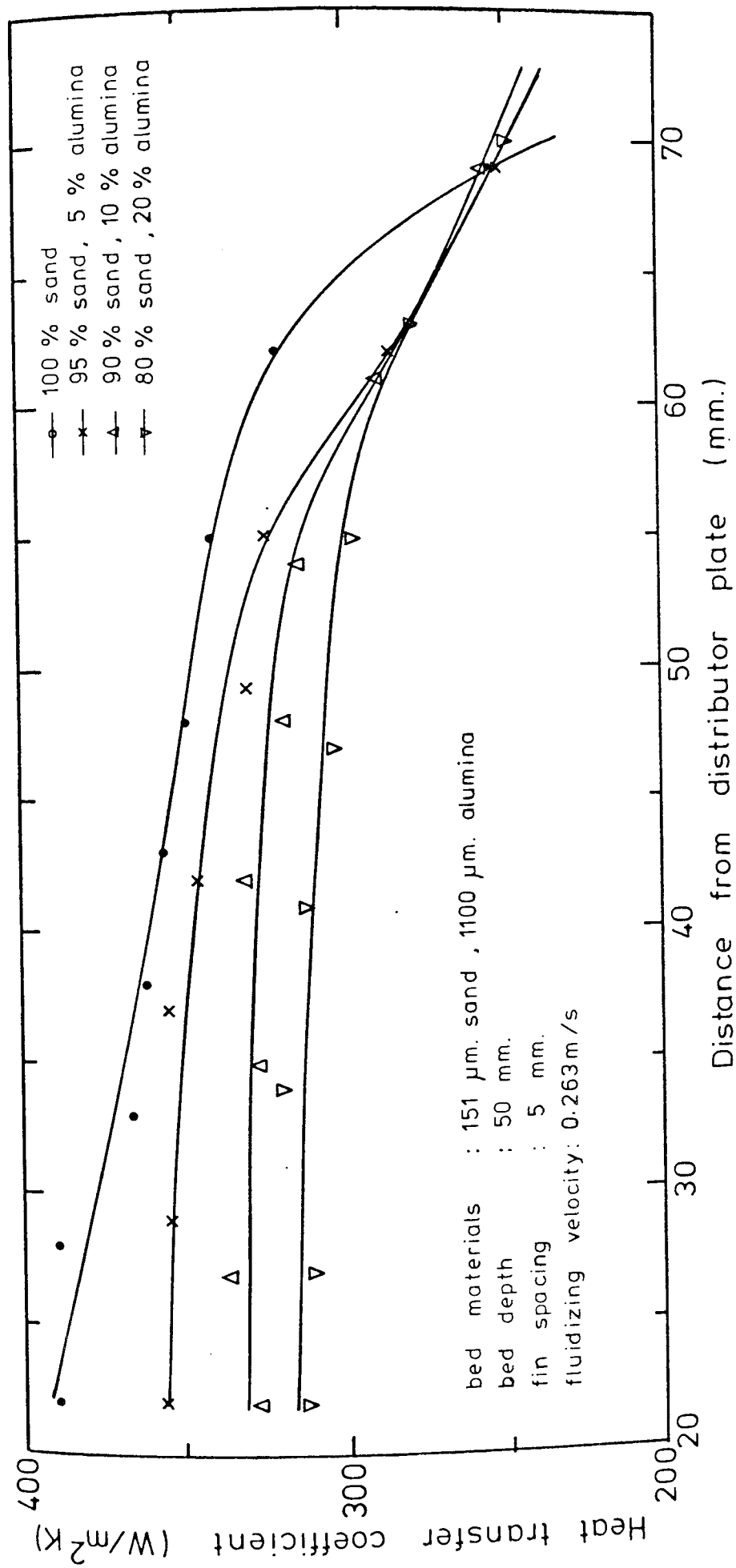

FIG.(9.7) VARIATION OF THE HEAT TRANSFER COEFFICIENT WITH TUBE POSITION FOR MIXTURES OF PARTICLES

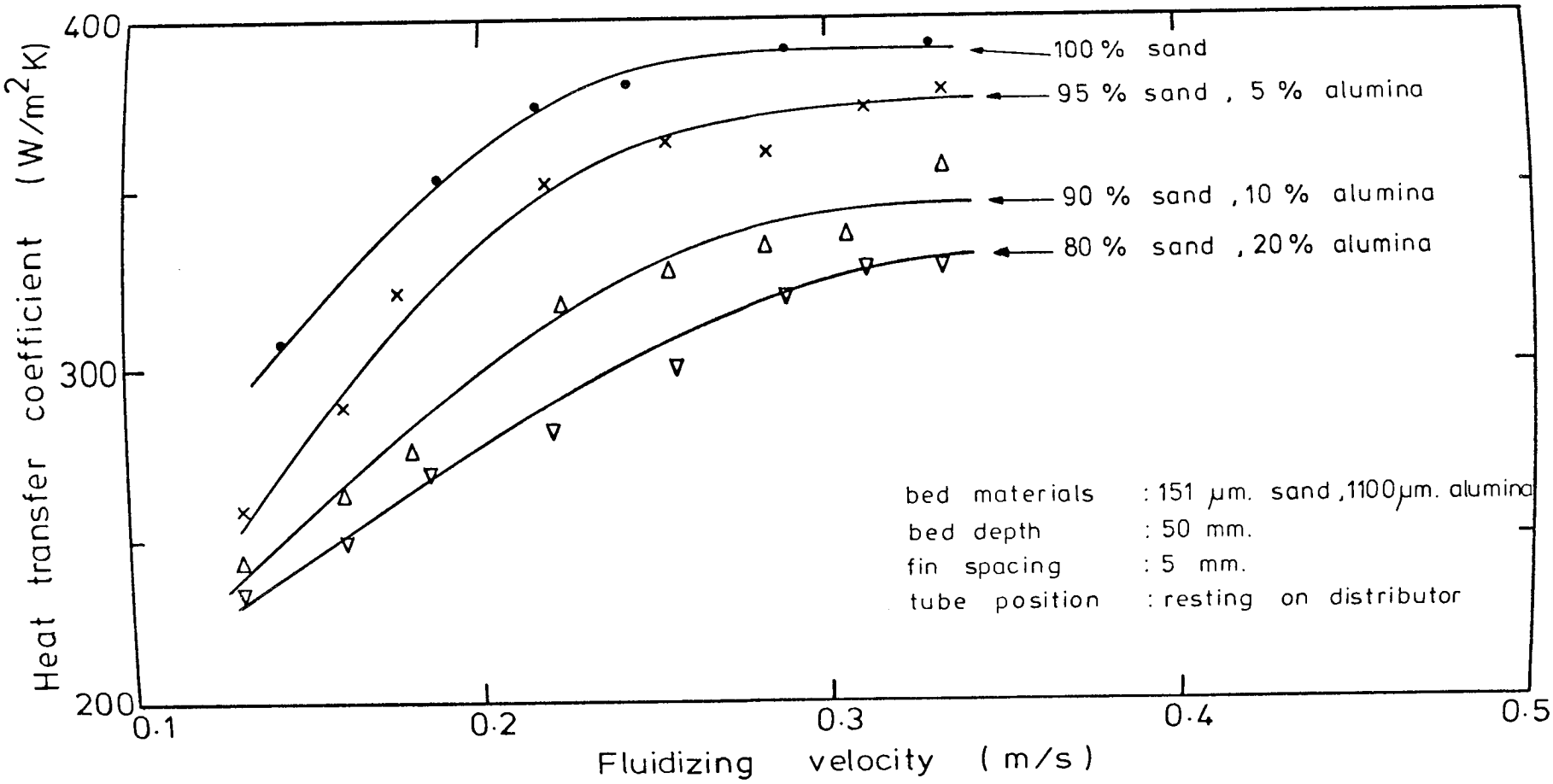

FIG. (9.8) VARIATION OF THE HEAT TRANSFER COEFFICIENT WITH FLUIDIZING VELOCITY FOR MIXTURES OF PARTICLES

Dp = 151 μm. magnification ×100

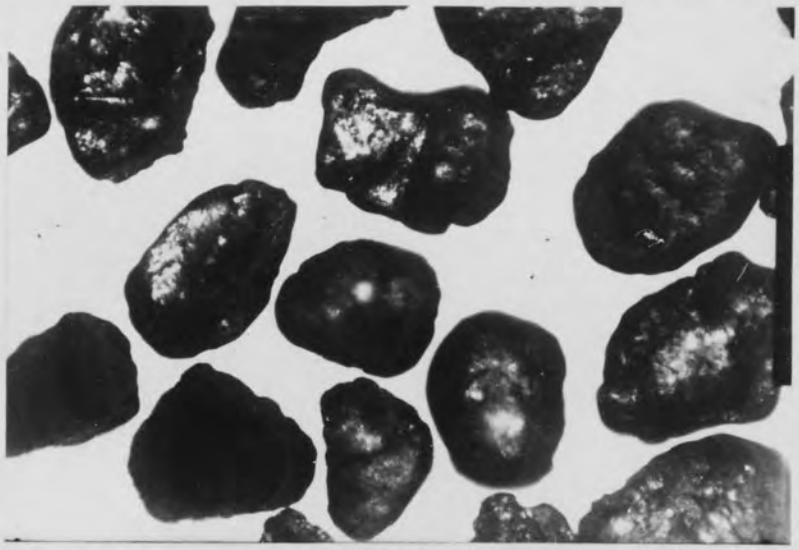

Dp = 253 μm. magnification ×100

Dp = 345 μm. magnification × 100

FIG (9.9) PROJECTION MICROSCOPE PHOTOGRAPHS OF SAND BED MATERIALS.

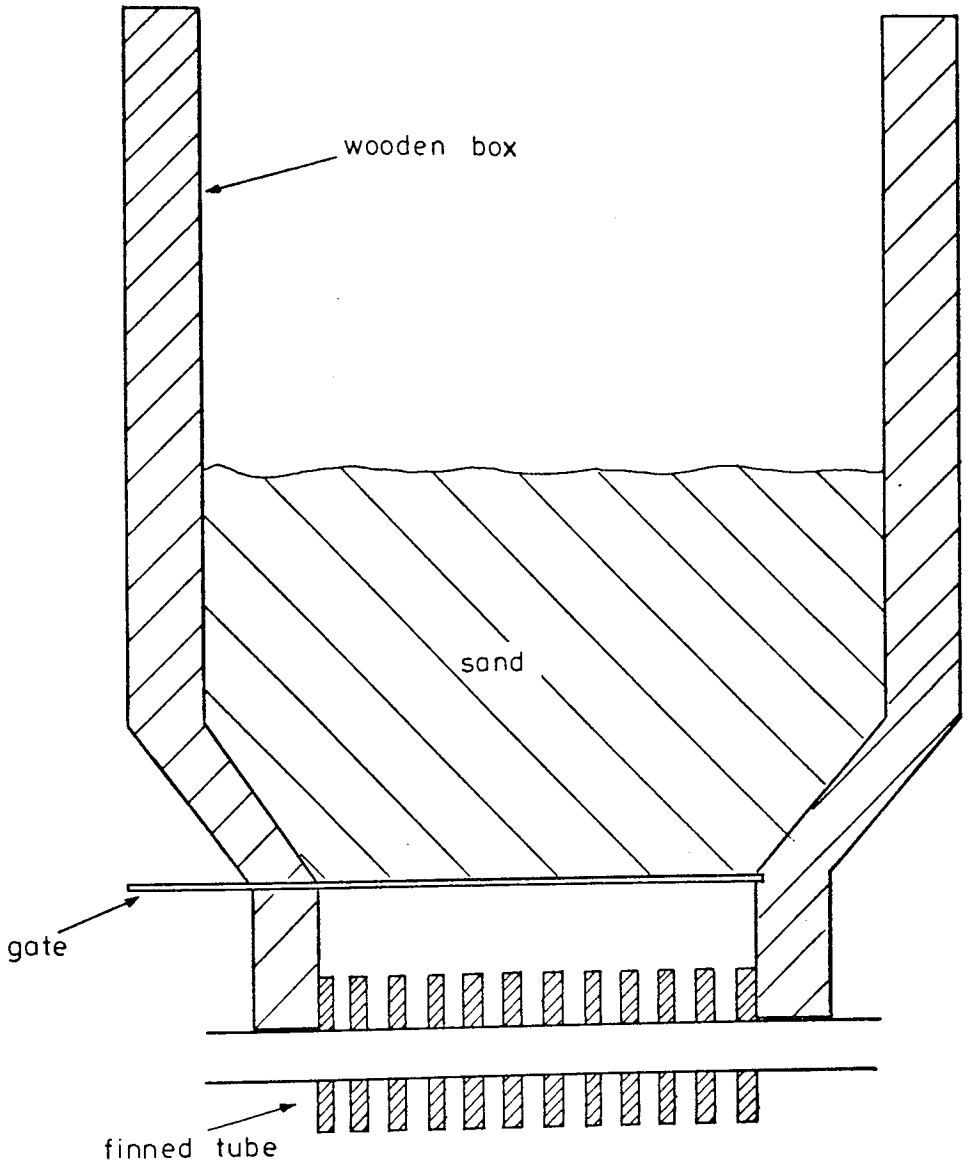

FIG. (9.10) TEST RIG FOR FLOW OF PARTICLES BETWEEN THE FINS

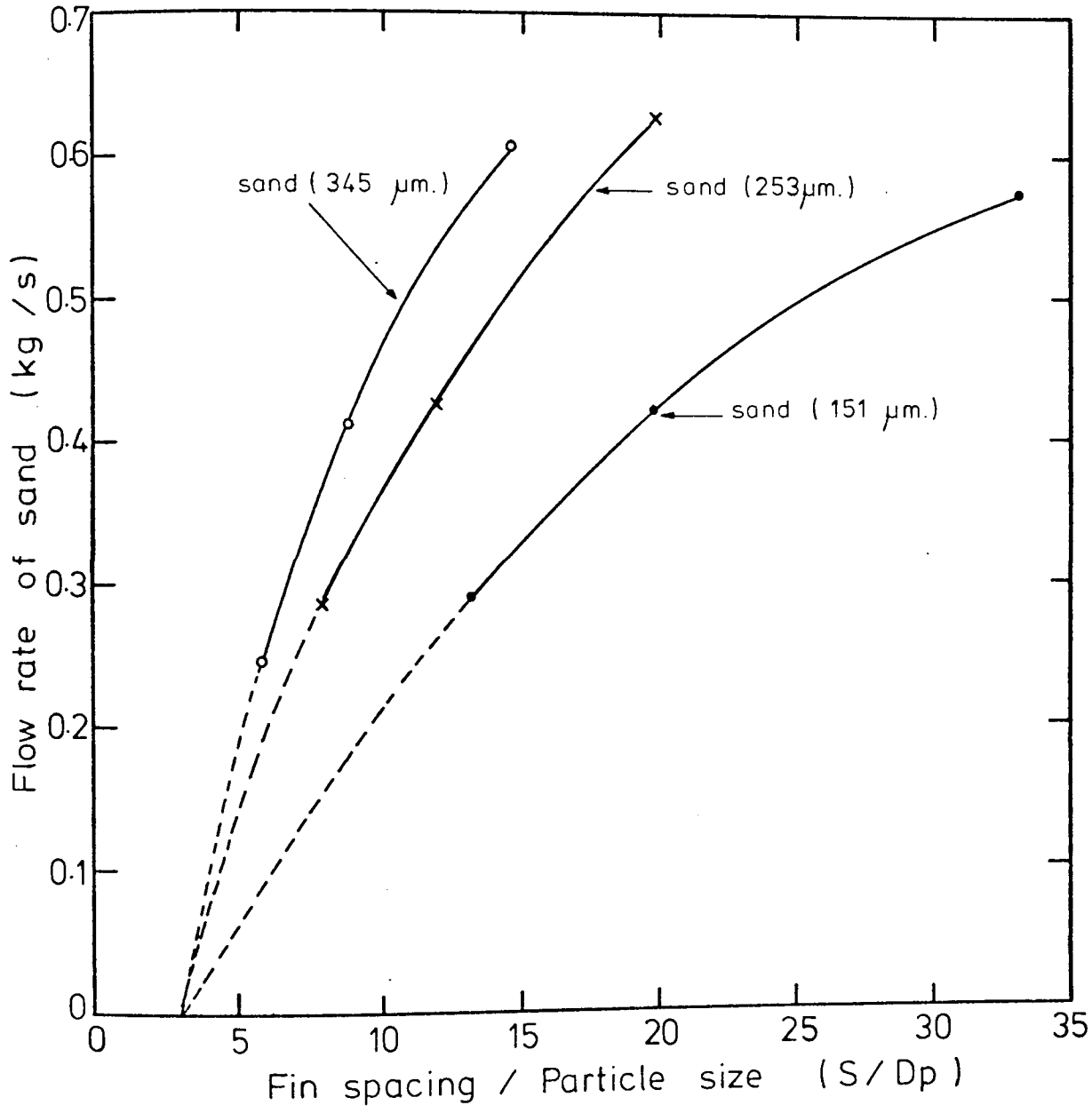

FIG. (9·11) INVESTIGATION OF FLOW OF SAND MATERIALS BETWEEN THE FINS

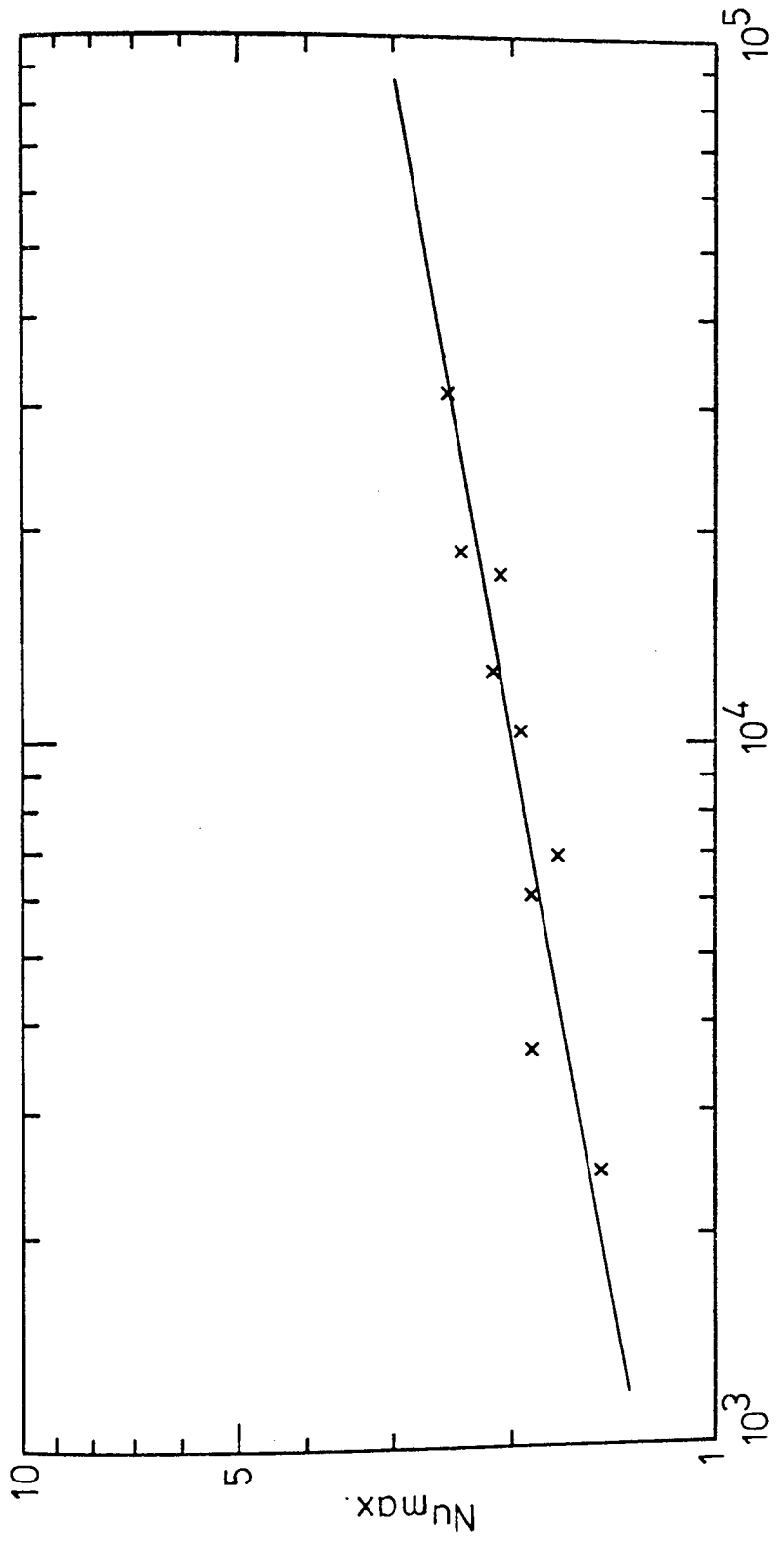

FIG. (9.12) PROPOSED CORRELATION FOR THE MAXIMUM HEAT TRANSFER COEFFICIENT IN FINNED TUBES

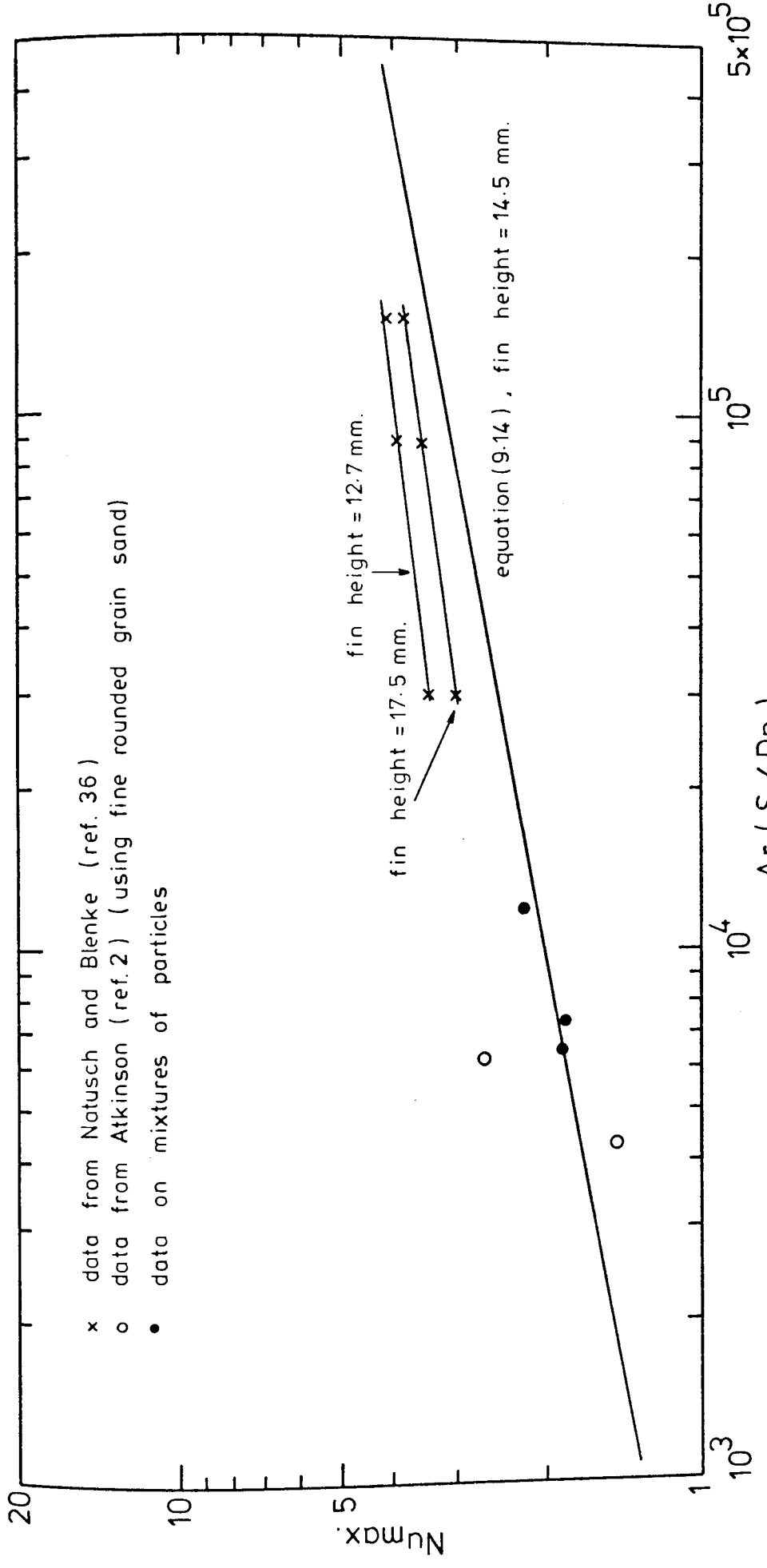

FIG.(9.13) COMPARISON OF FINNED TUBE RESULTS

CHAPTER 10

CONCLUSIONS

and

SUGGESTIONS FOR FURTHER WORK

CONCLUSIONS AND SUGGESTIONS FOR FURTHER WORK

10.1 Conclusions

The experimental work as well as the theoretical work have yielded very interesting information concerning the heat transfer performance of plain and finned tubes immersed in shallow gas fluidized beds and the phenomenon of fin gap/particle size interaction.

Theoretical calculations suggest that an increase in the profile near the root of a radial fin of a rectangular cross-section, which resulted from fins being soldered, brazed or welded onto tubes, was found to have very little effect on the fin efficiency which is considered to be the main performance criterion of fins.

The performance of a single horizontal plain tube was found to be dependent on its position in the bed. This performance was affected by particle size, as well as the fluidizing velocity and the static bed depth.

With fine particles, the heat transfer coefficient was highest with the tube positioned in the lean phase, i.e. the "cloud" above the bed. This effect was attributed to bubble coalescence and size in shallow beds which has a direct bearing on the bed expansion and the percentage of particles in the particle cloud above the bed and the height of this cloud. The effect becomes more marked as the bed depth decreases.

For plain tubes two correlations were proposed, which were,

$$Nu = 0.2\ N^{0.354}\ Ar^{0.331}$$

for the rising branch of the H-J curve, and

$$Nu_{max} = 0.562\ Ar^{0.255}$$

for the maximum heat transfer coefficient. An interesting point about this relatively simple correlation using the Archimedes number, is that it contains a "g" term which would be relevant in high gravitational field work such as that described by Broughton and Elliott[67] where Nu was estimated to be proportional to $Ar^{0.2}$.

Generally, the performance of plain tubes in shallow beds was not very different from that in deep beds with respect to orders of magnitude of the maximum heat transfer coefficient. It was interesting to observe that the maximum heat transfer coefficient obtained, when using 1100 μm alumina as the bed material, was higher than that in deep beds.

A spherical probe was successfully used to simulate a plain tube and was used to check the results of the plain tube. It was found that the spherical probe provided a useful method of obtaining a lot of data quite rapidly.

With finned tubes, the main factors influencing their performance was found to be the fin spacing and the interaction between the shape and profile of the particles with the surface of the fins.

A fin spacing of 20 times the average particle diameter was the critical value below which restriction to particle motion resulted when using rough angular particles. This was attributed to particle-surface interaction. With more rounded particles a fin gap/particle diameter ratio of 15 could be used with little fall off in performance. With the sands used the limit of the fin spacing was 5 times the particle diameter at which point heat transfer was some 15-20% reduced due to the particle motion being impaired. Below a value of fin gap/particle diameter of 5, the performance dropped very rapidly (50% reduction at a value of 2) even when using very smooth spherical particles.

The position of the finned tube in the bed did not have an effect on its performance provided that (S/Dp) did not exceed 20. Above this value, the best position of the tube was found to be near the distributor plate.

Three attempts were made to characterise particle shape which were :

1. The use of the angle of repose
2. Experimental investigation of the rate of flow of solids between the fins.
3. The use of a two-dimensional shape factor obtained from a projection microscope photograph of the particles.

Of the three methods, the rate of flow method appeared to be the one which best characterised the particle-fin interaction and could be useful in carrying out a series of "sorting" experiments with many different particles.

It was found that the restrained movement of particles between the fins resulting from the presence of fins themselves had the effect of improving the heat transfer coefficient at the centre tube.

A correlation was proposed for the maximum heat transfer coefficient of finned tubes which was

$$Nu_{max} = 0.359 \left|Ar(S/Dp)\right|^{0.186}$$

10.2 Suggestions for further work

The most important point that requires further investigation is the effect of particle shape and angularity. Characterising particle surface profile would enable the problem of interaction between the particle and the surface of the fins to be better evaluated and better understood.

It was felt that the whole aspect of particle motion in conjunction with finned tubes needs to be thoroughly investigated as this is one of the major limitations in the development of shallow bed extended surface heat exchangers.

The use of the spherical probe to simulate a plain tube is most helpful in obtaining a lot of reliable data in a short time. It is suggested that a similar approach to try to simulate a finned tube by an approximate flat probe, surrounded by dummy fins, would be very beneficial in evaluating the

performance of finned tubes.

Regarding the performance characteristics of fins, and in the light of the interaction between fins and particles, an investigation into the validity of the assumption of a constant heat transfer coefficient over the whole fin was thought to be necessary. Again in this work a small flat plate transient probe could be used very effectively. If the opposite was to be proven to be the case, the optimum fin shape would change which might result in fins being longer or shorter than the case is now, or the construction of fins with unequal thicknesses around their profile.

APPENDICES

APPENDIX 1

ANALYTICAL SOLUTION OF THE FIN EQUATION

The governing equation for the heat flow through the fin is equation (3.8)

$$\frac{d^2\theta}{dR^2} + \frac{1}{R}\frac{d\theta}{dR} - m^2\theta = 0 \qquad \text{(A1.1)}$$

This is a modified Bessel equation of order zero and the solution is

$$\theta = A_1 I_o(mR) + A_2 K_o(mR) \qquad \text{(A1.2)}$$

where I_o and K_o are modified Bessel functions of the first and second kind respectively and of order zero.

To evaluate the constants A_1 and A_2, the boundary conditions are used. These are

1. at $R=R_o$, $\theta=\theta_o$ at the fin root
2. at $R=R_e$, $\frac{d\theta}{dR} = 0$ at the fin tip

applying the first condition,we get

$$\theta_o = A_1 I_o(mR_o) + A_2 K_o(mR_o) \qquad \text{(A1.3)}$$

and from the second condition, we get

$$\frac{d\theta}{dR} = mI_1 mI_1(mR) - m K_1(mR)$$

hence $$0 = A_1 m I_1(mR_e) - mA_1 K_1(mR_e) \qquad \text{(A1.4)}$$

this gives $$A_2 = \frac{A_1 I_1(mR_e)}{K_1(mR_e)} \qquad (A1.5)$$

where I_1 and K_1 are modified Bessel functions of the first and second kind respectively and of the first order.

(I_1) and $(-K_1)$ are the derivatives of (I_o) and (K_o) respectively.

substituting (A1.5) into (A1.3) we get

$$\Theta_o = A_1 I_o(mR_o) + \frac{A_1 I_1(mR_e)}{K_1(mR_e)} K_o(mR_o)$$

$$= A_1 \left[\frac{I_o(mR_o)\ K_1(mR_e) + I_1(mR_e)\ K_o(mR_o)}{K_1(mR_e)} \right]$$

Therefore $$A_1 = \frac{\Theta_o K_1(mR_e)}{I_o(mR_o)K_1(mR_e) + I_1(mR_e)K_o(mR_o)} \qquad (A.1.6)$$

substituting (A1.6) into (A1.5) we get

$$A_2 = \frac{\Theta_o I_1(mR_e)}{I_o(mR_o)K_1(mR_e) + I_1(mR_e)K_o(mR_o)} \qquad (A1.7)$$

Finally substituting for A_1 and A_2 in (A.1.2), we get

$$\Theta = \frac{\Theta_o K_1(mR_e)\ I_o(mR\ ) + \Theta_o I_1(mR_e)K_o(mR)}{I_o(mR_o)\ K_1(mR_e) + I_1(mR_e)K_o(mR_o)}$$

Hence $$\frac{\Theta}{\Theta_o} = \frac{K_1(mR_e)\ I_o(mR) + I_1(mR_e)\ K_o(mR)}{I_o(mR_o)\ K_1(mR_e) + I_1(mR_e)\ K_o(mR_o)}$$

APPENDIX 2

NUMERICAL SOLUTION OF THE FIN EQUATION

A2.1 Procedure

The numerical solution was based on a predictor-corrector principle. Two values of the temperature gradient at the root of the fin were guessed, from each of which separate values of the temperature gradient at the tip of the fin were calculated. By interpolating between these final gradients, a corrected root gradient was obtained and then used with one of the initially guessed ones to obtain another two tip gradients for further interpolation. This was repeated until the boundary condition was satisfied that the temperature gradient at the tip of the fin was very close to zero. Using the final value of the root gradient the temperature difference (Θ) and its gradient ($\frac{d\Theta}{dR}$) along the fin was computed.

A2.2 Representation of differential equation

The differential equation was equation (3.8)

$$\frac{d^2\Theta}{dR^2} + \frac{1}{R}\frac{d\Theta}{dR} - m^2\Theta = 0$$

An approximation to this equation was made using finite differences for the derivatives. When expressed in discretised form, the differential equation became

$$\Theta_i'' = m^2\Theta - \frac{1}{R}\Theta_i' \qquad \text{(A2.1)}$$

where the suffix (i) refers to any point along the fin and

$$\theta''_{i+1} = m^2\theta_{i+1} - \frac{1}{R}\theta'_{i+1} \qquad \text{(A2.2)}$$

where $(i+1)$ refers to the next point after (i) along the fin. The distance between points (i) and $(i+1)$ is (ΔR) which was specified during computation.

The solution made use of the Taylor expansion series as follows

$$\theta_{i+1} = \theta_i + \Delta R\theta'_i \qquad \text{(A2.3)}$$

$$\theta'_{i+1} = \theta'_i + \Delta R\,\theta''_i \qquad \text{(A2.4)}$$

also $$\theta_{i+1} = \theta_i + \frac{\Delta R}{2}(\theta'_i + \theta'_{i+1}) \qquad \text{(A2.5)}$$

$$\theta'_{i+1} = \theta'_i + \frac{\Delta R}{2}(\theta''_i + \theta''_{i+1}) \qquad \text{(A2.6)}$$

where θ' and θ'' are first and second derivatives of θ respectively.

The computation was carried out as follows:

1. The assumed value of θ'_i was inserted into equation (A2.1) to obtain θ''_i (m, θ_i and R were known).
2. This value of θ''_i together with θ'_i (assumed) were substituted into equation (A2.4) to get a predicted value of θ'_{i+1}
3. The predicted θ'_{i+1} together with θ'_i (assumed) were substituted into equation (A2.5) to get a predicted value of θ_{i+1}

4. The predicted values of Θ_{i+1} were substituted into equation (A2.2) to obtain Θ''_{i+1}

5. Θ''_{i+1} and Θ''_i(predicted) with Θ'_i (assumed) were inserted into equation (A2.6) to get a corrected value of Θ'_{i+1}

6. This Θ'_{i+1} (corrected) and Θ_i (assumed) were inserted into equation (A2 .5) to obtain a corrected value of Θ_{i+1}

7. R was increased by ΔR and the above procedure was repeated using the corrected values of Θ_{i+1} and Θ'_{i+1} in place of Θ_i and Θ'_i

8. The above procedure was done until a final temperature gradient was reached at the tip of the fin.

A flow diagram of the computation procedure is presented in figure (A2.1).

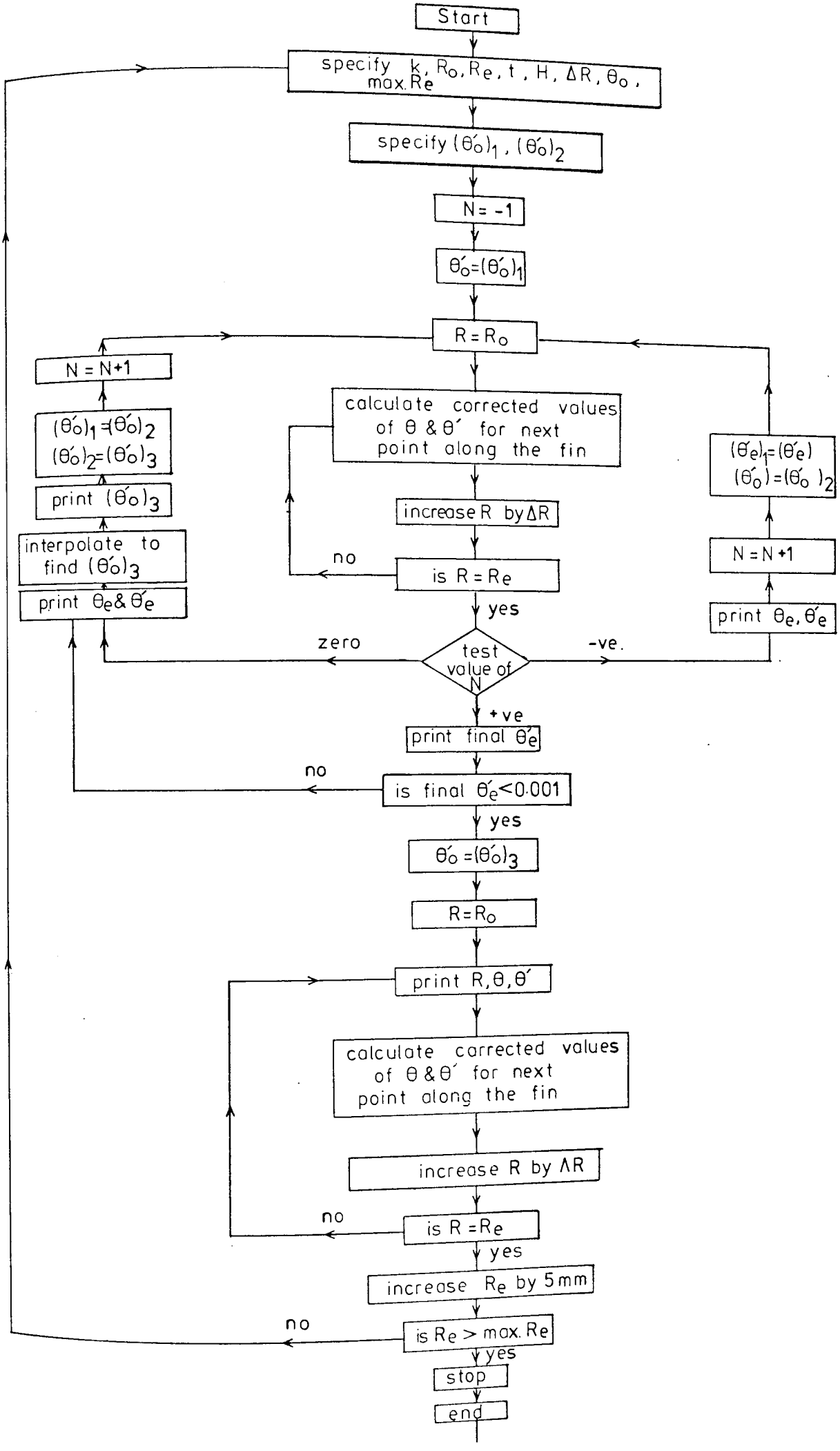

FIG. (A2.1) FLOW CHART FOR NUMERICAL SOLUTION OF FINS

APPENDIX 3

EFFICIENCY OF FINS

A.3.1 Analytical expression

The efficiency of fins is defined as the ratio of the heat transferred through the fin to that transferred if the whole fin was at the root temperature.

the heat flux $Q = +KA_o \left(\frac{dT}{dR}\right)_{R=R_o}$

$$= -KA_o \left(\frac{d\Theta}{dR}\right)_{R=R_o} \qquad \text{(A3.1)}$$

The expression for Θ derived in Appendix (1) is

$$\Theta=\Theta_o \left[\frac{K_1(mR_e)\ I_o(mR) + I_1(mR_e)K_o(mR)}{K_1(mR_e)\ I_o(mR_o)+I_1(mR_e)\ K_o(mR_o)}\right]$$

$$\text{hence } \frac{d\Theta}{dR} = m\Theta_o \left[\frac{K_1(mR_e)\ I_1(mR) - I_1(mR_e)K_1(mR)}{K_1(mR_e)\ I_o(mR_o) + I_1(mR_e)K_o(mR_o)}\right]$$

and at $R = R_o$

$$\left(\frac{d\Theta}{dR}\right)_{R=R_o} = m\Theta_o \left[\frac{K_1(mR_e)\ I_1(mR_o) - I_1(mR_e)K_1(mR_o)}{K_1(mR_e)\ I_o(mR_o) + I_1(mR_e)K_o(mR_o)}\right]$$

$$\text{Therefore } Q = -KA_o m\Theta_o \left[\frac{K_1(mR_e)\ I_1(mR_o) - I_1(mR_e)K_1(mR_o)}{K_1(mR_e)\ I_o(mR_o) + I_1(mR_e)K_o(mR_o)}\right] \qquad \text{(A3.3)}$$

The heat transferred if the fin is at root temperature is

$$Q' = HA_f\Theta_o$$

Hence the efficiency $\phi = \frac{Q}{Q'}$

$$= \frac{-KA_o m\Theta_o}{HA_f\Theta_o}\left[\frac{K_1(mR_e)I_1(mR_o) - I_1(mR_e)K_1(mR_o)}{K_1(mR_e)I_o(mR_o) + I_1(mR_e)K_o(mR_o)}\right] \quad (A3.4)$$

$$A_o = 2\pi R_o t$$

and $A_f = 2\pi(R_e^2 - R_o^2)$

Therefore $$\frac{-KA_o m}{HA_f} = \frac{-K2\pi R_o m t}{2\pi(R_e^2 - R_o^2)H}$$

$$= \frac{-2R_o m}{m^2(R_e^2 - R_o^2)}$$

Hence $$\phi = \frac{2R_o}{m(R_e^2 - R_o^2)}\left[\frac{I_1(mR_e)K_1(mR_o) - K_1(mR_e)I_1(mR_o)}{K_1(mR_e)I_o(mR_o) + I_1(mR_e)K_o(mR_o)}\right] \quad (A3.5)$$

A.3.2 Numerical evaluation

As can be seen from Appendix (2), the temperature gradient at the root of the fin is known at the end of the programme. Knowing this together with K, A_o, A_f, H and Θ_o, Q and Q' can be easily worked out using equations (A3.1) and (A3.3) respectively and the efficiency obtained.

APPENDIX 4

NUMERICAL SOLUTION FOR FINS WITH LARGE ROOT AREA

The solution used here is the same as the one explained in Appendix 2. The variation being that for the first part of the fin, where R is between R_o and R_o+R_1 the governing differential equation used is equation (3.16) which is

$$\frac{d^2\Theta}{dR^2} - \frac{2H}{KC_o} R\Theta = 0 \qquad \text{(A4.1)}$$

and when it is expressed in discretised form it becomes

$$\Theta_i'' = \frac{2H}{KC_o} R\Theta_i \qquad \text{(A4.2)}$$

and $$\Theta_{i+1}'' = \frac{2H}{Kc_o} R\Theta_{i+1} \qquad \text{(A4.3)}$$

Figure (A4.1) shows the flow diagram of the computer programme used to carry out the numerical solution.

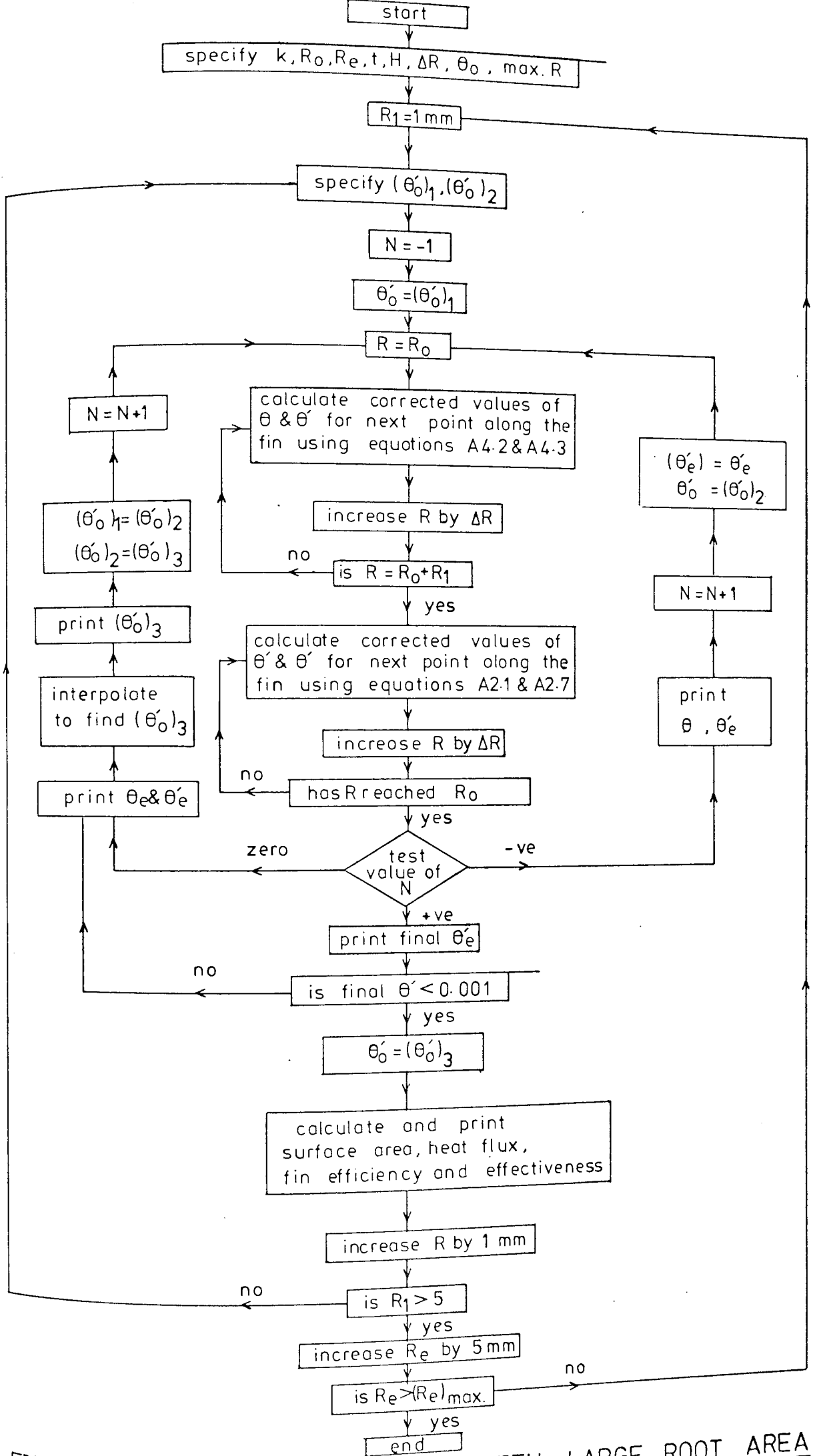

FIG.(A4.1) FLOW CHART FOR FINS WITH LARGE ROOT AREA

APPENDIX 5

BED PRESSURE MEASUREMENT

The arrangement used for measuring the pressure at any point in the fluidized bed is a simple one. A sketch of the arrangement is shown in figure A5.1. The probe used is a very fine tube of 1mm. internal diameter which was supported by a rod and was clamped in position by a clamp fitted at the top flange of the bed container. The tube was connected through a flexible plastic tube to an inclined manometer. The manometer used was a sensitive one and was accurate to 0.01cm. water gauge.

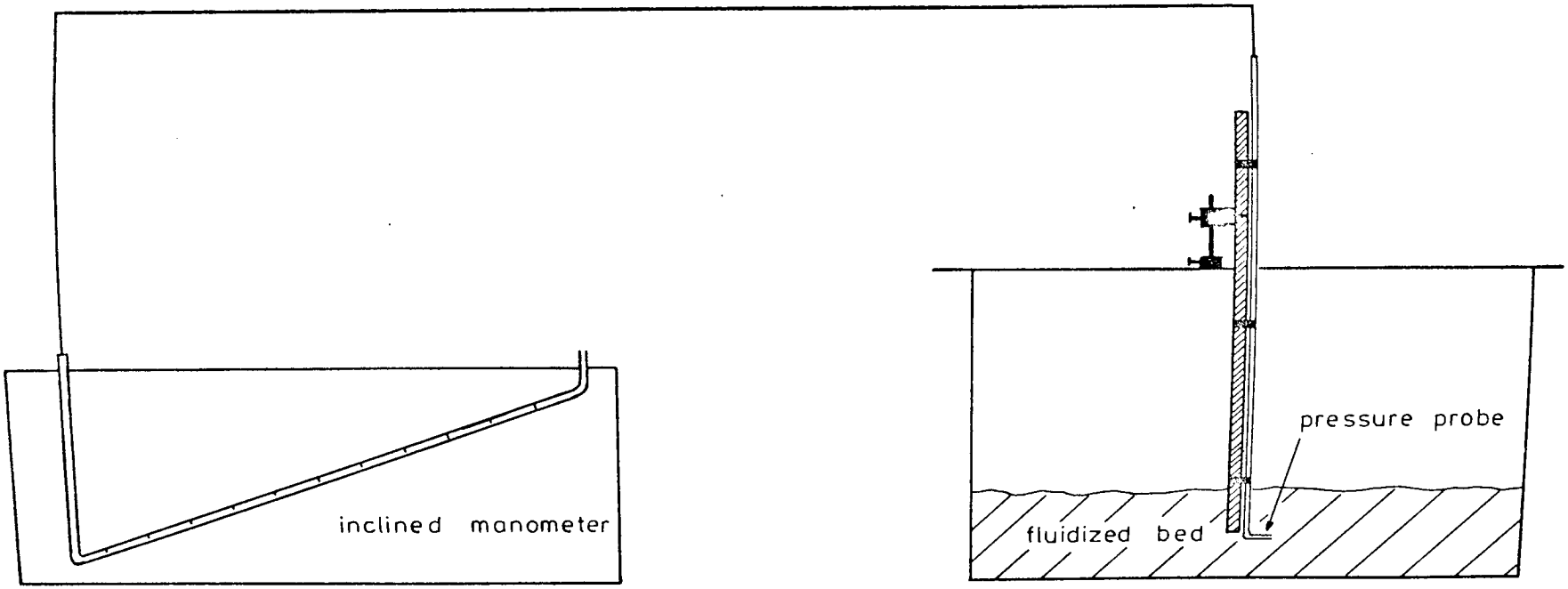

FIG. (A5·1) ARRANGEMENT OF BED PRESSURE MEASUREMENT

APPENDIX 6

PROPERTIES OF BED MATERIALS

A6.1 Mean Particle Size

A6.1.1 Introduction

Two bed materials were used in the research work: silica sand and blown alumina. The size ranges used were as follows:

100-200 μm. silica sand

200-300 μm. silica sand

300-400 μm. silica sand

1000-1200 μm blown alumina

From the first sand size range, two samples from two different sources, were obtained and were used for the bare tube and finned tube experiments. Only one sample was used, for all the experiments, from each of the other three size ranges.

The size distribution of each sample was obtained by conducting individual sieve analyses according to B.S.410 The particle diameter (for the sand samples) was then determined by two methods. The first was a mass averaging technique outlined by Kunii and Levenspiel[6] which is based on the idea that the specific surface area of the mean particle size is the same as the total specific areas of the fractions. This method expresses the mean size as

$$Dp = \left(\frac{X_i}{Dp_i} \right)^{-1}$$

The second method was outlined by Allen[65] which is based on a log-probability plot of the cumulative percentages of weight fractions against their respective sizes, from which the value of the median (i.e. the size corresponding to 50% weight fraction) was obtained using the least square technique to fit the best straight line, as shown in figure (A6.1) and (A6.2).

The second method is more representative in establishing the "mean particle size" since the size distributions did not exactly conform to the normal distribution

The procedure was adopted for the sand samples only since intermediate sieves were available to conduct sieve analyses. However, for the alumina, the mean size was taken as the arithmetic average of the two sieves limiting the size range, i.e. an average size of 1100 μm was used.

A6.1.2 Sieve Analyses and Particle Sizes

(a) 100-200 μm silica sand (used with bare tube)

size range (μm)	weight (gms)
-105 + 63	137.8
-125 + 105	207.11
-180 + 125	481.88
-210 + 180	35.87

size (Dp_i) (μm)	weight fraction (X_i) (per cent)	Cumulative fraction
84	15.951	15.951
115	23.975	39.926
152.5	55.782	95.708
195	4.292	100

$$\left(\Sigma \frac{x_i}{Dp_i}\right)^{-1} = 127.2 \text{ μm}$$

From figure (A6.1), Dp = 134 μm

(b) 100-200 μm silica sand (used with finned tube)

size range (μm)	weight (gms)
-90 + 63	13.78
-106 + 90	58.88
-125 + 106	39.74
-180 + 125	703.21
-212 + 180	109.99

size (Dp_i) (μm)	weight fraction (X_i) (per cent)	cumulative fraction
76.5	1.49	1.49
98	6.36	7.85
115.5	4.29	12.14
152.5	75.98	88.12
196	11.88	100

$$\left(\Sigma \frac{X_i}{Dp_i}\right)^{-1} = 147 \text{ μm}$$

From figure (A6.2), Dp = 151 μm

(c) 200-300 μm silica sand

size range (μm)	weight (gms)
-180 + 150	13.69
-210 + 180	63.52
-250 + 210	230.99
-300 + 250	466.15

size (Dp_i) (μm)	weight fraction (x_i) (per cent)	cumulative fraction
165	1.8	1.8
195	8.2	10.0
230	29.8	39.8
275	60.2	100.0

$$\left(\Sigma\frac{x_i}{Dp_i}\right)^{-1} = 244 \text{ μm}$$

From Figure A6.1, Dp = 253 μm.

(d) 300-400 μm silica sand

size range (μm)	weight (gm)
-300 + 250	61.41
-355 + 300	163.91
-420 + 355	158.1

size (Dp_i) (μm)	weight fraction (x_i) (per cent)	cumulative fraction
275	16.02	16.02
327.5	42.75	58.77
387.5	41.23	100.0

$$\left(\Sigma \frac{x_i}{Dp_i}\right)^{-1} = 338.8 \text{ μm}$$

From figure (A6.1), Dp = 345 μm

A6.2 Particle density

Densities of the bed materials used were determined experimentally by using a standard specific gravity bottle with the aid of a liquid which did not react chemically with the materials. The following steps were followed:

1. The bottle was weighed empty
2. The bottle was filled with water and then weighed to determine its exact volume
3. The bottle was filled with n-heptane and weighed again to determine the density of n-heptane.
4. A sample of the material, whose density was to be determined, was placed in the bottle and the weight was noted.
5. The bottle, with the material in it, was then filled with n-heptone making sure that no air bubbles were trapped within the solids.
6. From (5) and (4), the weight of n-heptane present with the material under test was calculated. This, together with the density of n-heptane obtained by (3), gave the volume occupied by the liquid. Eventually, the volume occupied by the material sample was calculated.
7. The weight of the material sample was calculated from (4) and the particle density of the material was then obtained knowing its weight and volume.

Values of the density of the materials used are presented in Table A6.1.

TABLE A6.1

DENSITIES OF BED MATERIALS

Type	Density (kg/m^3)
100-200 μm silica sand (used with bare tube)	2662
100-200 μm silica sand (used with finned tube)	2660
200-300 μm silica sand	2685
1000-1200 μm blown alumina	1777

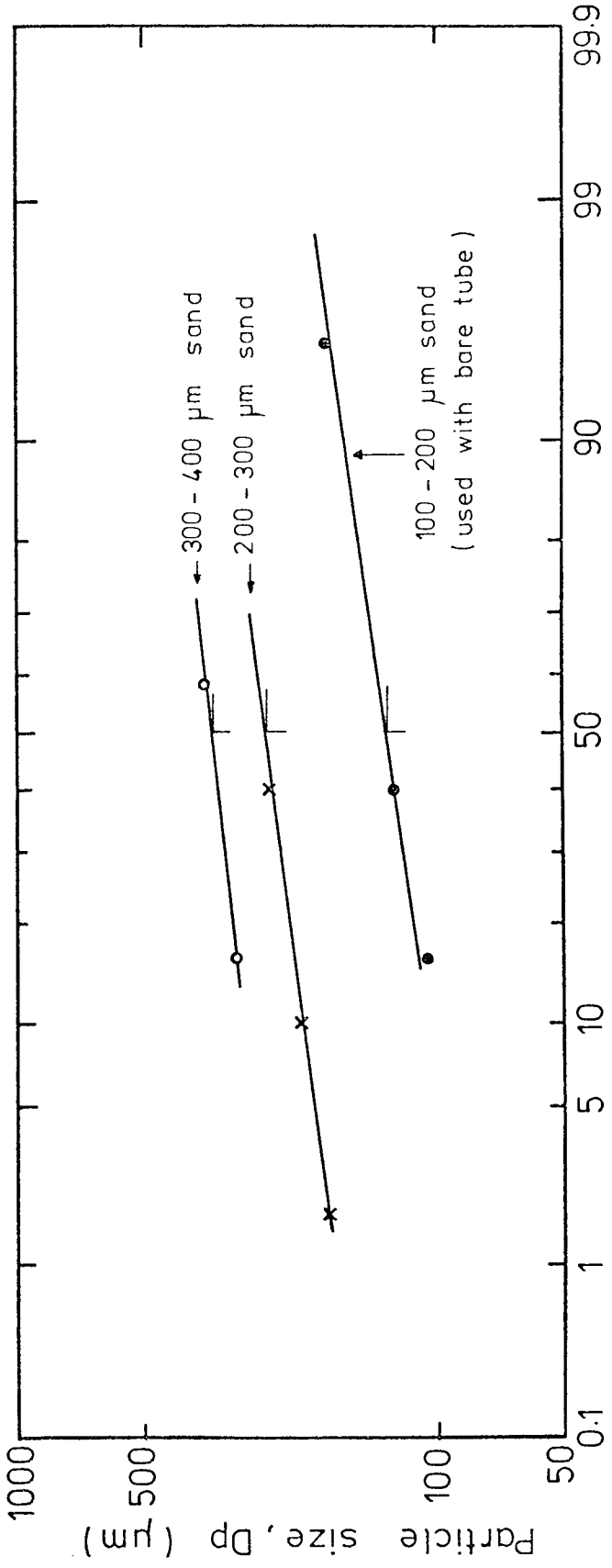

FIG. (A6.1) ESTIMATION OF MEAN PARTICLE SIZE

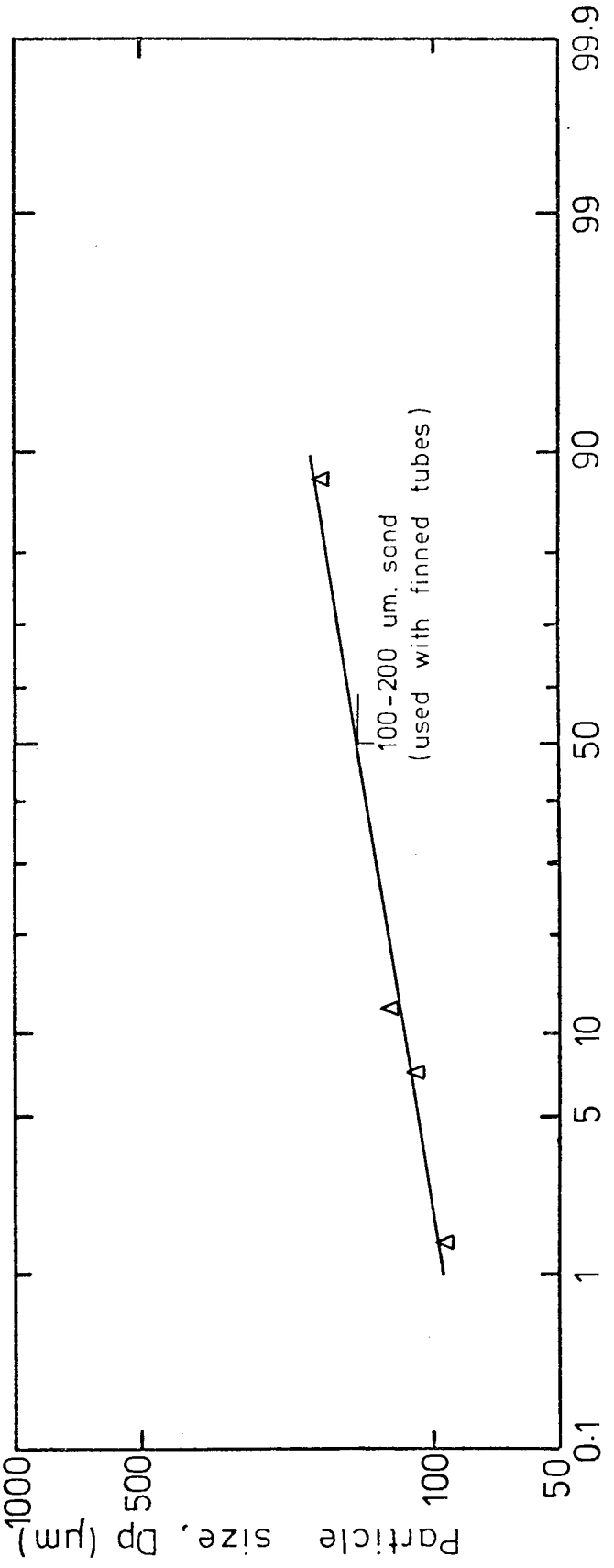

FIG. (A6.2) ESTIMATION OF MEAN PARTICLE SIZE

APPENDIX 7

EQUATION FOR THE SPHERICAL PROBE

In this appendix, the derivation of a simple expression which was used to calculate the heat transfer coefficient from the transient response of the spherical probe is presented.

The copper sphere was regarded as an isothermal one and accordingly the temperature measured at the centre of the sphere was taken as the temperature of the whole sphere.

Considering a small change in time (t), the heat absorbed by the sphere (Q_s) will be

$$Q_s = MC_s \frac{dT_i}{dt} \qquad (A6.1)$$

where M, C_s and T_i are the mass, specific heat and temperature of the sphere respectively. This absorbed heat is equivalent to the heat transferred across the surface of the sphere from the fluidised bed, which can be expressed as

$$Q_s = H\, A_s\, (T_b - T_s) \qquad (A6.2)$$

where H, A_s and T_b are the sphere surface average heat transfer coeffieient, the surface area of the sphere and the bed temperature respectively.

$$\text{Therefore, } MC_s \frac{dT_s}{dt} = H\, A_s (T_b - T_s) \qquad (A6.3)$$

By separating the variables, equation (A6.3) can be integrated to give

$$-\left[\ell n \ (T_b - T_s) \right]_{T_{s_i}}^{T_s} = \frac{HA_s}{MC_s} \left[t \right]_o^t \qquad (A6.4)$$

between the limits shown. This eventually yields

$$\ell n \left[\frac{T_b - T_s}{T_b - T_{si}} \right] = \frac{HA_s}{MC_s} \ t \qquad (A6.5)$$

from which the heat transfer coefficient (H) can be calculated.

Appendix -8-

Evaluation of the heat transfer coefficient of finned tubes

A8.1 Relationship between Hov., Hi, and H_{BM}

The heat transferred from the bed to the water (Q) can be expressed by the following equations

$$Q = H_i A_i (T_w - T_m) \quad \text{(A8.1)}$$

$$Q = H_{BM} A_{eff} (T_m - T_b) \quad \text{(A8.2)}$$

$$Q = Hov. A_T (T_w - T_b) \quad \text{(A8.3)}$$

where T_w, T_m and T_b are the water, tube and bed temperatures respectively and A_i, A_{eff}, and A_T are the inside, effective and total areas of the finned tube.

The three above equations can be written as

$$(T_w - T_m) = \frac{Q}{H_i A_i} \quad \text{(A8.4)}$$

$$(T_m - T_b) = \frac{Q}{H_{BM} A_{eff}} \quad \text{(A8.5)}$$

$$(T_w - T_b) = \frac{Q}{Hov. A_T} \quad \text{(A8.6)}$$

From equations (A8.4) and (A8.5) we get

$$(T_w - T_b) = \frac{Q}{H_i A_i} + \frac{Q}{H_{BM} A_{eff}} \quad \text{(A8.7)}$$

Hence by equating $(T_w - T_b)$ in equations (A8.6) and (A8.7), we get

$$\frac{Q}{Hov.A_T} = \frac{Q}{H_i A_i} + \frac{Q}{H_{BM} A_{eff}}$$

which finally becomes

$$\frac{1}{Hov. A_T} = \frac{1}{H_i A_i} + \frac{1}{H_{BM} A_{eff}} \qquad (A8.8)$$

A8.2 Iterative process to calculate H_{BM}

To find the heat transfer coefficient (H_{BM}), it was necessary that (A_{eff}) be known as can be seen from equation (A8.8). A_{eff} in itself is dependent on the fin efficiency (Ø) (see equation 8.7) which is a function of H_{BM} as can be seen from equation (3.10). It was, for this reason, necessary to use an iterative process to compute the heat transfer coefficient (H_{BM}) as follows:

1 - The overall heat transfer coefficient (Hov) was evaluated from the heat flux, bed and water temperatures and the total area (A_T) using equation (8.1)

2 - This value of Hov. was taken as the initial guessed value of H_{BM} from which the fin efficiency (Ø) was evaluated using the equation (3.10)

3 - Knowing the fin efficiency, the effective area was calculated from equation (8.7)

4 - A new value of H_{BM} was then calculated from equation (A8.8) which was then compared to the initial value of H_{BM}.

5 - The process was repeated until convergence was obtained so that the initial and final values of H_{BM} did not differ by more than 0.001.

To carry out this computation a programmable calculator (HP 9830) was employed using "BASIC" as the programming language. A flow chart of the programme is presented in figure (A8.1).

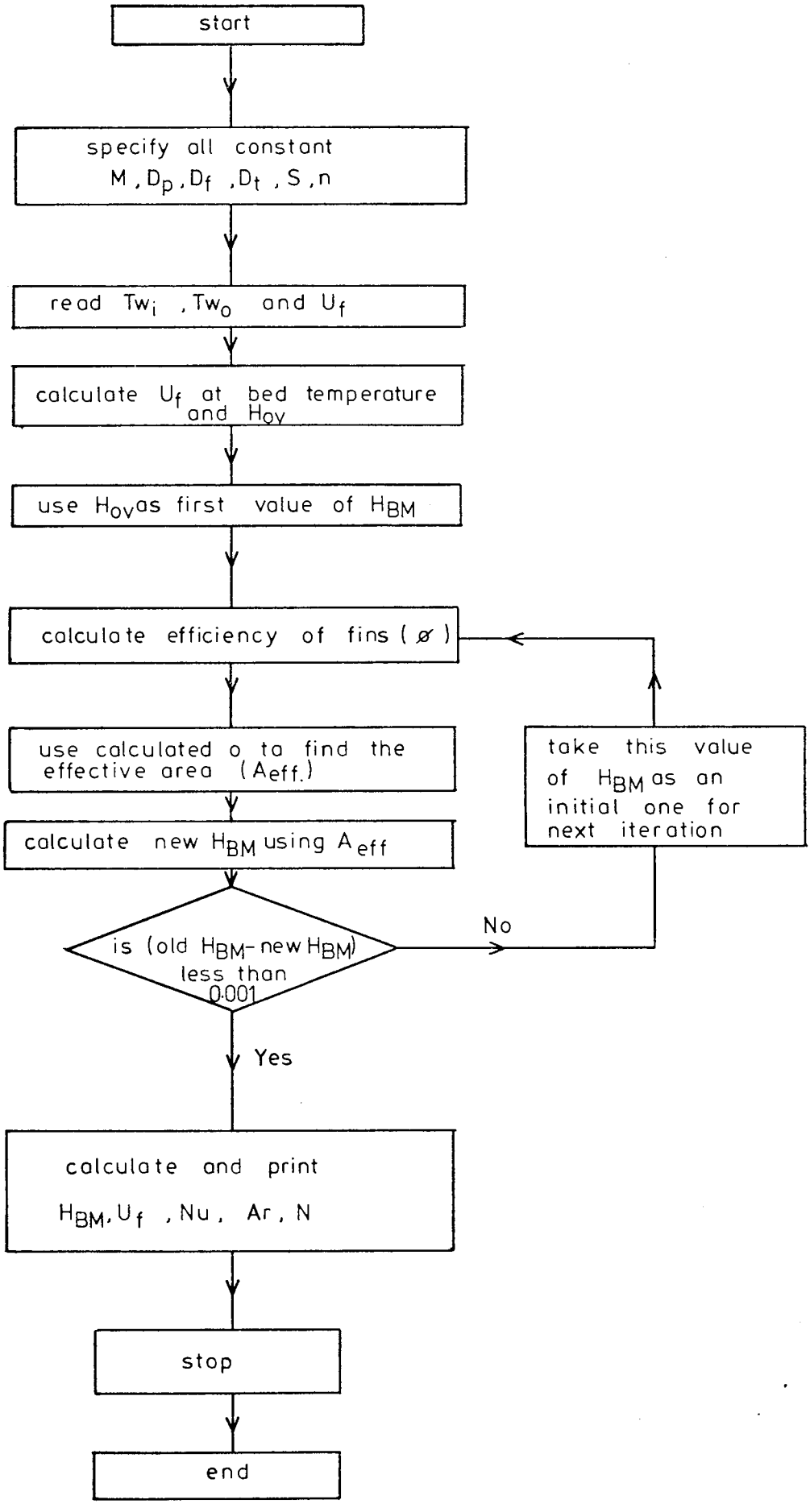

FIG. (A8·1) FLOW DIAGRAM OF COMPUTER PROGRAMME FOR FINNED TUBES

APPENDIX 9

DATA OF OTHER RESEARCHERS

A9.1 Bare tube data

Atkinson[2] presented data on the performance of bare tubes in shallow air fluidized beds. It was decided to use this data to compare with the experimental results of the present work.

For the rising branch of the H-J curve, the extracted data was for a bed depth of 50 mm so that a fair comparison could be made. For the maximum heat transfer coefficient, however, the data was limited to performance curves which showed that the heat transfer coefficient had attained its maximum. This data was only available for bed depth of 31 mm with the tube situated 15.5mm from the distributor. The data is shown in tables (A9.1) and (A9.2) for the rising branch of the H-J curve and for the maximum heat transfer coefficients respectively.

A9.2 Finned tube data

Data points were extracted from the works of Atkinson[2] and Natusch and Blenke[36] on the performance of a single horizontal finned tube in shallow and deep beds respectively for comparison with the results of the present work. Atkinson[2] used different types of fins and his data on radial manufactured fins were used where only two points could be used for the maximum heat transfer coefficients corresponding to two values

of fin spacing.

The data is presented in tables (A9.3) and (A9.4) corresponding to Atkinson[2] and Natusch and Blenke[36] respectively.

Table A9.1

Bare tube data (Atkinson[2]) for the rising branch of H-J curve

bed material : zircon sand

particle size : 138 μm

particle density : 4600 Kg/m^3

heat transfer coefficient (W/m^{2}K)	fluidizing velocity (m/s)
500	0.2
555	0.3
590	0.4
610	0.5

Table A9.2

Bare tube data (Atkinson[2]) for the maximum heat transfer coefficient

bed material	partical size (μm)	particle density (Kg/m^3)	max.heat transfer coefficient (W/m^{2}K)
zircon sand	138	4600	600
steel shot	432	7500	590
silica sand	157	2620	400

Table A9.3

Finned tube data (Atkinson[2]) for the maximum heat transfer coefficient

bed material : zircon sand

partical size : 138 μm

particle density : 4600 Kg/m^3

bed depth : 75 mm

fin height : 17.85 mm

max.heat transter coefficient (W/m^{2}K)	fin spacing (mm)
610	3.7
330	2.55

Table A9.4

Finned tube data (Natusch and Blenke[36]) for the maximum heat transfer coefficient

bed material : Glass

particle size : 450 μm

bed depth : 500 mm

max.heat transter coefficient (Kcal/m^{2}hr^{0}C)	fin spacing (mm)	fin height (mm)
206	10	12.7
197	6	12.7
172	2	12.7
189	10	17.5
166	6	17.5
149	2	17.5

BIBLIOGRAPHY

1. ELLIOTT, D.E.
Paper 22, The Total Energy Conference, Institute of Fuel, Nov. 1971, P.361.

2. ATKINSON, G.
Ph.D. Thesis, The University of Aston in Birmingham, 1974.

3. YUDITSKII, V.I. and ZABRODSKII, S.S.
"Investigation of Heat and Mass Transfer in Technological Processes and Apparatus" edited by A.V. LYKOV, Publishing House "Nawka:Tekhnika", Minsk 1966, p.19
English Translation ANL-Trans-587.

4. BOTTERILL, J.S.M.
"Fluid Bed Heat Transfer" Chapter 1,
Academic Press 1975

5. ZABRODSKY
"Hydrodynamics and Heat Transfer in Fluidized Beds", Chapter 10, M.I.T. Press, 1966.

6. KUNII, D. and LEVENSPIEL, O.
"Fluidization Engineering", Chapter 9,
John Wiley and Sons Inc. 1969.

7. DAVIDSON, J.F, and HARRISON, D.
"Fluidization", Chapter 10,
Academic Press 1971.

8. BOTTERILL, J.S.M.
"Fluid Bed Heat Transfer", Chapter 5.
Academic Press, 1975.

9. AINSHTEIN, V.G. and GELPERIN, N.I.
Int. Chem. Eng. vol. 6. No. 1, 1966, p.67.

10. DOW, W.M. and JAKOB, M.
Chem. Eng. Progress, vol. 47, No.12, 1951, p.637.

11. VAN HEERDEN, C., NOBEL, P. and VAN KREVELEN, D.W.
Chem. Eng. Science. Vol.1, No. 2, 1951, p.51.

12. VAN HEERDEN, C., NOBEL, P. and VAN KREVELEN, D.W.
Chem. Eng. Science, vol. 1, No. 1. 1951, p.37.

13. LEVENSPIEL, O., and WALTON, J.S.
Chem. Eng. Progr. Sym. series vol.50,(9),1954, p.2.

14. TOOMEY, R.D. and JOHNSTON, H.F.
Chem. Eng. Progr. Symp. series vol. 49,(5), 1953,p.51.

15. LEVA, M., WEINTRAUB, M., and GRUMMER, M.
Chem. Eng. Progr. vol. 45, 1949, p.563.

16. WEN, C.Y., and LEVA, M.
A.I.Ch.E. Journal, vol.2, 1956, p.482

17. BARTHOLEMEW, R.M. and KATZ, D.L.
Chem. Eng. Progr. Symp. series. vol.48,(4) 1953.

18. MICKLEY, H.S. and TRILLING, C.A.
Ind. Eng. Chem. vol.41, 1949, p.1135.

19. WENDER, L. and COOPER, G.T.
A.I.Ch.E. Journal, vol.4, 1958, p.15.

20. BAERG, A., KLASSEN, G., and GISHLER, P.E.
Can. J. of Res. vol. 28, Sec.F, No.8, 1950, p287.

21. MILLER, C.O., and LOGWINUK, A.K.
Ind. Eng. Chem. vol.43, 1951, p.1220.

22. VREEDENBERG, H.A.
J. Appl. Chem. vol. 2, suppl. No. 1, 1952, p.526.

23. VREEDENBERG, H.A.
Chem. Eng. Science, vol. 11, 1960, p.274.

24. VREEDENBERG, H.A.
Chem. Eng. Science, vol. 9, 1958, p.52.

25. OLIN, H.L. and DEAN, O.C.
Petrol. Eng., vol. 25, 1953, PC-23.

26. MICKLEY, H.S. and FAIRBANKS, D.F.
A.I.Ch.E. Journal, vol.1, 1955, p.374

27. WICKE, E., and FETTING, F.
Chem. Ing. Tech. vol.26, 1954, p.301.

28. JACOB, A. and OSBERG, G.L.
Can. J. Chem. Eng., vol. 35, 1957, p.5.

29. SHIRAI, T.
Chem. Eng. Japain, vol.26, 1962, p.637.

30. SHIRAI, T., YOSHITOME, H., SHOJI, Y., TANAKA., S.,
HOJO, K., and YOSHIDA, S.
Chem. Eng. Japan, vol. 29, 1965, p.880.

31. ZIEGLER, E.N., KOPPEL, L.B. and BRAZELTON, W.T.
Ind. Eng. Chem. Fundamentals, vol. 3, 1964, p.94.

32. PETRIE, J.C., FREEBY, W.A., and BUCKHAM, J.A.
Chem. Eng. Progr., vol. 64, No. 7, 1968, p.45.

33. BARTEL, W.J. and GENETTI, W.E. and GRIMMETT, E.S.
A.I.Ch.E. symp. series., vol.67, No.116, 1971, p.85.

34. BARTEL, W.J., and GENETTI, W.E.
A.I.Ch.E. Symp. series, vol.69, No.128, 1973, p.85.

35. GENETTI, W.E., SCHMALL, R.A. and GRIMMETT, E.S.
A.I.Ch.E. Symp. series, vol.67, No.116, 1971, p.90.

36. NATUSCH, H.J. and BLENKE, H.
Paper C4.4, 4th CHISA Congress, Prague,
Czechoslovakia, 1972.

37. SINCLAIR, R., WRIGHT, J.C.J., and THOMAS, C.G.
J. of Iron and Steel Inst., vol. 203, 1965, p.131.

38. BASKAKOV, A.P. and FILIPOVSKIY, N.F.
Heat Transfer-Soviet Research, vol.3, No.5, 1971, p.176.

39. MASKAEV, V.K., and BASKAKOV, A.P.
Int. Chem. Eng., vol. 14, No.1, 1974, p.80.

40. GELPERIN, N.I., AINSHTEIN, V.G.,KOROTYANSKAYA, L.A.
Int. Chem. Eng., vol. 9., No. 1, 1968, p.137.

41. BOTTERILL, J.S.M., and WILLIAMS, J.R.
Trans. Inst. Chem. Engrs., vol. 41, 1963, p.217.

42. BOTTERILL, J.S.M. and BUTT, M.H.D.
Br. Chem. Eng., vol.13, 1968, p.1000.

43. GABOR, J.D.
Chem. Eng. Progr. Symp. series, 66 No.105,1970,p.76.

44. BOTTERILL, J.S.M., BRUNDRETT, G.W., CAIN, G.L.
and ELLIOTT, D.E.
Chem. Eng. Progr. Symp. series, vol. 62, 1966, p.1.

45. KUBIE, J. and BROUGHTON, J.
Int. J. Heat and Mass Transfer, vol.18, 1975, p.289.

46. SYROMYATNIKOV, N.I.
Int. Chem. Eng. vol. 14, 1974, p.483.

47. GARDNER, K.A.,
Trans. A.S.M.E.,vol. 67,No. 8,1945,p. 621.

48. MURRAY, W.M.,
J. Applied Mechanics, Trans. A.S.M.E.,vol.60,1938,p. A-78.

49. CARRIER, W.H., and ANDERSON, S.W.
Heating, Piping and Airconditioning, vol.10,
1944, p.304.

50. PILLAI, K.K.
Int. J. Heat and Mass Transfer, vol. 18, 1975, p.341.

51. SINGH, J.
B.Sc. Project Report, University of Aston in Birmingham,
1972.

52. ELLIOTT, D.E., HEALY, E.M., and ROBERTS, A.G.
Paper presented at the Heat Exchangers Conference
Inst. of Fuel, Paris 1971.

53. McADAMS, W.H.
"HEAT TRANSMISSION", 3rd Edition,
McGraw Hill, 1954.

54. HSU, S.T.
"ENGINEERING HEAT TRANSFER"
Van Nostrand, 1963.

55. BASKAKOV, A.P., BERG, B.V., VANDANTSEVEENIY, B.,
ZUNDUYGIYN, T.S., and GALPERIN, L.G.
Heat Transfer Soviet Research, vol. 4, 1972, p.273.

56. BERG., B.V. and BASKAKOV, A.P.
Int. Chem. Eng. vol. 14, 1974, p.490.

57. ROWE, P.N., and EVERETT, D.J.
Trans. Inst. Chem. Engrs. vol. 50, 1972, p.42-60.

58. HAGER, W.R. and THOMSON, W.J.
A.I.Ch.E. Symp. series, vol. 69, No.128, 1973, p.68.

59. BOTTERILL, J.S.M., ELLIOTT, D.E., van der KOLK, M., and McGUIGAN, S.
Paper presented at "Powtech. International Powder Technology and Bulk Solids conference" 1971.

60. McGUIGAN, S.J.
Ph.D. Thesis, The University of Aston in Birmingham, 1975.

61. GOOSSENS, W.R.A., DUMONT, G.L., and SPAEPEN, G.L.,
Chem. Eng. Prog. Symp. series No. 116, vol. 67, 1971, p.38.

62. ROWE, P.N., NIENOW, A.W. and AGBIN, A.S.
Trans. Inst. Chem. Engrs., vol. 50, 1972, p.324.

63. CHURCH, T.
Powder Technology, vol. 2, 1968/69, p.27.

64. HAUSNER, H.H.
"Particle size Analysis", Proceedings of a Conference organised by the Society for Analytical Chemistry, Loughborough University of Technology, Sept. 1966, p.20.

65. ALLEN, T.,
"Particle Size Measurement"
Chapman and Hall, 1968.

66. HEERDAN, G.
"Small Particle Statistics"
Butterworth 1960.

67. BROUGHTON, J. and ELLIOTT, D.E.
I. Chem. E. Symp. series, No. 43, Paper No. 11.
"High Temperature Chemical Reaction Engineering Symposium", June 1975.